COMILLAS

UNIVERSIDAD PONTIFICIA

ICAI | ICADE | CIHS

ESCUELA TÉCNICA SUPERIOR DE INGENIERÍA (ICAI)

IMPROVING THE ELECTRICAL INFRASTRUCTURE OF DC-ELECTRIFIED RAILWAY SYSTEMS TO INCREASE ENERGY EFFICIENCY, TAKING INTO ACCOUNT COMPLEX TOPOLOGIES AND REPRESENTATIVE TRAFFIC SCENARIOS

Autor: Ing. D. David Roch Dupré

Directores: Prof. Dra. Dña. María Asunción Cucala García
Prof. Dr. D. Ramón Rodríguez Pecharromán

Madrid
Abril 2020

CONSTANCIA REGISTRAL DEL TRIBUNAL DEL ACTO

DE LA DEFENSA DE TESIS DOCTORAL

TÍTULO: Improving the electrical infrastructure of DC-electrified railway systems to increase energy efficiency, taking into account complex topologies and representative traffic scenarios

AUTOR: David Roch Dupré

DIRECTORES: María Asunción Cucala García y Ramón Rodríguez Pecharromán

TUTOR-PONENTE:

DEPARTAMENTO: Instituto de Investigación Tecnológica.

FACULTAD O ESCUELA: Escuela Técnica Superior de Ingeniería.

Miembros del Tribunal Calificador:

PRESIDENTE: Dr. D. Emilio Olías Ruiz **Firma**:

VOCAL: Dr. D. Masafumi Miyatake **Firma**:

VOCAL: Dr. D. Pablo Arboleya Arboleya **Firma**:

VOCAL:Dr. D. Aurelio García Cerrada **Firma**:

SECRETARIO: Dr. D. Adrián Fernández Rodríguez **Firma**:

Fecha de lectura:

Calificación:

Extended Abstract

In the current context of searching for measures to mitigate climate change, electrified railway systems have an important contribution to make. Particularly in large cities, promoting the use of Mass Transit Systems (MTSs), such as tramway or underground systems, can change the paradigm in urban transport and help solve the problems of traffic jams and pollution (as well as contribute to the mitigation of climate change).

To enable this change of paradigm, urban rail networks must become more attractive and, above all, more efficient. Among the possible ways to enhance MTSs, the installation of improvements in the electrical infrastructure, specifically the installation of Reversible Substations (RSs) and Energy Storage Systems (ESSs), are within the measures with the highest energy saving potentials. However, they require a considerable initial investment, which, in some cases, may call into question their profitability. Due to this, railway operators must have accurate methodologies to study in detail the impact that the installation of these improvements has on the system's energy efficiency as well as their associated profitability before taking the final decision on whether or not to undertake the installation.

Railway simulation models and **decision support mechanisms** are the key elements of any methodology meant to assess in a proper way the installation of infrastructure improvements**.** Despite their importance, none of them is sufficiently developed.

One problem found in the literature is that the tools in charge of computing the potential energy saving associated with the installation are unrealistic railway simulators. An unrealistic railway simulator provides inaccurate results that can have a great impact on the reliability of the assessments. One of the main sources of inaccuracies relies on the use of oversimplified traffic models, whose primary function is to represent the real traffic operation. The traffic models that are widespread in the literature consider small perturbations to take place during operation, neglecting traffic operation with large perturbations (perturbations being the deviations with respect to the commercial timetables). This is an error, since in real operation, especially during peak hours, large perturbations may appear, either punctually or even repetitively. Additionally, when modelling traffic operation with small perturbations, these traffic models apply a large number of simplifications, the main ones being: the consideration that the departures of trains from each terminal station are synchronized, the lack of stochastic models for dwell times and the use of only one speed profile (generally the flat-out one -minimum running time-).

Another disadvantage is that the literature only has focused on the assessment of improvements for the simplest type of line topology: lines with two terminal stations. Nevertheless, real railway lines may have more complex topologies, such as topologies with short-turn and terminal stations, topologies with branches, or topologies with branches, short-turn and terminal stations.

Finally, another drawback is that, once having the figures required for the assessment, the decisions about whether or not to undertake the installation and about the installation optimal configuration are usually based on the experience of railway operators.

This thesis covers some of the gaps existing in the literature with respect to the aforementioned fields (railway simulation and decision support mechanisms) and proposes a comprehensive methodology to determine the optimal installation of RSs or ESSs.

RAILWAY SIMULATION MODELS

The traffic and topology models, included within the traffic simulation models, have been considerably enhanced.

Regarding the **traffic models**, this thesis has developed a realistic traffic model for small and large perturbations able to generate representative traffic scenarios that properly represent the real traffic operation.

As previously explained, a perturbation is the deviation of train departures with respect to the commercial timetable. Two different traffic situations can take place depending on the perturbations level:

a) **Traffic with small perturbations**. In real operation there are always small deviations in the dwell time (stop-time at stations) since there are variations in the time required by the passengers to get in or off the train (which in turn depends on the number of passengers), as well as in the driver's response time to resume travel. These variations generate short delays in the departures from stations.
b) **Traffic with large perturbations**. In real operation, significant deviations may appear produced by the accumulation of trains in a certain stretch of track. This accumulation results in very irregular time intervals between trains and major delays.

The traffic model for small perturbations proposed in this thesis includes the traffic variables and features most important for the characterization of this type of operation: different headways (time interval between trains), different time shifts (gap between the departure instant of trains in each direction from the terminal stations), a dwell time model that observes the stochasticity associated with this variable, different train speed profiles and a specific module of the traffic regulation system in real time.

The traffic model for large perturbations proposed in this thesis introduces the big delays characteristic of this type of operation and replicates the traffic mechanisms that

regulate the operation: signalling system, use of perturbed speed profiles, dwell time model for large perturbations, etc.

Regarding the **topology models**, this thesis incorporates the information required by the railway simulation model to generate the commercial timetables of different types of topology, including the complex ones previously presented. Once having the commercial timetables of the complex topologies, the realistic traffic models for small and large perturbations can be applied to them in order to obtain the associated representative traffic scenarios.

As result of the improvements in the traffic and topology models, a new structure for railway simulation models is proposed. This structure, which implies an evolution with respect to the structure most common in publications and research papers, is divided into two main modules.

- **The operation module.** This module is the update of the **train movement module** (most common in the literature): while the **train movement module** only has the ***train movement simulator*** (in charge of calculating the train's speed, consumption, regeneration and position profile) and a very ***simplified traffic model*** that, in some cases, can be directly substituted by the commercial timetables, the **operation module,** apart from the ***train movement simulator***, also includes the ***timetable generator*** (in charge of generating commercial timetables with different characteristics), the ***realistic traffic model for small and large perturbations*** and the ***topology sub-module***.
- **The electrical network module**. This module includes the ***electrical scenarios generator*** (in charge of generating the circuits -also called snapshots- that electrically represent each moment of operation), the ***load flow solver*** (in charge of solving the snapshots using iterative processes) and the ***results aggregator*** (in charge of processing the results given by the load flow solver and providing the variables of interest)**.**

DECISION SUPPORT MECHANISMS BY MEANS OF OPTIMIZATION TECHNIQUES

Although very valuable, railway operators experience is not enough to take decisions on the installation of RSs or ESSs. Due to this reason, this thesis proposes the utilization of optimization algorithms.

Optimization algorithms use the information provided by the railway simulation models to find the optimal installation of RSs or ESSs. There are two types of optimization algorithms that can be used to tackle the optimal design of the infrastructure improvements: formal mathematical models or nature-inspired optimization algorithms. This thesis has focused on the latter, since they present high flexibility and a great capacity to successfully deal with the computationally intensive and highly non-linear and non-convex problem posed by the railway simulations.

The fitness function that guides the intelligent search of the algorithms has been defined as the Net Present Value (NPV), since it tries to find a balance between the energy saving and the installation costs associated with the infrastructure improvement required to achieve it. The variables of decision that must be optimized are:

- Number of RSs /ESSs to be installed.
- Location of the RSs /ESSs to be installed.
- Power (kW) of each RS / ESS to be installed.
- Capacity (kWh) of each ESS to be installed (this variable does not apply to the RSs optimization).

The optimization problem is addressed in two variants:

- Single-stage optimization: the whole budget for the installation of RSs/ESSs is available from the beginning.
- Multi-stage optimization: the whole budget is divided into stages, separated in time. Therefore, the improvement of the infrastructure must be undertaken gradually and the algorithm must try to find the optimum configuration for each stage without exceeding the budget limits of the stage and considering the installation as a whole.

While the single-stage optimization has already been addressed in the literature (but in few examples and with very simplified simulations), the multi-stage optimization is a true novelty that can be of great interest and application.

In order to fit with the optimization problem, the nature-inspired optimization algorithms selected from the literature have been reformulated according to the knapsack problem formulation. The knapsack problem consists in picking and choosing a set of items from a given larger set to put in the knapsack so as to maximize the total value, under certain constraints. The knapsack optimization problem is generally coded as a bit string containing zeros and ones – a “one” representing the fact that a certain item is selected and a “zero” representing the fact that a certain item is not selected. For the particular case of this optimization problem, each item represents one of the potential locations where an RS/ESS can be installed and, instead of having a bit string containing zeros and ones, each item has a value from a set of discrete values that represent the possible amounts of power or capacity that can be installed. The constraints are related to the maximum sizes and maximum admissible budget that cannot be exceeded.

For the single-stage optimization, three different optimization algorithms have been proposed in order to compare and validate their performance and results. The optimization algorithms proposed are the single-stage Genetic Algorithm (S-GA) as the main exponent of evolutionary algorithms, the single-stage Particle Swarm Optimization Algorithm (S-PSO) as the main exponent of swarm algorithms and the single-stage Fireworks Algorithm (S-FA) as another variant of swarm algorithms. The performance of all of them is excellent, although the S-GA outperforms the rest in terms of effectiveness, speed of convergence and robustness.

The two algorithms with the best performance in the single-stage optimization have been selected for the multi-stage optimization problem. Consequently, the optimization algorithms proposed are the multi-stage Genetic Algorithm (M-GA) and the multi-stage Fireworks Algorithm (M-FA). Again, although both algorithms demonstrate very good performance, the M-GA outperforms the M-FA in terms of effectiveness, speed of convergence and robustness.

METHODOLOGY TO ACCURATELY ASSESS THE INSTALLATION OF RSs OR ESSs

After presenting and explaining the improvements regarding railway simulation and decision support mechanisms, this thesis incorporates them into a comprehensive methodology to assess the installation of the infrastructure improvements. The steps of the methodology are:

- **Generation of the traffic space**: the traffic space represents in an accurate way the real operation of the railway line. It is composed of a big number of representative traffic scenarios so as to take into account the traffic variability and its impact on consumption. The traffic space is generated by the operation module.
- **Selection and compression of the traffic space:** with the aim of not making the optimization problem intractable in terms of computational burden, two procedures must be carried out:
    - A **selection procedure** has been applied to the whole set of representative traffic scenarios that compose the traffic space in order to obtain a reduced set of 'selected traffic scenarios' that contain most of the information of the initial set.
    - A **compression procedure** has been applied to the set of selected traffic scenarios in order to reduce the number of snapshots to be solved by the electrical network module without compromising the accuracy of the results.
- **Electrical simulation**: it is performed by the electrical network module.
- **Optimization**: it is performed by the nature-inspired optimization algorithms.

The methodology has been applied to optimize the installation of RSs and ESSs in a final case study. This final case study includes the simulation of representative traffic scenarios with large and small perturbations in a complex topology.

The results obtained are very satisfactory: the increase of the energy saving associated with the installation of the improvements is always accompanied with the economic profitability of the investment. Additionally, a sensitivity analysis for the ESSs optimization has been performed. In this sensitivity analysis different values for the ESSs unitary power costs have been given in order to study the influence of the installation costs on decision-making. The results clearly show how the installation of the infrastructure improvements varies depending on the economic factor, which means that the optimization algorithms are able to successfully combine this important factor with the main target of this thesis: increasing the energy efficiency.

The analysis of the solutions shows that the decisions taken by the optimization algorithms are very reasonable at the same time that difficult to achieve without the help of a proper methodology. This fact reinforces the idea defended in this thesis about the necessity of applying a comprehensive methodology, such as the one proposed, in order to provide an accurate assessment for the installation of infrastructure improvements.

Contents

List of symbols

Symbol	Description
AC	Alternating current
$Ac_{\overline{fw_i}}$	Amplitude of explosion of firework i
$Ad_{\overline{fw_i}}$	Discretized amplitude of explosion of firework i
$Adp_{\overline{fw_i}}$	Discretized power amplitude of explosion of firework i
$Adc_{\overline{fw_i}}$	Discretized capacity amplitude of explosion of firework i
ATO	Automatic Driving Systems
BPM	Bus power mismatch
c_1	Personal attractor in the PSO
c_2	Global attractor in the PSO
$C_0(ind_i)$	Installation cost of the RSs/ESSs configuration determined by ind_i
$cap(\overline{ind}_i, \dots)$	Capacity feature of $\overline{ind}_i$
$cap_{cost}(stage\ j)$	Unitary cost for capacity in stage j
CHR	Total population of chromosomes in the GA
$coeff$	Coefficient of Gaussian Explosion
DC	Direct-current
e_{cost}	Energy price
E_{abs}	Energy absorbed by the MTS
E_{cons}	Energy demand in pantographs
$E_{cons_{sub}}$	Energy fed by substations
$E_{cons_{sub},b}$	Energy fed by substations in the base case
E_{Regen}	Energy regenerated by trains
$E_{Regen_{sub}}$	Energy regenerated by trains delivered to the AC network through power inverters
E_{Rhe}	Energy lost in rheostats
$E_{infr.impr}^{ANNUAL}(ind_i)$	Annual energy consumption obtained with the RSs/ESSs configuration determined by ind_i
E_{Raw}^{ANNUAL}	Annual energy consumption without any infrastructure improvement
ELC	Energy Losses Coefficient
$E.sav._{selct.}$	Energy saving obtained in the selected case
$E.sav._{non-selct.}$	Energy saving obtained in the non-selected case
ESS	Energy Storage System

Symbol	Description
F	Total population of fireworks in the FA
F_{mech}	Tractive force
F_R	Tractive resistance
FA	Fireworks Algorithm
$f_{cost}(stage\ j)$	Installation fixed cost in stage j
$fit_{\overline{fw_i}}$	Fitness of firework i
fit_{BEST}	Best fitness
fit_{WORST}	Worst fitness
$\overline{fw_i}$	Firework i
g	Gravity
G	Conductance
GA	Genetic Algorithm
$gbest$	Global-best in the PSO
G-S	Gauss-Seidel method
$GSPK$	Number of Gaussian sparks in the FA
$\overline{headway}_{serv\ i}$	Average headway associated with service type i
HVDC	High-voltage DC
IA	Immune Algorithm
I	Current
I_{dI}	Inverter DC current
I_m	Coefficient for the rotary inertia
I_{MAX}	ESS maximum charging current
I_{MIN}	ESS maximum discharging current
$\overline{ind_i}$	Individual (i) of the population of any nature-inspired optimization algorithm
$iter$	Iteration of an optimization algorithm
LGM	Lagrange multipliers
m	Train mass
M	Number of stages in a multi-stage optimization problem
max_{budget}	Maximum amount of money available to undertake the infrastructure improvement
max_{cap}	Maximum capacity that can be installed for an ESS
max_{pow}	Maximum power that can be installed for an RS/ESS
M-FA	Multi-stage Fireworks Algorithm
M-GA	Multi-stage Genetic Algorithm
MILP	Mixed integer linear programming
MTS	Mass Transit System
mut_x	Probability to apply the mutation to x genes of the chromosome
n_{IR}	Turns ratio of the inverter transformer secondary winding to the rectifier transformer secondary winding
$n_{motored\ axles}$	Number of motored axles
$n_{selected}$	Number of selected traffic scenarios
$n_{services}$	Number of different types of train service in a railway line
n_{SH-T}	Number of short-turn stations in a railway line
$n_{sp_{\overline{fw_i}}}$	Number of regular sparks to be set off from firework i
$n_{sp_{max}}$	Maximum number of sparks that can be set off from a firework
$n_{sp_{min}}$	Minimum number of sparks that can be set off from a firework
n_T	Number of terminal stations in a railway line

Symbol	Description
n_{trains}	Number of trains
N	Number of potential locations for installing the infrastructure improvement
NPV	Net Present Value
N-R	Newton-Raphson method
$num\ iter_{max}$	Maximum number of iterations in the optimization algorithm
$nzd_{\overline{sp}_x}^{\ stage\ j}$	Number of non-zero dimensions in stage j of regular spark x.
p	Probability
p_{swap}	Probability to swap a gene
P	Active power
P_{aI}	Inverter-consumed rms fundamental active power
$P_{driveline}$	Power demanded by each driveline of the train
P^{spec}	Specified active power of a load bus
$pbest$	Particle-best in the PSO
$pow(\overline{ind}_i, \dots)$	Power feature of $\overline{ind}_i$
$pow_{cost}(stage\ j)$	Unitary cost for power in stage j
PMSM	Permanent magnet synchronous motors
P	Total population of particles in the PSO
PSO	Particle Swarm Optimization Algorithm
Q	Reactive power
Q^{spec}	Specified reactive power of a load bus
Q_{aI}	Inverter-consumed rms fundamental reactive power
r_x	Random numbers between 0 and 1 used for the velocity update of the PSO
RC	Recovery Coefficient
RS	Reversible Substation
RP	Rheostat Loss Projection
$R_{In^{\underline{o}}}$	Residual equation $n^{\underline{o}}$
R_c	Commutation resistance
$serv\ i$	Train service type i
S-FA	Single-stage Fireworks Algorithm
S-GA	Single-stage Genetic Algorithm
SIRS-Test	Single infinite Reversible Substation Test
SPK	Number of regular sparks in the FA
SPK_{ctrl}	Parameter to control the number of regular sparks that can be set off in the FA
S-PSO	Single-stage Particle Swarm Optimization Algorithm
SP0	Speed profile # 0 (flat-out)
SP1	Speed profile # 1
SP2	Speed profile # 2
SP3	Speed profile # 3
sp_{select}	Speed selection variable
$\overline{sp}_\alpha$	Regular spark α
$\overline{spg}_\delta$	Gaussian spark δ
SS	Substation
$step_{cap}$	Capacity step used to discretize the values of capacity that can be installed for an ESS
$step_{pow}$	Power step used to discretize the values of power that can be installed for an RS/ESS

Symbol	Description
$t_{arr_{i,j}}$	Arrival time of train i to station j
$t_{arr\ i,terminal\ station}$	Arrival time of train i to terminal station
$t_{comm\ arr_{i,j}}$	Arrival time of train i to station j according to the commercial timetable
$t_{comm\ dept_{i,j}}$	Departure time of train i from station j according to the commercial timetable
$t_{comm\ dwell_{i,j}}$	Dwell time of train i in station j according to the commercial timetable
$t_{dept_{i,j}}$	Departure time of train i from station j
$t_{dept\ i,\ interst[j,j+1]}$	Departure time of train i from intermediate stop between stations j and $j+1$
$t_{dept\ i,terminal\ station}$	Departure time of train i from terminal station
$t_{dept\ prov\ i,j}$	Provisional departure time of train i from station j
$t_{dwell_{i,j}}$	Dwell time of train i in station j
$t_{dwell\ delay\ not\ recovered}$	Dwell time in traffic with small perturbations but with a large perturbation delay not recovered
$t_{dwell\ under\ disturbance}$	Perturbed dwell time
t_{margin}	Time margin
t_j	Year when the improvements undertaken in stage j are installed.
$t_{target\ dwell_{i,j}}$	Target dwell time of train i in station j
$t_{turn.min.}$	Minimum turning time
$t_{SPx\ interst\ [j,j+1]}$	Interstation running time between stations j and $j+1$ associated with speed profile x (SPx)
$t_{up/down}^{trav.nom}$	Nominal travel time in up/down direction
$t_X^{schd.\ turn}$	Scheduled turning time in short-turn or terminal station X
T	Period to evaluate the investment (in years)
UN	United Nations
v	Train speed
$\overline{v_{PSO}}$	Velocity vector in the PSO
V	Voltage
V_{MIN}	Lowest admissible operating voltage
V_{REF}	Reference voltage level of the ESS control curve
V_{RHE}	Voltage threshold for the activation of the rheostatic braking
V_a	Rectifier transformer secondary rms line voltage
V_{dI}	Inverter DC average output voltage
V_1	Voltage level at which the ESS starts the discharging phase
$V_{1\ MIN}$	Voltage level at which the ESS reach its maximum discharging current
V_2	Voltage level at which the ESS starts the charging phase
$V_{2\ MAX}$	Voltage level at which the ESS reach the maximum charging current
w	Inertia weight in the PSO
w_{max}	Maximum inertia weight in the PSO
w_{min}	Minimum inertia weight in the PSO
$wacc$	Weighted Average Cost of Capital
$\overline{x_{PSO}}$	Position vector in the PSO
X_c	Commutation reactance
Y	Admittance
$z_{\overline{sp}_x}$	Number of randomly selected dimension for spark x

Symbol	Description
$\Delta\% \, E.sav._{selct.\ vs\ non-selct.}$	Energy saving overestimation/underestimation of the selected case with respect to the non-selected one
$\Delta size$	Vector with possible combinations for reducing the size when applying the mutation-as-repair
$\#RSs\left(\overline{ind}_i, stage\ j\right)$	number of RSs installed in stage j by individual i
γ	Inverter extinction angle
β	Inverter advance angle
ε	Very small constant used to avoid zero-division error and other numerical singularities

Acknowledgements

Escribiendo estas líneas y echando la vista atrás a lo que han supuesto para mí estos casi 4 años de tesis, me doy cuenta de que hay ciertas similitudes entre el proceso de tesis y el proceso interno que se vive durante los EE. En ambos procesos se va pasando por diferentes estados y por diferentes mociones. Y ambos procesos tienen un final. Continuando este paralelismo, creo que ha llegado el momento final del "reconocimiento agradecido de tanto bien recibido", y es que, realmente, hay mucho que agradecer.

Y como soy de los que piensan que el ser humano es un ser profundamente relacional y que son, precisamente, las relaciones que vamos desarrollando con los demás las que van entretejiendo lo más profundo de nuestro ser, en estas líneas quiero expresar mi más sincero agradecimiento a tantas personas que ya forman parte de mí.

En primer lugar, agradecer a tantos compañeros del IIT y de la Universidad su compañía y apoyo. Mención especial para mis amigos de Ricci. Y aún más especial para David, Pablo, Adri, Álvaro y Charlie. Os aseguro que habéis sido parte fundamental para mí en el proceso de esta tesis y en mi vida en general. Gracias por preocuparos conmigo en los momentos de las malas noticias, por alegraros conmigo en los momentos de las buenas y por haber estado siempre a mi lado. Que nuestra amistad, surgida o fortalecida durante esta tesis, pueda durar toda una vida.

Muchas de las personas que han marcado en mi vida un antes y un después pertenecen a mi "familia franciscana y jesuita". Gracias a todas y a cada una de ellas. Mención especial para quien, entre otras muchas cosas (y puedo asegurar que son muchísimas),

me ha ayudado a profundizar en el discernimiento de mi vocación y a enamorarme definitivamente de esta Universidad y de su misión de servicio a la sociedad. Han sido muchos paseos, muchos consejos y muchas charlas (de esas que tanto bien me hacen) compartidas desde que nos conocimos, casi por casualidad, el día del concierto de Navidad de la Universidad del año 2016. Que sean muchas más las que podamos compartir en el futuro.

Y hablando de personas que me han marcado, no puedo olvidarme de Tad. Te escribo en español, como a ti te gusta. Sin duda alguna, el elemento diferencial de mi estancia en Japón fuiste tú. Desde el primer minuto vimos que teníamos mucho en común (¡el mix Federer-Vivaldi fue providencial!). Durante las largas horas de investigación fuiste mi "sensei". Durante tantos momentos de diversión compartidos (me vienen rápidamente a la cabeza los inolvidables fines de semana en los que viajamos por Japón y los partidos de Federer en horas intempestivas) fuiste mi amigo. Y siempre me cuidaste como un padre. Gracias por todo, amigo y "sensei", ya estoy deseando poder volver a Japón para verte de nuevo (y de paso para ver tu nuevo GonKen lab!).

Gracias a Antonio, cuasi co-director de esta tesis, por tus consejos, tu ayuda y tus ideas, que tanto han enriquecido la investigación realizada.

Gracias a Álvaro, con quien, junto a Ramón, empecé en este apasionante mundo de la investigación ferroviaria cuando todavía estaba en cuarto de carrera. Recordaré siempre los primeros cafés que compartimos durante mi beca de colaboración en el IIT (¡qué ilusión me hacían!) y tu sentido del humor, que siempre conseguía hacerme reír. También han sido muchas las horas de "tabarra" que te he dado con mis innumerables dudas y preguntas y tu respuesta siempre ha sido superlativa. Gracias de corazón por tu amistad, generosidad, cercanía y disponibilidad.

Gracias a mis "jefes" de tesis: Paloma y Ramón. Habéis sido para mí el tándem perfecto y os habéis complementado a las mil maravillas. Habéis sabido gestionar mis "prisas", me habéis hecho aprender de los errores siempre de forma constructiva y me habéis hecho crecer como investigador y como persona. Gracias por vuestra creatividad, por vuestra experiencia y conocimiento, por vuestra entrega generosa, por sacar siempre un momento para mí cuando lo he necesitado (y sé que vuestras agendas no ayudaban) y, en definitiva, por haberme acompañado y guiado como verdaderos maestros.

Y, finalmente, llega el momento de dar las gracias a mi familia.

Gracias a Sara. Como decía el gran poeta y como dice el estribillo de una de nuestras canciones preferidas: "caminante no hay camino, se hace camino al andar". Gracias por haberme regalado estos casi 12 años de caminar juntos. Estoy seguro de que esto es solo el comienzo y deseo con todo mi corazón que podamos seguir haciendo juntos ese camino.

Y gracias a mi madre, a mi padre, a mi abuelo Antonio, a mi abuela Jacoba, a mi abuela Catalina y a mi abuelo Víctor (algunos ya no estáis aquí, pero sé que seguís cuidando de mí). Sin lugar a duda sois para mí un pilar fundamental en mi vida y es imposible escribir con palabras el agradecimiento que me brota desde lo más profundo de mi ser por

tanto, empezando por la vida. Me habéis criado, me habéis cuidado, me habéis educado, me habéis ayudado, me habéis escuchado y me habéis entendido, me habéis apoyado, me habéis dado todo lo que he necesitado (y muchísimo más). Con vosotros he vivido muchos de los momentos más importantes de mi vida (tanto de los buenos, como de los malos) y me habéis regalado un amor tan incondicional que sé que el vínculo que nos une es imborrable, ahora y por siempre.

CHAPTER 1

INTRODUCTION

The research of this PhD is motivated by one of the main challenges that must be faced nowadays: the Climate Change. This challenge is very present in several of the "*Sustainable Development Goals*" stablished by the United Nations (UN) to be achieved by 2030. Many voices from very different spheres advocate the need to face this problem with responsibility and determination. Examples of these voices go from international organizations such as the World Health Organisation (World Health Organization, 2019) or the aforementioned mentioned UN -including a number of UN organisms, among others, the Intergovernmental Panel on Climate Change (IPCC, 2018) and the United Nations High Commissioner for Refugees (Sanjula Weerasinghe, 2018)- to the Scientific Community (Ripple, Wolf, Newsome, Barnard, & Moomaw, 2019), passing through religious authorities (Pope Francis, 2015; Episcopal Church, Evangelical Lutheran Church in America, & Church of Sweden, 2019; National Religious Coalition on Creation Care, 2019). The challenge is of such relevance and urgency that, at the same time that this document is being written, the *"UN Climate Change Conference COP 25"* is taking place less than 10 km from this University with the aim of updating the commitments of "*Paris Agreement (CMA2)".*

There is no doubt that this big challenge must be addressed integrally and with an interdisciplinary approach as, more than ever, the big problems from today are interconnected (as evidence of this affirmation, the variety of entities and organizations from very different fields that have publicly expressed the need to take action against Climate Change cited in the previous paragraph). Therefore, there is no point in seeking

a technical solution to each problem because this can disconnect us from the interconnected reality and mask problems.

Although the humble contribution of this PhD to the fight against Climate Change is mainly made from a very technical approach, the conviction stated in the previous lines has guided the whole research. Especially, it has given light in those moments when the technical fascination about the models and algorithms described in the following chapters has run the risk of converting these technical solutions as ends by themselves and not as means to the service of a greater good (the fight against Climate Change).

Once stablished the general frame and motivation of this PhD, the following sections will introduce the relationship between Climate Change and transportation (and more specifically railway urban transportation) and present the objectives of this PhD in order to contribute, at least, to the mitigation of Climate Change.

1.1. INTRODUCTION TO THE ROLE OF MASS TRANSIT SYSTEMS IN THE MITIGATION OF CLIMATE CHANGE

In (IPCC, 2014) the Intergovernmental Panel on Climate Change urges the main actors in the international political and scientific scene to define the appropriate means for mitigating the Climate Change, as well as to generate the business models required to make them economically feasible.

Among the different sectors that can contribute to this objective, this PhD is focused on urban transport systems, as they are considered one of the most important energy consumers and, consequently, generators of greenhouse gas emissions globally (IPCC, 2015).

Currently, urban transport systems are highly dependent on light vehicles. As a consequence, large cities have notable traffic and pollution problems, which sometimes leads to the application of traffic restrictions (Holman, Harrison, & Querol, 2015; Huang, Fu, & Qi, 2017) and other public-sector initiatives to improve freight activity in metropolitan areas (Holguín-Veras, Amaya Leal, Sánchez-Diaz, Browne, & Wojtowicz, 2018a; Holguín-Veras, Amaya Leal, Sánchez-Diaz, Browne, & Wojtowicz, 2018b).

One of the possible solutions is to enhance the use of Mass Transit Systems (MTSs) such as tramway or underground systems. Nevertheless, urban rail networks must become more efficient and attractive in order to enable this change of paradigm in urban transport. Before presenting the different ways to improve the energy efficiency in MTSs, it is necessary to understand some of their main properties regarding the electrification.

1.2. MASS TRANSIT SYSTEMS ELECTRICAL PROPERTIES

MTSs are railway electrified systems. According to (López-López, Álvaro J., Pecharromán, Fernández-Cardador, & Cucala, 2017b), direct-current (DC) electrification spread in urban systems due to historical reasons (DC motors were easier to control).

Currently, some other advantages of DC power transmission still make railway infrastructure designers to use DC electrifications in new MTSs: reduced electro-magnetic emissions (avoiding interferences with the signalling system), lower number of conductors required for the supply systems, the fact that from the utility grid perspective DC railways are balanced loads, etc. Therefore, this PhD will focus on DC-electrified MTSs. Figure 1-1 shows the typical structure of a MTS power system.

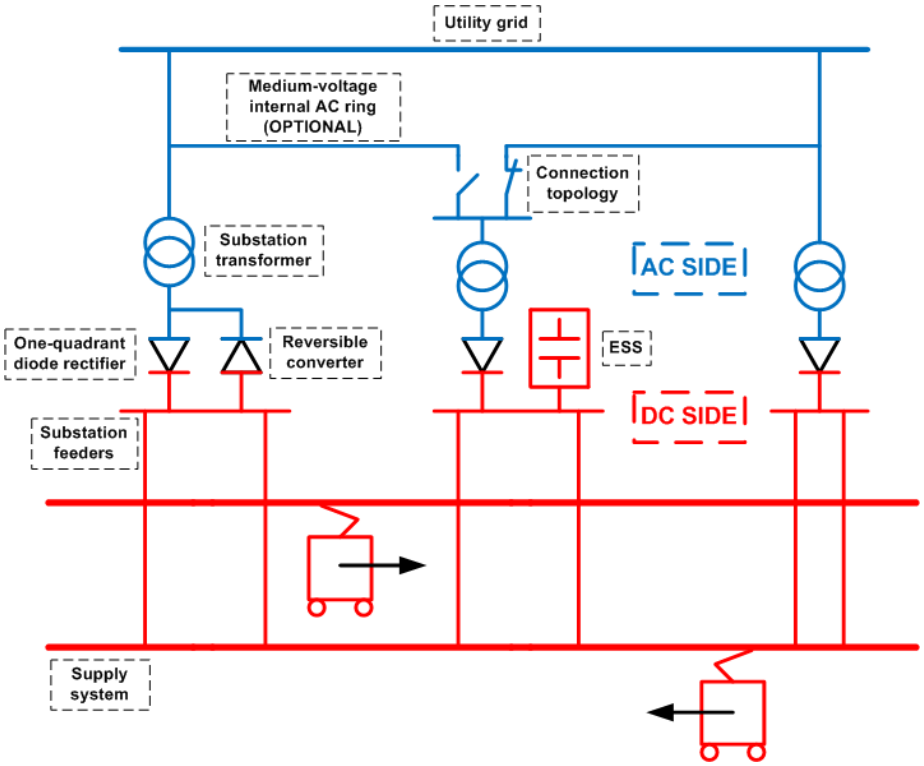

Figure 1-1: Structure of the typical MTS power system (López-López, Álvaro J. et al., 2017b)

As can be seen in Figure 1-1, there is an alternating current (AC) side and a DC side. The traction substations (SSs) connect both sides. According to (López-López, Álvaro J., 2016), the most widespread type of SS in DC-electrified MTSs only allows unidirectional power flows (from the utility grid to the supply system/catenary). This is because the converters used in most SSs are twelve-pulse rectifiers with diodes as semiconductor elements. This would not be a problem if the railway system only consumed energy, but nowadays it is very common to install regenerative braking equipment in the rolling stock, which allows kinetic energy to be transformed back into electrical energy during the moments when trains are braking. If the amount of regenerated energy produced by the braking trains at an instant of operation is greater than the amount of energy demanded by the motoring trains, the net energy consumption of the MTS is negative, which means than there is an excess of regenerated energy in the whole system. Since the excess of regeneration cannot be returned to the utility grid as a consequence of the unidirectional SSs, the catenary voltage can dangerously increase. The way to avoid dangerous over-voltages is the use of rheostats. They are large resistors installed on board trains that consume the excess of regenerated energy when a certain voltage limit is surpassed.

Although being a very bad measure in terms of energy efficiency, rheostats must be activated in some occasions for the sake of security. Therefore, a good way to improve the energy efficiency is limiting as much as possible the activation of the rheostats, as this implies a better use of the excess of regenerated energy.

The following section will describe the main ways of increasing energy efficiency. As will be seen, most of them are based on reusing the excess of regenerated energy (and, consequently, reducing the rheostats activation).

1.3. MAIN APPROACHES TO IMPROVE ENERGY EFFICIENCY IN MASS TRANSIT SYSTEMS

There are four main ways to re-use the regenerated energy:

- **Supplying train auxiliary consumption**. The regenerated energy is primarily used to supply the auxiliary and comfort functions, such as lighting of wagons, air conditioning, etc (González-Gil, Arturo, Palacin, & Batty, 2013). From the energy-efficiency point of view this is the best option since conduction losses are minimized (the regenerated energy is used by the train without the need to deliver it to catenary). Consequently, only the regenerated energy leftover after having supplied the auxiliaries will be delivered to catenary.

- **Supplying motoring trains close to the braking train**. Figure 1-2 graphically represents how the exchange of energy takes place. The timetable optimization is an optimization procedure that, among other objectives, is designed to maximize this energy exchange mechanism and will be explained in more detail in succeeding paragraphs.

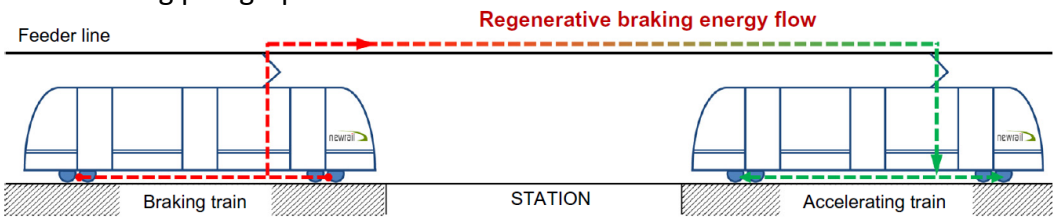

Figure 1-2: Regenerative energy exchange among trains (González-Gil, Arturo et al., 2013)

- **Store the excess of regenerated energy in Energy Storage Systems (ESSs)**. ESSs can be installed on board the trains (on-board ESSs) or in the electrical infrastructure (wayside ESSs). The energy stored will be returned to catenary when necessary. The uses that can be given to the stored energy are varied and will be explained in detail in Section 1.3.3.1. ESSs can provide better results than timetable optimization in terms of energy efficiency as well as in peak shaving. Nevertheless, they imply an additional cost that must be carefully studied. Figure 1-3 and Figure 1-4 graphically represent, respectively, the operation of on-board ESSs and wayside ESSs.

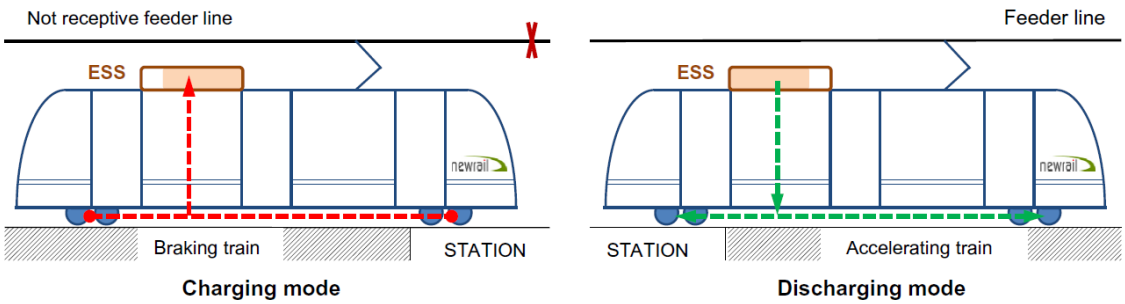

Figure 1-3: On-board ESS operation (González-Gil, Arturo et al., 2013)

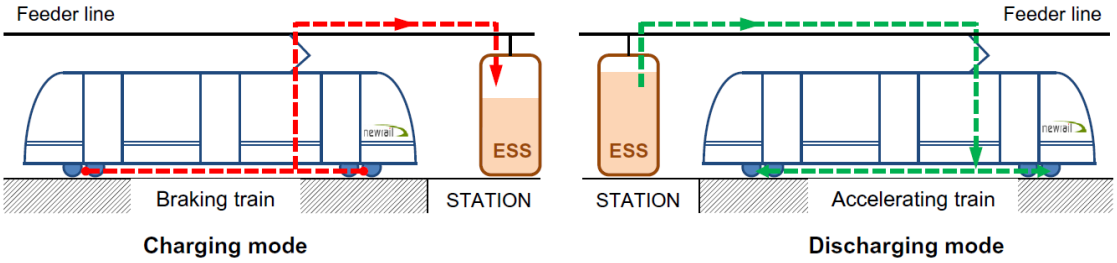

Figure 1-4: Wayside ESS operation (González-Gil, Arturo et al., 2013)

- **Deliver the excess of regenerated energy back to the utility grid by means of Reversible Substations (RSs).** Typically RSs yield better results than ESSs in terms of energy efficiency but their economic viability may be questioned if the regenerated energy returned to the grid is not remunerated. As with ESSs, their installation imply an additional cost that must be carefully studied. A more detailed explanation of the RSs will be provided in Section 1.3.3.2 . Figure 1-5 graphically represents the operation of an RS.

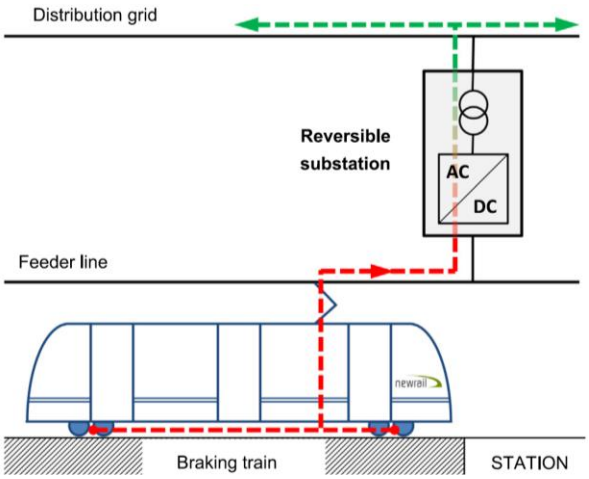

Figure 1-5: RS operation (González-Gil, Arturo et al., 2013)

There are different approaches to improve the energy efficiency of MTSs, being a lot of them directly related with the re-use of the excess of regenerated energy. The three main ones are: *a) Improving the train design, b) Improving the operation* and *c) Improving the infrastructure*.

1.3.1. TRAIN DESIGN IMPROVEMENT

The most important measures for **improving the train design** are:

- Installation of ESSs on board trains to store the excess of regenerated energy (Arboleya, Coto, González-Morán, & Arregui, 2014; Arboleya, Bidaguren, & Armendariz, 2016; Arboleya, Mohamed, & El-Sayed, 2020; Barrero, Mierlo, & Tackoen, 2008; Ciccarelli, Iannuzzi, & Tricoli, 2012; Kondo, K., 2010; Sumpavakup, Suwannakijborihan, Ratniyomchai, & Kulworawanichpong, 2018). Although on-board ESSs have the advantage of operating with higher efficiency than wayside ESSs (explained in Section 1.3.3.1) due to the absence of line losses, they require a large space on the vehicle and introduce a significant increase of weight (González-Gil, Arturo et al., 2013). Owing to these, their installation is not commonly considered when retrofitting rolling stock but when designing new vehicles.
- Improvement of trains' aerodynamics (Douglas, Roberts, & Hillmansen, 2016; Gunselmann, 2005).
- Reduction of train's weight (Douglas et al., 2016; Gunselmann, 2005).
- Reduction of the auxiliary consumption (Beusen, Degraeuwe, & Debeuf, 2013; Gunselmann, 2005).
- Improvement of the drive chain efficiency (Douglas et al., 2016; Kondo, K., 2010; Kondo, M., Miyabe, & Manabe, 2014; Matsuoka & Kondo, 2010). Particularly, (Kondo, K., 2010) establishes that there are two main domains in railway vehicle traction systems where there is room to improve:
    - Reduction of the losses in traction equipment, including the power traction converters and the traction motors. This can be achieved by improving the efficiency of the semiconductor power switching devices or using equipment producing less energy losses (for example using permanent magnet synchronous motors (PMSMs)).
    - Recuperation of more kinetic energy with the improvement of the regenerative brake control or with the installation of the on-board ESSs aforementioned.

1.3.2. OPERATION IMPROVEMENT

Two main fields study the measures to improve the operation: a) eco-driving and b) timetable optimization. The major advantage of these measures is that the associated costs are minor.

Eco-driving techniques have been extensively studied in (Bocharnikov, Tobias, Roberts, Hillmansen, & Goodman, 2007; Domínguez, Fernández-Cardador, Cucala, & Lukaszewicz, 2011; Domínguez, Fernández-Cardador, Cucala, Gonsalves, & Fernández-Rodríguez, 2014; Fernández-Rodríguez, Fernández-Cardador, Cucala, Domínguez, & Gonsalves, 2015; Fernández-Rodríguez, Fernández-Cardador, & Cucala, 2018; Miyatake, Haga, & Suzuki, 2009; Miyatake & Ko, 2010; Sheu & Lin, 2012). Eco-driving consists in increasing energy efficiency by calculating the speed profile with the minimum consumption for a target running time between stations (so that commercial running

times are not affected) and must take into account the speed restrictions and the track data. In order to achieve this goal, it is necessary to find the optimal balance among the parameters of the driving commands: the coasting speed, the remotoring speed, the holding speed and the braking rate. The design of the speed profiles can be made by means of mathematical optimization models or simulation-based optimization models. The latter are more flexible and give more accurate and practical results. The speed profiles obtained can be applied manually or with the use of Automatic Train Operation (ATO).

MTS lines are usually operated with ATO, which receives speed profiles from a pre-programmed set depending on the required arrival time, (Shigen Gao et al., 2013; Zhu, Zhang, Dai, Zhang, & Li, 2013). Among the possible speed profiles, (Domínguez et al., 2014) differentiates between two types:

- Speed profiles with the objective of achieving minimum running times.
- Slower speed profiles based on reducing energy consumption.

The **timetable optimization** is designed, among other objectives, to favour the exchange of regenerated energy among trains by synchronizing braking and motoring events. In order to re-use as much regenerated energy as possible without installing additional equipment, several authors have studied in detail this technique (Albrecht, 2004; Boizumeau, Leguay, & Navarro, 2011; Chen, Lin, & Liu, 2005; Gong, Zhang, Zhang, Jiang, & Wang, 2014; Ichikawa & Miyatake, 2019; Miyatake, 2011; Nasri, Moghadam, & Mokhtari, 2010; Nomura & Miyatake, 2016; Oettich, Albrecht, & Scholz, 2004; Pena-Alcaraz, Fernández-Cardador, Cucala, Ramos, & Pecharromán, 2012; S. Su, X. Li, T. Tang, & Z. Gao, 2013). With a proper timetable optimization -obtained basically from the variation of the dwell times- the regenerated energy can help reduce consumption from SSs up to 7% according to (Pena-Alcaraz et al., 2012), to 10% according to (Oettich et al., 2004), and even to 12 % according to (Boizumeau et al., 2011) (this variations depend on the characteristics and peculiarities of each railway system studied). In (Albrecht, 2004; Chen et al., 2005), apart from reducing the energy consumption in the SSs, there is also the implicit objective of reducing power peaks by means of modifying train running time in order to avoid simultaneous acceleration of several trains. Finally, although it is not a “pure” timetable optimization (Oettich et al., 2004) proposes to adapt traffic supply strictly to demand (flexible headway scheduling) as a long-term measure to increase energy efficiency considerably (with potential energy saving around 20-25%).

1.3.3. INFRASTRUCTURE IMPROVEMENT

The two main infrastructure improvements are the installation of wayside ESSs and RSs. As they are the two measures object of study of this PhD, they will be explained with more detail in Sections 1.3.3.1 and 1.3.3.2, respectively.

Other measures to be implemented in the electrification of DC-electrified MTSs in order to improve their efficiency are presented in the next paragraphs.

In (López-López, Á J. et al., 2014) the effect of the no-load voltage is studied. On the one hand, a high no-load voltage mitigates problems related to overloaded substations and voltage dips during rush hours and reduces transmission losses. On the other hand, a high no-load voltage also reduces the line receptivity (concept directly related to the line energy efficiency and explained in detail in Section 1.4) during off-peak hours, which would be counterproductive in terms of energy efficiency. The substation-transformer tap regulation proposed by this study allows operators to modify the no-load voltage according to a scheduled no-load voltage scheme that improves the energy efficiency of the system at the same time that successfully deals with the problems of substation overloads and voltage dips.

(Abrahamsson, Kjellqvist, & Östlund, 2012) proposes a high-voltage DC-feeder (HVDC-feeder) connected to the catenary through converters. This feeding system results in less material usage, lower transmission losses and higher controllability. The results are particularly satisfactory when there is a weak feeding or significant amounts of regenerated energy.

Another possible improvement is the installation of super-conducting cables in the power feeding network (Takagi, 2010; Takagi, 2012). The principal advantages of the theoretically zero resistance associated with these type of conductors are the reduction in the feeding losses and the increase of the line receptivity.

1.3.3.1. WAYSIDE ENERGY STORAGE SYSTEMS

The literature has described different uses for the regenerated energy stored in the ESSs:

- **Voltage stabilization**: installing ESSs between substations physically separated by large distances allows supplying the stored energy in situations when there is an increment of the load and the level of the voltage is below the operating margin. There are several studies related to this application such as (Ianuzzi, Ciccarelli, & Lauria, 2012; Lee, H. M., Oh, Lee, & Kim, 2008; Rufer, Hotellier, & Barrade, 2004).
- **Energy saving:** ESSs can help reduce the amount of energy demanded to substations by providing the stored energy at adequate moments (Barrero, Tackoen, & Van Mierlo, 2008; Gao et al., 2015; Ianuzzi et al., 2012; Konishi, Morimoto, Aihara, & Tsutakawa, 2010; Lee, Hansang, Jung, Cho, Yoon, & Jang, 2013; Roch-Dupré, López-López, Pecharromán, Cucala, & Fernández-Cardador, 2017).
- **Load levelling:** ESSs can reduce the big variations in consumption that characterize railway systems. This application is also known as peak regularization or peak shaving (Battistelli, Ciccarelli, Lauria, & Proto, 2009; Gao et al., 2015; Ise, Kita, & Taguchi, 2005; Lee, Hansang et al., 2013; Rahimi, Zarghami, Vaziri, & Vadhva, 2013; Roch-Dupré et al., 2017; Suzuki, Baba, Shutoh, & Masada, 2004). Several benefits are derived from load levelling, among them: (Rahimi et al., 2013) affirms that this practice offers direct and indirect benefits in generation costs, line loss reduction and even voltage support and (Roch-

Dupré et al., 2017) highlights the positive impact that ESSs can have in the reduction of the demand charge that MTSs operators must pay.

It must be noted that energy saving and load levelling can be also obtained with on-board ESSs (see Section 1.3.1). Nevertheless, as this PhD is focused on increasing the energy efficiency of MTSs by means of improving the electrical infrastructure, only wayside ESSs will be observed.

1.3.3.2. REVERSIBLE SUBSTATIONS INSTALLATION

RSs allow bidirectional power flows: from the utility grid to the catenary and vice versa. Their impact on the efficiency of the system has been extensively studied in (Arboleya et al., 2020; Gelman, 2013; Jefimowski & Szeląg, 2018; López-López, Á J., Pecharromán, Pilo de la Fuente, E., Cucala, & Fernández-Cardador, 2011; López-López, Álvaro J., Pecharromán, Fernández-Cardador, & Cucala, 2014; Mellitt, Mouneimne, & Goodman, 1984; Tian, Kamel, & Tricoli, 2019; Zhang, Tian, Tricoli, Hillmansen, & Liu, 2019). The excess of regenerated energy may be used in the operator's network or eventually sold back to the energy provider if the legislation allows it (González-Gil, Arturo et al., 2013).

According to (Cornic, 2010), the benefits from installing RSs can be categorized into three groups:

- 99% reutilization of braking energy at all time, while maintaining priority to natural energy exchange between trains.
- Regulation of their output voltage in traction and regeneration modes to reduce losses and increase the pick-up of energy from distant trains.
- Reduction in the level of harmonics and improvement of the power factor on the AC side.

Although they present exceptional results in terms of consumption reduction, they have no impact in power peak reduction (load levelling). Examples of real implementations of reversible substations can be found in (Cornic, 2010; Ibaiondo & Romo, 2010).

1.4. MEASURES OF ENERGY EFFICIENCY IN MASS TRANSIT SYSTEMS

It is very important to properly measure how much energy efficiency increases with the improvements presented in Section 1.3. In the case of this PhD, these measures are fundamental to study the impact of installing wayside ESSs or RSs. The following lines will explain some ways of measuring the MTS energy efficiency.

The most important measure is the receptivity. As previously stated, it is in direct relation with energy efficiency, as it represents the capacity of the system to reuse the regenerated energy. Several formulas haven been developed in the literature in order to measure the system's receptivity:

- Equation (1-1) defines a receptivity factor proposed by (Falvo, Lamedica, Bartoni, & Maranzano, 2011; Falvo et al., 2014). This factor studies the relationship between the energy lost in rheostats (E_{Rhe}) and the energy

regenerated by trains (E_{Regen}). In the ideal case of never activating the rheostats, the value of this receptivity factor would be 1, while in the case of dissipating all the regenerated energy in the rheostats the value would be 0.

$$Receptivity = 1 - \frac{E_{Rhe}}{E_{Regen}} \quad \textbf{(1-1)}$$

- Equation (1-2), proposed by (López-López, Álvaro J. et al., 2017b) defines the same receptivity factor with a different formulation. It studies the relationship between the regenerated energy reused/absorbed by the MTS (E_{Abs}) and the energy regenerated by trains (E_{Regen}). Equally to what happened with the receptivity factor of (Falvo et al., 2011; Falvo et al., 2014), if rheostats are not activated the value of the receptivity factor is 1, while if no regenerated energy can be reused the factor is 0.

$$Receptivity = \frac{E_{Abs}}{E_{Regen}} \quad \textbf{(1-2)}$$

There are other measures that are very useful to measure the MTS efficiency. Among them, the Recovery Coefficient, RC, proposed by (Domínguez, Fernandez-Cardador, Cucala, & Pecharroman, 2012) and defined in Equation (1-3). This coefficient represents the proportion between the total energy saving measured in substations in a certain scenario s (in which the recuperation of regenerated energy is observed) and the total available regenerated energy of all the trains ($\sum_t E^t_{regen}$). Total net energy consumption in substations is calculated as the subtraction of the energy fed by substations ($\sum_t E^t_{cons_{sub}}$) minus the energy sent to the AC network through power inverters, in case of having RSs installed, ($\sum_t E^t_{regen_{sub}}$). The savings are calculated regarding a base case with a non-receptive network ($\sum_t E^t_{cons_{sub},b}$).

$$RC_s = \frac{\sum_t E^t_{cons_{sub},b} - \left(\sum_t E^t_{cons_{sub}} - \sum_t E^t_{regen_{sub}}\right)}{\sum_t E^t_{regen}} \ \forall\ t, \text{(being } t \text{ any train)} \quad \textbf{(1-3)}$$

Finally, it is also very important to see how the potential improvements affect to the energy losses. Equation (1-4) defines the Energy Losses Coefficient, ELC, also proposed by (Domínguez et al., 2012). This coefficient characterizes, for a certain scenario s (in which the recuperation of regenerated energy is observed), the energy losses along the line and in substations by dividing the total demand of energy in pantograph ($\sum_t E^t_{cons}$) by the energy consumption in the base case with a non-receptive network ($\sum_t E^t_{cons_{sub},b}$).

$$ELC_s = \frac{\sum_t E^t_{cons}}{\sum_t E^t_{cons_{sub},b}} \; \forall \; t, \text{(being } t \text{ any train)} \qquad \textbf{(1-4)}$$

1.5. RAILWAY SIMULATION

Different ways to increase the MTS energy efficiency were explained in Section 1.3. At the end of the section, the infrastructure improvements and, in particular, the installation of RSs and ESSs were defined as the object of study of this PhD. The main reason for this choice is their high potential to increase energy efficiency. Indeed, according to several authors such as (Douglas, Roberts, Hillmansen, & Schmid, 2015; González-Gil, A., Palacin, Batty, & Powell, 2014) wayside ESSs and RSs are within the improvements with the highest energy saving, as can be seen in Figure 1-6.

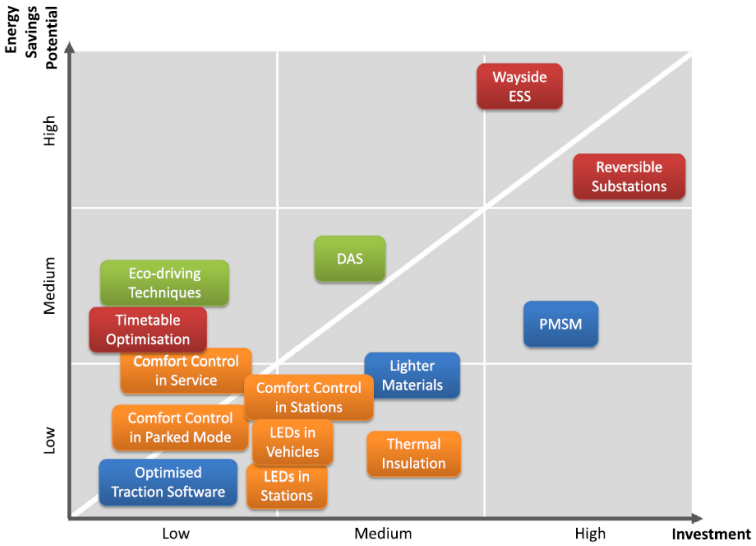

(González-Gil, A. et al., 2014)

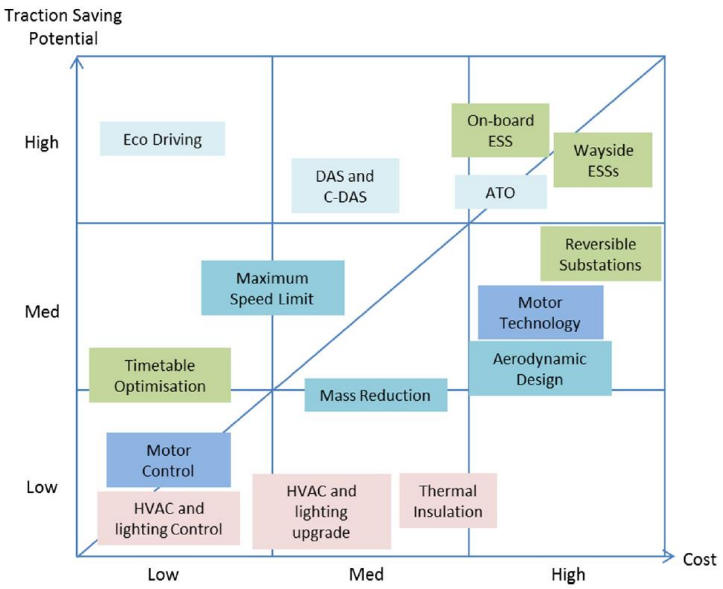

(Douglas et al., 2015)

Figure 1-6: Comparison of cost and saving potential for energy saving measures

Nevertheless, they require a high initial investment that, in some cases, may call into question their profitability. Due to this, railway operators must study in detail the impact of the potential energy saving achieved with the installation before taking the final decision. In order to properly asses the decision-making process, railway simulators turn to be the key tool.

They are proven to be the cheapest mean to carry out performance prediction and system behaviour characterization (Goodman, Siu, & Ho, 1998). Their design implies the development of suitable mathematical models of the traction equipment, the mechanics of the train performance and the behaviour of the power supply conductors and substations (Goodman & Chymera, 2013).

Research in railway simulation has been developed since the late 70s of the last century. In consequence, literature is neat in examples of railway simulators with different degrees of complexity: (Alnuman, Gladwin, & Foster, 2018; Arboleya, Diaz, & Coto, 2012; Arboleya, Mohamed, & El-Sayed, 2018; Cai, Irving, & Case, 1995; Chymera, M., Renfrew, & Barnes, 2006; Chymera, Martyn Z., Renfrew, Barnes, & Holden, 2010; Goodman et al., 1998; Goodman & Chymera, 2013; M. Khodaparastan, O. Dutta, M. Saleh, & A. A. Mohamed, 2019; Martin, 2010; Mellitt, Goodman, & Arthurton, 1978; Pilo, Rouco, Fernandez, & Hernandez-Velilla, 2000; Pilo, Rouco, Fernandez, Burleson, & Cackovic, 2003; Pires, Nabeta, & Cardoso, 2007; Tzeng, Wu, & Chen, 1995; Zhang et al., 2019).

The general structure of a railway simulator is depicted in Figure 1-7, which is based on (López-López, Á J. et al., 2011). Traditionally, it has been divided into two main modules: the **train movement module** and the **electrical network module** (Chymera, Martyn Z. et al., 2010).

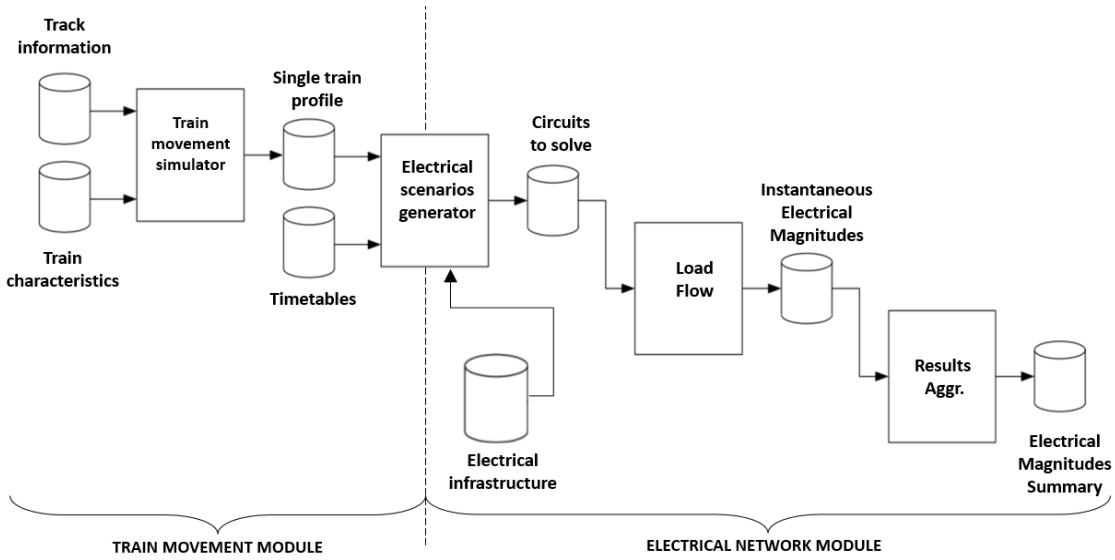

Figure 1-7: General structure of a railway simulator

1.5.1. TRAIN MOVEMENT MODULE

This module generates the traffic scenarios, which contain the power consumption and regeneration profiles of each train at each time instant and at each location of the railway line.

This module can be divided into two submodules: *1)* ***train movement simulator*** and *2)* ***traffic model***.

1.5.1.1. TRAIN MOVEMENT SIMULATOR

This submodule calculates train's speed, consumption, regeneration and position profile (Goodman et al., 1998). The train movement simulator module used for the railway simulator of this PhD is presented with all the details in (Domínguez et al., 2011). The following lines will highlight the main features of a train movement simulator.

As stated by (Goodman et al., 1998), firstly it is important to arrange the data representing the **track information**. It includes topography, topology, speed limitations in particular stretches, etc. Its influence on the variations in energy consumption is very considerable. One efficient way to manage all these data is by means of object oriented programming (Martin, 1997), where objects with similar properties and functions constitute a class linked with a data structure. In the case of the railway simulator used for this PhD there are two types of objects: 'node' objects that represent stations, junction points etc., and 'link objects' such as the tracks connecting the node objects. Trains move from one node to the next through a permitted link (Goodman et al., 1998).

The next step is to compute the **driving commands**. For any given line, different driving commands can be applied depending on whether the goal is minimizing consumption or reducing the running time (Martin, 2010). In the case of the railway simulator used for this PhD, they have been designed according to eco-driving techniques.

Once having the driving commands, the **behavior of the engines** and the train dynamics must be simulated. (Stephan, 2010) presents four modelling levels available for the propulsion simulation:

- Constant efficiency factors for the propulsion equipment.
- Driving state-related efficiency factors.
- Load-depending efficiency factors of single components
- Detailed mathematical engine component models.

Focusing on the last point, the following steps determine how to compute the energy flow in the system as well as the remaining train dynamics:

- In the first place, it is necessary to calculate the frictional force, also known as tractive resistance (F_R), which appears when the train is in movement. This force can be calculated using the Davis Equation (Equation (1-5)), see (Lukaszewicz, 2001) for further details).

$$F_R = a + b \cdot v + c \cdot v^2 \quad \textbf{(1-5)}$$

where a, b and c are determined empirically, and v stands for the speed of the train.

- Next step is to calculate the train acceleration and dynamics according to Equation (1-6):

$$\frac{dv}{dt} = \frac{F_R + m \cdot g \cdot \sin(\theta) - F_{mech}}{m_{eq}} \quad \textbf{(1-6)}$$

where the first term (F_R) corresponds to the tractive resistance previously explained, the second term $(m \cdot g \cdot \sin(\theta))$ corresponds to the force required to overcome gravity and the third term (F_{mech}) is the tractive force, obtained from complex ATO computations based on the driving commands, the speed limits and other parameters, such as the maximum traction effort curves of the engines. As can be seen, these three terms are divided by m_{eq}, which corresponds to the mass of the train plus the rotational inertial effect and the passengers load (see Equation (1-6)).

$$m_{eq} = m \cdot (1 + I_m) + passengers\ load \quad \textbf{(1-7)}$$

where I_m is the coefficient for the rotary inertia.

- Finally, the power demanded by each driveline of the train ($P_{driveline}$) is obtained from Equation (1-8), proposed by (Buckingham, 1988).

$$P_{driveline} = F_{mech} \cdot \frac{v}{n_{motored\ axles}} \quad \textbf{(1-8)}$$

where $n_{motored\ axles}$ is the number of motored axles.

It is also important to calculate the energy spent on the gear losses and the copper and iron losses, which can be attained by recursively solving the machine quasi-steady state circuit (Chymera, Martyn Z. et al., 2010).

Additionally, depending on the desired level of detail, train movement can be updated during simulation according to two different models, which correspond to different updating criteria (Goodman et al., 1998):

- Event-based simulation models: the progress of the train is followed by the occurrence of pre-defined events. Consequently, the pace of time is irregular and the updates are asynchronous. The low computational load is the main advantage of this model.
- Time-based simulation models: there is a sampling period at which information is updated. This method is closer to real performance of trains, easier to

implement, but takes more computational effort, which is directly related to the sampling time (the smaller the sampling time, the higher the effort).

For "pure" mechanical simulators, where train dynamics and consumption are the important aspects, event-based models can be used. This is because, from the "mechanical point of view", it is possible to spend some time in a scenario/event with the same characteristics (for example a flat stretch). Nevertheless, if the simulator incorporates electrical computations, event-based models are not recommendable because the electrical values of the simulated parameters are constantly changing, which makes every moment of time different from the previous one. Owing to this, time-based models are better for implementation into railway simulators with mechanical and electrical computations, such as the one used in this PhD (in particular, the train movement simulator used in this PhD has a sample time of 0.05 seconds).

1.5.1.2. TRAFFIC MODEL

The traffic model generates the traffic scenarios, which are the result of aggregating the information of each train (generated in the train movement simulator) and integrating it into timetables. The timetables can be directly the commercial timetables (with the information of trains' arrivals and departures when there are no deviations) or can be obtained from traffic models that, based on the commercial timetables, add traffic variability (due to different types of perturbations).

The traffic scenarios contain the power consumption and regeneration profiles of each train at each time instant and at each location of the railway line. They have a great impact when analysing the receptivity of the MTS line, as stated in (López-López, Álvaro J., 2016; Mellitt et al., 1984). Nevertheless, the vast majority of railway simulators from the literature have used either very simplified traffic models for generating the traffic scenarios or, directly, only use the commercial timetables (in Figure 1-7 there is not a traffic model as such, but data from timetables).

Using an oversimplified traffic model (or directly a single timetable -the commercial one-) can lead to significant errors in the results provided by the railway simulator. Since this PhD is going to assess the installation of ESSs and RSs, whose associated cost is very high, the energy saving estimations obtained from the simulator must be very precise. This implies to use a realistic traffic model in order to accurately assess the energy saving and the impact on the MTS receptivity associated with the installation of the improvements.

Due to the fact that there is a big gap in the literature with respect to the traffic models used for the railway simulators with mechanical and electrical computations, one of the main objectives of this PhD will be the development of a very realistic traffic model to be integrated in the railway simulator. This traffic model will allow generating **representative traffic scenarios** that will improve the accuracy and realism of the simulator.

Traffic models must include the use of traffic variables and topology data. While the use of relevant traffic variables has been observed to a certain extent in some of the models

presented in the literature, all the research studies (where railway simulation is used to assess the installation of MTS improvements) have been made with the simplest topology: a line with two terminal stations (Figure 1-8). Nevertheless, real MTS lines also present more complex topologies, such as topologies with short-turn and terminal stations (Figure 1-9), topologies with branches (Figure 1-10) and topologies with branches, short-turn and terminal stations (Figure 1-11). Therefore, this PhD will also develop the models of these complex topologies and integrate them in the railway simulator.

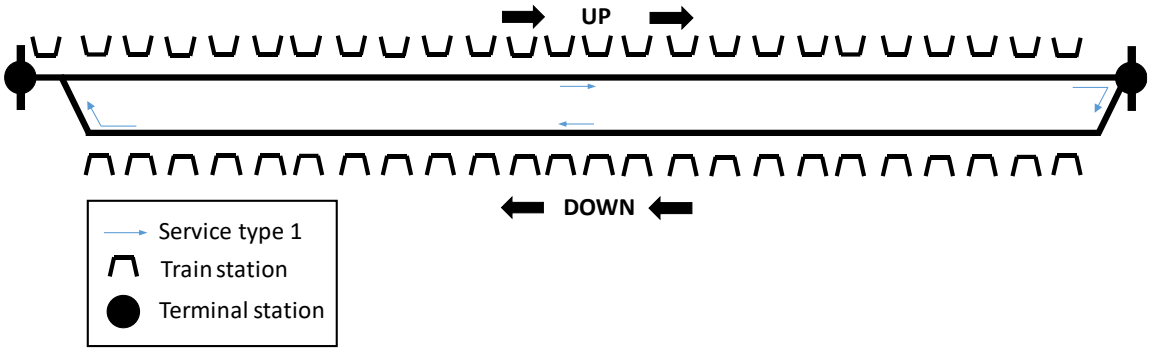

Figure 1-8: Line with two terminal stations

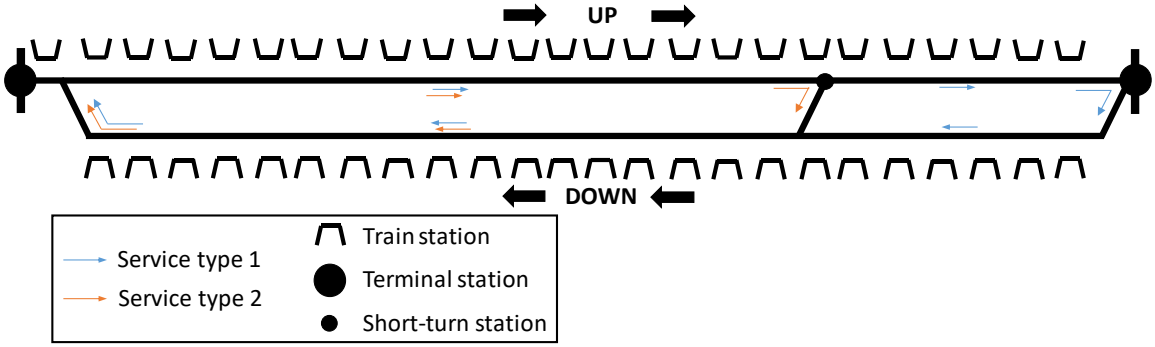

Figure 1-9: Line with short-turn and terminal stations

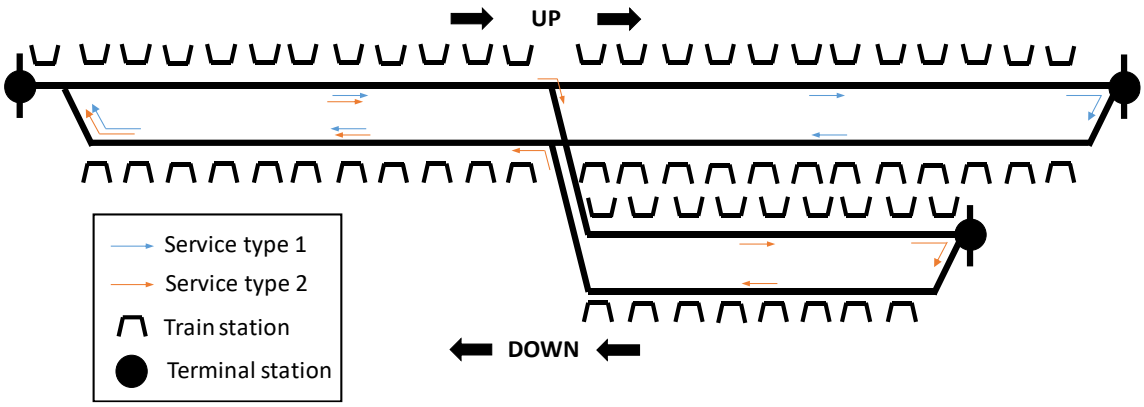

Figure 1-10: Line with branches

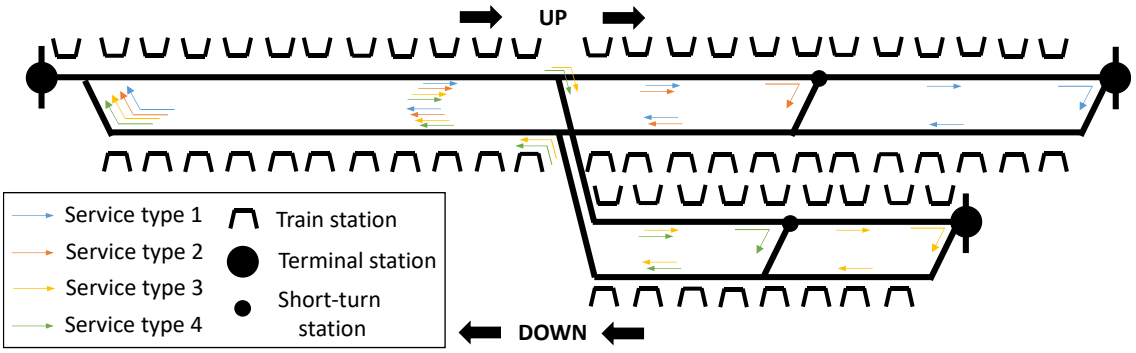

Figure 1-11: Line with branches, short-turn and terminal stations

1.5.2. ELECTRICAL NETWORK MODULE

As can be seen in Figure 1-7, this module can be divided into three submodules: *1)* ***electrical scenarios generator****, 2)* ***load flow solver*** and *3)* ***results aggregator****.*

1.5.2.1. ELECTRICAL SCENARIOS GENERATOR

The electrical scenarios generator used for the railway simulator of this PhD is presented with all the details in (López-López, Á J. et al., 2011; López-López, Álvaro J. et al., 2014). The following lines will highlight its main features.

This submodule generates the circuits (also called snaphots) that electrically represent the operation. As stated by (López-López, Á J. et al., 2011), trains are changing their position and consumption in time and, therefore, snaphots are not the same at each instant. It is hence necessary to generate a sequence of circuits at regular time intervals so that information is updated with time. The snapshots are generated from the following information:

- Train movement module output: the traffic scenarios
- Infrastructure data: it represents the time-invariant part of the circuits, i.e. the electrification elements. It includes, among others, the electrical features of the feeder line (overhead conductor or third rail), track and substations, track lengths, line topologies, supply voltage, substation positions, etc. (López-López, Á J. et al., 2011).

As can be inferred from the previous paragraph, this submodule works as an interface between the train movement module and the electrical network module.

1.5.2.2. LOAD FLOW SOLVER

After generating the snapshots, it is necessary to solve them with the application of load flow techniques. It must be noted that each snapshot is highly non-linear, since trains must be considered as power loads. Consequently, the snapshots must be solved using iterative processes.

In the specific case of DC-electrified MTS systems, there is another particularity that must be tackled: the existence of both AC and DC-electrified sides. On the one hand, many authors, such as (Cai et al., 1995; Chymera, Martyn Z. et al., 2010; Mellitt et al.,

1978), ignore the AC side of the system and only focus on the DC side, which is frequently solved by means of approximate linear methods. These methods can be called "***Iterative methods based on linear approximations to solve the DC side***". On the other hand, other authors, such as (Pires et al., 2007; Tzeng, Wu, & Chen, 1998; Tzeng & Wu, 1995), prefer what can be called "***Mixed AC-DC methods***", where both sides of the electrical network are studied and solved simultaneously. Although more complex, these methods are more realistic. The following paragraphs will explain with more detail each of these methods.

1.5.2.2.1. Iterative methods based on linear approximations to solve the DC side

Equation (1-9) defines the Nodal-voltage equations, which relate the node conductances and voltages to the node currents (Cai et al., 1995):

$$[G] \cdot [V] = [I] \quad \textbf{(1-9)}$$

where:

- ✓ $[G]$ is an $\boldsymbol{n\ x\ n}$ symmetrical nodal conductance matrix, being $\boldsymbol{n}$ the number of nodes in the system.
- ✓ $[V]$ is an $\boldsymbol{n\ x\ 1}$ nodal voltage vector.
- ✓ $[I]$ is an $\boldsymbol{n\ x\ 1}$ nodal injected-current vector.

The problem of non-linearity arises when power and voltage constraints appear, which makes it necessary to apply iterative techniques to achieve a solution. Among the methods using the Nodal-voltage equations, two of them must be remarked:

- **Conductance matrix iterative method**: in this method the nodal currents are zero, except for the substation positive and negative-bus-bar nodes. The solution procedure starts by assuming that the values of the voltages for train nodes are equal to the system voltage. From this assumption the conductance of every train can be calculated as indicated in Equation (1-10):

$$G_t = \frac{P_t}{V^2}\ (t = 1,2, \dots, T) \quad \textbf{(1-10)}$$

  where:

  - ✓ $\boldsymbol{G_t}$ is the equivalent conductance of train t.
  - ✓ $\boldsymbol{P_t}$ is the power consumed by train t.
  - ✓ $\boldsymbol{T}$ is the total number of trains.

  The values of G_t are introduced into the $[G]$ term of Equation (1-9) to obtain a new set of voltages. In the next step, the new set of voltages will be used to obtain new values for the train conductances by applying Equation (1-10). The process will iterate until the desired level of tolerance is achieved (Cai et al., 1995). This method can hold problems of slow convergence and unreliability.

- **Current-vector iterative method**: this method is an alternative to overcome the problems of slow convergence that the conductance matrix iterative method

might cause. Equation (1-9) remains without changing any term but in this case the train model is represented by an ideal current (I_t) source which can be calculated with Equation (1-11).

$$I_t = \frac{P_t}{V} \ (t = 1,2, \dots, T) \quad \textbf{(1-11)}$$

The initial solution is computed by applying Equation (1-11) with the assumption that train voltages are equal to the system voltage. With the values of I_t the voltages can be recomputed with Equation (1-9). After that, the new set of voltage values will be introduced in Equation (1-11) and the iterative process will be repeated until reaching the desired level of tolerance.

1.5.2.2.2. Mixed AC-DC methods

There are two different mixed AC-DC methods: sequential and unified.

In the **sequential mixed AC-DC methods**, the equations of the AC-DC systems are solved separately in each iteration until the conditions imposed by the connection points (rectifiers or inverters) are satisfied. In general, they are not too difficult to implement and it is possible to incorporate different control specifications of the converters easily (Pires et al., 2007).

In the **unified mixed AC-DC methods**, the equations of both sides of the network are combined with a set of equations that represents the performance of the converters. In this case, all the equations are solved together and simultaneously. They present better results in terms of convergence and computational efficiency. There are different iterative numerical unified methods to solve the power flow, such as the Gauss-Seidel method (G-S), the Newton-Raphson method (N-R) and the fast decoupled Newton-Raphson. According to (Tzeng et al., 1998; Yii-Shen Tzeng, Nanming Chen, & Ruay-Nan Wu, 1995), G-S needs accelerating factors because its convergence is slow, especially when approaching the solution. The fast decoupled N-R is based on associating the active power to voltage angles (P-δ) and the reactive power to voltage modules (Q-|V|). These associations are not totally true and the Jacobian matrix incorporated with the residual equations cannot be completely pre-inverted (Tzeng et al., 1998; Yii-Shen Tzeng et al., 1995). Finally, the N-R presents powerful convergence characteristics and can be considered the most appropriate method to be implemented.

The railway simulator used in this PhD applies the **unified mixed AC-DC Newton Raphson** method (for more details about the load flow solver, read Section 2.3.2 of (López-López, Álvaro J., 2016). The following variables are calculated with this method:

- Voltages and angles in AC nodes (e.g.: the AC nodes of the traction substations).
- Voltages in DC nodes (e.g.: the DC nodes of the tractions substations, the train pantographs, the catenary nodes, etc.).

As stated by, (López-López, Á J. et al., 2011), since the DC problem has plenty of nonlinearities, the simulator has to check that the solution at each iteration is feasible. For instance, if a non-reversible substation is considered and its current in the provisional results is negative, that means that the substation is likely to cut off. The

solution must be discarded and new calculations must be carried out taking this into account. In the same line, if a train reaches the maximum accepted voltage at its pantograph or collector shoe, which is common in strong braking combined with low line receptivity, a change in its behavior must be considered. In this situation, a fraction of the regenerated power must be dissipated in the rheostats for the voltage not to go on rising. Also energy storage devices have several operating modes (inactive, charging, discharging, etc.).

1.5.2.3. RESULTS AGGREGATOR

The result files generated by the load flow solver are processed in this module in order to make global studies. For instance, the integration of powers at each instant is carried out in this block in order to calculate energies. Net energy in substations, losses in substations and feeder line, energy dissipated in rheostats, regenerated energy, etc. are calculated in this block (López-López, Á J. et al., 2011).

In the case of this PhD, where the focus is on the energy saving achieved when installing RSs and ESSs, the most important electrical variable to obtain from this module is energy consumption at SSs. The value of this variable obtained from the simulation without improvements will be compared to the value obtained when simulating the infrastructure improvements in order to evaluate the potential energy saving. Other variables such as the rheostats and the losses will be also analysed in order to measure the receptivity, in particular, and the MTS energy efficiency, in general (see Section 1.4 for more details about these measures).

1.6. DESIGN OF THE INFRASTRUCTURE IMPROVEMENTS WITH NATURE-INSPIRED OPTIMIZATION ALGORITHMS

Once having presented the infrastructure improvements in which this PhD is going to focus -RSs and ESSs- and the tool used to assess the impact of their installation –the railway simulator-, it is necessary to introduce to the optimization algorithms that are going to be used to find the optimal design of the infrastructure improvements.

In the case of the RSs, the optimization will consist in finding the optimal number, location and power sizing. In the case of ESSs, the optimization will also include the capacity sizing.

There are two types of optimization algorithms that can be used to tackle the optimal design of the infrastructure improvements: formal mathematical models or nature-inspired optimization algorithms. This PhD will focus on the second ones. The following paragraph, extracted from (Fernández-Rodríguez, 2018), will briefly justify the choice.

Nature-inspired methods have been developed during the last thirty years. According to (Glover & Kochenberger, 2006), Nature-inspired Computational Intelligence includes “any procedures that employ strategies for overcoming the trap of local optimality in complex solution spaces, especially those procedures that utilise one or more neighbourhood structures as a mean of defining admissible moves to transition from

one solution to another, or to build or destroy solutions in constructive and destructive processes". These methods usually make use of stochastic components, they are problem independent and they are not gradient based (as formal mathematical optimization methods are). Moreover, they can describe and solve complex relationships with practically no knowledge of the search space. These methods have become very popular to solve complex optimisation problems, most of them using detailed simulation models, and have been applied in a variety of engineering fields such as: computer networks, power systems, security, robotics, production engineering, biomedical engineering, control systems, data mining, etc… (Binitha & Sathya, 2012). The reasons for their popularity can be found in the flexibility and efficiency of these algorithms that, nevertheless, tend to be easy to implement.

Additional reasons that explain why formal mathematical optimization models have been discarded for this PhD are the following:

- Formal optimization models must solve a highly non-linear and non-convex load flow problem (see Section 1.5.2.2), while deciding the optimal configuration of the electrical infrastructure (López-López, Álvaro J., 2016). This causes very complex and time-consuming optimization processes. On the contrary, nature-inspired optimization algorithms have been proved to be very flexible and successful in dealing with computationally-intensive and highly non-linear and non-convex problems (Ertenlice & Kalayci, 2018; Mavrovouniotis, Li, & Yang, 2017; Saka, Hasançebi, & Geem, 2016).
- Formal optimization models use a large number of simplifications for the traffic model that does not ensure that they are capable of dealing with complex metropolitan lines, where there are different time intervals between trains and many possible traffic scenario (López-López, Álvaro J., 2016). On the contrary, nature-inspired optimization algorithms can use detailed simulation models, which make them clearly more aligned with one of the objectives of this PhD: developing a realistic traffic model where many representative traffic scenarios will be used (see Section 1.5.1.2).

Three different nature-inspired optimization algorithms have been selected: the Genetic Algorithm (GA), the Particle Swarm Optimization Algorithm (PSO) and the Fireworks Algorithm (FA). The GA and the PSO are, respectively, the main exponents of evolutionary and swarm algorithms and have been used in multiple applications (Long, Wu, Huang, & Wang, 2015; Lynn & Suganthan, 2015). The FA is an interesting and novel proposal within the swarm algorithms with promising results (He, Li, Zhang, & Cao, 2019). The remainder of this section will briefly introduce them, although the detailed state of the art about the application of nature-inspired optimization algorithms in the design of infrastructure improvements will be presented in Chapter 5.

The GA (Goldberg & Holland, 1988) is a well-known optimization metaphor based on the natural selection process. It begins with a population of random solutions called chromosomes, and evolves them through several cycles of selection, crossover and mutation operations. The better fit selected chromosomes exchange the promising

genetic information, which is further mutated to give rise to ever evolving and best fit or optimal solutions.

The PSO (Kennedy & Eberhart, 1995) is a metaphor in the swarm intelligence paradigm. It has become a popular meta-heuristic algorithm in the optimization domain and has been successfully applied to optimization problems ranging from business, engineering, healthcare, etc. Based on the food-gathering behaviour of swarms of bees, birds and schools of fish, PSO optimally balances exploration and exploitation. Simplicity in implementation, negligible computational overhead and rapid convergence have made it one of the outstanding swarm intelligence paradigms.

The FA (Tan & Zhu, 2010) is a recent Swarm Intelligence optimization algorithm, which derives its inspiration from the fireworks exploding in the night sky. The algorithm generates random initial positions of N fireworks. The fireworks explode generating sparks, depending on their respective amplitudes. Fireworks with higher fitness values have a smaller explosion amplitude and a larger number of explosion sparks, while fireworks with lower fitness values have a larger explosion amplitude and a smaller number of explosion sparks. In addition, random sparks are also generated based on a Gaussian mutation process. A new population of N fireworks is selected at the end of each iteration. This may include the original fireworks, as well as the regular and Gaussian sparks. The elitist strategy is maintained by always inserting the current best location in the new population.

1.7. THESIS OBJECTIVES

1.7.1. MAIN OBJECTIVE

In the current context of looking for measures to mitigate climate change, Mass Transit Systems are a sustainable alternative for urban transport. Railway operators have a great interest in improving the infrastructure of these systems in order to reach the maximum levels of energy saving. The installation associated with these improvements involve big investments that need to be adequately assessed. However, the methodology to determine the optimal design of these installations is not sufficiently developed in the scientific literature; decisions are usually made by means of unrealistic railway simulators or even based on the experience of railway operators. This chapter has introduced the reader to some of the gaps existing in the literature with respect to the railway simulators used for the assessments:

- Traffic models are too simplified and, in worst cases, they are directly substituted by a single operation timetable.
- Line topology models are always simple lines with two terminal stations.

In consequence, providing a rigorous and detailed methodology for designing the installation of the MTSs' infrastructure improvements has become a demand of railway operators and a necessity for society. This PhD will try to cover this demand and will address the proposal of a methodology with those requirements. The methodology will be based on the application of nature-inspired optimization algorithms to optimize the

installation of Reversible Substations and Energy Storage Systems. The algorithms will make use of a realistic railway simulator to properly assess the impact of installing these improvements on the MTS energy efficiency. The realistic railway simulator will develop some features missing in the literature: a detailed traffic model able to generate representative-enough traffic scenarios and the capability of dealing with any type of line topology.

1.7.2. SPECIFIC OBJECTIVES

The main objective can be divided into four specific objectives that have constituted the main contributions of this PhD.

1. <u>Development of a realistic traffic model</u>

This objective consists in developing a realistic traffic model to be integrated in the railway simulator. In previous research of our group, important traffic variables have been included in the traffic model:

- The headway: time interval between two consecutive trains.
- The dwell time.
- The time shift at terminal stations: the gap between the departure instant of trains in each direction from the terminal stations.

This PhD will also implement:

1) A realistic traffic model for small perturbations. The proposed traffic model has to include different headways, different time shifts at terminal stations, non-constant dwell times, different train speed profiles and a specific module of the traffic regulation system in real time (being the last two features a big novelty with respect to literature).
2) A realistic traffic model for large perturbations. This model has to replicate the traffic mechanisms that regulate the operation in this type of situations, which have never been observed in the literature before.

The improved traffic model will be able to generate representative traffic scenarios that properly replicate the real behaviour of railway operation. From the whole set of representative scenarios a reduced set of them, called 'selected traffic scenarios', will be obtained. The selected scenarios must contain most of the information included in the whole set of representative traffic scenarios (specially the important information for assessing the impact that the potential installation of RSs and ESSs can have on the system efficiency: energy saving, receptivity measures, etc.) and will make it possible to reduce the computational burden of the simulations performed when applying the nature-inspired optimization algorithms.

2. <u>Complex line topologies modelling and integration in the railway simulation model</u>

As explained in Section 1.5.2.1, literature only has focused on the assessment of improvements for the simplest type of line topology: line with two terminal stations. Nevertheless, railway lines may have more complex topologies, such as topologies with

short-turn and terminal stations, topologies with branches, or topologies with branches, short-turn and terminal stations. In addition, and associated with these complex topologies, different types of service (train itineraries) can be offered. This PhD will develop the models of the different types of complex topologies (and their associated services) and implement them in the railway simulator. This will enable to apply the methodology proposed in this PhD to any existing railway line.

3. **Development of optimization algorithms to design the optimal installation of Reversible Substations and Energy Storage Systems**

The aim is to optimize the installation of RSs and ESSs in order to maximize the use of the energy coming from the regenerative braking of the trains. The optimization algorithms will use the detailed and realistic railway simulator already integrating the improvements presented in the previous objectives. They must be able to find the optimal number, location and sizing of the improvements (power in the case of RSs and power and capacity in the case of ESSs). Since the economic aspect is essential to undertake the investments, the solutions provided by the algorithms must find the optimal balance between energy saving and installation costs.

4. **Update of the railway simulation model**

Together with the two first objectives, which greatly enhance the railway simulation model, the development of this thesis makes necessary to update, improve and incorporate simulation features to different modules of the railway simulation model. These improvements will focus on two main aspects:

- The electrical models of the RSs and ESSs used in the load flow solver.
- Computational efficiency and reduction of simulation time.

As the entity of this objective is minor in comparison to the previous ones, this objective will not have devoted a chapter itself but will be splitted among the different chapters of this document.

1.8. STRUCTURE OF THE DOCUMENT

This thesis is structured into eight chapters:

- Chapter 1 has presented the context in which this thesis is framed as well as its motivation and objectives.
- Chapter 2 presents the realistic traffic model for small perturbations developed during the thesis. In order to illustrate the risk of using too simplified traffic models, an illustrative case study compares the energy saving resulting from the installation of an RS obtained with the accurate model proposed in this chapter and the model most commonly used in the literature.
- Chapter 3 is devoted to the realistic model for traffic with large perturbations. The chapter also includes an illustrative case study that offers a comparison among the energy saving results from installing an RS obtained with three different traffic models: the simplified traffic model more extended in the literature, the realistic

traffic model for small perturbations proposed in Chapter 2 and the realistic traffic model for large perturbations of this chapter. This will show the impact of including traffic scenarios with high perturbations in the energy saving estimations.

- Chapter 4 addresses the study of the complex line topologies.
- Chapter 5 explains the nature-inspired optimization algorithms used to find the optimal installation of RSs or ESSs, as well as the implementation details and the adjustments required to properly working with the railway simulator. The algorithms are presented in two different approaches: the single-stage approach (the whole budget for the installation is available from the beginning) and the multi-stage approach (the whole budget is not available from the beginning, but is divided into separate stages over time). The performance of the algorithms is analysed in optimizations tests.
- Chapter 6 formalizes the methodology proposed in this thesis to assess the installation of electrical infrastructure improvements. It integrates all the knowledge obtained from the research of this PhD and presents a case study where the optimization of RSs and ESSs is addressed by the application of the single and multi-stage optimization algorithms of Chapter 5. These algorithms will use the realistic railway simulator already incorporating the improvements with respect to the traffic model presented in Chapters 2 and 3 and able to work with complex topologies thanks to the models developed in Chapter 4.
- Chapter 7 summarizes the main conclusions and the most relevant contributions of this PhD. Some suggestions for future work are also proposed in this chapter.

The results presented in Chapters 2 and 3 have been published in 2 journal papers (Roch-Dupré, Cucala, R. Pecharromán, López-López, & Fernández-Cardador, 2018; Roch-Dupré, Cucala, Pecharromán, López-López, & Fernández-Cardador, 2020). Therefore, some materials from these papers have been used to write previously mentioned chapters.

CHAPTER 2

TRAFFIC MODEL FOR SMALL PERTURBATIONS

The traffic model has a great impact on the receptivity of a line and, in general terms, on the efficiency. Thus, an oversimplified traffic model consisting of a single traffic timetable with constant dwell times can lead to significant errors in the computation of the energy saving associated with the installation of RSs or ESSs and, therefore, to an incorrect decision-making about the best improvements to be installed.

There are two main types of traffic scenarios according to the degree of perturbations that take place in operation*: a) traffic with small perturbations* and *b) traffic with large perturbations*. A perturbation is the deviation of train departures with respect to the commercial timetable. Two different traffic situations can take place depending on the perturbations level:

a) **Traffic with small perturbations**. In real operation there are always small deviations in the time that trains remain stopped at the stations since there are variations in the time required by the passengers to get in or off the train (which in turn depends on the number of passengers), as well as in the driver's response time to resume travel. These variations generate short delays in the departures from stations.
b) **Traffic with large perturbations**. In real operation, especially during peak hours, there may appear, either punctually or repetitively, big deviations produced by

the accumulation of trains in a certain stretch of track. This accumulation results in very irregular time intervals between trains and major delays.

This chapter will focus on the model developed for traffic with small perturbations while Chapter 3 will focus on the model for traffic with large perturbations.

Section 2.1 summarizes the state of the art in the literature with respect to traffic models for small perturbations. Section 2.2 provides an overall description about the way the new traffic model for small perturbations proposed in this PhD must be used to assess possible railway infrastructure improvements. Section 2.3 gives the details about this traffic model. Section 2.4 contains the characteristics of the case study that is going to be used to compare the traffic model more extended in the literature and the proposed in this chapter. Section 2.5 analyses and compares the simulation results obtained with both models. Finally, the main conclusions are presented in Section 2.6.

2.1. INTRODUCTION

Three of the main parameters that define a traffic scenario are:

1) **Headway:** time interval between two consecutive trains (Roch-Dupré et al., 2017). In order to represent the different types of operation during the day (peak hours, off-peak hours, etc.) several values must be used for this variable.
2) **Dwell time:** stop-time at stations. As previously explained, dwell time is variable in real operation because it depends on several factors, such as the number of passengers waiting at the station or the driver's response time.
3) **Time shift at terminal stations**: gap between the departure instant of trains in each direction from the terminal stations (López-López, Álvaro J., Pecharromán, Fernández-Cardador, & Cucala, 2017a). Different values for the time shift must be considered to accurately represent the real traffic operation.

The vast majority of studies uses oversimplified traffic models: a single traffic timetable, with just one headway and with constant dwell times (Calderaro, Galdi, Graber, & Piccolo, 2015; de la Torre, Sánchez-Racero, Aguado, Reyes, & Martínez, 2015; Fazel, Firouzian, & Shandiz, 2014; Pereira, Pires, & Nabeta, 2014; Ratniyomchai, Hillmansen, & Tricoli, 2014; Ratniyomchai, Hillmansen, & Tricoli, 2015; Xia, Chen, Yang, Lin, & Wang, 2015). Few papers consider different headways (operation at peak and off-peak hours), which slightly enhances the variety of the traffic scenarios simulated (Bae, 2009; Gao et al., 2015; Tian et al., 2019; Wang, Yang, Lin, & Zhao, 2014).

A first step in the direction of enhancing the traffic model is taken by (López-López, Álvaro J. et al., 2017a), where it is stated that traffic variables such as dwell time must be modelled stochastically and that they have an important impact on the energy interactions between trains in the line. In this line, (Chuang, 2005; Hui-Jen, Chao-Shun, Chia-Hun, & Shi-Hong, 2005) consider "stochastic operation characteristics" to find the optimal placement of RSs. Nevertheless, the only improvement of the traffic model explicitly described in these studies is the use of different headways to represent peak and off-peak operation hours, without giving more details about any other traffic variable.

In (Mellitt et al., 1984), in order to obtain accurate results in the simulation of a DC railway line with RSs, different headways are used as well as a range of values for a parameter called 'synchronization delay'. The synchronization delay measures the shift between two trains on adjacent tracks (up and down direction) along their entire trajectory (not only at the departure instants, as happens with the time shift previously defined). Using a range of values for the synchronization delay involves a variable probability of coincidence between braking and motoring events of different trains, which has a direct impact on the receptivity of the line. This way, the traffic variability that must be included in a detailed traffic model is observed to some extent, but with less accuracy than by separately introducing time shifts and non-constant dwell times.

In (Roch-Dupré et al., 2017) there is a step forward by explicitly using different headways and non-constant dwell times in order to determine the impact that the installation of ESSs can have on the demand charge of a railway line, but different time shifts are not included in this study. Finally, in (López-López, Álvaro J. et al., 2017a), apart from different headways and non-constant dwell-times, the use of variable time shifts is included in order to carry out an energy saving study with RSs.

In addition to the traffic variables previously presented, another element that plays a pivotal role in the traffic model is the speed profile (Domínguez et al., 2012). In railway systems, different speed profiles are used: the flat-out profile (minimum travel time and maximum energy consumption) and other speed profiles that require higher travel times and typically have lower energy consumption. These speed profiles can be designed with the eco-driving techniques explained in Section 1.3.2, which make it possible to increase the energy efficiency through the computation of the speed profile with the lowest consumption for a given travel time. Eco-driving design usually includes coast commands (null traction). Currently in metro-lines, the speed profile to be selected among the available ones is determined by the traffic regulation needs.

The impact that the use of different speed profiles has on the assessment of infrastructure improvements has not been studied in the literature in detail. There are very few studies about this topic and the existing ones are very simplified. In (Mellitt et al., 1984), two cases regarding the use of different speed profiles are considered: flat-out and coasting allowance of 7.4%. (Bae, 2009) states that different driving patterns are used in the study of the optimal installation of RSs without giving more details. In the rest of the literature, the most common practice is to use the flat-out profile to perform the analysis.

In railway lines equipped with ATO (Automatic Train Operation), speed profiles are selected in real time by the traffic regulation system at the control center. This system selects and sends the driving commands to every train in order to accomplish with the target schedule. The speed profiles are automatically executed by the on-board ATO equipment. The traffic regulation system has a big influence on the real-time traffic behavior. Nevertheless, there are no examples where a traffic regulator model is integrated within the electrical railway simulator in order to study the impact that the traffic regulation has on the consumption, as well as on the installation of RSs or ESSs.

Consequently, and with the aim of filling the gap existing in the literature, this chapter develops an accurate traffic model with different headways, different time shifts, stochastic modelling of dwell times based on statistical distributions and a specific module of the traffic regulation system with different speed profiles. In addition, the results obtained from applying the proposed model to an illustrative case study, which is particularized to the installation of an RS, are analyzed and compared to the results obtained when applying the most common model in the literature (much more simplified).

2.2. MODEL TO ASSESS INFRASTRUCTURE IMPROVEMENTS TAKING INTO ACCOUNT SMALL PERTURBATIONS

This model has the goal of helping in the decision-making process about the investments required for the infrastructure improvements, by analyzing in detail the energy saving that can be obtained with them (see Figure 2-1).

The model must be realistic enough from the point of view of the energy saving obtained with each type of investment. With this aim, the model, based on simulation, contains a traffic model for small perturbations that improves in different ways the models presented in the literature as it introduces more complete information about the traffic of the railway line.

As can be seen in Figure 2-1 (and will be explained in detail in the following sections) this traffic model uses different headways (taking into account the different operation periods during the day), introduces variations in the time shift, models the stochastic behavior of the dwell time and observes the possibility of using different speed profiles at each interstation. Besides, a simplified model of a traffic regulator for small perturbations has been included.

This allows generating not only one traffic scenario, but a high number of traffic scenarios that represent better the possible situations that can take place in the railway line. Once having the traffic scenarios, the electrical simulation is the one presented in Section 1.5.2. As a reminder, the next paragraph briefly describes it.

The traffic scenarios contain the information about train positions and consumptions for every time instant. These scenarios are introduced into the electrical scenarios generator, which integrates the traffic scenarios within the electrical infrastructure (including the possible improvements that can be installed on it, such as RSs and ESSs), giving as a result the electrical scenarios (also called ‘snapshots’) at each time instant. The electrical scenarios represent the consecutive electrical circuits to be solved by the application of the load flow techniques. They are solved in the load flow solver that, after some data processing in the results aggregator, provide the final results (consumption in SSs, rheostats losses, receptivity, efficiency, energy losses, etc.).

The steps to assess the impact of an infrastructure improvement are the following:

1. Generate a big enough number of traffic scenarios so as to take into account the traffic variability.
2. Generate, for each traffic scenario, the consecutive electrical scenarios.
3. Simulate these electrical scenarios with the current infrastructure characteristics in order to compute the consumption in SSs and the rest of the electrical variables required.
4. Introduce the infrastructure improvements (for example the installation of an RS) and simulate, for each traffic scenario, the corresponding consecutive electrical scenarios, in order to compare the previous results with those obtained with the new infrastructure, as well as to compute the energy saving that can be achieved.

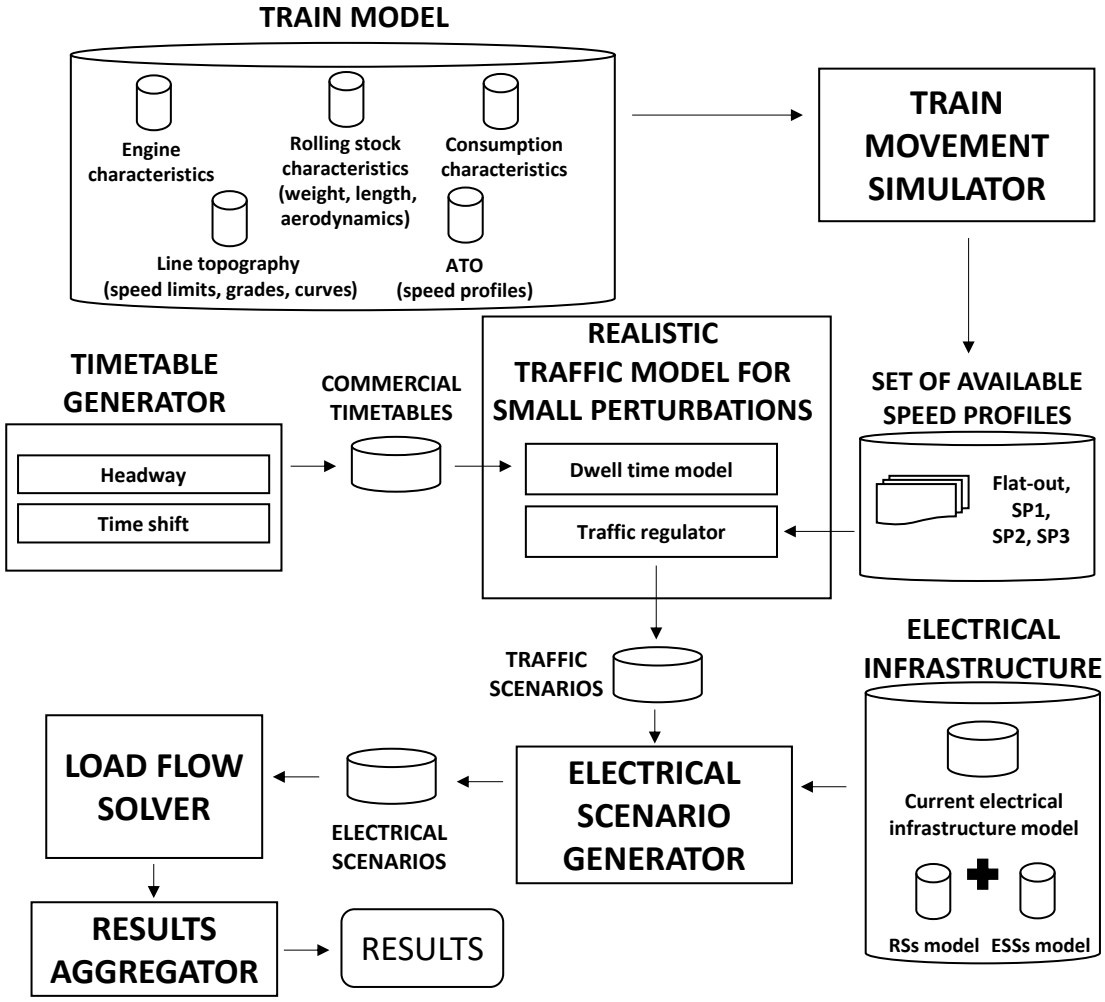

Figure 2-1: Model to assess railway infrastructure improvements including a realistic traffic model for small perturbations

Among all the modules that compose this model, this chapter is going to focus on the traffic model, as well as on its impact on the evaluation of the electrical infrastructure improvements.

2.3. TRAFFIC MODELLING

2.3.1. TIMETABLE GENERATOR

It generates the commercial timetables, which have the information of trains' arrivals and departures when there are no deviations.

Several headways are taken into account for timetable generation, in order to represent in a realistic way peak, off-peak and sparse traffic conditions. As stated in (Roch-Dupré et al., 2017), the lower the headway is, the higher the consumption, the amount of regenerated energy and the receptivity. Additionally, trains have been simulated with different loads depending on the headway in order to take into account that depending on the operational period, the average number of passengers is different.

Then, for each headway, multiple timetables are generated by varying the time shift value. This represents in a realistic way that passengers can be given the same service with timetables that have different time shifts. Changing the time shift means to change the moment when trains departure from terminal stations. Positive values of the time shift implies that trains going in up direction departs with a delay, in relation to the corresponding train going in down direction, equivalent to the absolute value of the time shift and vice-versa. No time shift (time shift = 0) implies that the departures of the trains in both directions are synchronized. Once the commercial timetables are obtained (there are multiple due to the use of different headways and time shifts) the realistic traffic simulation is performed.

2.3.2. REALISTIC TRAFFIC MODEL FOR SMALL PERTURBATIONS

The realistic traffic model for small perturbations generates deviations in the departure of trains with respect to each commercial timetable provided by the timetable generator. These deviations are obtained by introducing 'traffic noise' in the dwell time (the variation of the dwell time is within a range short enough to consider only situations of traffic with small perturbations). Then, the traffic regulator tries to compensate these deviations by using the most appropriate speed profile -selected among the set of predesigned ATO speed profiles (flat-out, SP1, SP2 and SP3 in Figure 2-1)- according to its associated running time.

As a result, a great number of traffic scenarios is obtained for each timetable. These scenarios take into account the deviations from schedule produced by the traffic noise and the strategies to recover them applied by the traffic regulator, which involve the use of different ATO speed profiles.

This traffic model can be divided into two sub-modules: *a) dwell time model* and *b) traffic regulator.*

2.3.2.1. DWELL TIME MODEL

Figure 2-2 graphically represents the model for the traffic noise and for the time regulation at station. It calculates the dwell time for each train $\boldsymbol{i}$ at each passenger station $\boldsymbol{j}$. The inputs for this model are:

- The arrival time of train $\boldsymbol{i}$ to station $\boldsymbol{j}$ ($t_{arr_{i,j}}$).
- The arrival time of train $\boldsymbol{i}$ to station $\boldsymbol{j}$ according to the commercial timetable ($t_{comm\ arr_{i,j}}$).
- The departure time of train $\boldsymbol{i}$ from station $\boldsymbol{j}$ according to the commercial timetable ($t_{comm\ dept_{i,j}}$).
- The dwell time of train $\boldsymbol{i}$ in station $\boldsymbol{j}$ according to the commercial timetable ($t_{comm\ dwell_{i,j}}$).

The output is the departure time of train $\boldsymbol{i}$ from station $\boldsymbol{j}$ ($t_{dept_{i,j}}$).

Dwell time has been modelled according to a lognormal distribution that, as stated in (Martínez, Vitoriano, Fernandez-Cardador, & Cucala, 2007), is the best way to represent the real behavior of this variable. Additionally, the mean value of this distribution changes depending on whether the train is delayed or not with respect to the commercial timetable:

- If the train $\boldsymbol{i}$ is delayed when arriving to station $\boldsymbol{j}$ ($t_{arr_{i,j}} > t_{comm\ arr_{i,j}}$), the mean value of the distribution corresponds to that required to recover the delay ($t_{target\ dwell_{i,j}} = t_{comm\ dept_{i,j}} - t_{arr_{i,j}}$).
- If the train is ahead or in time ($t_{arr_{i,j}} \leq t_{comm\ arr_{i,j}}$), the mean value of the distribution is constant and equal to the dwell time of the commercial timetable ($t_{comm\ dwell_{i,j}}$).

This modification in the mean value of the distribution tries to represent the driver's behavior, who tries to shorten the dwell time at station when the train is delayed.

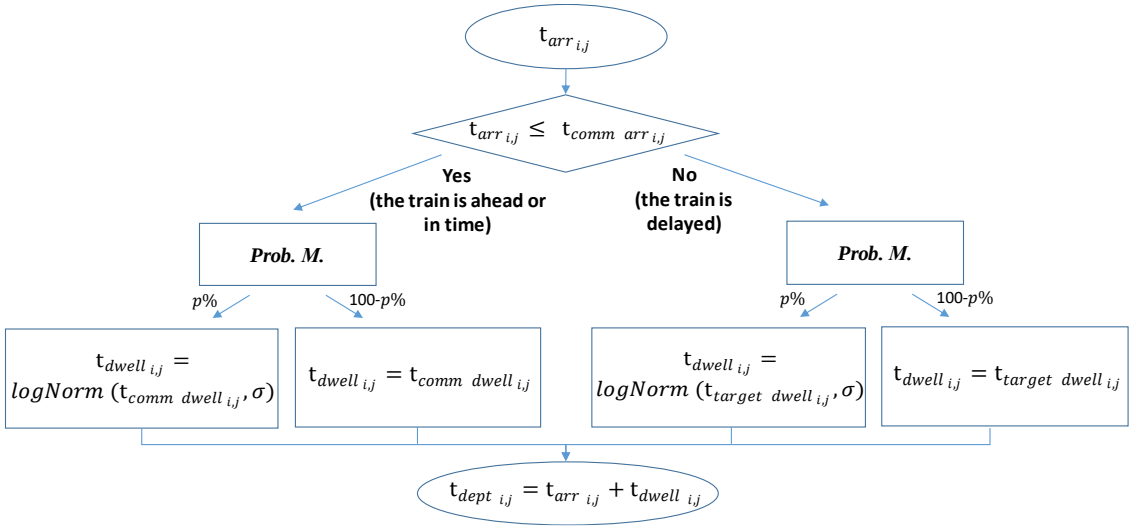

Figure 2-2: Dwell time model

Finally, a probability model (***Prob. M.***) decides whether to obtain the values of the dwell time from the lognormal distribution (with a probability $p\%$) or directly from the mean value itself (with a probability 100-$p\%$). This represents that sometimes the number of passengers is very low and then, the real dwell time ($t_{dwell_{i,j}}$) can be exactly equal to the dwell time desired by the driver ($t_{target\ dwell_{i,j}}$ or $t_{comm\ dwell_{i,j}}$ depending on whether the train is delayed or not). It must be remarked that, in any case, all the values of dwell time obtained will be always greater than a minimum operative dwell time and lower than a maximum operative dwell time.

2.3.2.2. TRAFFIC REGULATOR

When a train is going to depart from the station, the traffic regulator decides the speed profile to be sent to the train to be executed along the next interstation, according to the required running time for that train. This will depend on whether the train is delayed or not with respect to the commercial timetable. Typically, traffic regulators use a set of four different pre-programmed speed profiles (Fernández-Rodríguez et al., 2015; Domínguez et al., 2011; Fernández-Cardador, Cucala, Vitoriano, & de Cuadra, 2006), but this number could change without varying the general behavior of the regulator. The four different speed profiles used for this study have been designed with the train movement simulator described in (Domínguez, Cucala, Fernández, Pecharromán, & Blanquer, 2011): SP0 (the flat-out), SP1, SP2 and SP3. The specifications for the design are given in (Domínguez et al., 2011). As stated in (Domínguez et al., 2011), the speed profiles are practically equidistant in travel time and consumption decreases while running time increases.

Commercial timetables are designed with time margins to recover from possible delays in both dwell times and interstations. This means that if there are no delays, commercial timetables can be accomplished by a train circulating with a speed profile slower that the flat-out. Therefore, among the four different speed profiles, SP1 is typically the nominal speed profile for the commercial timetable, in order to have, at least, a faster speed profile (SP0/flat-out) that allows the traffic regulator to recover the time delay when necessary.

Figure 2-3 graphically represents the model of the traffic regulator. The inputs for this model are:

- The departure time of train $\boldsymbol{i}$ from station ($t_{dept_{i,j}}$).
- The departure time of train $\boldsymbol{i}$ from station $\boldsymbol{j}$ according to the commercial timetable ($t_{comm\ dept_{i,j}}$).
- The arrival time of train $\boldsymbol{i}$ to the next station (station $\boldsymbol{j+1}$) according to the commercial timetable ($t_{comm\ arr_{i,j+1}}$).
- The interstation running times between stations $\boldsymbol{j}$ and $\boldsymbol{j+1}$ associated with the different speed profiles ($t_{\mathrm{SP}\ 0/1/2/3\ interst\ [j,j+1]}$)

The output is the arrival time of train $\boldsymbol{i}$ to station $\boldsymbol{j+1}$, ($t_{arr_{i,j+1}}$). The logic of the traffic regulator model is explained bellow:

- If train ***i*** departs delayed from station ***j*** ($t_{dept_{i,j}} > t_{comm\ dept_{i,j}}$), the traffic regulator has to choose between SP0 (faster than the used in the commercial timetable) and SP1 (the used in the commercial timetable):
  - If the delay cannot be recovered with SP0 ($t_{dept_{i,j}} + t_{SP0\ interst_{[j,j+1]}} \geq t_{comm\ arr_{i,j+1}}$), SP0 (which is the fastest speed profile) is chosen in order to recover as much delay as possible.
  - If the delay can be recovered with SP0 ($t_{dept_{i,j}} + t_{SP0\ interst_{[j,j+1]}} < t_{comm\ arr_{i,j+1}}$), there is an election between speed profiles SP0 and SP1.
    - ✓ If SP1 is chosen, the train continues having a delay, which can be acceptable in the case of being very small, as it can be recovered in the following station by shortening the dwell time or in succeeding interstations with the use of SP0. In return for maintaining a small delay, there is an energy saving as a more economic speed profile is used.
    - ✓ On the contrary, if SP0 is chosen, the delay is completely recovered and the train arrives a bit ahead at the following station. In this case, the consumption increases in return of recovering the delay.

    In these situations the decision of recovering or not the delay at the cost of increasing the energy consumption is made according to a variable (sp_{select}) which is computed from Equation (2-1). If this variable is greater or equal than a threshold ($sp_{select} \geq Train\ Delayed\ Factor$), the delay derived from using a more economic speed profile (SP1 in this case) would not be acceptable and therefore a faster but less economic speed profile must be selected (SP0 in this case). If the variable is lower than the threshold, the delay obtained with a more economic speed profile is admissible as it can be easily recovered later and, therefore, this speed profile can be chosen.

$$sp_{select} = \frac{|delay\ accum.\ with\ a\ more\ economic\ SP|}{|delay\ accum.\ with\ a\ more\ economic\ SP| + |advance\ accum.\ with\ a\ less\ economic\ SP|} \quad \textbf{(2-1)}$$

- If the train ***i*** is ahead or on time when leaving station ***j*** ($t_{dept_{i,j}} \leq t_{comm\ dept_{i,j}}$), the traffic regulator has to decide between SP1 (the used in the commercial timetable), SP2 (slower but less energy consuming than SP1 and faster but more energy consuming than SP3) and SP3 (the slowest but with the least energy consumption):
  - If using SP2 generates a delay when the train arrives at the following station ($t_{dept_{i,j}} + t_{SP2\ interst_{[j,j+1]}} \geq t_{comm\ arr_{i,j+1}}$), there is an election between speed profiles SP1 and SP2. This situation is similar to that when the traffic regulator has to choose between using SP0 and SP1. If SP2 is used, the train arrives with delay to the next station but less energy is consumed. If SP1 is used, the train arrives in advance to the following station but the energy consumption is higher. The decision again depends on the variable (sp_{select}). The only difference is that in this case, the threshold to which sp_{select} must be compared ($Train\ Ahead\ Factor$) can be different from that used when the train is delayed before leaving the station ($Train\ Delayed\ Factor$).

- If using SP2 does not generate a delay when the train arrives at the following station ($t_{dept_{i,j}} + t_{SP2\ interst_{[j,j+1]}} < t_{comm\ arr_{i,j+1}}$), there is an election between speed profiles SP2 and SP3. The selection procedure is exactly equal to that used to decide between SP1 and SP2 (explained in the previous paragraph).

Finally, the arrival time to station $\boldsymbol{j+1}$ is computed by the addition of the departure time from the previous station ($t_{dept_{i,j}}$) and the interstation running time obtained with the selected speed profile x ($t_{SPx\ interst_{[j,j+1]}}$).

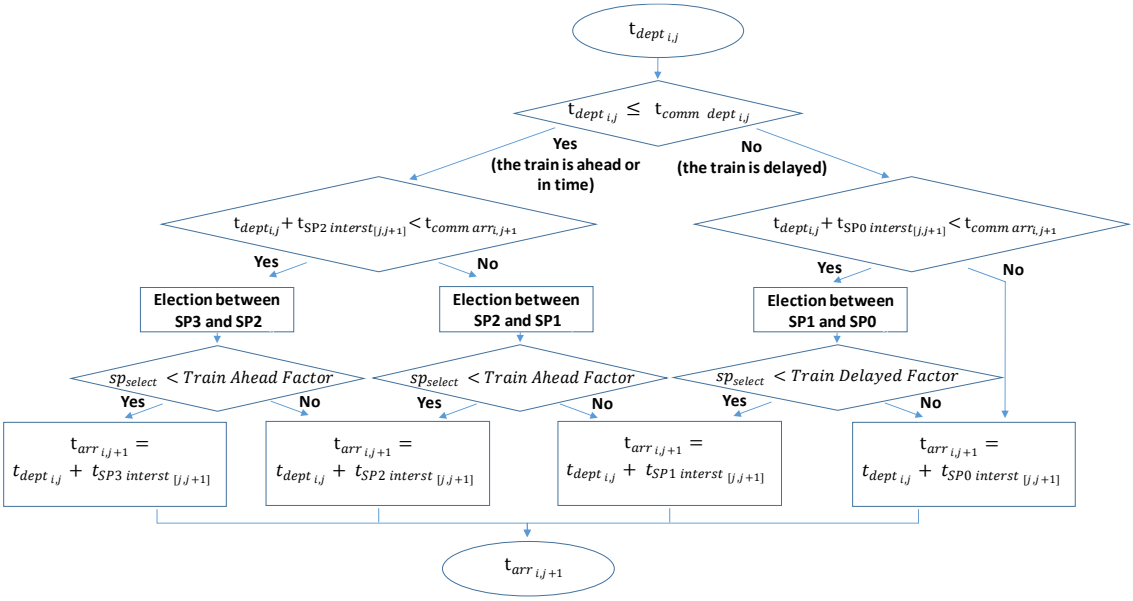

Figure 2-3: Traffic regulator model

2.4. CASE STUDY

2.4.1. TOPOLOGY, INFRASTRUCTURE AND ROLLING STOCK CHARACTERISTICS

A real Spanish metro line is used for the case study. It consists in a line with two terminal stations. The turn-back maneuvers at terminal stations are the following: turn-back in front of the station at terminal station A and turn-back beyond the station at terminal station B. The case-study line topology is depicted in Figure 2-4.

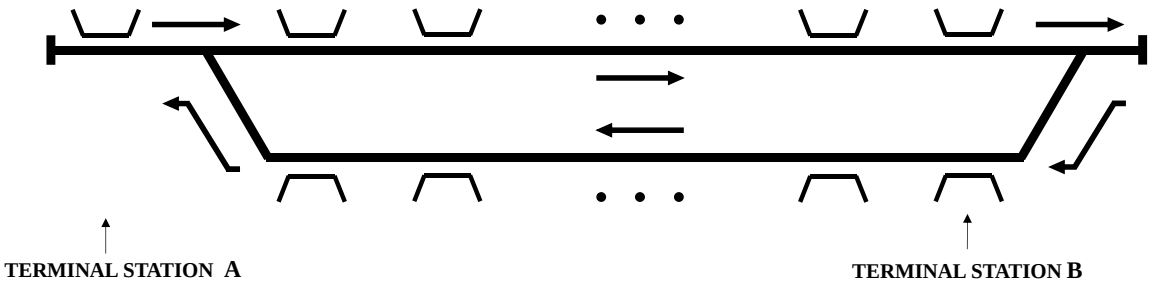

Figure 2-4: Case-study line topology

Figure 2-5 provides information about the location of passenger stations, electrical SSs and the line topography.

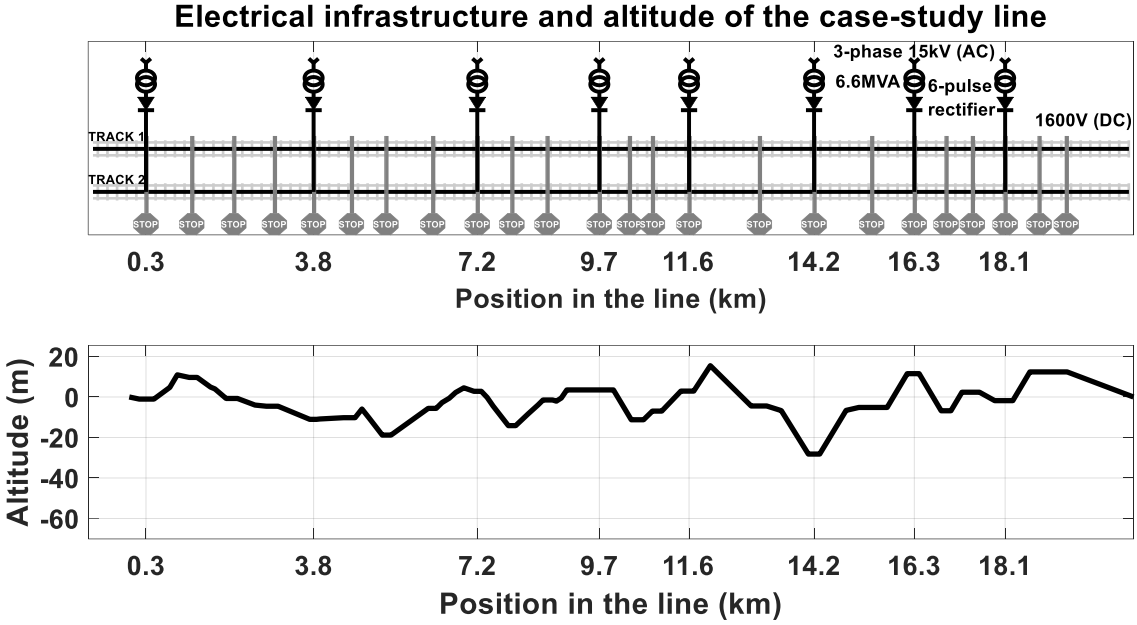

Figure 2-5: Case-study line passenger stations, SSs and topography

Table 2-1 shows the main electrical and topological characteristics of this line and Table 2-2 provides the most relevant information regarding the rolling stock.

Table 2-1: Electrical and topological characteristics

• **Line length:** 19.3 km. • **Maximum speed:** 70 km/h. • **Passenger stations:** 24 • **Traction SSs:** 8. • **Rectifier type (all SSs):** 6-pulse diode rectifiers (one-quadrant) • **Rectifier nominal power (all SSs):** 6.6 MVA. • **Nominal voltage of the line / No-load voltage:** 1600 / 1650 V	• **Feeder lines:** Conventional overhead conductor with a support feeder connected to the contact lines every 700 m (at these points, both track overhead conductor lines are paralleled). • **Return circuit:** Both rails are used to carry the return current. • **Total impedance of the active + return line:** 26 mΩ/km.

Regarding the RS management, the regenerated energy not used by other trains is sent back to the grid when the inversion mode is activated. The activation of this mode takes place when the catenary voltage exceeds the threshold of 1665.5 V (this value is obtained from multiplying by 1.01 the no-load voltage). There are two main methods for defining the behavior of the RS in the inversion mode: the constant advance angle control and the constant voltage control (Tzeng et al., 1998). The latter has been selected and implemented in the electrical network module of the railway simulator. This control method is preferable to the constant advance angle control as it is more robust and more powerful in terms of recovering regenerated energy from the

catenary. The only disadvantage from this method is the high harmonic content generated, but thanks to the advances in power electronics, this is no longer a problem. The equations that must be included in the Jacobian matrix of the N-R used by the load flow solver in order to implement this control method are given in Appendix 1.

Table 2-2: Rolling stock characteristics

• T**rain length:** 108.3 m • **Empty train mass:** 192.96 tons (only one type of train composition used). • **Train maximum load:** 76.58 tons. • **Train load in the study:** varies depending on the headway (see Section 2.4.2). • **Type of braking:** Blend of pneumatic and electrical braking. The pneumatic braking is only used when the electrical braking is not able to provide the braking force commanded.	• **Electrical braking:** Regenerative. Trains feed braking power into the railway line if possible. If the maximum voltage is reached, the power surplus is sent to rheostats. • **Maximum motoring power:** 5MW • **Maximum regenerating power:** 4MW • **Type of guidance:** Automatic Train Operation (ATO) guided trains. • **Auxiliary consumption power:** 270 kW. • **Voltage threshold for the activation of the rheostatic braking:** 1800 V

2.4.2. OPERATION CHARACTERISTICS

The headways chosen for the simulations are 5, 7 and 15 min, which respectively represent peak hour operation, off-peak hour operation and sparse traffic conditions. The train load varies depending on the headway:

- At peak hours (5 minute headway), the train is practically full of passengers and, therefore, the load is near the maximum (90% Max. Load).
- At off-peak hours (7 minute headway), the number of passengers is low (50% Max. Load).
- At sparse traffic conditions (15 minute headway), the train is practically empty and therefore the load is lower than in the other two cases (25% Max. Load).

The values for the time shifts are ($\frac{-headway}{4}$, 0, $\frac{headway}{4}$, $\frac{headway}{2}$]. These values are equally separated and the interval covered is equivalent to the headway (notice that $\frac{headway}{2}$ is equivalent to $\frac{-headway}{2}$), with the aim to explain most of the variability in the final results that can be associated with this traffic variable.

The comparison between each SP and SP0, in terms of running time and energy consumption, is shown in Figure 2-6. As can be seen, the reference for the comparison is the flat-out SP0 (minimum running time).

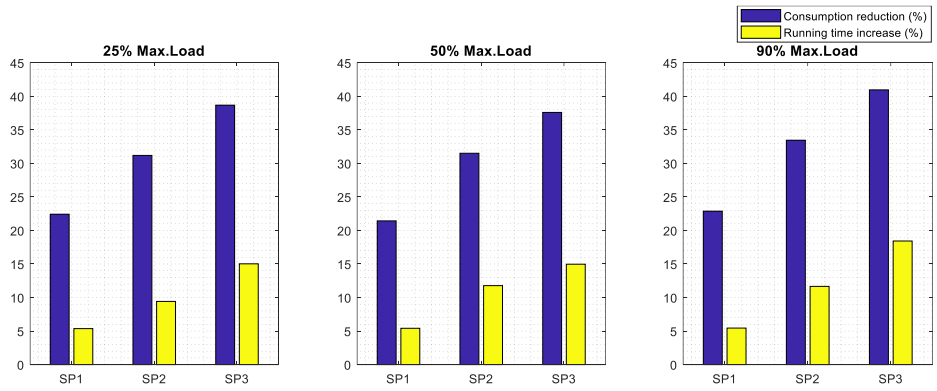

Figure 2-6: Comparisons of speed profiles SP1, SP2, and SP3 with respect to flat-out (SP0)

2.4.3. SIMULATION CHARACTERISTICS

The length of the simulation of each traffic scenario is 2600 seconds, which is the approximate time required by a train to go from one terminal station to the other. This way, a typical operation cycle is represented.

The number of scenarios simulated for each headway and time shift ensures the stabilization of the mean values of the variables of interest and is depicted in Table 2-3, together with the total number of traffic scenarios per headway. It must be noted that the criterion used to select the number of traffic scenarios (stabilization of the average values of the variables of interest) will be explained in more detail in Chapter 6, where the whole methodology to assess the infrastructure improvements will be presented.

Table 2-3: Number of different traffic scenarios simulated

	5 minute headway	**7 minute headway**	**15 minute headway**
Total number of scenarios per time shift	12	17	35
Total number of scenarios per headway	48	68	140

The sample time of the electrical simulations is 1 second, a commonly used value, as stated in (López-López, Álvaro J. et al., 2017b).

2.4.4. DESCRIPTION OF THE CASES USED FOR THE COMPARISON

Two different cases will be used to show the influence of the traffic model:

- Case A: simplified traffic model. Only one traffic scenario is used for each headway. This single traffic scenario has been obtained from the most common traffic model in the literature: no time shift, constant dwell times, no traffic regulation model and use of only one speed profile (the flat-out SP0).
- Case B: detailed traffic model for small perturbations. A high number of traffic scenarios are simulated at each headway (see Table 2-3). These traffic scenarios have been obtained from the detailed traffic model presented in this chapter: 4

different time shifts, non-constant dwell times obtained from the model presented in Section 2.3.2.1 and use of a traffic regulation model that decides among 4 different ATO speed profiles (flat-out/SP0, SP1, SP2, SP3) according to the model presented in Section 2.3.2.2.

2.4.5. ENERGY CALCULATION PROCEDURE

The results of Section 2.5 are given in terms of the energy saving obtained when simulating the installation of an RS in each traffic scenario (units in [kWh]). Energy saving has been computed and normalized for an hour (normalization consisting in converting from kWh to kWh/h). After that, the normalized results from all the scenarios with the same headway have been averaged in order to obtain an averaged normalized value of consumption for each headway. Finally, each averaged and normalized headway consumption is multiplied by the total number of hours of operation during a year at each headway (see Table 2-4), obtaining the annual consumption values required for the assessment of the traffic infrastructure improvements (operation is from 6:00 AM to $2:00^{+1}$ AM, while maintenance is from 2:00 AM to 6:00 AM).

Table 2-4: Hours of operation during a year at the different headways

	5 minute headway	7 minute headway	15 minute headway
Hours of operation during a year	3770	2782	728
Percentage of total operation	51.8%	38.2%	10%

2.5. RESULTS

As already stated, the main purpose of this section is to analyze the impact of the rail traffic model for small perturbations on the assessment of the infrastructure improvements. It does not aim to optimize neither the number, nor the location, nor the size of the RSs to be installed (task that will be tackled with the application of the nature-inspired optimization algorithms of Chapter 5). Nevertheless, some reasonable considerations related to the installation of RSs have been observed:

- After an initial study of the railway line of the case study, it was concluded that the installation of just one RS would be enough to obtain significant reductions in the rheostat losses. Therefore, only one RS has been installed per simulation (which significantly reduces the simulation time required).
- At the beginning of this study, every SS was a candidate location to install the RS. Nevertheless, the first simulations clearly showed that the locations with the best improvements in terms of energy efficiency were always at SSs 6, 7 and 8 (at kilometers 14.2, 16.3, 18.1 of Figure 2-5 respectively). Therefore, the results presented in this Section will only focus on these three possible locations (which reduces, even more, the simulation time required).

- When simulating the effect of installing an RS, different sizes have been considered: 1, 2 and 3 MW. An RS of 3 MW is underused most of the time, reason why higher sizes have not been included in this study.

The energy saving associated with the installation of the RS have been drawn from the comparison of the results obtained with and without the RS. The simulations have been carried out following the indications of Section 2.4.3 and the energy consumption have been computed according to the calculation procedure explained in Section 2.4.5.

Table 2-5: Annual energy saving in cases A and B from installing an RS of different sizes in different positions. Numerical comparison

		Number of the SS converted into RS		
RS size	**Case**	**6**	**7**	**8**
1 MW	***A***	0.45 GWh	0.47 GWh	0.48 GWh
	B	0.34 GWh	0.35 GWh	0.36 GWh
2 MW	***A***	0.68 GWh	0.69 GWh	0.68 GWh
	B	0.49 GWh	0.51 GWh	0.51 GWh
3 MW	***A***	0.75 GWh	0.75 GWh	0.73 GWh
	B	0.55 GWh	0.56 GWh	0.55 GWh

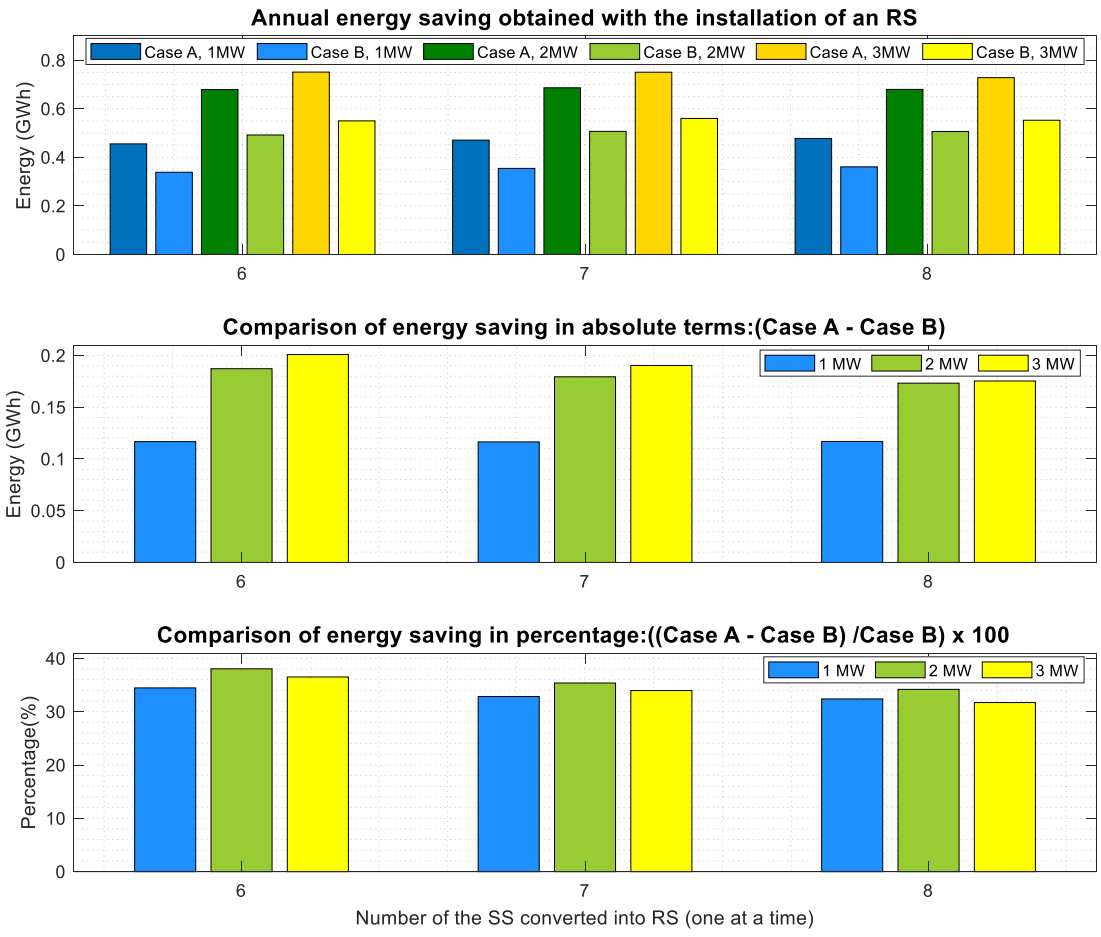

Figure 2-7: Impact of the traffic model in the evaluation of the energy saving associated with the RS installation

Table 2-5 and Figure 2-7 depicts the differences (in terms of energy saving) that appear when simulating the installation of the same infrastructure improvement (an RS installed in SS no.6,7 or 8 whose size can be 1,2 or 3 MW) with the two simulation cases presented in Section 2.4.4. The analysis of Figure 2-7 leads to the followings results:

- The differences in the savings obtained in Case A are very considerable with respect to those obtained in Case B: with exactly the same infrastructure improvement (the same RS size and location), the lack of accuracy in the traffic model of Case A leads to an overestimation in the energy saving above 30%, as can be seen in Table 2-6. This strongly affects the decision-making about the infrastructure improvements.
- The decision on the size to be installed can be also affected by the traffic model used. For example, with independence from the location of the RS, the energy saving expected with the installation of a 1 MW-RS in Case A is only achieved with the installation of a 2 MW-RS in Case B.

Table 2-6: Overestimation in the energy saving when using Case A for assessing the RS installation

No. of the SS converted into RSS	**6**	**7**	**8**
Intervals of overestimation in GWh	[0.12-0.2]	[0.12-0.19]	[0.12-0.18]
Intervals of overestimation in percentage $\left(\frac{savings\ over\text{-}estimation}{savings\ with\ Case\ B} \cdot 100\right)$	[34.5% - 38%]	[32.9% - 35.4%]	[31.7% - 34.2%]

It must be observed that the relevance of this analysis does not rely on whether the simplified model (represented by Case A) overestimates or underestimates the savings, but on the fact that there is a big difference in the results provided by this model with respect to the results provided by the model proposed in this chapter (represented by Case B) due to the lack of accuracy of the simplified model. For the case-study line and the traffic scenario selected for Case A, the difference results in an overestimation, but it is perfectly possible to obtain underestimations if another traffic scenario is selected to represent the case A (for example with values of dwell time that, although being constant, favor the utilization of the regenerated energy by synchronizing motoring and braking trains).

Since the main aim is to increase, in average, the energy saving (not for any particular scenario or situation) the results presented are given in terms of average values (see Section 2.4.5). Nevertheless, it must be noted that, although results focus on the average, the traffic variability is observed in a much more accurate way when generating a great number of scenarios with the realistic traffic model for small perturbations (although later working with their average) than when using just one

traffic scenario per headway (as happens with the simplified traffic model). Figure 2-8 illustrates this fact, representing the point cloud associated with all the scenarios simulated for the installation of a 3 MW RS at 5 minute headway with the realistic traffic model for small perturbations and comparing it to the single point that represents the scenario generated with the simplified traffic model for the same RS installation and headway (the energy saving overestimation of Case A with respect to Case B for this particular headway is of 28%).

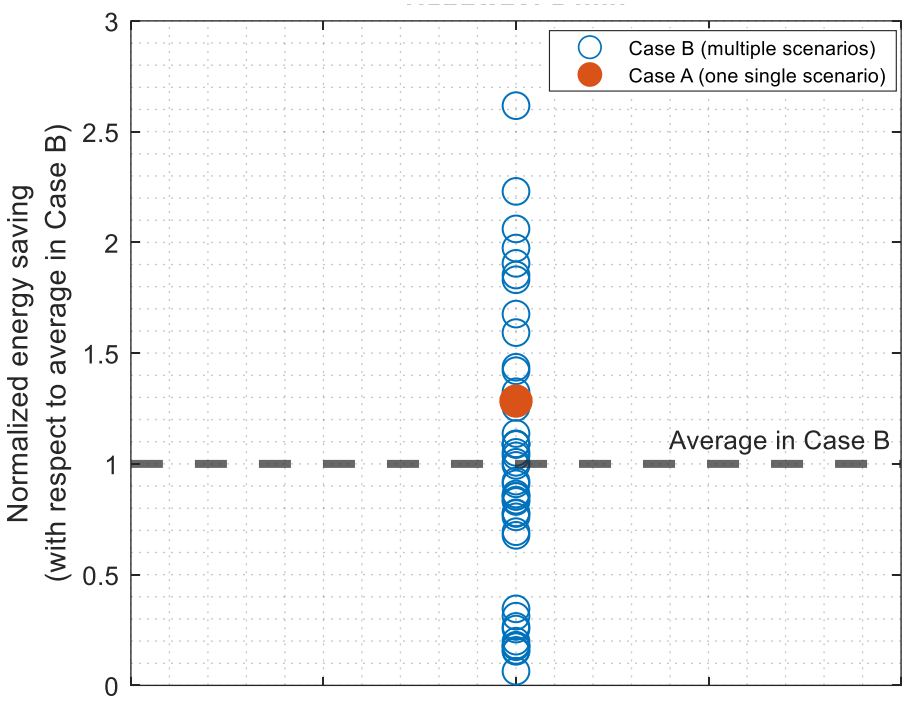

Figure 2-8: Energy saving obtained with each traffic scenario at 5 minute headway when simulating the same installation (a 3 MW RS in position no.8)

Finally, the annual energy consumption without RS is 74.06 GWh in Case A. If this value is compared with the energy saving obtained with each of the RS configurations presented in this chapter, there is a reduction in consumption between 0.6% and 1%. These savings could be enough to justify the infrastructure investment (although the final decision cannot be made without an economic analysis, which is out of the scope of this chapter). In Case B, the annual energy consumption without RS is 67.65 GWh and the energy saving obtained with the different configurations of the RS is between 0.5% and 0.8%.

2.6. CONCLUSIONS AND CONTRIBUTIONS

This chapter proves that the results obtained in electric railway simulations can be significantly different depending on the accuracy of the traffic model used. The most common traffic model in the literature is too simplified and produces inaccurate results. This lack of accuracy can have a great impact on several railway operator decisions, including those related with the installation of railway infrastructure improvements to increase the energy efficiency, which is the object of study of this PhD.

The main simplifications of the traffic model used in the literature are: the consideration that the departures of trains from each terminal station are synchronized (null time shift), the lack of stochastic models for dwell times and the use of only one speed profile, generally the flat-out one (minimum running time).

Opposite to this model, this chapter proposes a novel traffic model for small perturbations with the following features:

- Use of different values of time shift to cover the variability associated with this variable.
- Use of realistic dwell times, taking into account the stochastic behavior of this variable and the behavior of the driver, who tries to shorten the dwell time when the train is delayed.
- Use of four different speed profiles (flat-out and three additional speed profiles with higher travel times and less energy consumption).
- Integration of a traffic regulator module to decide about the speed profile to be used in each interstation.

To prove the necessity of improving the accuracy of the traffic model, the results obtained with both traffic models (the common in the literature and the proposed in this chapter) have been compared in an illustrative case study, where the installation of an RS is simulated and the energy saving associated with this installation is analyzed. The comparison showed that the simplified traffic model used in the literature can yield non-accurate results (energy saving overestimations higher than the 30% have been obtained).

CHAPTER 3

TRAFFIC MODEL FOR LARGE PERTURBATIONS

This chapter will explain the model developed during this PhD to represent traffic operation with large perturbations.

Section 3.1 summarizes the characteristics of traffic with large perturbations. Section 3.2 provides an overall description about the way the new traffic model for large perturbations proposed in this PhD must be used to assess possible railway infrastructure improvements. Section 3.3 gives the details about this traffic model. Section 3.4 contains the characteristics of the case study that is going to be used to study the influence of three different traffic models: the simplified traffic model more extended in the literature, the realistic traffic model for small perturbations proposed in Chapter 2 and the realistic traffic model for large perturbations of this chapter. Section 3.5 illustrates the effect of these perturbations on the power flow of the MTS line. Section 3.6 analyses and compares the simulation results obtained with the three models. Finally, the main conclusions are presented in Section 3.7.

3.1. INTRODUCTION

In the literature, the studies evaluating the possibility of installing ESSs or RSs hardly cover situations of traffic with small perturbations. Some of the most important traffic variables and features to include in a railway traffic model for traffic with small perturbations have been described in Chapter 2. They can be briefly summarized in:

- Dwell time: stop time at stations. In real operation, dwell time is variable because it depends on several factors, such as the number of passengers waiting at the station.
- Headway: time interval between two consecutive trains. In order to represent the different types of operation during the day (peak hours, off-peak hours, etc.) several values must be used for this variable.
- Time shift: the gap between the departure instant of trains in each direction from the terminal stations. Different time shift values must be considered to accurately represent the real traffic operation.
- Speed profiles: apart from the flat-out (minimum travel time and maximum energy consumption), the eco-driving techniques allow obtaining speed profiles with the lowest consumption for a given travel time (higher than the travel time of the flat-out).
- Traffic regulation system: determines the most appropriate speed profile to be used at each interstation (travel between two stations) by each train in order to accomplish with the target schedule.

Only the traffic model for small perturbations from Chapter 2 takes into account all of them but, as can be supposed, it does not observe situations of traffic with large perturbations.

Traffic with large perturbations presents major delays at certain points of the line, which produces a mismatch in the distance among trains: there will be stretches of track where trains will accumulate and other stretches where trains will be too separated.

This way, in the part of the line where trains are accumulated, the headway is lower than the nominal one (without large perturbations) and trains are so close one to the other that the signalling system is activated and forces the speed profile of the "pursuing" train (the one that goes behind) to be perturbed. This means that the speed profile is affected by speed limitations and eventually the train may stop in an interstation. On the other hand, in the part of the line where trains are separated, the headway is higher than the nominal one and trains try to recover the accumulated delay. In this part of the line, trains' speed profiles are not perturbed by the trains that go ahead and the traffic regulation system will send the flat-out speed profile to be executed by trains (in order to recover the delay).

Due to the perturbed operation, the line consumption profile is very different from the nominal one:

- Trains consuming and regenerating energy are less uniformly distributed than in nominal operation, as consumption and regeneration accumulate in the part of the line where trains are very close one to the other.

- Consumption profiles in the perturbed interstations (both with speed limits activated and with intermediate stops) largely differ from those of the non-perturbed ones.

Traffic with large perturbations is usual in some metro lines at peak hours and, generally, trains accumulate at the terminal stations of a line. This is the reason why it is very relevant to analyze the impact that these traffic situations can have on the consumption and on the potential energy saving that can be obtained with the installation of infrastructure improvements.

3.2. MODEL TO ASSESS INFRASTRUCTURE IMPROVEMENTS TAKING INTO ACCOUNT LARGE PERTURBATIONS

Figure 3-1 depicts the model for the assessment of infrastructure improvements when including large perturbations in the traffic modelling.

The model and the steps of the assessment are the same as the presented in Section 2.2, with the exception of the traffic model used, which now also observes traffic scenarios with large perturbations. Therefore, the new set of traffic scenarios generated by the traffic model represents in an accurate way the real operation of the railway line in both traffic conditions: small and large perturbations.

3.3. TRAFFIC MODELLING

The traffic model explained in this chapter adds, with respect to the model presented in Chapter 2 , traffic scenarios with large perturbations, in order to take into account all type of traffic situations (along the day, there are moments when the traffic has small perturbations and moments when the traffic may have large perturbations, generally during peak hours). This is a total novelty in the literature that will improve the realism and the accuracy of the energy saving results provided by the model, which, in turn, will facilitate the decision-making process about the most appropriate infrastructure improvements to install.

3.3.1. TIMETABLE GENERATOR AND DELAYS

As depicted in Figure 3-1, the traffic scenarios with large perturbations are generated from two main inputs: the **commercial timetables** and the **delays** at certain track points.

The ***timetable generator*** (see Section 2.3.1) generates the **commercial timetables**. As already explained, these timetables have the information of trains' arrivals and departures when there are no deviations. In off-peak operation (and therefore, with the majority of headways), only small perturbations take place and, consequently, the traffic model that must be used to obtain the representative traffic scenarios is the traffic model for small perturbations of Chapter 2. Large perturbations may appear in peak operation, when the headway is very small. Indeed, in certain metro lines these

large perturbations appear not just occasionally, but are typical during peak operation. In these cases, the model for large perturbations proposed in this paper must be applied to obtain the representative traffic scenarios. The reason why large perturbations usually appear at small headways is that the number of passengers is very high and, as a consequence, dwell times extends. In addition, the number of trains is also very high. The combination of these factors increases considerably the probability of trains to accumulate at a certain stretch of track (usually close to a terminal station) and generate big **delays**.

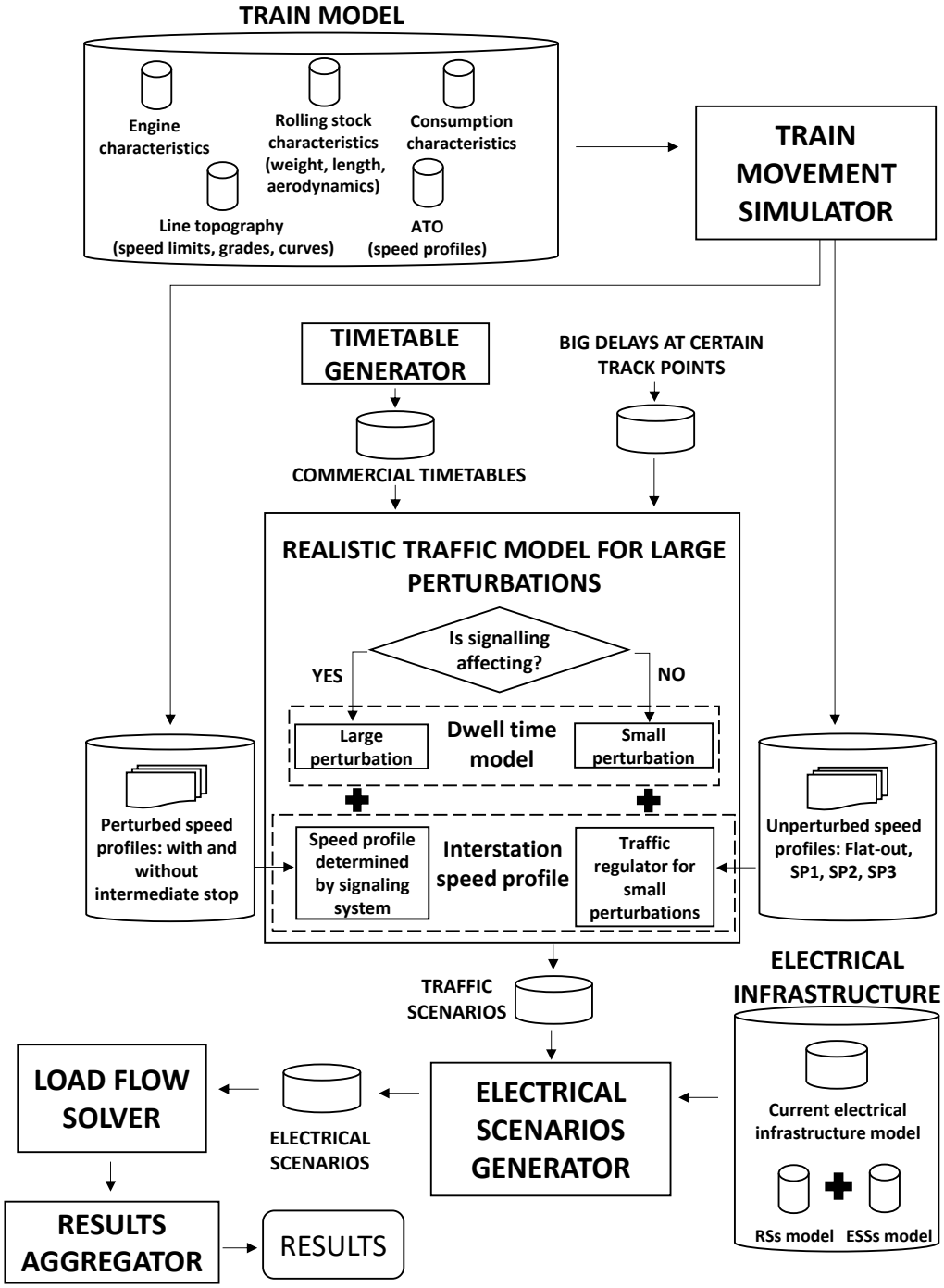

Figure 3-1: Model for the assessment of railway infrastructure improvements including a realistic traffic model for large perturbations

3.3.2. REALISTIC TRAFFIC MODEL FOR LARGE PERTURBATIONS

The following lines will describe qualitatively the management of traffic with large perturbations emulated by the realistic traffic model for large perturbations designed in this thesis. The details of this model will be given in Sections 3.3.2.1 and 3.3.2.2.

Delays make trains get closer one to another, forcing the signalling system to be activated in order to maintain the minimum safety distance between consecutive trains (minimum interval). The activation of the signalling system has two main consequences:

- Dwell times at stations with values considerably higher, overpassing the nominal ones (dwell time with large perturbation in Figure 3-1).
- Perturbed speed profiles: when a train has departed from a station and is affected by the train that goes ahead, the signalling system reduces the speed limits affecting the train and this could even lead to stop the train in the interstation. Therefore, the traffic model proposed observes two levels of perturbed speed profiles, depending on the location of the previous train: speed profiles with speed limits lower than the nominal ones (perturbed speed profiles without intermediate stop in Figure 3-1) and speed profiles that make stops in the interstation (perturbed speed profiles with intermediate stop in Figure 3-1).

As a consequence of the delays, one part of the line has an accumulation of trains and the signalling system affecting the operation, while another part of the line has the trains more distanced from each other than in normal operation. Therefore, two 'operation modes' must be clearly distinguished:

- 'Large perturbation mode' in the part of the line with accumulation of trains and the signalling system affecting dwell times and driving.
- 'Small perturbation mode' in the rest of the line. This operation mode has the following characteristics:
    - The signalling system is not affecting the driving of the trains.
    - The traffic regulator tries to recover the accumulated delay by selecting the fastest speed profiles (from the set of unperturbed speed profiles of Figure 3-1). Once having recovered the delay, the traffic regulator will behave according to the rules of the traffic model for small perturbations (see Section 2.3.2.2).
    - Dwell time at stations are always within the nominal limits and only affected by small deviations (dwell time with small perturbation in Figure 3-1). These small deviations model the variability associated with the number of passengers waiting at the station and with the driver's response time.

3.3.2.1. DWELL TIME MODEL

Figure 3-2 graphically represents the model for the time regulation at station and for the traffic noise. It calculates the dwell time for each train $\boldsymbol{i}$ at each passenger station $\boldsymbol{j}$.

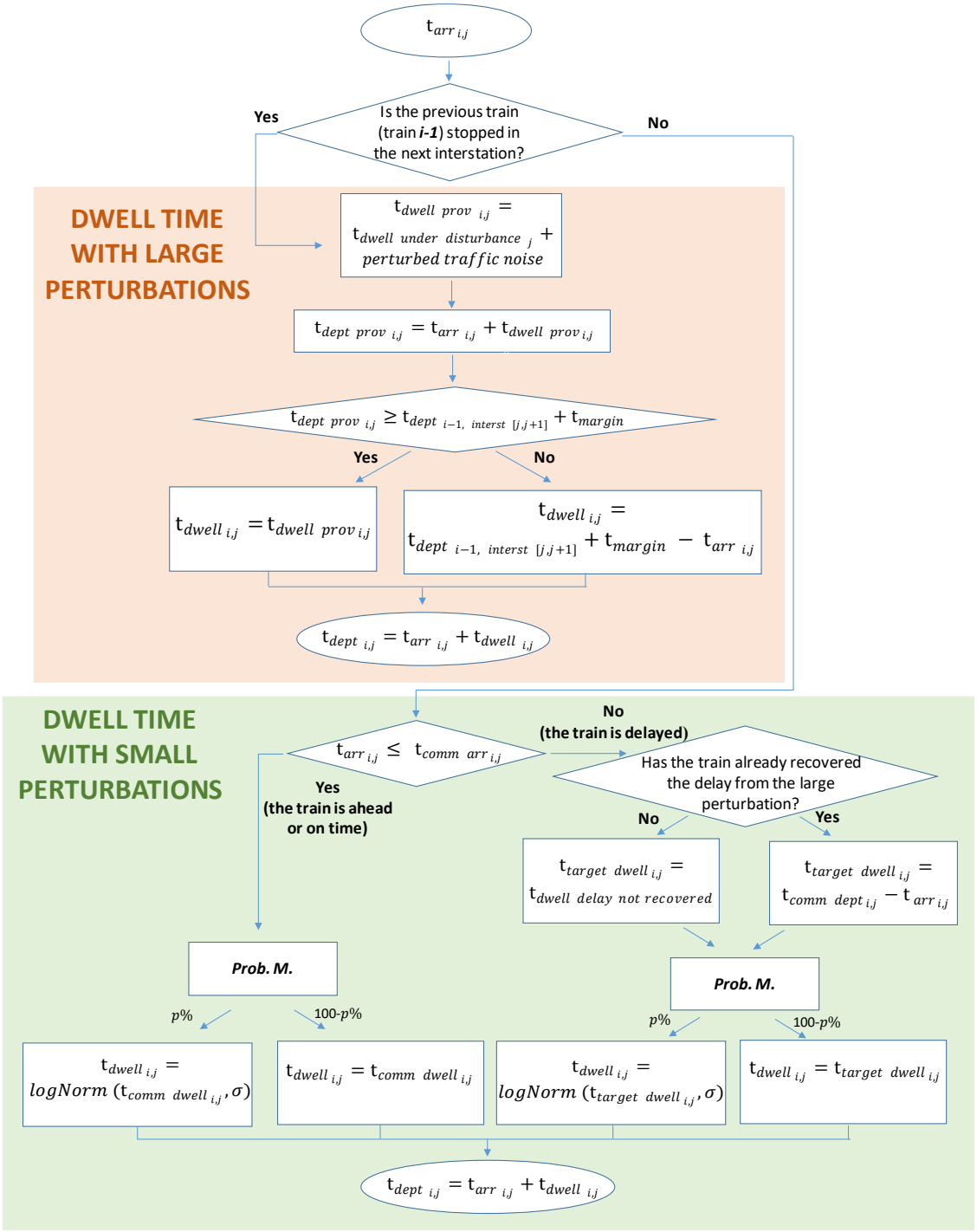

Figure 3-2: Dwell time model

The inputs for this model are:

- The arrival time of train $\boldsymbol{i}$ at station $\boldsymbol{j}$ ($t_{arr_{i,j}}$).
- The location of the previous train (train $\boldsymbol{i-1}$).
- The arrival time of train $\boldsymbol{i}$ at station $\boldsymbol{j}$ according to the commercial timetable ($t_{comm\ arr_{i,j}}$).
- The departure time of train $\boldsymbol{i}$ from station $\boldsymbol{j}$ according to the commercial

timetable ($t_{comm\ dept_{i,j}}$).

- The dwell time of train $\boldsymbol{i}$ in station $\boldsymbol{j}$ according to the commercial timetable ($t_{comm\ dwell_{i,j}}$).

The output is the departure time of train $\boldsymbol{i}$ from station $\boldsymbol{j}$ ($t_{dept_{i,j}}$). As can be seen, the way to determine the output will vary depending on the operation mode: large or small perturbation.

3.3.2.1.1. Dwell time with large perturbations

If train $\boldsymbol{i}$ arrives at station $\boldsymbol{j}$ and the previous train (train $\boldsymbol{i-1}$) is stopped in the immediately following interstation (interstation $\boldsymbol{j,j+1}$), train $\boldsymbol{i}$ cannot depart from station $\boldsymbol{j}$ until train $\boldsymbol{i-1}$ resumes the travel because the signalling system does not allow the departure. The consequence is that the dwell time of train $\boldsymbol{i}$ at station $\boldsymbol{j}$ increases significantly (dwell time with large perturbation in Figure 3-1).

Perturbed dwell times with values much higher than the nominal ones are called $t_{dwell\ under\ disturbance}$ ($t_{dwell\ under\ disturbance_j}$ particularized for station $\boldsymbol{j}$), to which some traffic noise called 'perturbed traffic noise' is added. The perturbed traffic noise is represented by a uniform distribution and aims to include small variations in the train's departure associated with driver's reactions (e.g.: some drivers react faster than others when the traffic signal allows them to depart).

The departure time obtained is provisional ($t_{dept\ prov\ i,j}$) and it is necessary to check if train $\boldsymbol{i-1}$ has resumed its travel with a time margin (t_{margin}) before allowing train $\boldsymbol{i}$ to depart ($t_{dept\ prov\ i,j} \geq t_{dept\ i-1,\ interst[j,j+1]} + t_{margin}$). This time margin is the minimum interval of time that train $\boldsymbol{i}$ must wait after train $\boldsymbol{i-1}$ has departed and it is imposed by the signalling system. If this condition is fulfilled, the provisional departure time is validated ($t_{dwell_{i,j}} = t_{dwell\ prov_{i,j}}$). If not, the dwell time changes its value in order to comply with the time margin stablished by the signalling system ($t_{dwell_{i,j}} = t_{dept\ i-1,\ interst[j,j+1]} + t_{margin} - t_{arr\ i,j}$).

3.3.2.1.2. Dwell time with small perturbations

If train $\boldsymbol{i}$ arrives at station $\boldsymbol{j}$ and the previous train (train $\boldsymbol{i-1}$) is not stopped in the immediately following interstation (interstation $\boldsymbol{j,j+1}$), the moment of departure of train $\boldsymbol{i}$ from station $\boldsymbol{j}$ is not determined by train $\boldsymbol{i-1}$**.** In such cases, the dwell time is modelled according a lognormal distribution (Martínez et al., 2007). The traffic noise associated with this distribution will be called 'non-perturbed traffic noise' and tries to represent the small perturbations in dwell time, mainly due to the fluctuating number of passengers at the station.

The mean value of the lognormal distribution will vary depending on the state of the traffic. This variation in the mean value represents the driver's behavior.

- If train $\boldsymbol{i}$ is ahead or on time ($t_{arr_{i,j}} \leq t_{comm\ arr_{i,j}}$), the mean value of the distribution is constant and equal to the dwell time of the commercial timetable ($t_{comm\ dwell_{i,j}}$).

- If train $\boldsymbol{i}$ is delayed when arriving to station $\boldsymbol{j}$ ($t_{arr_{i,j}} > t_{comm\ arr_{i,j}}$) there are two possibilities for selecting the mean value of the distribution:
    - If the big delay produced by the accumulation of trains is recovered, the delay of train $\boldsymbol{i}$ is due to small perturbations and, therefore, the mean value of the distribution corresponds to that required to recover a small delay and depart from the station at the moment specified by the commercial timetable ($t_{target\ dwell_{i,j}} = t_{comm\ dept_{i,j}} - t_{arr_{i,j}}$).
    - If the big delay produced by the accumulation of trains is still not recovered, the delay of the train is too big (it cannot be recovered in just one or two stations). Therefore the mean value of the distribution ($t_{dwell\ delay\ not\ recovered}$) is close to the minimum admissible dwell time (the time required for opening and closing the doors plus some time margin for passengers to get out or into the train).

Finally, a probability model (***Prob. M.***) decides whether to obtain the values of the dwell time from the lognormal distribution (with a probability $p\%$) or directly from the mean value itself (with a probability 100-$p\%$). This represents that sometimes the number of passengers is very low and then, the real dwell time ($t_{dwell_{i,j}}$) can be exactly equal to the target time.

3.3.2.1.3. Dwell time in terminal stations

Trains' departures from terminal stations in the small perturbation mode are determined by the commercial timetable, as delays are always recovered before trains begin their journey in the new direction. Therefore, the dwell time in terminal stations is defined as the difference between the departure instant (determined by the commercial timetable) and the moment of arrival at the terminal station (determined by the realistic traffic model).

This situation changes qualitatively in the large perturbation mode, where there are major delays produced by large perturbations. In these cases, the delayed trains depart from the terminal station as soon as possible in order to recover part of the delay accumulated, and not in the moment determined by the commercial timetables (although never before it). Indeed, it is very likely that, in case of having very big delays, the trains have not even arrived to the terminal station in the moment when, according to the commercial timetables, they would have to depart from it. This means that, in the large perturbation mode, the moment of departure from the terminal station is also determined by the realistic traffic model, according to Equation (3-1).

$$t_{dept\ i,terminal\ station} = t_{arr\ i,terminal\ station} + t_{turn.min.} + noise \qquad \textbf{(3-1)}$$

where:

- $t_{dept\ i,terminal\ station}$ is the departure time of train $\boldsymbol{i}$ from the terminal station.
- $t_{arr\ i,terminal\ station}$ is the arrival time of train $\boldsymbol{i}$ to the terminal station.
- $t_{turn\ min.}$ is the minimum turning time, defined as the minimum admissible time

between the departure instant and the moment of arrival at the terminal station (this concept will be explained in detail in Chapter 4).

- $noise$ is a parameter whose value is determined by a uniform distribution between 0 and x seconds. It represents that the moment of departure can be slightly delayed.

3.3.2.2. SPEED PROFILES

Depending on the level of perturbation in traffic operation, the speed profile between two stations is determined by the traffic regulation system or by the signalling system.

3.3.2.2.1. Speed profiles in small perturbation mode

If the train is under the so called small perturbation mode, the traffic regulator must select among a set of four predesigned and unperturbed speed profiles (see Figure 3-1). The speed profile selected by the traffic regulator is sent to the train, which applies it without being affected by the previous train (as the signalling system is not activated).

If the big delay produced by the accumulation of trains has not been recovered yet, the traffic regulator will always choose the fastest speed profile (the flat-out one), although it is the most energy consuming. Once the big delay produced by the accumulation of trains is recovered, the traffic regulator will choose the most appropriate unperturbed speed profile by finding the best balance between travel time and energy consumption. This balance is explained in detail in Section 2.3.2.2. As a reminder, the following lines summarize it:

- If the train departs with some delay from a station (with respect to the commercial timetable), a faster and more energy-consuming speed profile than the one used in the commercial timetable will be selected. Nevertheless, using a slower and less energy-consuming speed profile than the required to recover the delay will be accepted if this delay is small enough to be recovered in the next station.
- If the train departs in advance from a station (with respect to the commercial timetable), a slower and less energy consuming speed profile than the one used in the commercial timetable will be selected.

3.3.2.2.2. Speed profiles in large perturbation mode

When a train is in the stretch of track where trains are accumulated, its speed profile is affected by the signalling system, in order to keep enough distance to the previous train. To represent the behavior of the line in these cases, the model proposed in this chapter makes use of a speed profile within the set of perturbed speed profiles (see Figure 3-1). The perturbations on the speed profile can go from activating speed limits to making intermediate stops.

- **Perturbed speed profile with an intermediate stop:** Figure 3-3 graphically explains the application of this type of perturbed speed profile:
  - *Moment no.1 of Figure 3-3*: train $\boldsymbol{i}$ is at station $\boldsymbol{j}$ and the previous train (train $\boldsymbol{i-1}$) is stopped at station $\boldsymbol{j+1}$. Train $\boldsymbol{i}$ is allowed to depart from station $\boldsymbol{j}$ (the traffic signal that regulates the departures from station $\boldsymbol{j}$ is green) but it has no permission to enter in the following station (the traffic signal that regulates the arrivals at station $\boldsymbol{j+1}$ is red).
  - *Moment no.2 of Figure 3-3*: train $\boldsymbol{i}$ departs from station $\boldsymbol{j}$ with an unperturbed speed profile. At the moment of departure it has no permission to enter at station $\boldsymbol{j+1}$, because train $\boldsymbol{i-1}$ is still stopped at that station.
  - *Moment no.3 of Figure 3-3:* once train $\boldsymbol{i}$ has made part of the travel between stations $\boldsymbol{j}$ and $\boldsymbol{j+1}$ (interstation $\boldsymbol{j, j+1}$), it still does not have permission to enter at station $\boldsymbol{j+1}$ (the traffic signal that regulates the arrivals at station $\boldsymbol{j+1}$ is still red). As a consequence, train $\boldsymbol{i}$ must stop at a certain point of interstation $\boldsymbol{j, j+1}$**.**
  - *Moment no.4 of Figure 3-3*: train $\boldsymbol{i-1}$ departs from station $\boldsymbol{j+1}$ and train $\boldsymbol{i}$ remains stopped.
  - *Moment no.5 of Figure 3-3*: train $\boldsymbol{i}$ resumes its trip after a minimum time interval has passed from the departure of train $\boldsymbol{i-1}$ from station $\boldsymbol{j+1}$, so that the arrival of train $\boldsymbol{i}$ at station $\boldsymbol{j+1}$ is allowed. The moment of departure of train $\boldsymbol{i}$ from its intermediate stop is defined by Equation (3-2).

$$t_{dept\ i,interst_{[j,j+1]}} = t_{dept\ i-1,j+1} + t_{margin} \quad \textbf{(3-2)}$$

    where:

    - $t_{dept\ i,interst_{[j,j+1]}}$ is the moment when train $\boldsymbol{i}$ departs from the intermediate stop between stations $\boldsymbol{j}$ and $\boldsymbol{j+1}$.
    - $t_{dept\ i-1,j+1}$ is the moment when train $\boldsymbol{i-1}$ departs from station $\boldsymbol{j+1}$.
    - t_{margin} is the time margin, given by the signalling system, that train $\boldsymbol{i}$ must wait before resuming its trip.

  In the particular case of the last interstation of a track with turn-back maneuver in front of the terminal station, the train would stop before the railroad switch and t_{margin} includes the time required to move it. Figure 3-4 provides the graphical explanation of this particular restriction.

- **Perturbed speed profile without intermediate stop:** when train $\boldsymbol{i}$ and train $\boldsymbol{i-1}$ are not so close one to the other so as to stop train $\boldsymbol{i}$, there is no need to apply an intermediate stop but maybe it is still necessary to activate some speed limits. Particularly, the speed limitations are applied to train $\boldsymbol{i}$ if the minimum interval between train $\boldsymbol{i}$ and train $\boldsymbol{i-1}$ is not complied with the use of unperturbed speed profiles.

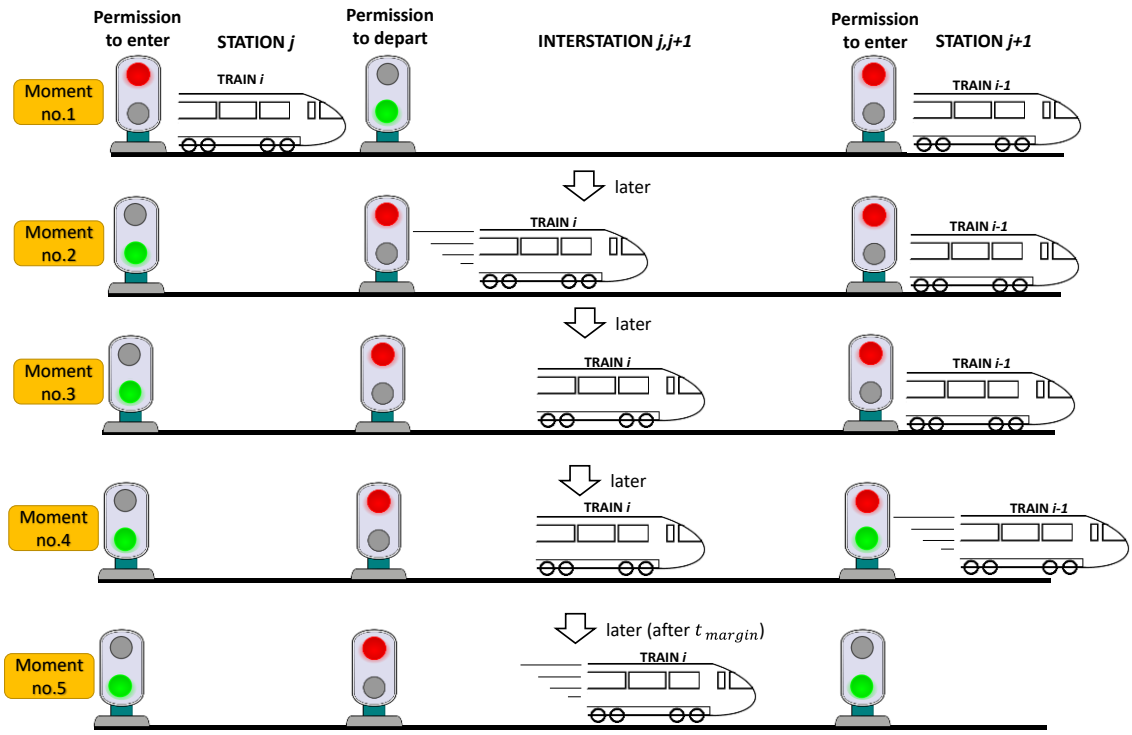

Figure 3-3: Application of perturbed speed profile with intermediate stop

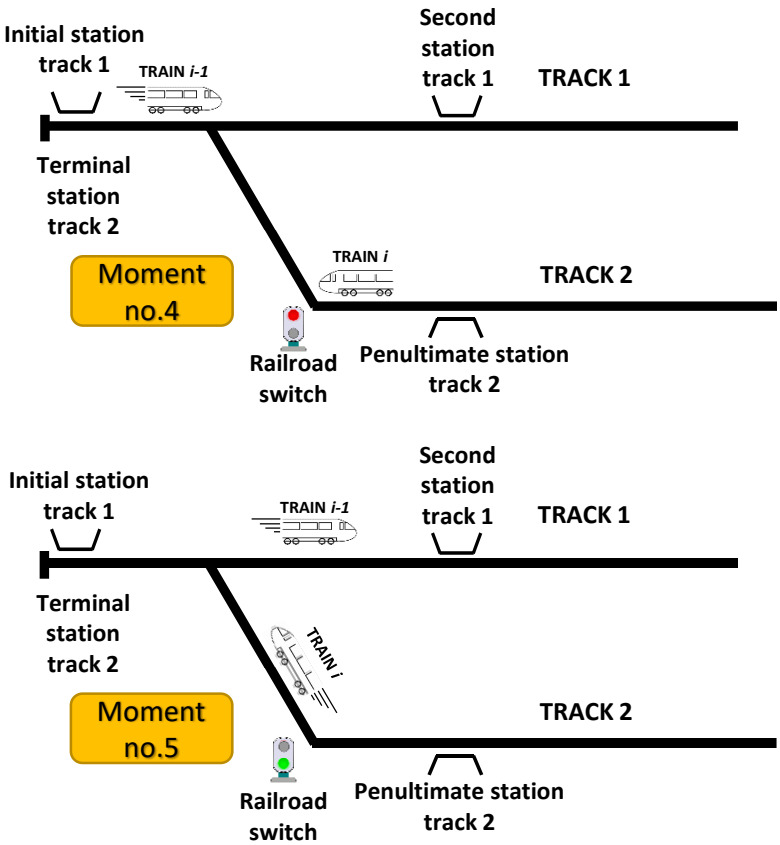

Figure 3-4: Application of perturbed speed profile with intermediate stop in the particular case of the last interstation of a track with turn-back maneuver in front of the terminal station

3.4. CASE STUDY

3.4.1. TOPOLOGY, INFRASTRUCTURE AND ROLLING STOCK CHARACTERISTICS

The case study, in terms of topology, infrastructure and rolling stock characteristics, is the same as the one presented in Section 2.4.1. The only difference is that, in order to highlight the differences, in terms of energy saving, that can appear with the different models that are going to be compared in Section 3.6, the train auxiliary consumption power has been reduced to 200 kW (nevertheless, it must be noted that this value has also been obtained from real data).

3.4.2. OPERATION CHARACTERISTICS

Although this chapter is focused on the traffic with large perturbations, in Section 3.6 some of the comparisons and results presented will also include situations of traffic with small perturbations, in order to observe all type of traffic conditions. In this section, the operation characteristics for both traffic conditions are explained.

Four different headways have been chosen: 3.5, 5, 7 and 15 minute headways. Simulations with small and large perturbations will be performed with 3.5 minute headway, while only simulations with small perturbations will be performed with the rest of headways. As happened in Section 2.4.2, train load varies depending on the headway:

- At peak hours, represented by 3.5 minute headway, and semi-peak hours, represented by 5 minute headway, the number of passengers is very high and train load is 90% of the maximum load.
- At off-peak hours, represented by 7 minute headway, the number of passengers is less and train load is 50% of the maximum load.
- At sparse traffic conditions, represented by 15 minute headway, the train is almost empty, thus its load is 25% of the maximum load.

When generating the commercial timetables with the headway (see Figure 3-1), the values of the time shift change depending on the traffic conditions:

- In traffic with small perturbations, the value of the time shift is relevant. This is because part of the variability in the results obtained with the different scenarios simulated is due to this variable (the rest of this variability is associated with the non-constant dwell time and with the use of different speed profiles). The same four different headways as the ones used in Section 2.4.2 have been selected: $(\frac{-headway}{4}, 0, \frac{headway}{4}, \frac{headway}{2}]$.
- In traffic with large perturbations it has been explained that the moment of departure from the terminal stations is determined by Equation (3-1) and not by the commercial timetables. Consequently, the time shift is not very relevant in these cases, since changing the time shift means to change the moment of departure from the terminal stations in the commercial timetables (a more detailed explanation about the relationship between these two variables –time

shift and departures from terminal stations- will be given in Section 4.1). Therefore, commercial timetables have been obtained considering null time shift (the standard one).

All speed profiles have been simulated with the traffic movement simulator explained in (Domínguez et al., 2011). It is necessary to distinguish between perturbed and non-perturbed speed profiles:

- There is a set of four predesigned and unperturbed speed profiles: flat-out, SP1, SP2, SP3. They are the same as the presented in Section 2.4.2. Just as a reminder, the flat-out has the lowest travel time and the highest energy consumption, while the rest of speed profiles (SP1, SP2, SP3) require higher travel times and lower consumptions (in terms of travel time: SP1< SP2 < SP3 and in terms of energy consumption SP1> SP2 > SP3, for more details see Figure 2-6).
- For the case study of this chapter, the delays that create the accumulation of trains are introduced at the end of track no.2 (see Figure 3-5). As a consequence, the interstations with perturbed speed profiles are the last three interstations of this track and both types of perturbed speed profiles -with and without intermediate stops- have been simulated.

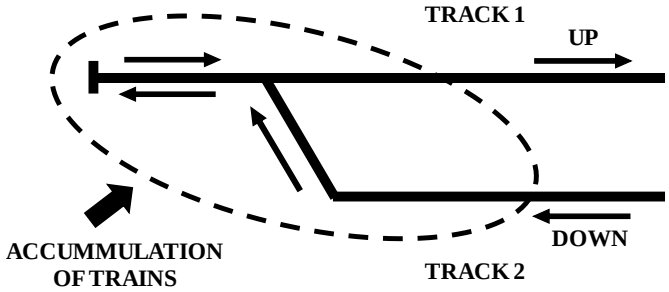

Figure 3-5: Stretch of track with the accumulation of trains

Figure 3-6 shows an example of the speed-time and power-time diagrams of different speed profiles available for a specific interstation.

For the sake of clarity, not all the speed profiles are shown, but the followings:

- The speed profile used in the nominal timetable: NOM-SP (NOM-SP= SP1).
- An unperturbed speed profile faster (and more energy consuming) than the used in the nominal timetable: FLAT-OUT.
- An unperturbed speed profile slower (and less energy consuming) than the used in the nominal timetable: ECO- SP (ECO- SP=SP3).
- A perturbed speed profile with intermediate stop: PERT-SP.

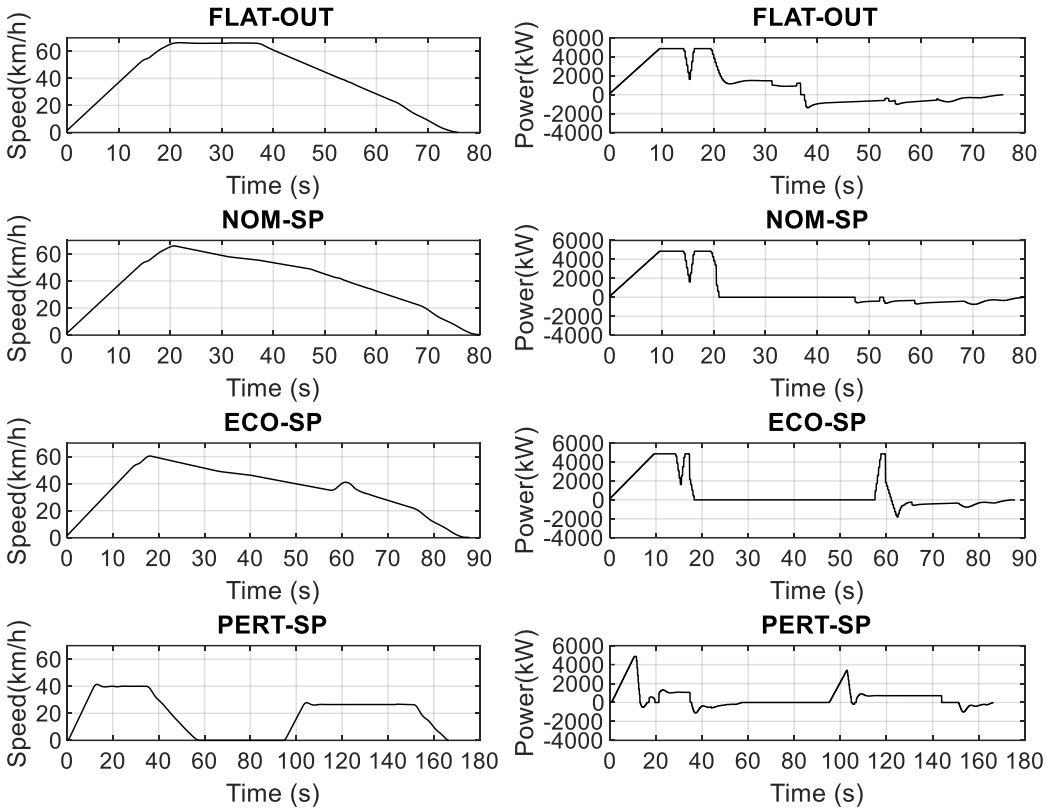

Figure 3-6: Speed-time and power-time diagrams of different speed profiles available for a specific interstation

3.4.3. SIMULATION CHARACTERISTICS

The number of scenarios simulated for each headway (and time shift if applicable) is depicted in Table 3-1. The amount of scenarios selected ensures the stabilization of the mean values of the variables of interest (specially the energy saving).

Table 3-1: Number of different traffic scenarios simulated per headway

	3.5 minute headway with large perturbations	3.5 minute headway with small perturbations	5 minute headway	7 minute headway	15 minute headway
Number of scenarios per time shift	(-)	32	32	37	55
Number of scenarios per headway	70	128 (=32x4)	128 (=32x4)	148 (=37x4)	220 (=55x4)

As in Section 2.4.3, the criteria to select the simulation length is to approximately cover the time required by a train to go from one terminal station to the other. Since the line is the same as in the case study of Chapter 2, the simulation length is also 2600 seconds. Finally, the sample time of the electrical simulations is also the same: 1 second.

3.4.4. DESCRIPTION OF THE CASES USED FOR THE COMPARISON

In Section 3.6, the influence of the traffic with large perturbations is going to be analyzed in two steps:

- In the first step, a direct comparison among the energy saving obtained at 3.5 minute headway (peak hour) in three different cases is provided. This comparison will show the clear impact that the different traffic conditions represented in each case have on the possible energy saving associated with the installation of an RS. This comparison will be called ***Peak-H Comparison.*** The three cases defined for this comparison are:
  - *PEAK-H.I*: simplified traffic model. This case represents the results obtained from the most common traffic model used in the literature, which is very simplified. It does not observe any kind of traffic perturbation (neither large nor small) and therefore, there is only one scenario, obtained with constant dwell time, no time shift and the flat-out speed profile.
  - *PEAK-H.II*: traffic model for small perturbations. This model, explained in Section 2.3, includes the use of different time shifts, variable dwell times and a traffic regulator which decides among a set of unperturbed speed profiles. A high number of scenarios is simulated (see Table 3-1).
  - *PEAK-H.III*: traffic model for large perturbations (presented in Section 3.3). A high number of scenarios is simulated (see Table 3-1).
- In the second step, a global comparison of the annual energy saving obtained in three different cases is provided. This comparison will be called ***Annual Comparison*** and takes into account all possible headways: 3.5, 5, 7 and 15 minute headways. The three cases defined for this comparison are:
  - *ANNUAL.I*: is the extension of case *PEAK-H.I* to all the headways. Therefore, there is only one scenario per headway, obtained with constant dwell time, no time shift and the flat-out speed profile.
  - *ANNUAL.II*: is the extension of case *PEAK-H.II* to all the headways: 3.5, 5, 7, and 15 minute headways with traffic operation with small perturbations represented by the simulations made with the traffic model for small perturbations explained in Section 2.3. A high number of scenarios is simulated for each headway (see Table 3-1).
  - *ANNUAL.III*: traffic model with small and large perturbations, depending on the headway chosen: with 3.5 minute headway the traffic is supposed to have large perturbations and is represented by the simulations made with the traffic model for large perturbations explained in Section 3.3, while with 5, 7, and 15 minute headways the traffic is supposed to have small perturbations and is represented by the simulations made with the traffic model for small perturbations explained Section 2.3. A high number of scenarios is simulated for each headway (see Table 3-1).

3.4.5. ENERGY CALCULATION PROCEDURE

The results of 3.6 are given in terms of the energy saving obtained when simulating the installation of an RS in each traffic scenario generated by the traffic models (units in

[kWh]). Energy saving has been computed and normalized for an hour (normalization consisting in converting from kWh to kWh/h). In case of having more than one traffic scenario simulated per headway (cases *PEAK-H.II*, *PEAK-H.III*, *ANNUAL.II*, *ANNUAL.III*), the normalized results from all the scenarios with the same headway have been averaged in order to obtain the averaged normalized energy saving for each headway. Finally, in the case of the ***Annual Comparison,*** the annual energy saving has been computed by multiplying the averaged and normalized energy saving of each headway by the annual number of hours of operation at the correspondent headway, depicted in Table 3-2 (operation is from 6:00 AM to $2:00^{+1}$ AM, while maintenance is from 2:00 AM to 6:00 AM).

Table 3-2: Distribution of the hours of operation during a year at the different headways

	3.5 minute headway	**5 minute headway**	**7 minute headway**	**15 minute headway**
Hours of operation in a year	1885	1885	2782	728
Percentage of total operation	25.9%	25.9%	38.2%	10%

3.5. IMPACT OF PERTURBATIONS IN THE POWER FLOW ALONG THE LINE

Just to illustrate the effect of perturbations on energy consumption, Figure 3-7 shows the voltage and the power consumption of an RS in two consecutive snapshots (separation in time of 1 second) as well as the power consumption and voltage profiles of the two trains closest to the RS.

This figure has been obtained by comparing the same two consecutive snapshots in two different traffic scenarios with the same headway: one scenario with large perturbations (in blue color) and other scenario with small perturbations (in red color). For each scenario, one train is in track no.1 (represented by a circle) and the other train is in track no.2 (represented by a cross).

The first subplot represents the positions of the trains along the line and the position of the RS. The second and third subplots are bar graphs that represent, respectively, power consumption (regeneration if the value is negative) and voltages of the trains (the voltage is represented in parts per unit ***(p.u.)***, with the no-load voltage (1650 V) as reference. To facilitate the identification of a train with its power and voltage, the x-axis of these subplots are exactly equal to the x-axis of the first subplot. Therefore, the bar representing the power or the voltage of a train is placed in the position of that train and has the color associated with the scenario to which it corresponds. Finally, the subplot in the bottom-left represents the power demanded (sent back to the grid if the value is negative) from the RS in each scenario and the subplot in the bottom-right represents the voltage of the RS in each scenario.

Focusing on the **first snapshot** (***Snapshot no.1***), the train that is in track 2 is in a very similar situation in both scenarios: approximately in the same position and coasting

(consumption is 200 kW, which corresponds to the auxiliary consumption). On the contrary, the train that is in track 1 is in a very different situation in each scenario:

- **In the traffic scenario with small perturbations,** the train is **in traction phase**, as it has already departed from the station where the RS is located.
- **In the traffic scenario with large perturbations**, the train is arriving at that station and, therefore, it is **in braking phase** and regenerating energy.

The reason for this big difference is given bellow:

- In the traffic scenario with large perturbations, the train in track no. 2 has recovered every previous delay and, therefore, its situation is similar to that of the train of the same track in the traffic scenario with small perturbations.
- In the traffic scenario with large perturbations, the train in track no.1 is very delayed and, consequently, its situation (regarding position and power consumption) is absolutely different from that of the train of the same track in the traffic scenario with small perturbations.

This difference is even bigger regarding the RS:

- **In the traffic scenario with large perturbations, there is not power demanded, neither sent back to the grid in the RS**. This is because there is a balance between the regeneration of the train in track no.1, the auxiliary consumption of the train in track no.2 and other trains more distant to the RS (that have smaller influence).
- **In the traffic scenario with small perturbations, the power demanded to the RS is higher than 3 MW**. Although the sum of the consumptions of the two trains that appear in Figure 3-7 is higher than the power demanded to the RS, it can be assumed that a small part of the power consumed by these two trains come from more distant trains in braking phases and from other tractions substations.

When analyzing the **second snapshot** (***Snapshot no.2***), the situation is the same from the point of view of the trains, except that the power regeneration of the train in track no.1 of the traffic scenario with large perturbations has increased considerably. As there are no close trains able to use this regenerated energy (the closest train is the train in track no.2 and it is coasting), there is an excess of regenerated energy that is sent to the RS. Therefore, while in the traffic scenario with small perturbations the RS is providing power to the catenary, in the traffic scenario with large perturbations the RS is sending more than 2 MW back to the utility grid.

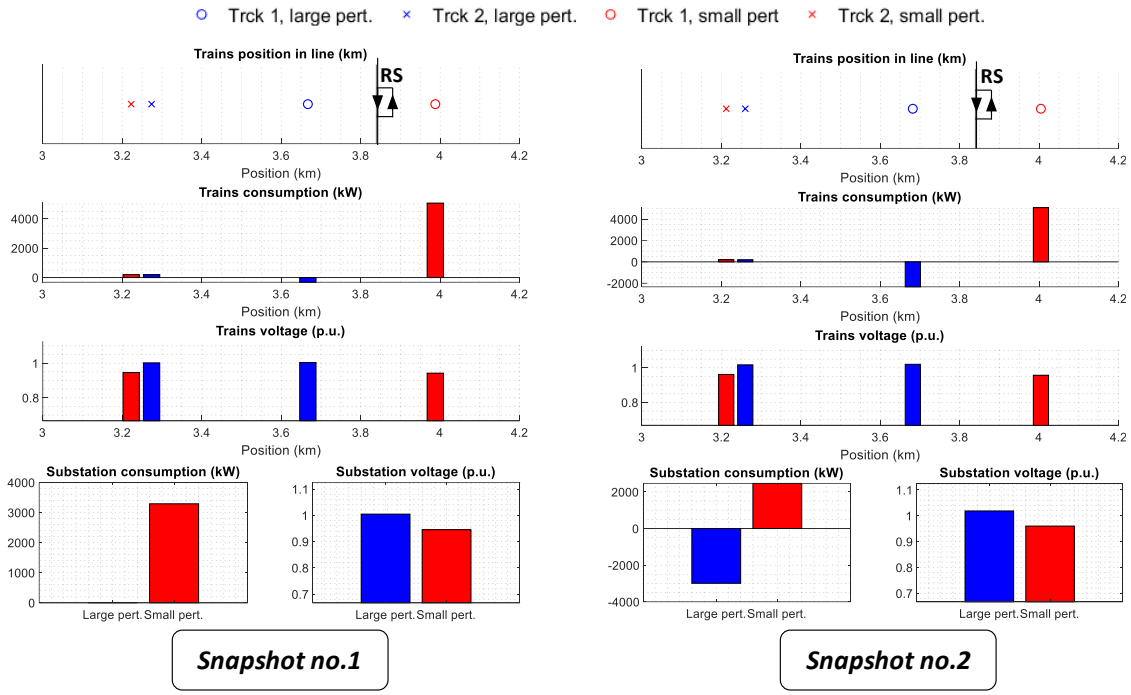

Figure 3-7: Example of power flows along the line for two different traffic scenarios

The example given in this section has illustrated how large perturbations can completely change energy consumption at a certain instant, nevertheless their global impact (during the whole operation period) is shown in Section 3.6.

3.6. RESULTS

This section analyzes the influence of the traffic model with large perturbations on the decision-making process of the installation of an RS. It must be noted that this chapter does not focus on optimizing neither the size nor the location of the RS to be installed (this task will be tackled in Chapter 5). Nevertheless, in order to provide realistic results, reasonable values for this variables of decision have been selected from a preliminary analysis of the case-study line characteristics:

- The installation of an RS with a size higher than 3 MW does not make sense, as having peaks of regeneration higher than this value is very rare. Therefore, 3 MW is the size selected for the RS.
- Each SS of the case study may be converted into an RS. Therefore, as there are eight SSs in the case-study line, there are eight candidate locations for the installation of the RS.

The following paragraphs will compare some of the most interesting results obtained for ***Peak-h comparison*** and ***Annual Comparison***. Equation (3-3) will be used to make these comparisons. It computes the energy saving overestimation (underestimation if the value is negative) of the result obtained with the traffic model selected with respect to the result that would be obtained if another traffic model had been selected.

$$\Delta\%\ E.sav._{selct.\ vs\ non-selct.} = \frac{E.sav._{selct.} - E.sav._{non-selct.}}{E.sav._{non-selct.}} \cdot 100 \qquad \textbf{(3-3)}$$

where:

- $\Delta\%\ E.sav._{selct.\ vs\ non-selct.}$ is the energy saving over/underestimation of the selected case with respect to the non-selected one.
- $E.sav._{selct.}$ is the energy saving obtained in the selected case.
- $E.sav._{non-selct.}$ is the energy saving obtained in the non-selected case.

3.6.1. PEAK-H COMPARISON

The results from comparing cases *PEAK-H.I* (peak hour operation represented by the simulation of only one scenario with the simplified traffic model), *PEAK-H.II* (peak hour operation represented by the simulation of a high number of scenarios with the traffic model for small perturbations) and *PEAK-H.III* (peak hour operation represented by the simulation of a high number of scenarios with the traffic model for large perturbations) are depicted in Table 3-3 and Figure 3-8.

A qualitative analysis of this figure shows that the results obtained with the realistic traffic models (cases *PEAK-H.II and PEAK-H.III*) are completely different to the result obtained with the simplified traffic model (case *PEAK-H.I*). This is because the single scenario from case *PEAK-H.I* is not representative at all of traffic operation.

Besides, the results from *PEAK-H.II and PEAK-H.III* present the same patterns with respect to the energy saving distribution: the highest energy saving is obtained when installing the RS in position 3 and there is a gradual reduction in the energy saving figures while moving away from this location. Nevertheless, the behavior of this variable is somehow smoothed in case *PEAK-H.III* with respect to the results in case *PEAK-H.II*. The reason is that, while in traffic with small perturbations (case *PEAK-H.II*) trains are equally distributed, in traffic with large perturbations (case *PEAK-H.III*) there are parts of the line with trains more accumulated than in normal operation and other parts where trains are more spread than in normal operation, which directly impacts on the use of the regenerated energy. Concretely, there is an increase of the receptivity in the places where trains are accumulated (and, consequently, a reduction of the regenerated energy that must be sent to the RS) at the same time that there is a decrease of the receptivity in the places where trains are more spread (and, consequently, an increase of the regenerated energy that must be sent to the RS). This behavior perfectly fits with the distribution of trains associated with this case study: the accumulation of trains takes place at the end of track 2 (corresponding to location 1) and the separation takes place along the whole track 1 until arriving to the place where the delay is recovered (which is variable but always around location 8).

The main consequences derived from the differences between these three cases are given in the next paragraphs.

Table 3-3: Normalized energy saving (kWh/h) with 3 MW RS at 3.5minute headway. Numerical comparison

Number of the SS converted into RS	*PEAK-H.I (simplified)*	*PEAK-H.II (small pert.)*	*PEAK-H.III (large pert.)*
1	56.36	170.28	75.89
2	66.46	205.64	99.89
3	55.61	215.06	114.68
4	51.07	191.22	112.06
5	58.07	154.63	105.89
6	81.49	80.31	102.84
7	119.51	68.02	100.28
8	127.35	61.09	97.90

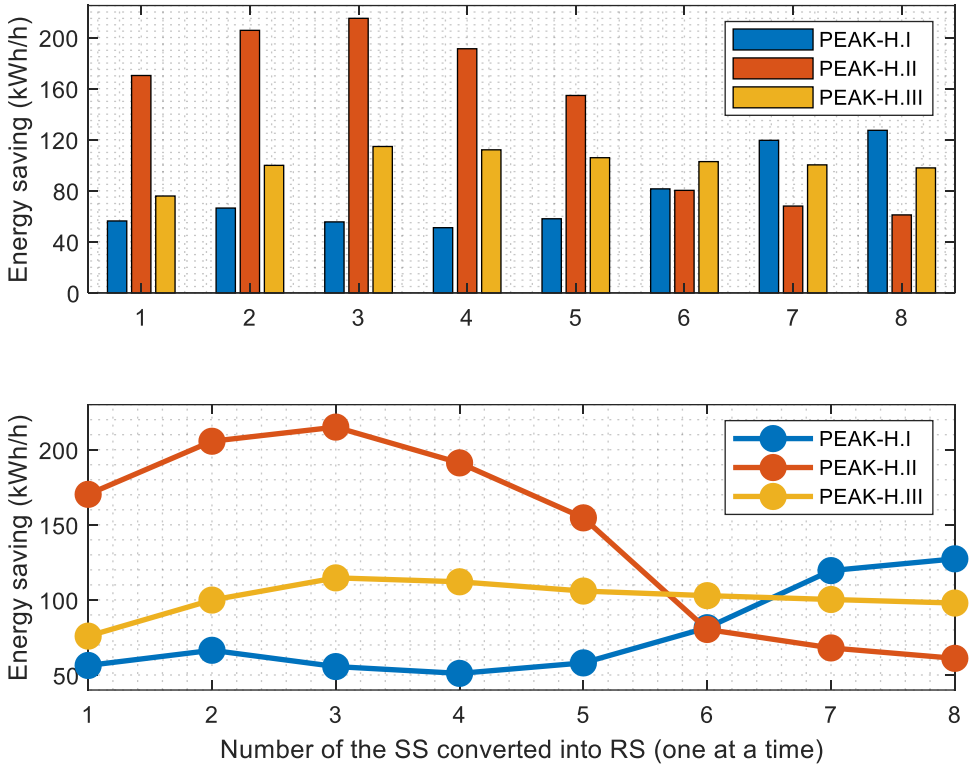

Figure 3-8: Normalized energy saving (kWh/h) with 3MW RS at 3.5 minute headway. Graphical comparison

If the simplified traffic model from the literature (case *PEAK-H.I*) would be chosen to assess the installation of the RS, position no.8 would be selected and the energy saving estimation with this model would be 127.3 kWh/h. It can be seen that the energy saving obtained for that RS location from the assessment with the simplified traffic model is very high in comparison to the energy saving results obtained with the realistic traffic models. This means an overestimation around 108.5% with respect to the realistic traffic model with small perturbations and around 30.1% with respect to the realistic traffic model with large perturbations (see Table 3-4).

Table 3-4: Energy saving of cases *PEAK-H.I, PEAK-H.II and PEAK-H.III when installing an RS in position no.8*

	PEAK-H.I	*PEAK-H.II*	*PEAK-H.III*
Normalized energy saving (kWh/h)	127.35	61.09	97.90
Energy saving overestimation of *PEAK-H.I with respect to PEAK-H.II and PEAK-H.III*	(-)	108.5 %	30.1 %

Besides, in the case of estimating the energy saving with the realistic traffic model with large or with small perturbations, the best position for installing the RS is position no. 3. This makes a big difference with respect to the decision that would have been made with the simplified traffic model (position no.8).

Even in case of using the realistic traffic model, the fact of assuming small or large perturbations is determinant because, although the best position for the RS is the same, the amount of energy saving is very different. If the traffic model used in the estimation of the energy saving is the realistic traffic model with small perturbations, but in real operation the traffic has large perturbations, the overestimation in the energy saving is around the 87.5% with respect to the estimation provided by the realistic traffic model with large perturbations (see Table 3-5). The big difference in the amount of energy saving can be determinant in order to assess positively or not the installation of the RS.

Table 3-5: Energy saving of cases *PEAK-H.II and PEAK-H.III when installing an RSS in position no.3*

	PEAK-H.II	*PEAK-H.III*
Normalized energy saving (kWh/h)	215.06	114.68
Energy saving overestimation of *PEAK-H.II* with respect to *PEAK-H.III*	(-)	87.5 %

Although all headways (not only 3.5 min-headway) must be taken into account for the decision-making process of installing an RS, these results, together with Section 3.5, prove that traffic with large perturbations have a great influence on the energy saving estimations and, therefore, an appropriate model to represent these traffic conditions can help make the best decision.

3.6.2. ANNUAL COMPARISON

This section computes the annual energy saving that can be obtained when taking into account all the headways. The results obtained in three different cases: *ANNUAL.I* (one scenario per headway and use of the simplified traffic model), *ANNUAL.II* (a high number of scenarios per headway and use of the traffic model for small perturbations to simulate every headway) and *ANNUAL.III* (a high number of scenarios per headway and use of the traffic model for large or small perturbations depending on the headway: the model for large perturbations for 3.5 minute headway and the model for small perturbations for the rest of headways) are depicted in Table 3-6 and Figure 3-9.

Table 3-6: Annual energy saving (GWh) with 3 MW RS. Numerical comparison

Number of the SS converted into RS	*ANNUAL.I (simplified)*	*ANNUAL.II (small pert.)*	*ANNUAL.III (combination of small and large pert.)*
1	0.861	0.779	0.601
2	0.953	0.899	0.699
3	0.959	0.949	0.760
4	0.987	0.973	0.823
5	1.040	0.950	0.858
6	1.105	0.847	0.890
7	1.174	0.834	0.894
8	1.163	0.811	0.880

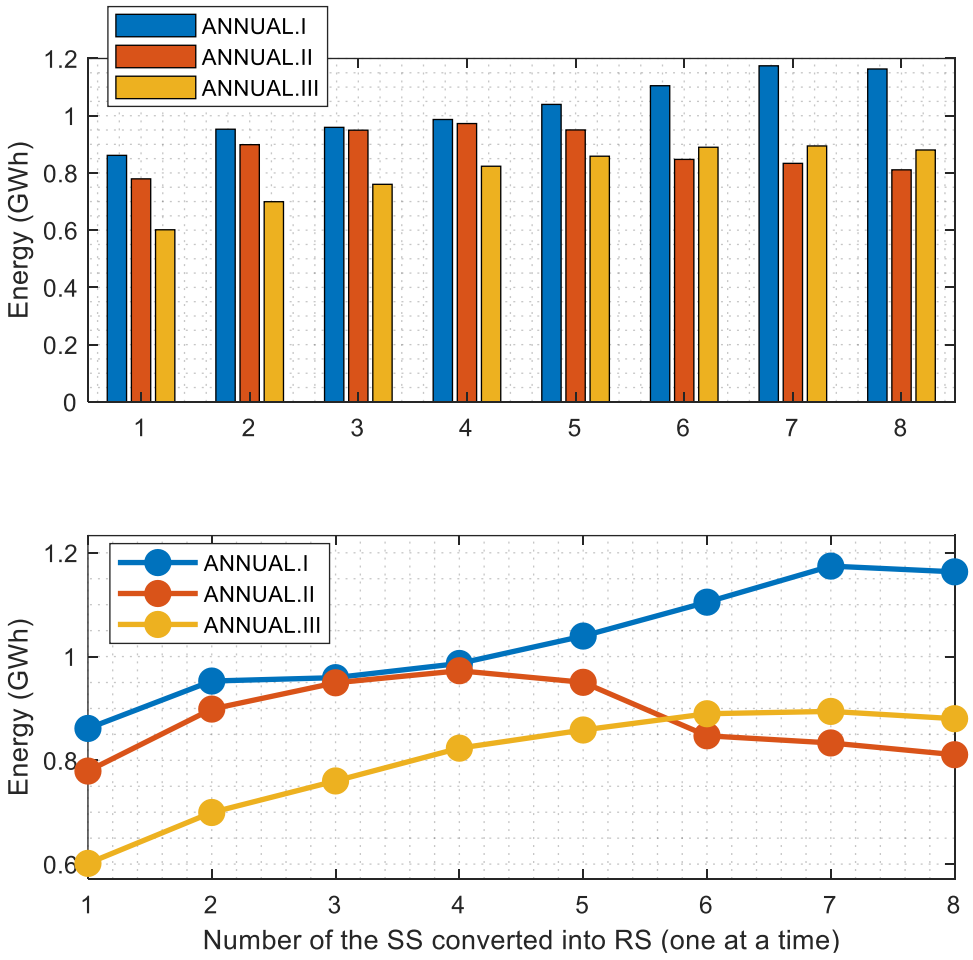

Figure 3-9: Annual energy saving (GWh) with 3MW RS. Graphical comparison

If the simplified traffic model from the literature (case *ANNUAL.I*) is used for estimating the potential energy saving achieved with the installation of the RS, position no. 7 would be chosen, obtaining around 1.17 GWh saved in a year. If this value is compared to the energy saving estimation obtained in case *ANNUAL.II* or in case *ANNUAL.III*, there is an overestimation in the energy saving around 40.8% and 31.3% respectively (see Table 3-7).

Table 3-7: Energy saving of cases *ANNUAL.I, ANNUAL.II and ANNUAL.III when installing an RS in position no.7*

	ANNUAL.I	*ANNUAL.II*	*ANNUAL.III*
Annual energy saving (GWh)	1.174	0.834	0.894
Energy saving overestimation of *ANNUAL.I with respect to ANNUAL.II and ANNUAL.III*	(-)	40.8 %	31.3 %

Additionally, the best location for the RS varies depending on the case selected: while cases *ANNUAL.I* and *ANNUAL.III* agree on installing the RS in position no.7, *ANNUAL.II* presents the highest energy saving when installing the RS in position no.4.

In case of supposing that there are only small perturbations, the realistic traffic model for small perturbations of Chapter 2 would be used (case *ANNUAL.II*), position no.4 would be selected and the estimation of the annual energy saving would be around 0.973 GWh. Nevertheless, if in real operation there are large perturbations at 3.5 minute headway and small perturbations in the rest of the headways (situation represented by case *ANNUAL.III*), there is an overestimation in the energy saving obtained from installing an RS in position no. 4 around 18.2% (see Table 3-8).

	ANNUAL.II	*ANNUAL.III*
Annual energy saving (GWh)	0.973	0.823
Energy saving overestimation of *ANNUAL.II* with respect to *ANNUAL.III*	(-)	18.2 %

Table 3-8: Energy saving of cases *ANNUAL.II and ANNUAL.III when installing an RS in position no.4*

Even more, in the latter case (case *ANNUAL.III*) the RS would be installed in position no.7, which would result in around an 8.6% more of energy saving with respect to the obtained in position no.4, as shown in (3-4).

$$\Delta\%\ E.sav._{RS_{no.7}\ vs\ RS_{no.4}} = \frac{E.sav._{RS_{no.7}} - E.sav._{RS_{no.4}}}{E.sav._{RS_{no.4}}} \cdot 100 = \left(\frac{0.894 - 0.823}{0.823} \cdot 100\right) = 8.6\% \qquad \textbf{(3-4)}$$

It must be remarked that the importance of this analysis is not based on whether one case is under or overestimating the energy saving with respect to the other cases (which will depend on the characteristics of the case-study line), but on the fact that the energy saving estimations are significantly different and also that the best location for the RS may vary. With respect to the accuracy of the estimations, the most accurate cases are *ANNUAL.II* and *ANNUAL.III* and the less accurate is *ANNUAL.I*. The energy estimation in case *ANNUAL.I*, which represents the estimation made with the simplified traffic model from the literature, depends on a single non-representative traffic scenario per headway, while the energy saving estimations of cases *ANNUAL.II* and *ANNUAL.III* are obtained from a set of representative traffic scenarios for each headway, ensuring that the margin of error in the estimation of the energy saving is very low.

Finally, the decision of selecting case *ANNUAL.II* or case *ANNUAL.III* will depend on the traffic characteristics. Real operation is usually characterized by a combination of small and large perturbations, reason why case *ANNUAL.III* is preferable.

3.7. CONCLUSIONS AND CONTRIBUTIONS

It has been proven that traffic with large perturbations has a direct impact on the energy saving that can be obtained with infrastructure improvements. This chapter proposes a realistic traffic model for traffic with large perturbations with the following features:

- Introduction of big delays, characteristic of the operation with large perturbations, which generate great decompensations in the distribution of trains along the line (with some parts where trains are accumulated and other parts where they are very disperse).
- Realistic dwell times (non-constant). They are obtained from the model explained in Section 3.3.2.1, which takes into account the traffic conditions (if trains are accumulated or not), the stochasticity inherent to dwell times and the driver's behavior.
- Realistic speed profiles which take into account the traffic conditions (if trains are accumulated or not). In case of not having trains accumulated (traffic with small perturbations) the speed profiles are designed with eco-driving techniques.
- Simulation of the most appropriate speed profile, for each train in each moment, based on the traffic conditions:
    - When trains are not accumulated and the signalling system is not activated, the traffic regulator selects the most appropriate unperturbed speed profile.
    - When there is an accumulation of trains, the speed profiles are perturbed by the signalling system. The application of different types of perturbed speed profiles is considered in the model: speed reduction or train stop at the interstation.

The use of the realistic traffic model for small perturbations of Chapter 2 together with the realistic traffic model for large perturbations of this chapter will allow taking into account all type of traffic situations. This improves the realism and the accuracy of the energy saving results provided by the simulator, which, in turn, will facilitate decision-making process about the most appropriate investments required for the electrical infrastructure.

The results presented in this chapter have proven that using *a) the simplified traffic model of the literature, b) only the realistic traffic model for small perturbation*s *or c) a combination of both realistic traffic models (with small and large perturbations)*, can lead to different decisions about the most appropriate infrastructure improvement to be installed. The ones provided by the realistic traffic models are the most reliable and accurate ones. More concretely, for the case study of this chapter, where the energy saving obtained from installing an RS was evaluated, differences in the energy saving estimations higher than the 30% were obtained when comparing the results provided

by the simplified traffic model and the realistic ones. Additionally, there are also significant differences (higher than the 18% for the case study) between the results obtained only with the realistic traffic model for small perturbations or with the combination of both realistic traffic models (for small and for large perturbations). Finally, it has also been proven that even the decision about the location of the RS may differ depending on the traffic model used for the simulations.

CHAPTER 4

COMPLEX TOPOLOGIES

As explained in Section 1.5.2.1, only the simplest line topology (line with two terminal stations) has been used in all the studies of the literature about simulation-based assessments of infrastructure improvements. Nevertheless, real MTS lines also present more complex topologies.

This chapter will give the details about the variables required by the timetable generator to generate the commercial timetables associated with different types of topology (including the complex ones). Once having the commercial timetables of the complex topologies, the realistic traffic models explained in sections 2.3 and 3.3 can be applied to them in order to obtain the associated representative traffic scenarios (the selection of the traffic model to apply will depend on the traffic conditions).

Sections 4.1 to 4.4 focuses, respectively, on the following line topologies:

- Line with two terminal stations.
- Line with short-turn and terminal stations.
- Line with branches.
- Line with branches, short-turn and terminal stations.

Finally, Section 4.5 presents the main conclusions and contributions of the chapter.

4.1. LINE WITH TWO TERMINAL STATIONS

Depending on the topology selected, the commercial timetable will be different. For a proper understanding of the complex topology models explained in the succeeding sections, this section focuses on the simplest line topology: line with two terminal stations, represented by Figure 4-1. It must be noted that the terminal stations are the places in the end of the line where trains change the direction of the travel. In particular, in Figure 4-1 trains change from down to up direction in terminal station A and from up to down direction in terminal station B.

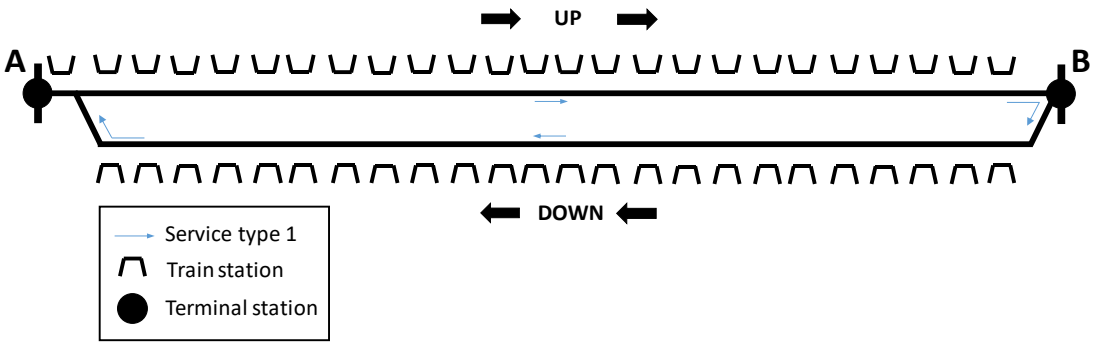

Figure 4-1: Line with two terminal stations

Figure 4-2 represents the time-position diagram of the commercial timetable of a line with two terminal stations. As shown, the variables defining the commercial timetable are:

- Nominal travel times (two in total, one per direction): time required by a train to make its entire journey in one direction, using its nominal speed profile (SP1) and the commercial dwell time in the stations ($t_{comm\ dwell}$). In Figure 4-2 it is represented by $t_{up/down}^{trav.nom}$.
- Headway: time interval between two consecutive trains.
- Scheduled turning times (two in total, one per terminal station): it is defined as the difference between the departure instant and the moment of arrival at the terminal stations. In Figure 4-2 it is represented by $t_X^{schd.\ turn}$ (X being the associated terminal station). The scheduled turning time can change depending on the type of turn-back maneuver:
    - In case of a turn-back in front of the station, as happens with terminal station A in Figure 4-1, the terminal station coincides with a passenger station. According to (van Oort & van Nes, 2010) the turning time in these cases consists of:
        - Technical turning time: time to start up the vehicle to depart in the opposite direction (e.g.: walking time of the driver to go the other part, start up the board computer…, etc.)
        - Break: the time the driver is allowed to rest (if not relieved).
        - Synchronization time: the time needed to depart by schedule.
        - Dwell time: time needed for passengers to alight or board.
    - In case of a turn-back beyond the station, as happens with terminal station B in Figure 4-1, the terminal station is after the last passenger

station. In these cases the turning time consists of the technical turning time, the break and the synchronization time (the dwell time does not exist, since all the passengers have already left the train in the last passenger station).

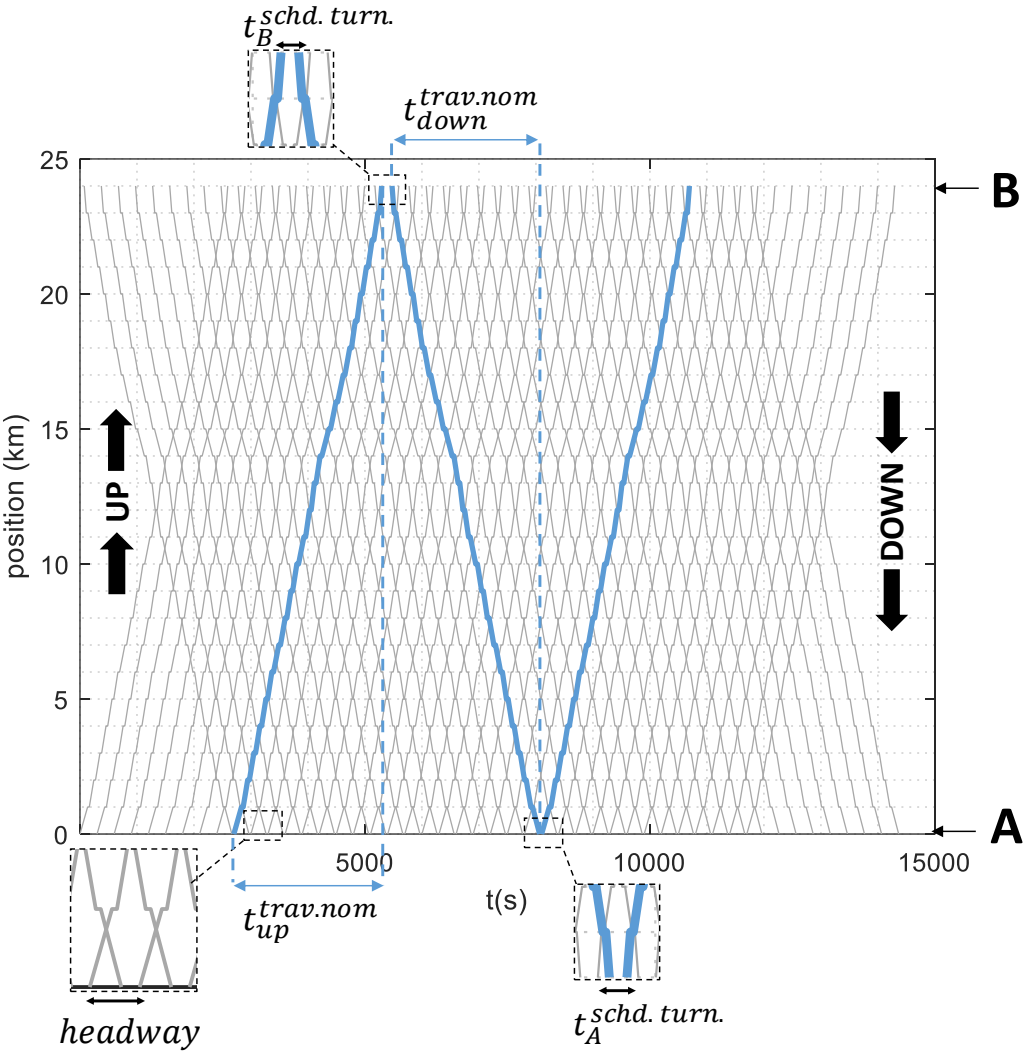

Figure 4-2: Time-position diagram of the commercial timetable of line with two terminal stations

It must be noted that there is a direct relation between the so-called dwell time in terminal stations presented in Section 3.3.2.1.3 and the scheduled turning time. Indeed, the difference between both variables is due to the traffic perturbations, which means that, in absence of them, both variables will coincide. Nevertheless, in traffic with small perturbations departures are determined by the realistic traffic model (which takes into account the perturbations) and in traffic with large perturbations both moments are determined by the realistic traffic model, which sets the dwell time in terminal stations to a different value from the correspondent scheduled turning time.

In a line with two terminal stations, the input variables required to completely determine the commercial timetable are:

1) *The nominal travel times.*
2) *The headway.*
3) *The scheduled turning time in one of the terminal stations*.
4) *The minimum admissible values for the turning times* ($t_{turn.min.}$).

With the values of these variables, the scheduled turning time in the other terminal station is given by the timetable, as illustrated in Figure 4-3. In the particular case of this figure, the input variables are the headway, $t_{up}^{trav.nom}$, $t_{down}^{trav.nom}$, and $t_A^{schd.\ turn}$. This variables set the moments of arrival and departure in both terminal stations. Therefore, the remaining scheduled turning time ,$t_B^{schd.\ turn}$, is obtained from subtracting the moment of arrival to terminal station B of the train in down direction to the moment of departure from that terminal station of the first train that departs in up direction after that arrival. This time has to comply with the restrictions of the minimum admissible values for the turning times, $t_{turn.min.}$, which are obtained when considering neither breaks for the drivers nor synchronization times and the minimum admissible values for the technical turning times and dwell times (the latter only applicable when having the turn-back in front the station). If the value for that time is lower than $t_{turn.min.}$, the linkage is with the following train and the value for the scheduled turning time increases considerably, as shown in Figure 4-4.

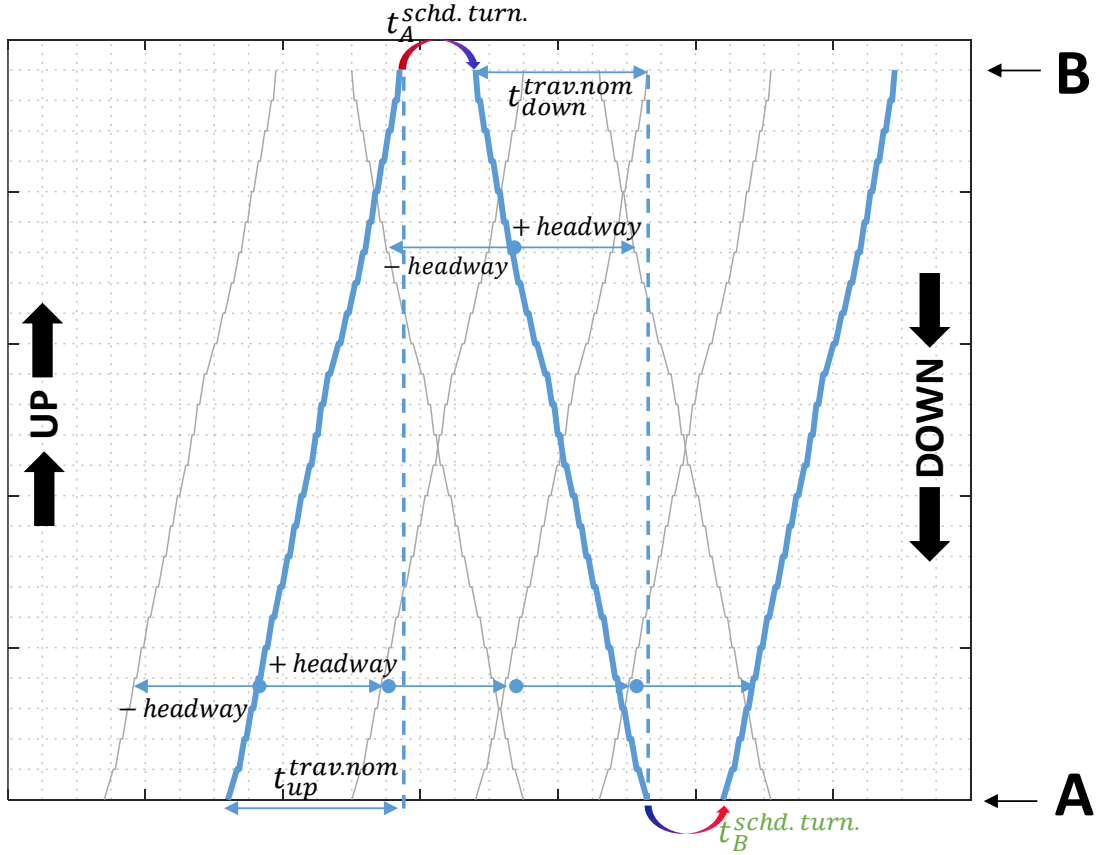

Figure 4-3: Example of *input* (in black) and *given* (in green) variables in the commercial timetable of a line with two terminal stations

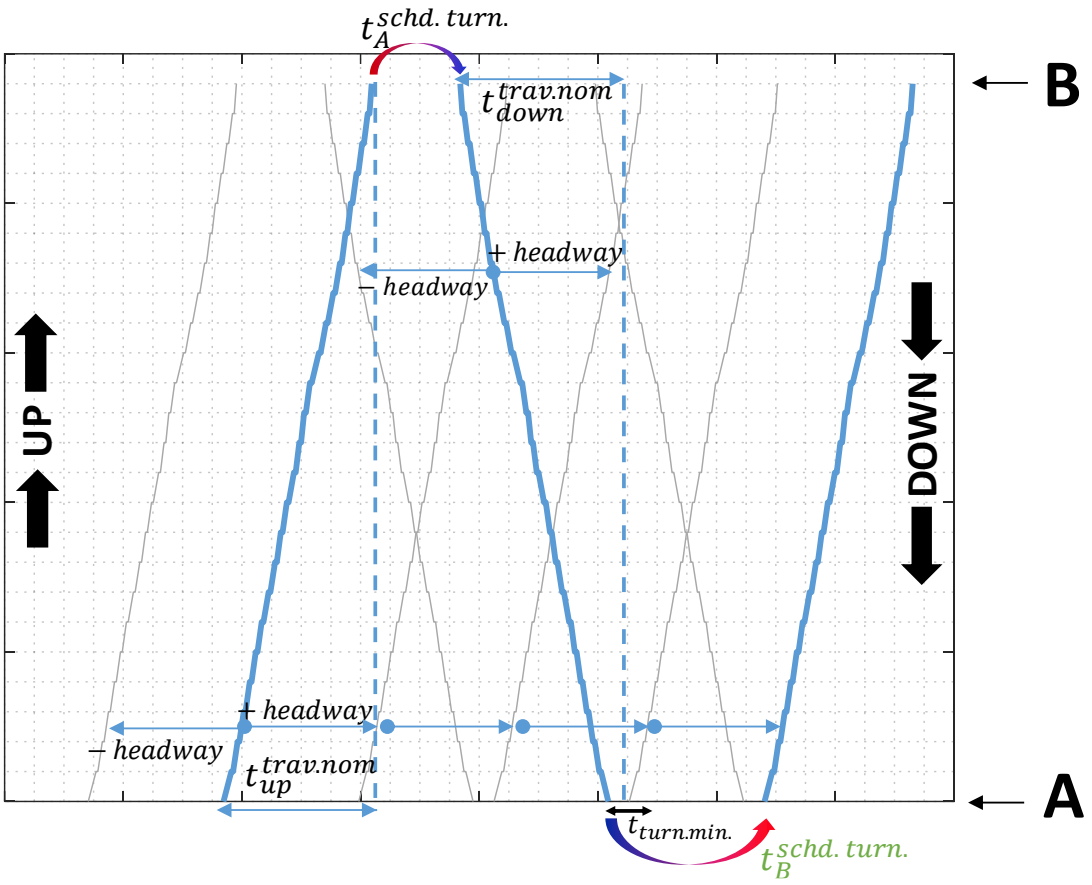

Figure 4-4: Example of an increase in the scheduled turning time due to a no compliance with $t_{turn.min.}$

At this point, it can be interesting to clarify that the concept of the time shift is directly related with the scheduled turning time. Indeed, changing the time shift is equivalent to change the scheduled turning times, which, in turn, is equivalent to generate different commercial timetables with the same headway. This is depicted in Figure 4-5, where it is clearly shown the difference between the scheduled turning times when applying null time shift ($t_{A/B\ null\ t-s}^{comm.\ return}$) and positive time shift $t_{A/B\ pos.\ t-s}^{comm.\ return}$).

At the light of this explanation, it can be clearly understood the reason why in the last chapter (specifically in Section 3.4.2) it was stated that using different time shifts only makes sense in traffic with small perturbations. Since commercial timetables determine train departures from terminal stations in traffic with small perturbations and changing the time shift is equivalent to generate different commercial timetables (with a same headway), the time shift must be taken into account with these traffic conditions. On the contrary, due to the fact that in traffic with large perturbations the departures and arrivals in the terminal stations are determined by the realistic traffic model and not by the commercial timetables, using just one commercial timetable per headway (with any value for the time shift) is enough.

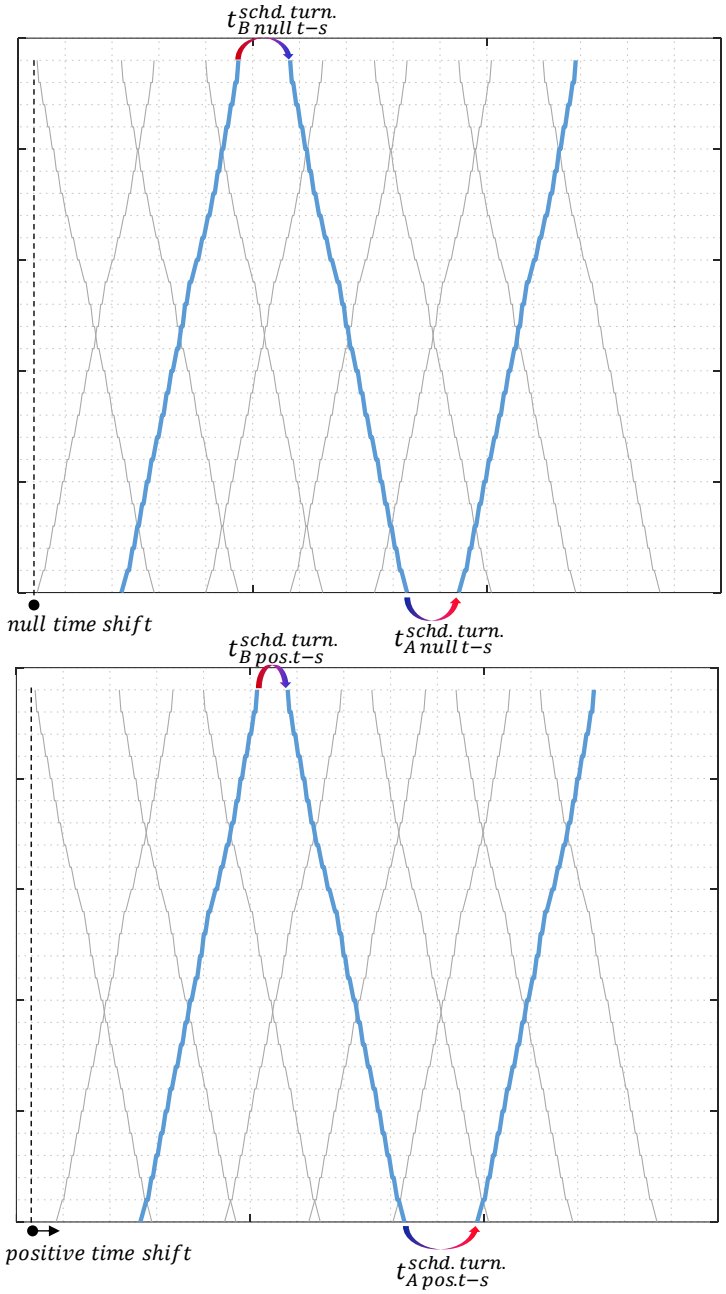

Figure 4-5: Relationship between time shift and scheduled turning time

Finally, Equation (4-1) determines the number of trains, n_{trains}, required to enable the operation associated with the commercial timetable generated. The value given by this equation must be an integer number in order to verify that the value of all the variables defining the commercial timetable are correct.

$$n_{trains} = \frac{t_{up}^{trav.nom} + t_{down}^{trav.nom} + t_{A}^{schd.turn.} + t_{B}^{schd.turn.}}{headway} \qquad \textbf{(4-1)}$$

4.2. LINE WITH SHORT-TURN AND TERMINAL STATIONS

This type of topology is represented by Figure 4-6 (particularized for the case of a line with two services, one short-turn station and two terminal stations) and has the following main characteristics:

- There are two types of stations where trains can change direction:
  - Terminal stations: they are located at the end of the line. The number of terminal stations in this type of topology is fixed: 2 (one at each end of the line).
  - Short-turn stations: they are located at intermediate points of the line. There can be as many short-turn stations as necessary.
- There are $n_{services}$ different types of service, taking each one a different itinerary that, in turn, depends on the short-turn or terminal stations selected to change direction.

In the case of Figure 4-6, the terminal stations are represented by A and B and there is one short-turn station in C. Besides, there are two different types of service ($n_{services} = 2$): trains with service type 1 change direction in A and B, while trains with service type 2 change direction in A and C.

A consideration that must be taken into account for this type of topology is that there must be always a part of the line common for all the services, where the time interval between trains is regular (this value will be called **common headway**). In the case of Figure 4-6, this part of the line is between A and C.

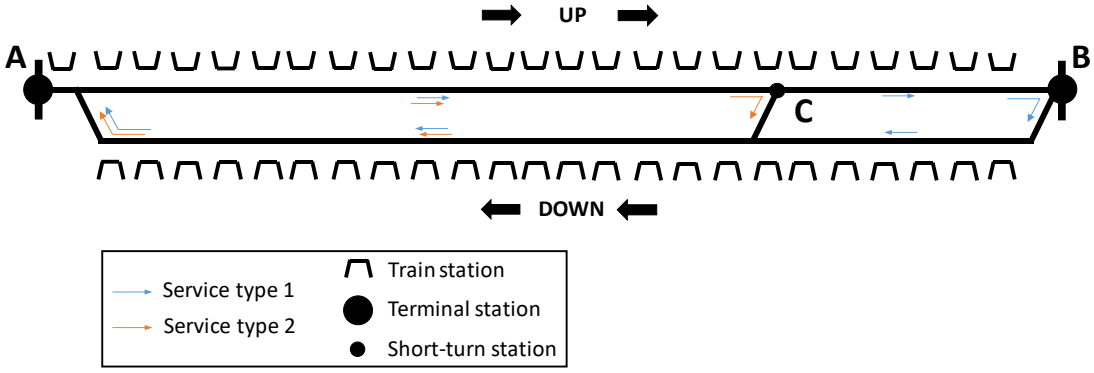

Figure 4-6: Line with two services, one short-turn station and two terminal stations

The commercial timetables associated with a line with $n_{services}$ services, n_{SH-T} short-turn stations and n_T terminal stations are characterized by the following variables:

- Nominal travel times ($2 \cdot n_{services}$ in total, $n_{services}$ per direction). In Figure 4-7, the nominal travel times in up/down direction for service type i are represented by $t^{trav.nom}_{up/down\ serv\ i}$.
- Common headway.

- Scheduled turning times ($n_{SH-T} + n_T$ in total). In Figure 4-7, the scheduled turning times are represented by $t_X^{schd.\ turn}$ (X being the associated short-turn or terminal station).
- The distribution of train services according to a service pattern that is repeated periodically (e.g.: [*type 1, type 2*] or [*type 1, type 1, type 2*]). It must be noted that when the service pattern is not symmetric (different number of services of each type within the pattern, e.g.: [*type 1, type 1, type 2*]), the scheduled turning times in any of the short-turn or terminal stations may not be constant.

In order to completely determine the commercial timetable it is necessary to have the values of:

1. *The nominal travel times.*
2. *The common headway.*
3. *The service pattern.*
4. *One of the scheduled turning times, provided that the turning time is constant.*
5. *The minimum admissible values for the turning times* ($t_{turn.min.}$).

With the values of these variables, the remaining scheduled turning times are set by the timetable.

Figure 4-7 represents the time-position diagram of the commercial timetable for the topology represented by Figure 4-6. In order to illustrate the variable scheduled turning time, service pattern [*type 2, type 2, type 1, type 2, type 1*] has been selected, so that $t_B^{schd.\ turn}$ is variable.

In this figure, trains with service type 1 change from up to down direction in terminal station B (around PK. 24), trains with service type 2 change from up to down direction in short-turn station C (around PK. 15) and trains with both types of service change from down to up direction in terminal station A (around PK. 0). If the input variables are $t_{up\ serv\ 1}^{trav.nom}$, $t_{down\ serv\ 1}^{trav.nom}$, $t_{up\ serv\ 2}^{trav.nom}$, $t_{down\ serv2}^{trav.nom}$, the common headway, the service pattern ([*type 2, type 2, type 1, type 2, type 1*]) and $t_A^{schd.\ turn}$ or $t_C^{schd.\ turn}$ (both being constant), the moments of arrival and departure in all the stations where trains change direction are set and the remaining scheduled turning times are obtained from linking these moments of arrival and departure in the short-turn or terminal stations whose turning time has not been given as input (taking into account that these values must comply with $t_{turn.min.}$).

In case of having different scheduled turning times in any short-turn or terminal station X, the average scheduled turning time, $t_{\bar{X}}^{schd.\ turn}$, must be computed according to Equation (4-2).

$$t_{\bar{X}}^{schd.\ turn} = \frac{1}{\sum_{i=MEMB(X)}(TOT(serv\ i))} \cdot \sum_{i=MEMB(X)} \left(\sum_{tr=ORD(serv\ i)} \left(t_{X_{tr}}^{schd.\ turn} \right) \right) \qquad \textbf{(4-2)}$$

where:

- $MEMB(X)$ is a "membership" function that determines the types of train services that change direction in X (e.g.: in Figure 4-6, $MEMB(A) = [type\ 1, type\ 2]$, $MEMB(B) = [type\ 1]$ and $MEMB(C) = [\ type\ 2]$).
- $ORD(serv\ i)$ is a function that determines the ordinal position of trains with service type i within the service pattern (e.g.: in service pattern [*type 1, type 2, type 1*], $ORD(serv\ 1) = [1,3]$ and $ORD(serv\ 2) = [2]$).
- $t_{X_{tr}}^{schd.\ turn}$ is the scheduled turning time in X particularized for train tr (tr being a train that changes direction in X).
- $TOT(serv\ i)$ is a function that determines the total amount of trains with service type i within the service pattern (e.g.: in service pattern [*type 1, type 2, type 1*], $TOT(serv\ 1) = 2$ and $TOT(serv\ 2) = 1$).

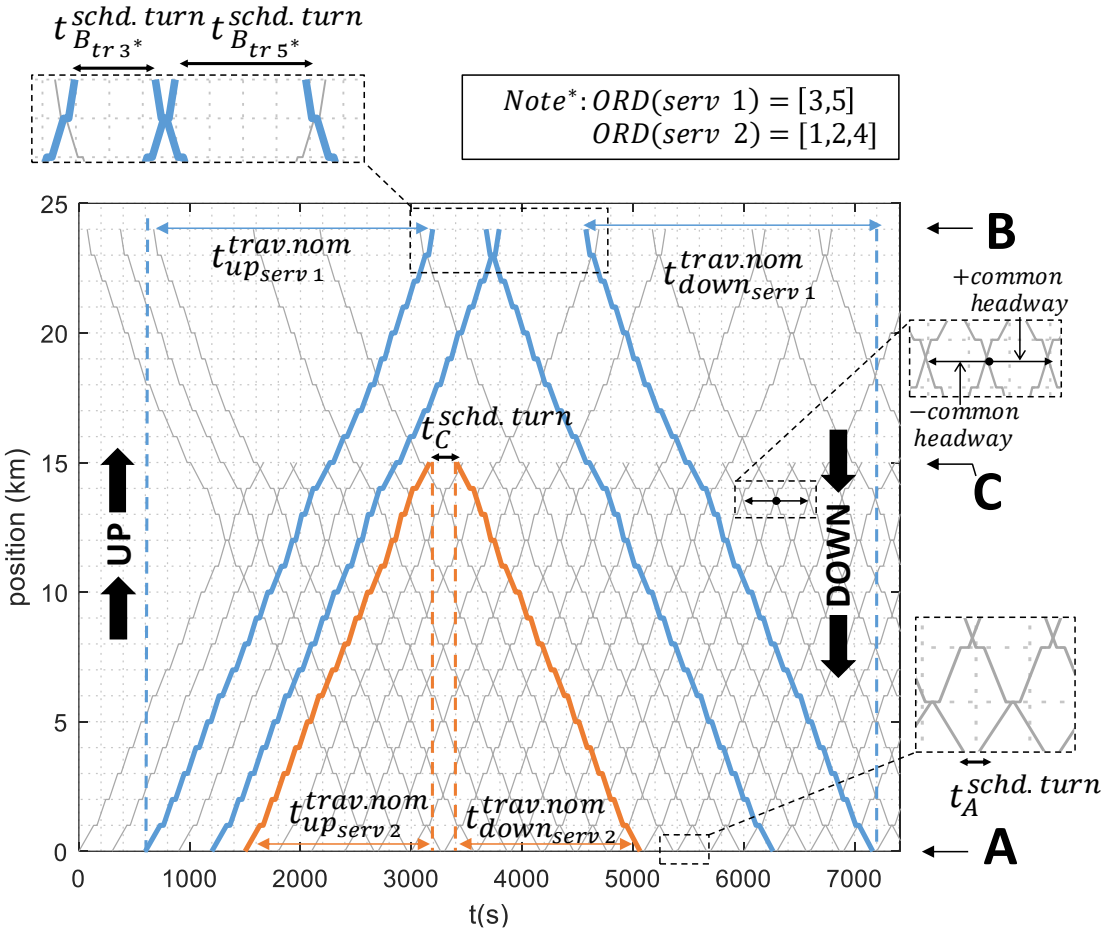

Figure 4-7: Time-position diagram of the commercial timetable of a line with two services, one short-turn station and two terminal stations

Finally, equation (4-3) determines the number of trains required.

$$n_{trains} = \sum_{i=1}^{n_{services}} n_{trains \in serv\ i} \qquad \textbf{(4-3)}$$

where $n_{trains \in serv\ i}$ is the number of trains giving the service type i, computed according to Equation (4-4).

$$n_{trains \in serv\ i} = \frac{t^{trav.nom}_{up\ serv\ i} + t^{trav.nom}_{down\ serv\ i} + t^{schd.\ turn}_{up \to down_{serv\ i}} + t^{schd.\ turn}_{down \to up_{serv\ i}}}{\overline{headway}_{serv\ i}} \quad \textbf{(4-4)}$$

where:

- $t^{schd.\ turn}_{up \to down_{serv\ i}}$ is the scheduled turning time in the station where trains with service type i change from up to down direction.
- $t^{schd.\ turn}_{down \to up_{serv\ i}}$ is the scheduled turning time in the station where trains with service type i change from down to up direction.
- $\overline{headway}_{serv\ i}$ is the average headway associated with service type i. This value is obtained from Equation (4-5).

$$\overline{headway}_{serv\ i} = \frac{\left(\sum_{j=1}^{n_{services}} TOT(serv\ j)\right) \cdot common\ headway}{TOT(serv\ i)} \quad \textbf{(4-5)}$$

It must be noted that the total number of trains (n_{trains}) must be an integer number, although the number of trains giving each type of service ($n_{trains \in serv\ i}$) can be rational, which means that some trains will be varying the type of service in succeeding travels.

4.3. LINE WITH BRANCHES

This type of topology is represented by Figure 4-8 (particularized for the Y-shaped case, which has a common section and two branches) and has the following main characteristics:

- There are only terminal stations, which correspond to the terminal locations of the common section and branches not being bifurcation points.
- There are several types of service, sharing all of them the travel along a common section and taking different branches when arriving to the bifurcation point (BPT in Figure 4-8).

In the case of Figure 4-8, there is a common section, two branches, a bifurcation point (BPT) and three terminal stations (n_T=3): A in the common section, B in branch 1 and C in branch 2. Besides, there are two different types of service ($n_{services} = 2$): trains with service type 1 take branch 1, while trains with service type 2 take branch 2.

As can be seen, this type of topology is very similar to the previous one: line with short-turn and terminal stations. The only difference relies on the fact that, while in the previous case the type of service depended on its associated short-turn or terminal stations, in the current one the type of service depends on the selected branch.

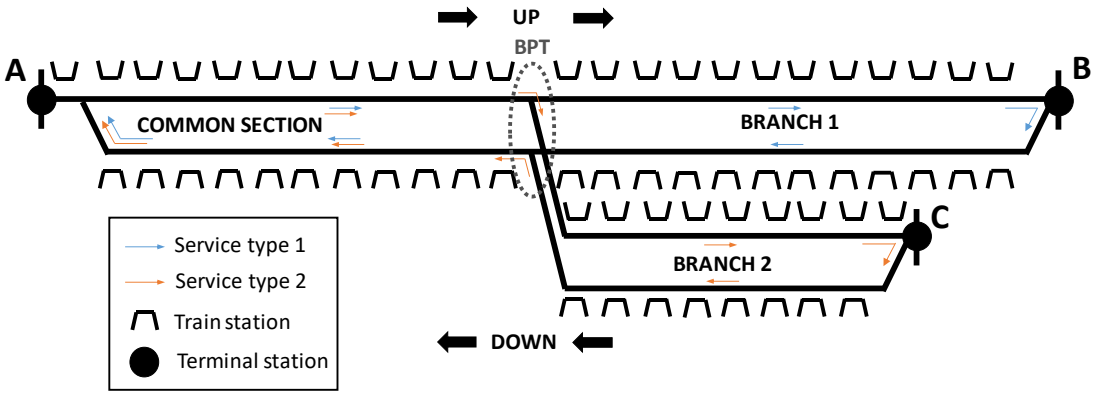

Figure 4-8: Y-shaped line (line with a common section and two branches)

A consideration that must be taken into account for this type of topology is that, although it can become as complex as needed (branches in both sides of the common section, sub-branches within the branches, etc…), there must be always a common section with a regular time interval between trains (the **common headway**).

The commercial timetables associated with a line with $n_{services}$ services and n_T terminal stations (it must be noted that the number of branches is not relevant) are characterized by the following variables:

- Nominal travel times ($(2 \cdot n_{services}$ in total, $n_{services}$ per direction).
- Common headway.
- Scheduled turning times (n_T in total).
- The distribution of train services according to a service pattern that is repeated periodically (e.g.: [*type 1, type 2*] or [*type 1, type 1, type 2*]). As happened in the previous topology, if the service pattern is not symmetric, the turning times in some terminal stations may not be constant, in which case the average scheduled turning time must be computed according to Equation (4-2).

In order to completely determine the commercial timetable, the values of the variables that must be defined are also the same as in the line with short-turn and terminal stations:

1. *The nominal travel times.*
2. *The common headway.*
3. *The service pattern.*
4. *One of the scheduled turning times, provided that the turning time is constant.*
5. *The minimum admissible values for the turning times* ($t_{turn.min.}$).

With the values of these variables, the remaining scheduled turning times are set by the timetable. The procedure to obtain them is exactly the same as the one explained in Section 4.2.

Figure 4-9 represents the time-position diagram of the commercial timetable for the topology of Figure 4-8 and the service pattern [*type 2, type 2, type 1*]. This figure is

subdivided into two subplots. Both subplots represent all the trains in the part of the travel corresponding to the common section (trains with any type of service change from down to up direction in the terminal station A, located at this branch (around PK.0)). Nevertheless, from the bifurcation point (around PK.10) the first subplot only represents the trains giving service type 1 (which goes along branch 1 and changes from up to down direction in terminal station B (around PK. 24)), while the second subplot only represents the trains giving service type 2 (which goes along branch 2 and change from up to down direction in terminal station C (around PK. 20)).

Additionally, the value of $t_C^{schd.\ turn}$ in this figure is variable (it has two different values that must be averaged according to Equation (4-2)) and it is shown the effect that restrictions regarding the minimum turning time has on the generation of the commercial timetables. Particularly, the minimum turning time is not complied between the arrivals at terminal station C and the immediately following departures, reason why the scheduled turning times in terminal station C are determined as the time between the arrivals and the second of the departures after the arrival.

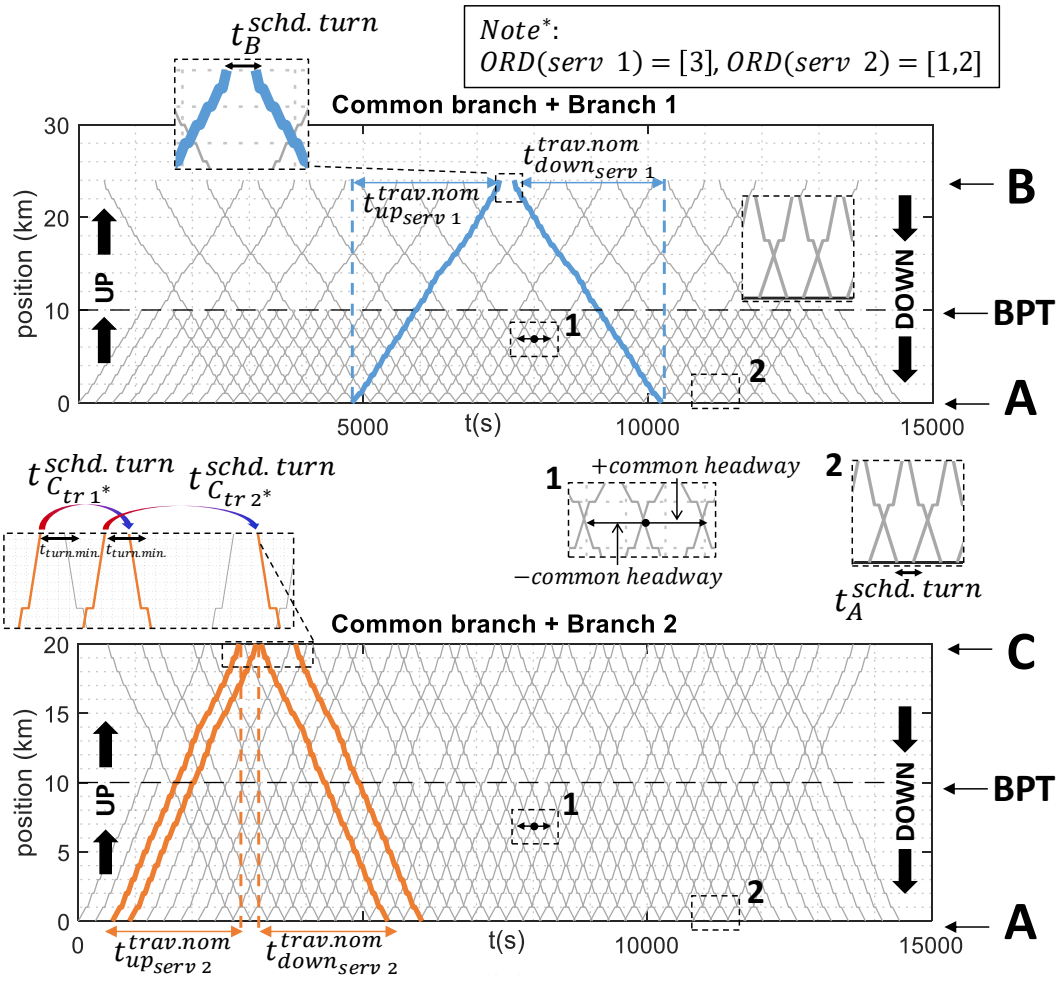

Figure 4-9: Time-position diagram of the commercial timetable of a Y-shaped line

The number of trains required (n_{trains}) is calculated from Equations (4-3), (4-4) and (4-5). Although n_{trains} must be an integer number, the number of trains giving each

type of service ($n_{trains \in serv\ i}$) can be rational, which means that some trains will be varying the type of service in succeeding travels.

4.4. LINE WITH BRANCHES, SHORT-TURN AND TERMINAL STATIONS

This type of topology is a combination of the topologies presented in Sections 4.2 and 4.3 and, therefore, the most complex one. It is represented by Figure 4-10 (particularized for the Y-shaped case with short-turn and terminal stations in the branches and a terminal station in the common section) and has the following main characteristics:

- There are two types of stations where trains can change direction:
  - Terminal stations: they are located at the terminal locations of the branches and common section where there are no bifurcation points.
  - Short-turn stations: they are located at intermediate points of the branches and common section. There can be as many short-turn stations as necessary.
- There are $n_{services}$ different types of service, each one going along the common section but taking different branches and different short-turn or terminal stations (it is even possible to have different types of service going exactly along the same branches but changing direction in different short-turn or terminal stations).

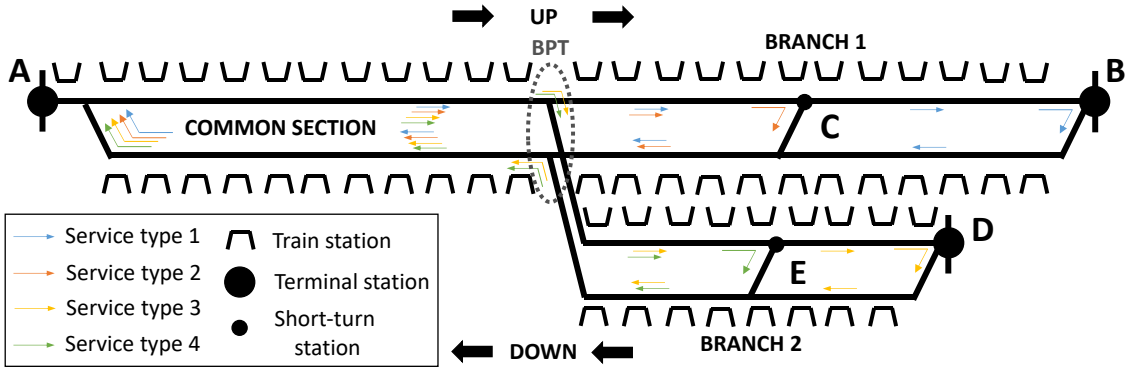

Figure 4-10: Y-shaped line with short-turn and terminal stations in the branches and a terminal station in the common section

In the case of Figure 4-10, there is a common section, two branches, a bifurcation point (BPT) and three terminal stations (n_T=3): A in the common section, B in branch 1 and D in branch 2. Additionally, there are two short-turn stations ($n_{SH-T} = 2$), one in each of the two branches: C in branch 1 and E in branch 2. The different possibilities of itinerary selection makes it possible to have four different types of service ($n_{services} = 4$).

- Service type 1 takes the common section and branch 1. The change from down to up direction is made in terminal station A (in the common section), while the change from up to down direction is made in terminal station B (in branch 1).

- Service type 2 takes the common section and branch 1. The change from down to up direction is made in terminal station A (in the common section), while the change from up to down direction is made in short-turn station C (in branch 1).
- Service type 3 takes the common section and branch 2. The change from down to up direction is made in terminal station A (in the common section), while the change from up to down direction is made in terminal station D (in branch 2).
- Service type 4 takes the common section and branch 2. The change from down to up direction is made in terminal station A (in the common section), while the change from up to down direction is made in short-turn station E (in branch 2).

Similarly to what happened in the previous topology, this type of topology can become as complicated as needed (branches in both sides of the common section, sub-branches within the branches, short-turn stations in any branch or sub-branch, etc.), but there must always be a common section shared by all the services, where the time interval between trains is regular (the **common headway**). In the case of Figure 4-10, the common section goes from terminal station A to the bifurcation point (BPT).

The commercial timetables associated with a line with $n_{services}$ services, n_{SH-T} short-turn stations and n_T terminal stations (it must be noted that the number of branches is not relevant) are characterized by the following variables:

- Nominal travel times ($2 \cdot n_{services}$ in total, $n_{services}$ per direction).
- Common headway.
- Scheduled turning times ($n_{SH-T} + n_T$ in total).
- The distribution of train services according to a service pattern that is repeated periodically (e.g.: [*type 1, type 2*] or [*type 1, type 1, type 2*]). As happened in the previous topology, if the service pattern is not symmetric, the turning times in some short-turn or terminal stations may not be constant, in which case the average scheduled turning time must be computed according to Equation (4-2).

As can be seen, the variables defining the commercial timetables are exactly the same as those of the topology with short-turn and terminal stations. Indeed, the only difference between both topologies is the fact that in this topology, since there are branches, there are more than two terminal stations.

The number of different services is usually much higher than in the other topologies, which makes the service patterns much more complex. The level of complexity can be so high that it can be divided into a 'branch pattern' that determines the branch selected for each service and 'branch sub-patterns' that determine, for each branch, the short-turn or terminal stations where each type of service change direction.

In order to graphically illustrate the complexity that may arise in the service patterns of this type of topologies, Figure 4-11 shows one of the possible service patterns that can take place in the topology represented by Figure 4-10. As can be seen, the complete service pattern is [type 1, type4, type2, type 3, type 1, type 1, type 4, type 2, type 4, type 1, type 1, type 3, type 2, type 4, type 1]. To make this pattern more understandable, it can be divided into:

- Branch pattern: [1,2,1,2,1].
- Branch 1 sub-pattern: [B,C,B].
- Branch 2 sub-pattern: [E,D,E].

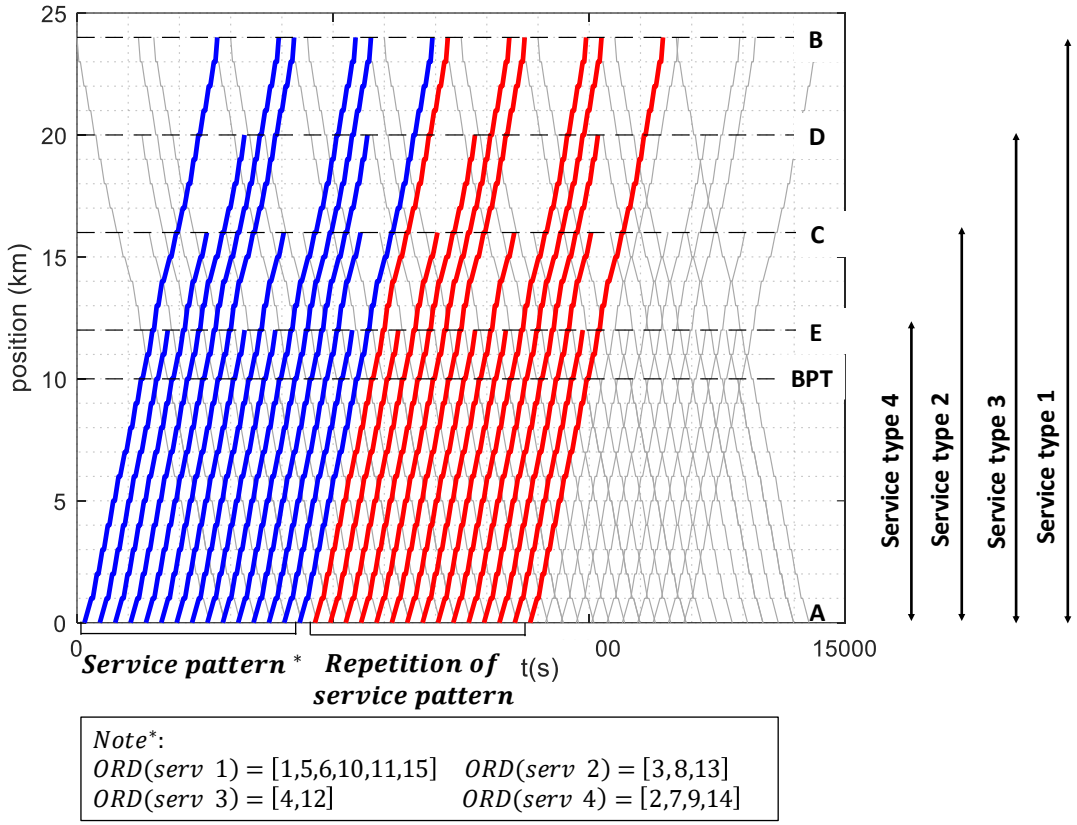

Figure 4-11: Example of a complex service pattern in the line represented by Figure 4-10

In order to completely determine the commercial timetable, the values of the variables that must be defined are also the same as in the previous sections:

1. *The nominal travel times.*
2. *The common headway.*
3. *The service pattern.*
4. *One of the scheduled turning times, provided that the turning time is constant.*
5. *The minimum admissible values for the turning times* ($t_{turn.min.}$).

With the values of these variables, the remaining scheduled turning times are set by the timetable. The procedure to obtain them is also the same as the one explained in Section 4.2.

Figure 4-12 represents the time-position diagram of the commercial timetable for the topology of Figure 4-10 and with the service pattern presented in Figure 4-11. This figure is subdivided into two subplots. Both subplots represent all the trains in the part of the travel corresponding to the common section. Nevertheless, from the bifurcation, the first subplot only represents the trains giving services type 1 and type 2 (which go

along branch 1), while the second subplot only represents the trains giving services type 3 and type 4 (which go along branch 2). As depicted in the legend of the figure, the values of $t_A^{schd.\ turn}$, $t_B^{schd.\ turn}$ and $t_C^{schd.\ turn}$ are unique, while $t_D^{schd.\ turn}$ and $t_E^{schd.\ turn}$ are variable (in particular, there are two different values for $t_D^{schd.\ turn}$ and four different values for $t_E^{schd.\ turn}$) and must be averaged according to Equation (4-2).

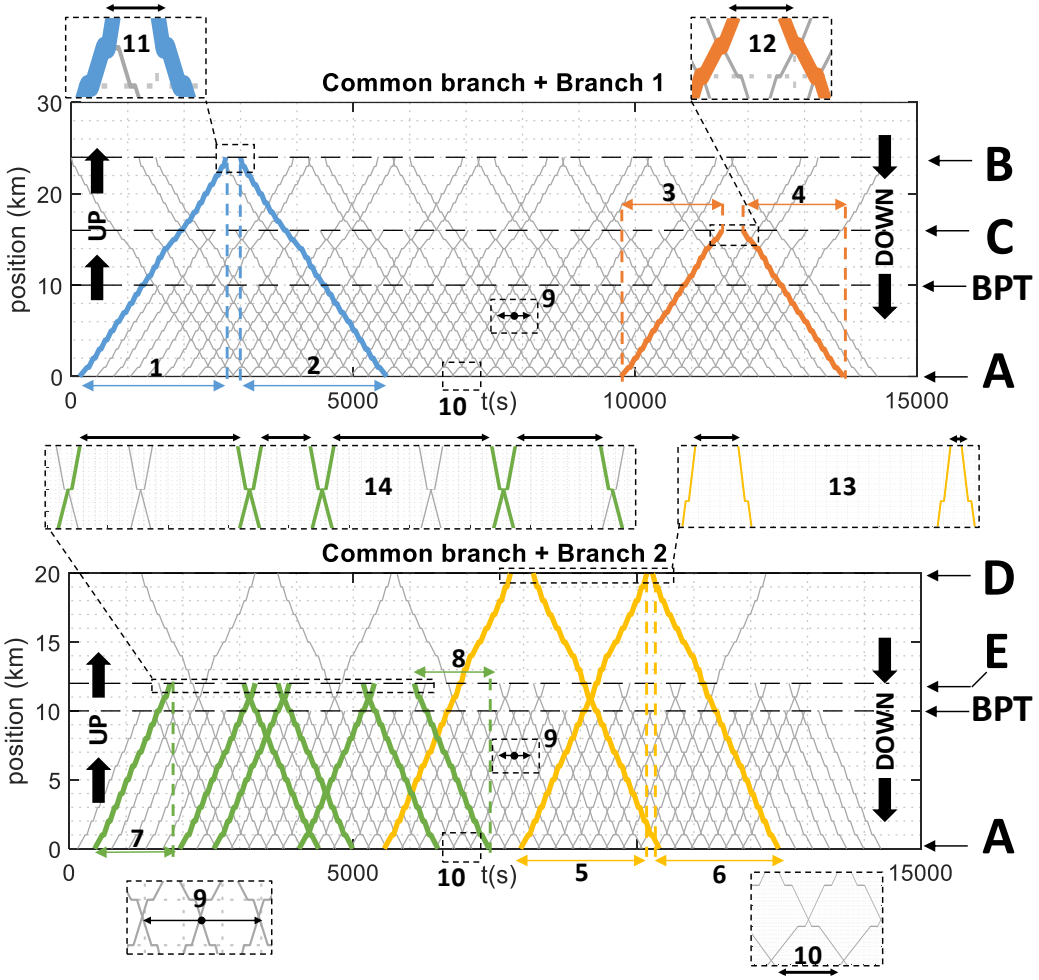

LEGEND

1: $t_{up\ serv\ 1}^{trav.nom}$	2: $t_{down\ serv\ 1}^{trav.nom}$	3: $t_{up\ serv\ 2}^{trav.nom}$
4: $t_{down\ serv\ 2}^{trav.nom}$	5: $t_{up\ serv\ 3}^{trav.nom}$	6: $t_{down\ serv\ 3}^{trav.nom}$
7: $t_{up\ serv\ 4}^{trav.nom}$	8: $t_{down\ serv\ 4}^{trav.nom}$	9: *common headway*
10: $t_A^{schd.\ turn}$	11: $t_B^{schd.\ turn}$	12: $t_C^{schd.\ turn}$
13:From left to right: $\left[t_{D_{tr4}}^{schd.\ turn}, t_{D_{tr12}}^{schd.\ turn}\right]$		
14: From left to right: $\left[t_{E_{tr2}}^{schd.\ turn}, t_{E_{tr7}}^{schd.\ turn}, t_{E_{tr9}}^{schd.\ turn}, t_{E_{tr14}}^{schd.\ turn}\right]$		

Figure 4-12: Time-position diagram of the commercial timetable of a Y-shaped line with short-turn and terminal stations in the branches and a terminal station in the common section

The number of trains required (n_{trains}) is calculated from Equations (4-3), (4-4) and (4-5). Although n_{trains} must be an integer number, the number of trains giving each

type of service ($n_{trains \in serv\ i}$) can be rational, which means that some trains will be varying the type of service in succeeding travels.

4.5. CONCLUSIONS AND CONTRIBUTIONS

This chapter fills the gap in the literature with respect to the studies about simulation-based assessments of infrastructure improvements using complex topologies, as it produces the information required by the simulator (the tool in charge of the assessments) in order to work with these types of topology.

For a better understanding and modularization of the railway simulator, all the developments made in this chapter with respect to the topologies can be grouped in a ***topology sub-module***, which is the one that provides the information to the ***timetable generator*** in order to obtain the commercial timetables associated with the different types of topology (the structure of the updated railway simulation model including the topology sub-module, as well as all the advances made in the traffic modelling, will be given in Section 6.1).

The details about the variables required for the generation of the commercial timetables have been explained, as well as the procedure to determine the number of trains that must be in service in order to comply with the operation requirements. As seen in Section 2.3 and 3.3, commercial timetables are one of the main inputs required by the realistic traffic models developed in this PhD. Therefore, obtaining the representative traffic scenarios associated with the complex topologies presented in this chapter is straightforward once having their commercial timetables.

The topologies studied in this chapter have been the following ones:

- Line with two terminal stations.
- Line with short-turn and terminal stations.
- Line with branches.
- Line with branches, short-turn and terminal stations.

The line with branches, short-turn and terminal stations will be used for the remaining chapters of this document, since it is the most complex one and it integrates the features of the other complex topologies studied (the line with short-turn and terminal stations and the line with branches).

CHAPTER 5

DESIGN OF NATURE-INSPIRED OPTIMIZATION ALGORITHMS

As already explained in this document, undertaking infrastructure improvements, and more concretely the installation of RSs or ESSs, implies a great investment that must be carefully studied. Railway simulators are usually the tool in charge to assess the impact of these improvements. Therefore, the more precise and realistic the simulator, the better assessment will be obtained and the more confidence on the investment will have the railway operators. Chapters 2, 3 and 4 have focused on the development of different features of the railway simulator in order to improve its accuracy and realism.

Once having the improvements of the simulator, the next step is to design the optimization algorithms that, working with the information provided by the railway simulator, determine the optimal configuration of the infrastructure improvements. This task is going to be tackled in this chapter. In particular, the optimization of the infrastructure improvements will be addressed in two variants: the single-stage and the multi-stage optimization. In the single-stage optimization, the whole budget for the installation of the infrastructure improvements is available from the beginning. In the multi-stage optimization the whole budget is divided into stages, separated in time.

The optimization algorithms designed in this chapter have been applied to a case study in order to compare their performance. The case study takes into account the improvements in the railway simulator model proposed in Chapters 2 and 3, which makes it possible the simulation of representative traffic scenarios with large and small perturbations, and uses one of the complex topologies presented in Chapter 4, in particular a line with branches, short-turn and terminal stations.

Therefore, this case study can be considered the final case study of the thesis. For the sake of clarity, instead of giving its details in this chapter, which focuses on the design of the optimization algorithms, they are going to be given in Chapter 6, which formalizes the methodology proposed in this thesis to assess the installation of electrical infrastructure improvements and applies it to this final case study.

Section 5.1 provides a brief introduction to the research in the literature that addresses, by different means, the design of improvements in the MTS electrical infrastructure. Section 5.2 describes the way the optimization algorithms communicate with the railway simulator. Sections 5.3 and 5.4 focus, respectively, on the single-stage and the multi-stage optimization problems. Finally, Section 5.5 presents the main conclusions and contributions of the chapter.

5.1. INTRODUCTION

Table 5-1 and Table 5-2 show a summary of the state of the art on the application of methodologies for designing the improvements of the electrical infrastructure by means of installing, respectively, RSs and ESSs. All these studies use simulation tools and apply analysis or optimization techniques to provide a reasonable solution.

Regarding the studies in the literature that focus on the improvement of the infrastructure with the installation of RSs, few of them deal with the problem of the optimal location and size. (Chuang, 2005; Hui-Jen et al., 2005; Jefimowski & Szeląg, 2018; López-López, Álvaro J., 2016; Pereira et al., 2014) use Nature-Inspired optimization algorithms. In particular (Hui-Jen et al., 2005; Jefimowski & Szeląg, 2018; Pereira et al., 2014) use the Genetic Algorithm (GA), while (Chuang, 2005) uses the Immune Algorithm (IA) and (López-López, Álvaro J., 2016) uses the Particle Swarm Optimization algorithm (PSO).

There are also a few works that study the optimal location and sizing for the ESSs. (Calderaro et al., 2015; Wang et al., 2014; Xia et al., 2015) use Nature-Inspired optimization algorithms. In particular, (Wang et al., 2014; Xia et al., 2015) propose the Genetic Algorithm (GA), while (Calderaro et al., 2015) proposes the Particle Swarm Optimization Algorithm (PSO). There are also some authors who apply mathematical optimization models, such as the nonlinear optimization based on Lagrange multipliers (LGM) proposed by (Ratniyomchai et al., 2014; Ratniyomchai et al., 2015), or the mixed integer linear programming (MILP) proposed by (de la Torre et al., 2015).

Table 5-1: Research works assessing the installation of RSs

Analysis / Optimization	Opt. Method	Traffic model				Reference
		Variable headway	Variable time shift	Variable dwell time	Different speed profiles	Traffic regulation system	
Optimization	GA	YES	NO	NO	NO	NO	(Jefimowski & Szeląg, 2018)
Optimization	GA	NO	NO	NO	NO	NO	(Pereira et al., 2014)
Optimization	GA	YES	" stochastic operation" (without details)		NO	NO	(Hui-Jen et al., 2005)
Optimization	IA	YES			NO	NO	(Chuang, 2005)
Analysis	-	NO	NO	NO	NO	NO	(Fazel et al., 2014)
Analysis	-	YES	NO	NO	YES	YES	(Bae, 2009)
Optimization	PSO	YES	YES	YES	NO	NO	(López-López, Álvaro J., 2016)

Table 5-2: Research works assessing the installation of ESSs

Analysis / Optimization	Opt. Method	Traffic model					Reference
		Variable headway	Variable time shift	Variable dwell time	Different speed profiles	Traffic regulation system	
Optimization	GA	YES	NO	NO	NO	NO	(Wang et al., 2014)
Optimization	GA	NO	NO	NO	NO	NO	(Xia et al., 2015)
Optimization	LGM	NO	NO	NO	NO	NO	(Ratniyomchai et al., 2014)
Optimization	LGM	NO	NO	NO	NO	NO	(Ratniyomchai et al., 2015)
Optimization	MILP	NO	NO	NO	NO	NO	(de la Torre et al., 2015)
Optimization	PSO	NO	NO	NO	NO	NO	(Calderaro et al., 2015)
Analysis	-	YES	NO	NO	NO	NO	(Gao et al., 2015)
Analysis	-	YES	NO	YES	NO	NO	(Roch-Dupré et al., 2017)

As can be seen, the vast majority of studies in both tables use railway simulators with very simplified traffic models. Additionally, the entire research in the literature only works with the simplest line topology: line with two terminal stations.

Therefore, it is necessary to design optimization algorithms capable, on the one hand, to work with a railway simulator with an accurate and realistic traffic model (such as the one developed in Chapters 2 and 3) and, on the other hand, to tackle with complex topologies (such as the ones presented in Chapter 4).

It must be also noted that all the papers previously cited only address the single-stage optimization, which makes the multi-stage optimization proposed in Section 5.4 of this chapter a novelty that can be of great interest and application.

The search for the optimum configuration will be made with several nature-inspired optimization algorithms: GA, PSO and FA. These algorithms have proved to be very flexible and successful in dealing with computationally-intensive and highly non-linear and non-convex problems (Ertenlice & Kalayci, 2018; Mavrovouniotis et al., 2017; Saka et al., 2016), such as the one presented by the realistic railway simulator used in this PhD. The detailed explanation of the reasons for selecting this type of algorithms instead of formal mathematical optimization models has already been given in Section 1.6.

5.2. COMMUNICATION BETWEEN OPTIMIZATION ALGORITHMS AND RAILWAY SIMULATOR

The optimization algorithms decide which, among all the possible configurations for the infrastructure improvements, produces the best result in a balance between energy saving and installation costs. This balance is stablished by the fitness function, which is the Net Present Value (NPV) computed from evaluating the cash flows in the period studied (the positive cash flows being associated with the energy saving and the negative cash flows with the investments).

The attributes of each configuration are the following:

- Number of RSs /ESSs to be installed.
- Location of the RSs /ESSs to be installed.
- Power (kW) of each RS / ESS to be installed.
- Capacity (kWh) of each ESS to be installed (this variable does not apply to the RSs optimization).

Figure 5-1 depicts the communication process between any optimization algorithm and the simulator. The communication is made up of the following steps for every iteration:

1. The algorithm gives the configuration -locations, powers and capacities (the last one only in the case of ESSs)- of the installations to be tested as the input data for the simulator.

2. The electrical network module simulates each RSs/ESSs configuration provided by the algorithm for all the traffic scenarios generated in the traffic simulation. After performing the electrical simulations, the energy saving associated with this configuration is given as the output data to the optimization algorithm.
3. The NPV of each configurations is computed from its associated energy saving and installation cost (see Sections 5.3.1 and 5.4.1 to see the way NPV is computed for, respectively, the single-stage and the multi-stage optimization). The NPV will be used as the fitness value of the optimization problem, which provides the information required by the algorithms to update the configurations to be tested by the simulator in the next iteration.

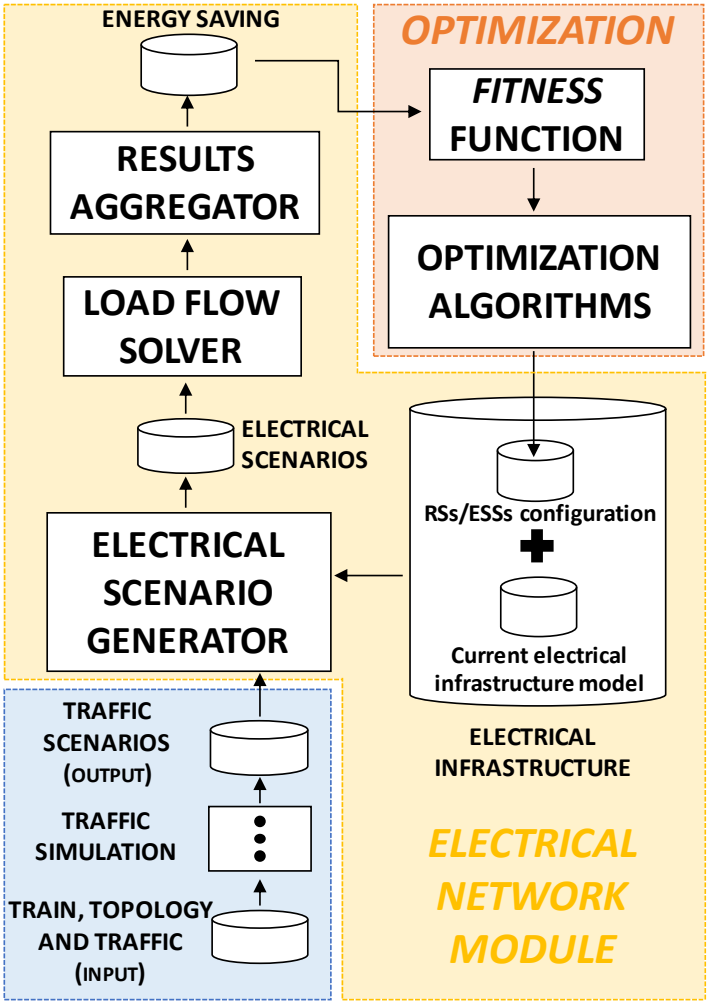

Figure 5-1: Communication between optimization algorithms and railway simulator

5.3. SINGLE-STAGE OPTIMIZATION

The three optimization algorithms selected for the single-stage optimization are the Genetic Algorithm (GA) (Goldberg & Holland, 1988), the Particle Swarm Optimization Algorithm (PSO) (Kennedy & Eberhart, 1995) and the Fireworks Algorithm (FA) (Tan & Zhu, 2010). As explained in Section 1.6, the GA and the PSO are, respectively, the main exponents of evolutionary and swarm algorithms and have been used in multiple

applications (Long, Wu, Huang, & Wang, 2015; Lynn & Suganthan, 2015), while the FA is an interesting and novel proposal within the swarm algorithms with promising results (He, Li, Zhang, & Cao, 2019).

It must be noted that, for a first approximation, the two variables that are going to be optimized are the location and the power of the RSs/ESSs. As previously stated, although these are all the variables required for the RSs optimization, the capacity is also a variable of decision in the case of the ESSs. Nevertheless, its importance as a variable of decision is residual in comparison with the location and power, which can be considered as the main variables of the optimization (as a note, in the optimum solution provided by the algorithms the cost associated with the power of the ESS is more than 10 times higher than the cost associated with the capacity).

Therefore, in this first approximation, the capacity will be set to a reasonable value when optimizing the installation of ESSs, so that significant energy saving is not lost due to lack of storage capacity. The main aim of this simplification is to focus on the analysis of the behavior of the algorithms with respect to the two main variables and have a first insight on the optimization problem. Once having tested the behavior of the optimization algorithms, the capacity will be included in the formulation of the multi-stage optimization problem, which can be also applied to the single-stage optimization just by setting the number of stages to one.

5.3.1. SINGLE-STAGE OPTIMIZATION PROBLEM FORMULATION

In order to fit with this optimization problem, the standard GA, PSO and FA have been reformulated as knapsack problems with some changes. The knapsack problem is a well-known problem found in the optimization literature (Gonsalves, 2017) and consists in picking and choosing a set of items from a given larger set to put in the knapsack so as to maximize the total value, under certain constraints. The knapsack optimization problem is generally coded as a bit string containing zeros and ones – a "one" representing the fact that a certain item is selected and a "zero" representing the fact that a certain item is not selected. For the particular case of this optimization problem, each item represents one of the potential locations where an RS/ESS can be installed and, instead of having a bit string containing zeros and ones, each item has a value from a set of discrete values that represent the possible amounts of power that can be installed. The constraints are related to the maximum sizes and maximum admissible budget that cannot be exceeded.

Therefore, each individual $i(\overline{ind}_i)$ of the population contains the characteristics of one configuration of RSs/ESSs according to the structure given by Equation (5-1).

$$\overline{ind}_i = \left[pow(\overline{ind}_i, 1)\ , pow(\overline{ind}_i, 2)\ \cdots pow(\overline{ind}_i, k)\ \cdots\ pow(\overline{ind}_i, N)\ \right] \quad \textbf{(5-1)}$$

where:

- $pow(\overline{ind}_i, k)$ is the item associated with position k and represents the power (kW) for the RS/ESS installed in that position. The possible values for this variable are discrete, going from 0 kW (no RS/ESS installed in position k) to max_{pow} kW

(maximum power that can be installed) in steps of $step_{pow}$ kW. Therefore, each item must take one value out of the set of $\frac{max_{pow}}{step_{pow}}$ discrete values available (being max_{pow} a multiple of $step_{pow}$).

- N is the number of potential locations for installing the RS/ESS. This means that each $\overline{ind}_i$ will have N items.

The optimal solution is the one that yields the highest Net Present Value (NPV) of the installation. Therefore, the fitness function for a given individual i ($\overline{ind}_i$) is the NPV of its associated RSs/ESSs configuration. Equation (5-2) defines the fitness function.

$$NPV(\overline{ind}_i) = \sum_{t=1}^{T} \frac{\left(E_{Raw}^{ANNUAL} - E_{infr.impr}^{ANNUAL}(\overline{ind}_i)\right) \cdot e_{cost}}{(1+wacc)^t} - C_0(\overline{ind}_i) \qquad \textbf{(5-2)}$$
$$\boldsymbol{s.t} \qquad C_0(\overline{ind}_i) \leq max_{budget}$$

where:

- E_{Raw}^{ANNUAL} is the annual energy consumption without any infrastructure improvement. This value is obtained from the railway simulator.
- $E_{infr.impr}^{ANNUAL}(\overline{ind}_i)$ is the annual energy consumption obtained with the RSs/ESSs configuration determined by ind_i. This value is obtained from the simulation of that configuration in the railway simulator.
- e_{cost} is the energy price. This parameter allows transforming the energy saving, which is computed by comparing the total energy consumption with and without infrastructure improvement $\left(E_{Raw}^{ANNUAL} - E_{infr.impr}^{ANNUAL}(\overline{ind}_i)\right)$ into economic cash flows.
- $C_0(\overline{ind}_i)$ is the installation cost of the RSs/ESSs configuration determined by ind_i.
- $wacc$ is the Weighted Average Cost of Capital.
- T is the period to evaluate the investment (in years).
- max_{budget} is the maximum amount of money available to undertake the infrastructure improvement.

The reason why the NPV has been selected as fitness function is that it is capable of finding a balance between what is important from the environmental point of view -the energy saving- and what is important from the economic point of view -justifying the investment in the infrastructure improvement and obtaining economic benefits from it-. The investment will be economically profitable if the NPV is positive in T. Therefore, the optimization algorithms will try to determine the configuration with the highest NPV (the higher the NPV, the better the balance between the energy saving and the cost of the installation).

5.3.2. IMPLEMENTATION OF THE SINGLE-STAGE OPTIMIZATION ALGORITHMS

5.3.2.1. SINGLE-STAGE GENETIC ALGORITHM (S-GA)

For the sake of clarity, the nomenclature used in the general formulation of Section 5.3.1 will be adapted to a nomenclature that fits better with the GA:

- The individuals will be referred to as chromosomes.
- The items will be referred to as genes.

The Genetic Algorithm (GA) is a well-known optimization metaphor based on the natural selection process. It begins with a population of random solutions called chromosomes, and evolves them through several cycles of selection, crossover and mutation operations. The better-fit selected chromosomes exchange the promising genetic information, which is further mutated to give rise to ever evolving and best fit or optimal solutions.

Following the structure presented in Equation (5-1), each chromosome has N genes that can take one of the $\frac{max_{pow}}{step_{pow}}$ discrete values available, according to the knapsack formulation previously explained.

The steps of the S-GA (the GA particularized for the single-stage optimization problem) are based on (Gonsalves, 2017), listed below and depicted in Figure 5-2.

S-GA 1. Random generation of a population of chromosomes: a population of CHR chromosomes is generated. At the beginning all the genes of all the chromosomes are initialized with null values and during the generation process of each chromosome, one of the N genes is randomly selected and given a value from the set of non-zero discrete values available. This process is repeated until having an associated budget higher than a fraction of the maximum budget, discarding in every new selection the genes already selected.

S-GA 2. Fitness evaluation of the initial population of chromosomes: the infrastructure configurations of the initial chromosomes are simulated in the railway simulator, obtaining the energy saving associated with them. With this information and the cost of the installation associated with each chromosome, the NPV is computed by applying Equation (5-2).

S-GA 3. Selection: the ***tournament selection*** has been selected and the population resulting from this procedure is called *parent population.* A pair of chromosomes is randomly selected from the *children population* of the previous iteration or from the initial population in case of the first iteration. The fitness of both chromosomes are compared and the chromosome with the highest fitness is selected as a 'parent' chromosome for the next generation. This selection procedure is repeated until the number of selected parents equals the population size and the same chromosome can be selected more than once (every pair is randomly selected from the whole *children population* of the previous iteration/initial population). After having the parents for the new population, one of them is randomly selected and replaced by the chromosome

with the best fitness of the *children population* of the previous iteration/initial population.

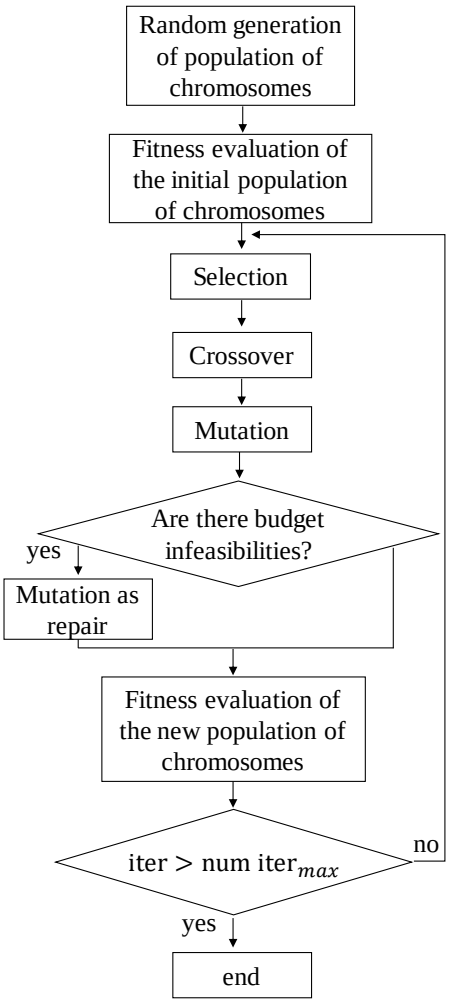

Figure 5-2: Single-stage GA flowchart

S-GA 4. Crossover: two types of crossover mechanisms have been selected (each one has been applied in a different optimization scenario, as will be seen in Section 5.3.3.1).

a. ***One-point crossover***: chromosomes of the *parent population* are randomly selected in pairs as well as a single crossover point for each pair. The part of the chromosome after the crossover point is exchanged between the parents.
b. ***Uniform crossover***: chromosomes of the *parent population* are randomly selected in pairs and each gene is swapped between each pair with a probability p_{swap}.

The population resulting from the crossover will be called *children population.*

S-GA 5. Mutation: it is a small modification consisting in adding or subtracting $step_{pow}$ (each possibility with a 50% probability) to the genes randomly selected for the mutations. Every chromosome of the *children population* can be modified in

one of its genes with a probability mut_1, in two of them with a probability mut_2 or in none of them with a probability mut_0. The relationship among these probabilities is shown in Equation (5-3).

$$mut_2 < mut_1 \ll mut_0$$
$$mut_1 + mut_2 + mut_0 = 1 \quad \textbf{(5-3)}$$

If any mutated gene crosses the maximum or minimum limits in power, the maximum or minimum power, respectively, is selected for that gene.

S-GA 6. Mutation as repair: it may happen that some chromosomes of the *children population* become not feasible in terms of budget (installation cost higher than the maximum budget) after the mutation. In order to avoid these budget infeasibilities, the mutation as repair mechanism is applied to those chromosomes. This mechanism consists in randomly selecting genes with non-zero values and reducing its size in $step_{pow}$ (the minimum admissible change in size) until the installation cost of the chromosome becomes feasible.

S-GA 7. Fitness evaluation of the new population of chromosomes: the chromosomes of the *children population* are evaluated in the same way as described in step 2 (**S-GA 2**). Once the new fitness values are obtained, the algorithm proceeds to the next iteration, which starts in step 3 (**S-GA 3)**. This process is repeated for a number of iterations given by $num\ iter_{max}$.

5.3.2.2. SINGLE-STAGE PARTICLE SWARM OPTIMIZATION ALGORITHM (S-PSO)

For the sake of clarity, the nomenclature used in the general formulation of Section 5.3.1 will be adapted to a nomenclature that fits better with the PSO:

- The individuals will be referred to as particles.
- The items will be referred to as dimensions.

The Particle Swarm Optimization (PSO) is a metaphor in the swarm intelligence paradigm. It has become a popular meta-heuristic algorithm in the optimization domain and has been successfully applied to optimization problems ranging from business, engineering, healthcare, etc. Based on the food-gathering behavior of swarms of bees, birds and schools of fish, PSO optimally balances exploration and exploitation. Simplicity in implementation, negligible computational overhead and rapid convergence have made it one of the outstanding swarm intelligence paradigms.

Each particle maintains a history of its flying over the search space. In every cycle of flying, the swarm also records two important pieces of information: the particle-best (*pbest*), which is the best position found by a particle in the course of flying, and the global-best (*gbest*), which is the best position found by the swarm as a whole. These two values act as beacons to guide the flying of the rest of the particles towards the global optimum during the search.

Unlike the GA, which is designed for discrete search spaces, the PSO was originally designed to deal with continuous search spaces. Nevertheless, the formulation of the PSO as a knapsack problem allows it to successfully deal with discrete search spaces.

According to this reformulation, each particle of the population has N dimensions that can take $\frac{max_{pow}}{step_{pow}}$ possible values (see Equation (5-1)). In the case of the PSO, the position of the particle in a given iteration will be defined by the value taken by each of its N dimensions. The steps of the S-PSO (the PSO particularized for the single-stage optimization problem), are based on (Gonsalves, 2017), listed below and depicted in Figure 5-3.

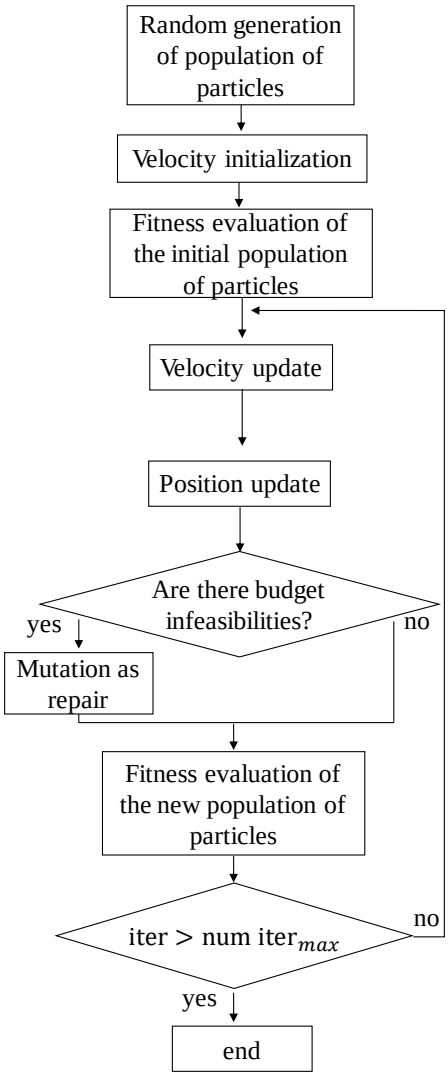

Figure 5-3: Single-stage PSO flowchart

S-PSO 1. Random generation of a population of particles: a population of P particles is generated. At the beginning all the dimensions of all the particles are initialized with null values and during the generation process of each particle, one of the N dimensions is randomly selected and given a value from the set of non-zero discrete values available. This process is repeated until having an associated budget higher than a fraction of the maximum budget, discarding in every new selection the dimensions already selected.

S-PSO 2. Velocity initialization: each particle has a position change known as velocity. The velocity is also a vector with N dimensions. In the initialization, each of the

N dimensions of the velocity take any value (with the same probability) in the continuous interval $[-step_{pow} : +step_{pow}]$.

S-PSO 3. Fitness evaluation of the initial population of particles: the infrastructure configurations of the initial particles are simulated in the railway simulator, obtaining the energy saving associated with them. With this information and the cost of the installation associated with each particle, the NPV is computed by applying Equation (5-2).

S-PSO 4. Velocity update: for a given iteration, $iter$, the velocity of each particle is updated according to Equation (5-4). It must be noted that every vector in this equation has N dimensions.

$$\overline{v_{PSO}}(iter) = w \cdot \overline{v_{PSO}}(iter-1) + c_1 \cdot r_1 \cdot \left(\overline{pbest} - \overline{x_{PSO}}(iter-1)\right) + c_2 \cdot r_2 \cdot \left(\overline{gbest} - \overline{x_{PSO}}(iter-1)\right) \quad \textbf{(5-4)}$$

where:

- $\overline{v_{PSO}}$ is the particle velocity vector.
- $\overline{x_{PSO}}$ is the particle position vector.
- w is the inertia weight.
- $\overline{pbest}$ is the vector with the best position found by the particle in the course of flying.
- $\overline{gbest}$ is the vector with the best position found by the swarm as a whole.
- c_1, c_2 are called social factors (being $c_1$the personal attractor and $c_2$the global attractor).
- r_1, r_2 are random numbers between 0 and 1.

If any velocity dimension crosses the minimum or maximum velocity limits ($-step_{pow}\ and\ +step_{pow}$, respectively), the exceeded limit is selected for that dimension.

S-PSO 5. Position update: for a given iteration, $iter$, the position of each particle is updated according to Equation (5-5). The value of each dimension of the particle obtained from updating the position is rounded to the nearest discrete value from the set of possible values.

$$\overline{x_{PSO}}(iter) = \overline{x_{PSO}}(iter-1) + \overline{v_{PSO}}(iter) \quad \textbf{(5-5)}$$

If any position dimension crosses the maximum or minimum limits in power, the maximum or minimum power, respectively, is selected for that dimension.

S-PSO 6. Mutation as repair: it may happen that some particles become not feasible in terms of budget (installation cost higher than the maximum budget) after the position update. In order to avoid these budget infeasibilities, the mutation as repair mechanism explained for the S-GA is also applied to the S-PSO.

S-PSO 7. Fitness evaluation of the new population of particles: the new particles are evaluated in the same way as described in step 3 (**S-PSO 3**). Once the new fitness values are obtained, the algorithm proceeds to the next iteration, which starts in step 4 (**S-PSO 4**). This process is repeated for a number of iterations given by $num\ iter_{max}$.

5.3.2.3. SINGLE-STAGE FIREWORKS ALGORITHM (S-FA)

For the sake of clarity, the nomenclature used in the general formulation of Section 5.3.1 will be adapted to a nomenclature that fits better with the FA:

- The individuals will be referred to as fireworks or sparks.
- The items will be referred to as dimensions.

The Fireworks Algorithm (FA) is a recent Swarm Intelligence optimization algorithm, which derives its inspiration from the fireworks exploding in the night sky. The algorithm generates random initial positions of F fireworks. The fireworks explode generating SPK regular sparks, depending on their respective amplitudes. Fireworks with higher fitness values have a smaller explosion amplitude and a larger number of explosion sparks, while fireworks with lower fitness values have a larger explosion amplitude and a smaller number of explosion sparks. In addition, $GSPK$ random sparks are also generated based on a Gaussian mutation process. A new population of F fireworks is selected at the end of each iteration. This may include the original fireworks, as well as the regular and Gaussian sparks. The elitist strategy is maintained by always inserting the current best individual (firework or spark) in the new population.

Like the PSO, the FA was originally designed to deal with continuous search spaces. Nevertheless, the formulation of the FA as a knapsack problem allows it to successfully deal with discrete search spaces. According to this reformulation, each spark of the population has N dimensions that can take $\frac{max_{pow}}{step_{pow}}$ possible values (see Equation (5-1)). In the case of the FA, the location of the spark in a given iteration is defined by the value taken by each of its N dimensions. Apart from the reformulation as a knapsack problem, some parts of the standard FA defined by (Tan & Zhu, 2010) have been discretized. The steps of the discretized S-FA (the discretized FA particularized for the single-stage optimization problem) are listed below and depicted in Figure 5-4.

S-FA 1. Random generation of a population of fireworks: a population of F fireworks is generated. At the beginning all the dimensions of all the fireworks are initialized with null values and during the generation process of each firework, one of the N dimensions is randomly selected and given a value from the set of non-zero discrete values available. This process is repeated until having an associated budget higher than a fraction of the maximum budget, discarding in every new selection the dimensions already selected.

S-FA 2. Fitness evaluation of the initial population of fireworks: the infrastructure configurations of the initial fireworks are simulated in the railway simulator, obtaining the energy saving associated with them. With this information and the

cost of the installation associated with each firework, the NPV is computed by applying Equation (5-2).

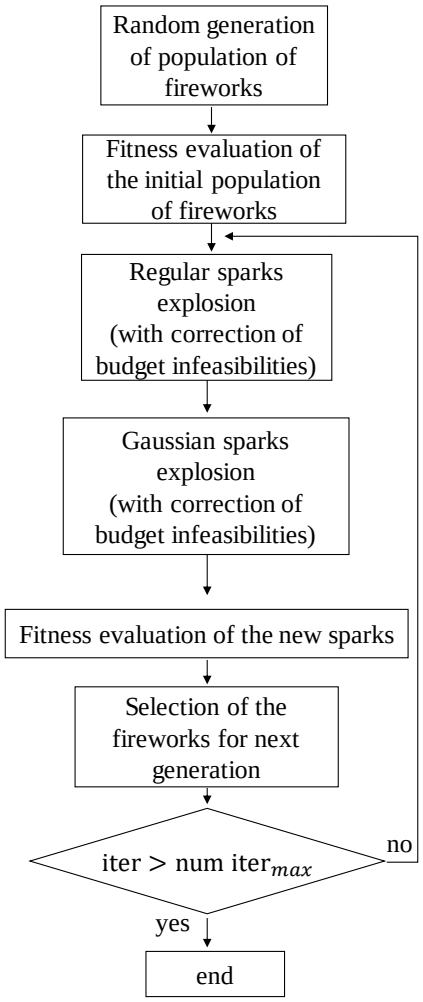

Figure 5-4: Single-stage FA flowchart

S-FA 3. Regular sparks explosion: from each firework a variable number of regular sparks is set off. The explosion has the following steps:

S-FA 3.1. Selecting the number of regular sparks per firework: each firework has a different amount of regular sparks to set off, which directly depends on the fitness of the firework: the higher the fitness of the firework -more concretely, the higher the difference with respect to the worst fitness-, the higher the number of sparks to set off from that firework. The number of regular sparks per firework is determined by Equation (5-6).

$$\begin{cases} n_{sp_{\overline{fw_i}}} = round\left(SPK_{ctrl} \cdot \dfrac{fit_{\overline{fw_i}} - fit_{WORST} + \varepsilon}{\sum_{j=1}^{F}\left(fit_{\overline{fw_j}} - fit_{WORST}\right) + \varepsilon}\right) & if\ n_{sp_{min}} \leq n_{sp_{\overline{fw_i}}} \leq n_{sp_{max}} \\ n_{sp_{min}} & if\ n_{sp_{\overline{fw_i}}} < n_{sp_{min}} \\ n_{sp_{max}} & if\ n_{sp_{\overline{fw_i}}} > n_{sp_{max}} \end{cases} \quad \textbf{(5-6)}$$

where:

- $n_{sp_{\overline{fw_i}}}$ is the number of regular sparks to be set off from firework i $(\overline{fw_i})$.
- F is the number of fireworks, which corresponds to the population size.
- SPK_{ctrl} is a parameter that controls the number of regular sparks that can be set off from the F fireworks.
- $fit_{\overline{fw_i}}$ is the fitness of firework i $(\overline{fw_i})$.
- fit_{WORST} is the worst fitness of the F fireworks.
- ε is a very small constant used to avoid zero-division error and other numerical singularities.
- $n_{sp_{min}}$ is the minimum number of sparks that can be set off from a firework.
- $n_{sp_{max}}$ is the maximum number of sparks that can be set off from a firework.

It must be noted that the total number of regular sparks, SPK, generated from the F fireworks is variable in every iteration due to rounding effects and to the restrictions in the minimum and maximum number of sparks that can be set off from a firework, although $SPK \cong SPK_{ctrl}$.

S-FA 3.2. Selecting the amplitude of explosion per firework: the amplitude of explosion of each firework depends directly on the fitness of the firework: the smaller the fitness of the firework -more concretely, the higher the difference with respect to the best fitness-, the bigger the amplitude. The bigger the amplitude, the lower the exploitation and the higher the exploration (on the contrary, the smaller the amplitude, the higher the exploitation and the lower the exploration). The reason for having different amplitudes depending on the fitness is to find the best ratio between exploration and exploitation. On the one hand, in those fireworks where the fitness value is high, the algorithm will select a small amplitude so that it can exploit the area near to the solution of the firework in order to try to find a better one but with small differences. On the other hand, in those fireworks where the fitness value is low, the algorithm will select a big amplitude to explore new areas of the search space, where there may be solutions that can lead to higher fitness values but that present big differences with respect to the solution of the firework. In the original fireworks algorithm, the value of the amplitude is continuous. Nevertheless, as the search space in this case is discrete, some changes with respect to the original formula of (Tan & Zhu, 2010) have been applied.

Initially, a continuous normalized amplitude, $Ac_{\overline{fw_i}}$, is computed for each firework i $(\overline{fw_i})$ according to Equation (5-7).

$$Ac_{\overline{fw_i}} = \frac{fit_{BEST} - fit_{\overline{fw_i}} + \varepsilon}{\sum_{j=1}^{F}(fit_{BEST} - fit_{\overline{fw_j}}) + \varepsilon} \quad \textbf{(5-7)}$$

where fit_{BEST} is the best fitness of the F fireworks in the current iteration. Then, a discrete amplitude will be obtained for each firework i depending on the associated $Ac_{\overline{fw_i}}$:

- $step_{pow}$ when $Ac_{\overline{fw_i}}$ is within the x[th] percentile of the smallest continuous radii (which is equivalent to be within the x% of fireworks with the best fitness).
- $2 \cdot step_{pow}$ when $Ac_{\overline{fw_i}}$ is out of the x[th] percentile of the smallest continuous radii (which is equivalent to be within the (100-x)% of fireworks with the worst fitness).

After this transformation from continuous to discrete, each firework i will have an associated discrete amplitude of explosion $Ad_{\overline{fw_i}}$.

S-FA 3.3. Generating the regular sparks: each regular spark differs from the firework from which it is set off in z number of dimensions, z being a random number between 0 and the total number of dimensions (N). The z dimensions selected to be modified as well as the order in which they are going to be modified is also determined randomly. The formula to apply the changes in each selected dimension k of firework i ($\overline{fw_i}$) to obtain the values of regular spark α ($\overline{sp_\alpha}$) for that dimension is defined by Equation (5-8). This equation will be applied to each of the $z_{\overline{sp_\alpha}}$ randonmly selected dimensions for regular spark α.

$$\overline{sp_\alpha}(k) = \overline{fw_i}(k) + randsample\left(\left[-Ad_{\overline{fw_i}} : step_{pow} : 0\right) \cup \left(0 : step_{pow} + Ad_{\overline{fw_i}}\right]\right) \quad \textbf{(5-8)}$$

where:

- $\overline{fw_i}(k)$ is the value for dimension k of firework i.
- $\overline{sp_\alpha}(k)$ is the value for dimension k of regular spark α.
- $randsample$ is a logical operator that randomly selects one of the values of the input vector- $\left([-Ad_{\overline{fw_i}} : step_{pow} : 0) \cup (0 : step_{pow} + Ad_{\overline{fw_i}}]\right)$ in this case- according to a uniform distribution.

If dimension k of regular spark α crosses the maximum or minimum limits in power, the maximum or minimum power, respectively, is selected for dimension k of regular spark α.

If an increment in the power of dimension k of regular spark α makes the spark infeasible in terms of budget, that increment is reduced to a feasible increment (this mechanism emulates, somehow, the mutation as repair mechanism of the S-GA and the S-PSO and ensures that the new regular sparks comply with the budget).

S-FA 4. Gaussian sparks explosion: according to (Tan & Zhu, 2010), in order to keep the diversity of sparks, another type of explosion must also be applied to set off a very reduced amount of sparks. This type of explosion is called Gaussian Explosion and is only applied to $GSPK$ number of sparks. Each

Gaussian spark is set off from a different firework and differs from it in z randomly selected dimensions, z being a random number that goes from 0 to the total number of dimensions (N). The z dimensions selected to be modified as well as the order in which they are going to be modified is also determined randomly. The algorithm to apply the changes in each selected dimension k of firework i ($\overline{fw_i}$) to obtain the values of Gaussian spark δ ($\overline{spg_\delta}$) for that dimension is described by Equation (5-9). This algorithm will be applied to each of the $z_{\overline{spg_\delta}}$ randonmly selected dimensions for Gaussian spark δ.

$$\begin{aligned} &while\ coeff < 0 \\ &\quad coeff = Gaussian\ (1{,}1) \\ &end \end{aligned} \qquad \textbf{(5-9)}$$

$$\overline{spg_\delta}(k) = round\left(\overline{fw_i}(k) \cdot coeff \Big/ step_{pow}\right) \cdot step_{pow}$$

where:

- $coeff$ is the coefficient of Gaussian Explosion. It must be noted that $coeff$ must not be negative because the power of the RS/ESS cannot be negative, just 0 (which means no installation of an RS/ESS in the location associated with dimension k).
- $\overline{spg_\delta}(k)$ is the value for dimension k of Gaussian spark δ.

If dimension k of Gaussian spark δ crosses the maximum limit in power (in this case it is not possible to cross the minimum), the maximum power is selected for dimension k of Gaussian spark δ.

If an increment in the power of dimension k of Gaussian spark δ makes the spark infeasible in terms of budget, that increment is reduced to a feasible increment (this mechanism emulates, somehow, the mutation as repair mechanism of the S-GA and the S-PSO and ensures that the new Gaussian sparks complies with the budget).

S-FA 5. Fitness evaluation of the new sparks: the new sparks (the regular and the Gaussian ones) are evaluated in the same way as described in step 2 (**S-FA 2**).

S-FA 6. Selection of the locations of fireworks for the next generation: F new fireworks to set off the sparks of the next generation must be selected from the fireworks and sparks of the current generation. Among the F fireworks, SPK regular sparks and $GSPK$ Gaussian sparks of the current generation, the one with the best fitness is directly selected. The $F-1$ remaining fireworks are selected according to their distance to other locations in order to keep diversity among fireworks. For this optimization problem, distance measure is computed according to the Manhattan distance (sum of the absolute value of the differences in every dimension of the sparks/fireworks).

A firework/spark x is selected to become a firework in the next generation with a probability p, which depends on its distance to the rest of fireworks and sparks. This probability p is defined by Equation (5-10).

$$p(x) = \frac{R(x)}{\sum_{i=1}^{F} R(\overline{fw_i}) + \sum_{\alpha=1}^{SPK} R(\overline{sp_\alpha}) + \sum_{\delta=1}^{GSPK} R(\overline{spg_\delta})} \quad \textbf{(5-10)}$$

where $R(\dots)$ is the sum of the distances between the spark/firework selected and the rest of fireworks and sparks. In the case of firework/spark x, this value is computed according to Equation (5-11).

$$R(x) = \sum_{i=1}^{F}\sum_{k=1}^{N}\left|x(k) - \overline{fw_i}(k)\right| + \sum_{\alpha=1}^{SPK}\sum_{k=1}^{N}|x(k) - \overline{sp_\alpha}(k)| + \sum_{\delta=1}^{GSPK}\sum_{k=1}^{N}|x(k) - \overline{spg_\delta}(k)| \quad \textbf{(5-11)}$$

As a reminder, k stands for the dimensions of the fireworks and sparks, i for the fireworks, α for the regular sparks and δ for the Gaussian sparks.

Once the new fireworks are obtained, the algorithm proceeds to the next iteration, which starts in step 3 (**S-FA 3)**. This process is repeated for a number of iterations given by $num\ iter_{max}$.

5.3.3. COMPARISON OF THE PERFORMANCE OF THE SINGLE-STAGE OPTIMIZATION ALGORITHMS

A test has been used to compare the performance of the single-stage optimization algorithms. This test uses the final case study of this thesis (explained in detail in Chapter 6) that, in short, simulates representative traffic scenarios with large and small perturbations in a line with the following main characteristics:

- **Topology**: Y-shaped line with short-turn and terminal stations in the branches and a terminal station in the common section.
- **Electrical infrastructure**: 11 traction substations (4 in the common section, 4 in the longest branch and 3 in the shortest one). The nominal voltage is 1600 V and the no-load voltage is 1650 V.

Since the main aim of this test is to compare the performance and not to analyze the configuration of the solutions or the NPV obtained with them (this will also be done in Chapter 6), the results obtained will be normalized with respect to the best fitness achieved.

The infrastructure improvement selected for the comparison test has been the ESSs and the energy storage capacity value has been set to 5 kWh (this value is big enough -but not too big- for not losing significant amounts of regenerated energy due to lack of storage capacity and allows to focus on the two main decision variables: location and power).

With respect to the variables of decision:

- Locations: Every SS location in the final case study is considered as a candidate to install an ESS, therefore $N = 11$. This choice is mainly due to operational reasons, since the installation and maintenance of the ESSs in these locations is much easier and simpler than in any other point of the line. Additionally, although installing the ESSs between Traction Substations can be better from the voltage regulation point of view, the case-study line does not have voltage drop problems.
- Power to be installed in each location: this variable of decision can take any value from the set $[0: step_{pow}: max_{pow}]$, where:
  - $step_{pow} = 500\ kW$
  - $max_{pow} = 3000\ kW$

5.3.3.1. OPTIMIZATION CASES AND ALGORITHMS' PARAMETERS

The test comprises:

- Two optimization cases for each algorithm (S-GA, S-PSO and S-FA) in order to check their robustness.
- Ten instances to be run for each algorithm and case.

Parallel computing has been used to speed up the simulation of this test: the configurations to be simulated in each iteration have been distributed among a number of workers equivalent to the number of logical processors of the server. Two type of servers have been used:

- Server type 1:
  - CPU: AMD Ryzen Threadripper 2990WX , 32 Cores - 3000 MHz (64 logical processors).
  - RAM: 64 GB.
  - Disk: NVMe 512 GB.
- Server type 2:
  - CPU: Intel(R) Xeon(R) Silver 4116, 24 Cores-2100 MHz (48 logical processors).
  - RAM: 128 GB.
  - Disk: DELL PERC H330 1.65 TB.

The average simulation time required by these servers to perform the simulations associated with a single iteration of any optimization algorithm is around 40 minutes (having variations in time that mainly depend on the number of logical processors of the server). The time required to perform the whole test is around a month.

The two cases of the S-GA differ in the crossover mechanism used: the one-point crossover has been used for Case 1 and the uniform crossover has been used for Case 2. The parameters of the S-GA have been selected experimentally and are depicted in Table 5-3.

Table 5-3: S-GA parameters

	Case 1 (S-GA1)	**Case 2 (S-GA2)**
Population size (number of chromosomes)	128	
Probability for a chromosome to mutate one gene, mut_1	20%	
Probability for a chromosome to mutate two genes, mut_2	10%	
Probability to swap each gene among parents in the uniform crossover mechanism, p_{swap}.	-	50%
Maximum number of iterations, $num\ iter_{max}$	100	

The two cases of the S-PSO differ in the way the velocity is updated. In Case 1, the inertia weight, w, is a constant parameter, while in Case 2 it changes its value in every iteration according to the formula of the "*Linear Decreasing Inertia Weight*" proposed by (J. Xin, G. Chen, & Y. Hai, 2009) and defined in Equation (5-12).

$$w(iter) = w_{max} - \frac{w_{max} - w_{min}}{num\ iter_{max}} \times iter \quad \textbf{(5-12)}$$

where:

- w_{max} is a preset maximum inertia weight.
- w_{min} is a preset minimum inertia weight.

The parameters of the PSO have been selected experimentally and are depicted in Table 5-4.

Table 5-4: S-PSO parameters

	Case 1 (S-PSO1)	**Case 2 (S-PSO2)**
Population size (number of particles)	128	
Inertia weight, w	0.5	w_{max}=0.9 w_{min}=0.4
Personal attractor, c_1	0.2	
Global attractor, c_2	0.3	
Maximum number of iterations, $num\ iter_{max}$	100	

Before giving the parameters of the two cases selected for the S-FA, a clarification regarding the population of sparks must be made: although the population of fireworks and Gaussian sparks are constant (F and $GSPK$, respectively), the number of regular sparks, SPK, is variable in every iteration, reason why it must be approximated with SPK_{ctrl} (as a reminder, it is ensured that $SPK \cong SPK_{ctrl}$). In consequence, the parameter named average population of sparks is obtained from adding SPK_{ctrl} to the number of Gaussian sparks, $GSPK$.

The two cases of the S-FA differ in the proportion between fireworks and regular sparks. Maintaining the average population of sparks in both cases, in Case 2 the number of fireworks doubles the number of fireworks of Case 1. Consequently, the number of

regular sparks per firework, $n_{sp_{\overline{fw_i}}}$, in Case 2 is on average half than in Case 1. The parameters of the S-FA have been selected experimentally and are depicted in Table 5-5.

Table 5-5: S-FA parameters

	Case 1 (S-FA1)	**Case 2 (S-FA2)**
Average population of sparks ($SPK_{ctrl} + GSPK$)	128	
SPK_{ctrl} (percentage with respect to the average population of sparks)	93%	
$GSPK$ (percentage with respect to the average population of sparks)	7%	
Number of fireworks, F	13	26
x^{th} percentile to determine the radius of explosion	40	
Min. number of regular sparks that can be set off from a firework, $n_{sp_{min}}$	$\left(\frac{SPK_{ctrl}}{F}\right) \cdot 0.1$	
Max. number of regular sparks that can be set off from a firework, $n_{sp_{max}}$	$\left(\frac{SPK_{ctrl}}{F}\right) \cdot 1.5$	
Maximum number of iterations, $num\ iter_{max}$	100	

5.3.3.2. RESULTS

Ten instances have been run for each optimization algorithm and case. The same best fitness value has been achieved by the three algorithms. The results presented in this section have been normalized with respect to it.

Figure 5-5 shows the evolution of the normalized fitness average and median for each algorithm and case with respect to the number of iterations.

The average of the fitness is very sensitive to outlier instances. This high sensitivity results in two effects:

- Effectiveness: if just one instance of a case does not reach the optimum fitness (this instance can be considered an outlier), the average of all the instances will not reach it.
- Speed of convergence: even in the case that all instances reach the optimum, the average will only do it in the iteration where the slowest instance, in terms of speed of convergence, reach the optimum (this instance can be considered an outlier if it is much slower than the rest of the instances of the case).

The median filters these outliers to a certain extent and represents what can be considered the normal behavior of the algorithm for a given optimization case. Therefore, the presentation of both metrics helps to have a better insight on the algorithms' performance.

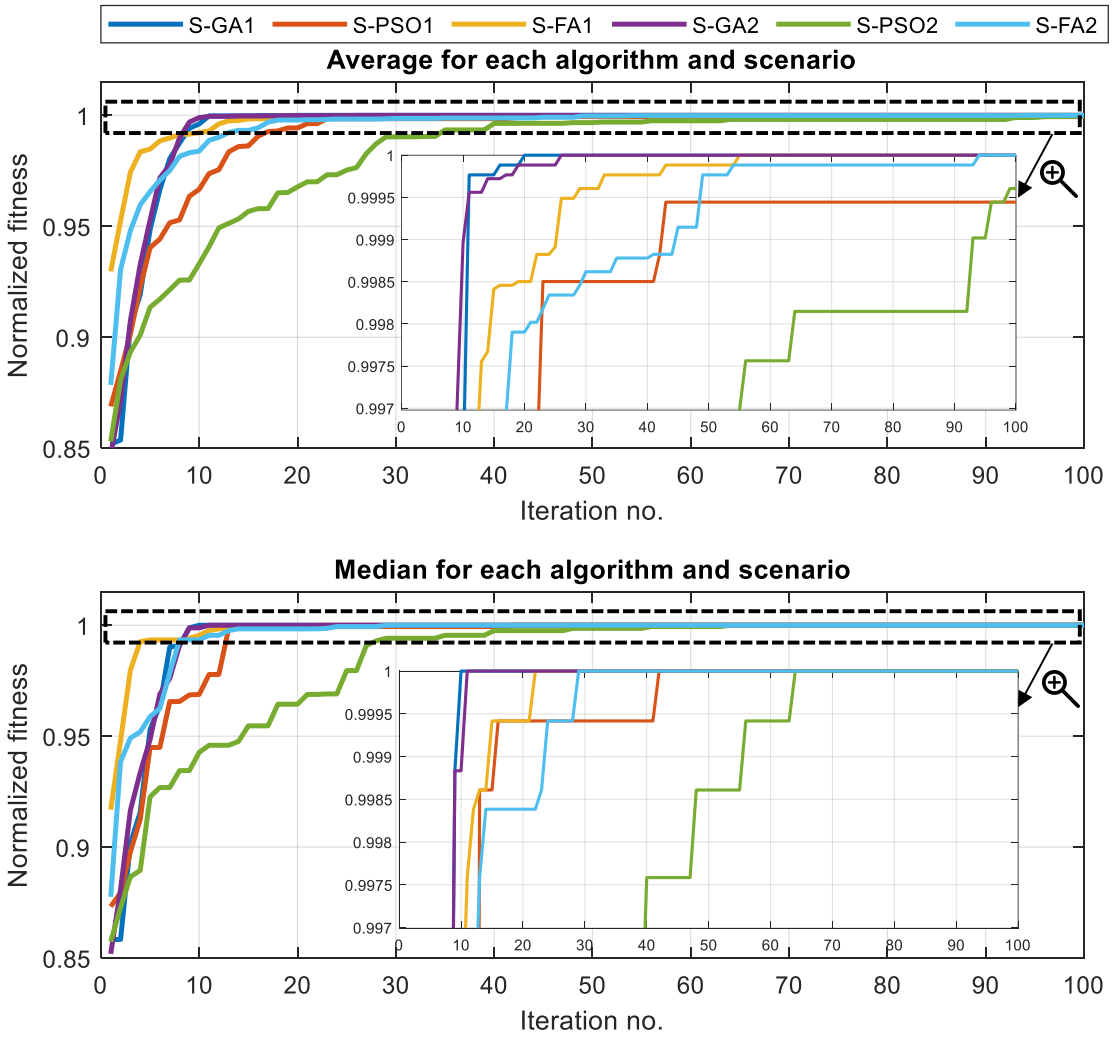

Figure 5-5: Evolution of the average and median of the normalized fitness for each algorithm and simulation case. Single-stage optimization

Regarding the effectiveness of the algorithms, the S-GA and S-FA always reach the optimum solution, while the S-PSO does not reach it in all its instances. This is clear when analyzing the evolution of the average: while this value is stabilized to 1 (as the results are normalized, this is the best fitness value obtained) in the two cases of the S-GA and the S-FA (S-GA1, S-GA2, S-FA1, S-FA2), the average obtained in the two cases of the S-PSO (S-PSO1, S-PSO2) is bellow it. Nevertheless, in a normal situation, the S-PSO reaches the optimum solution, as can be seen when analyzing the median: all the cases of all the algorithms stabilize their value to 1.

Regarding the speed of convergence of the algorithms, the S-GA is faster than the S-FA, which, in turn, is faster than the S-PSO. This is clearly seen in the vertical evolution of the averages and medians (especially in the medians, as they filter the outlier instances): the two cases of the S-GA are the first to stabilize, then the two cases of the S-FA and, finally, the two cases of the S-PSO.

Additionally, the S-GA and the S-FA are very robust, since they present a very similar performance in both optimization cases. On the contrary, the S-PSO is less robust, as its

performance is more affected by the optimization case (S-PSO1 being faster than S-PSO2).

In conclusion, the S-GA presents the best performance, followed by the S-FA and the S-PSO.

- The main difference in performance between S-GA and S-FA is on the speed of convergence, not in the effectiveness, as both algorithms reach the best solution in all the instances run. The S-GA requires less iterations to reach the optimum than the S-FA, although the S-FA is faster in the initial iterations.
- The S-PSO is worse than the S-GA and S-FA in effectiveness, in speed of convergence and in robustness.

The detailed analysis of the solutions provided by the algorithms will be given in Chapter 6. Nevertheless, it must be noted that, although it is not possible to assure that the algorithms have reached the global optimum- this is only possible with mathematical optimization- it is very likely that they have reached it. This is because the three of them (run each one ten instances per optimization case and having two optimization cases per algorithm) have reached the same best solution (in all the instances run with the S-GA and S-FA and in most of the instances run with the S-PSO). Besides, the optimization algorithms selected present good exploration features that generally prevent them from getting "trapped" in local optima.

Additionally, those configurations provided by the instances of S-PSO1 and S-PSO2 that have not achieved the highest fitness are very close to the best solution in both fitness (the normalized fitness of the worst solution is 0.9984) and configuration (same number of ESSs installed, same power installed and only one location different).

5.4. MULTI-STAGE OPTIMIZATION

Unlikely to what happens in the single-stage optimization, where the whole budget for the installation of RSs/ESSs is available from the beginning, in the multi-stage optimization the whole budget is divided into stages, separated in time. Therefore, the improvement of the infrastructure must be undertaken gradually and the algorithm must try to find the optimum configuration for each stage without exceeding the budget limits of the stage. As will be seen, the key idea of this approach is that the algorithms must take the decisions for each stage considering the installation as a whole (not separately per stages).

The two optimization algorithms selected to solve the multi-stage optimization problem are the Genetic Algorithm (GA) and the Fireworks Algorithm (FA), as they have presented the best performance in the single-stage optimization problem.

5.4.1. MULTI-STAGE OPTIMIZATION PROBLEM FORMULATION

Once having tested the proper behavior of the optimization algorithms in their single-stage formulation with a fixed capacity (for the case of the ESSs), the formulation of the

multi-stage problem made in this section will include the capacity as a variable of decision. In the case of applying the algorithms to optimize the installation of RSs, the parts of the formulation in relation with the capacity must be ignored.

In line with the formulation of the single-stage optimization algorithms of Section 5.3.1, the multi-stage GA and FA have been reformulated as a knapsack problem with some changes.

In the multi-stage formulation, each individual, $\overline{ind}_i$, of the population has a tridimensional structure, where the two first dimensions contain the information of the RSs/ESSs' configuration for each stage and the third dimension correspond to the stage. This structure is depicted in Equation (5-13).

$$\overline{ind}_i = \left[\overline{ind}_i^{\,stage\ 1}, \dots \overline{ind}_i^{\,stage\ j}, \dots \overline{ind}_i^{\,stage\ M}\right] \quad \textbf{(5-13)}$$

where M is the total number of stages and $\overline{ind}_i^{\,stage\ j}$ is a matrix that represents the RSs/ESSs' configuration of individual i in stage j.

Each row of $\overline{ind}_i^{\,stage\ j}$ corresponds to one feature of the RS/ESS (therefore, in the case of the RSs there is only one row -associated with the power- and in the case of the ESSs there are two rows -the first one associated with the power and the second one with the capacity-) and each column corresponds to one of the N potential locations where the RS/ESS can be installed. Unlike the knapsack problem, where values are binary (0/1), each position in the matrix must take a value from a set of discrete values that represent the possible amounts of power or capacity that can be installed. In the case of ESSs, the two elements in the same column are linked and there must be a coherency among them, since they represent the values of the different features of the element installed in the position associated with the column (the way to ensure this coherency will be explained in Section 5.4.2). The general structure of $\overline{ind}_i^{\,stage\ j}$ is indicated in Equation (5-14).

$$\overline{ind}_i^{\,stage\ j} = \begin{bmatrix} pow(\overline{ind}_i, stage\ j, 1) & \dots\ pow(\overline{ind}_i, stage\ j, k) \dots & pow(\overline{ind}_i, stage\ j, N) \\ cap(\overline{ind}_i, stage\ j, 1) & \dots cap(\overline{ind}_i, stage\ j, k) \dots & cap(\overline{ind}_i, stage\ j, N) \end{bmatrix} \quad \textbf{(5-14)}$$

where:

- $pow(\overline{ind}_i, stage\ j, k)$ is the power item of $\overline{ind}_i$ associated with position k in stage j and represents the power (kW) for the RS/ESS installed in that position. The values for this variable are discrete, going from 0 kW (no RS/ESS installed in position k) to max_{pow} kW (maximum power that can be installed) in steps of $step_{pow}$ kW. Therefore, each power item must take one value out of the set of $\frac{max_{pow}}{step_{pow}}$ discrete values available (being max_{pow} a multiple of $step_{pow}$).
- $cap(\overline{ind}_i, stage\ j, k)$ is the capacity item of $\overline{ind}_i$ associated with position k in stage j and represents the capacity (kWh) for the ESS installed in that position.

The values for this variable are discrete, going from 0 kWh (no ESS installed in position k) to max_{cap} kWh (maximum capacity that can be installed) in steps of $step_{cap}$ kWh. Therefore, each capacity item must take one value out of the set of $\frac{max_{cap}}{step_{cap}}$ discrete values available (being max_{cap} a multiple of $step_{cap}$).

In summary, each individual of the population will be structured as a matrix with dimension $[number\ of\ features\ x\ N\ x\ M]$, which can be divided into sub-matrices, each one representing a different feature, with a dimension $[1\ x\ N\ x\ M]$ and with an element-to-element correspondence among them: the first sub-matrix will refer to the power feature and the second one will refer to the capacity feature (this one only applicable for the case of the ESSs optimization).

The fitness function for the multi-stage optimization will consist in the evaluation of the Net Present Value (NPV) of the installation associated with each individual. It is calculated by Equation (5-15).

$$NPV\left(\overline{ind}_i\right) = \sum_{t=1}^{T}\left(\frac{\left(E_{Raw}^{ANNUAL} - E_{infr.impr}^{ANNUAL}\left(\overline{ind}_i^{\ stage\ J(t)}\right)\right)\cdot e_{cost}}{(1+wacc)^t}\right) - \sum_{j=1}^{M}\frac{C_0\left(\overline{ind}_i^{\ stage\ j}\right)}{(1+wacc)^{Y(j)}}$$

$$\boldsymbol{s.t}$$

$$C_0\left(\overline{ind}_i^{\ stage\ j}\right) \leq max_{\ budget}^{\ stage\ j} + \sum_{stg=1}^{j-1}\left(max_{\ budget}^{\ stage\ stg} - C_0\left(\overline{ind}_i^{\ stage\ stg}\right)\right) \quad \textbf{(5-15)}$$

where:

- E_{Raw}^{ANNUAL} is the annual energy consumption of the railway system without any RS/ESS installation.
- $E_{infr.impr}^{ANNUAL}\left(\overline{ind}_i^{\ stage\ J(t)}\right)$ is the annual energy consumption obtained with the installation associated with individual i in year t. In this year the installed improvements are those made from the initial stage until stage $J(t)$, where J is a function defined in Equation (5-16).

$$J(t) = j, \qquad if\ t_j \leq t < t_{j+1} \quad \textbf{(5-16)}$$

  where t_j is the year when the improvements undertaken in stage j are installed.
- e_{cost} is the cost of the energy.
- $C_0\left(\overline{ind}_i^{\ stage\ j}\right)$ is the cost of the installation associated with individual i in stage j.
- $wacc$ is the Weighted Average Cost of Capital.
- T is the period to evaluate the investment (in years).
- $Y(j)$ is the function, defined in Equation (5-17), which determines the number of years passed between stage j (installed in year t_j) and the first stage (installed in year t_1).

$$Y(j) = t_j - t_1 \quad \textbf{(5-17)}$$

- $max\ {}^{stage\ j}_{budget}$ is the maximum budget allocated to stage j.

As can be seen from Equation (5-15), positive cash flows in the NPV are associated with the energy saving achieved in each year $\left(E_{Raw}^{ANNUAL} - E_{infr.impr}^{ANNUAL}\left(\overline{ind_i}^{\,stage\ J(t)}\right)\right)$. The energy saving is translated into money by multiplying it by the cost of the energy (e_{cost}). As the energy saving in each year depends on the RSs/ESSs already installed, which in turn depends on the stage of investment already undertaken, the annual positive cash flows will vary between years in different stages (Equation (5-16) stablishes to which stage corresponds each year). Negative cash flows are associated with the investments undertaken in each stage.

The budget constraint of Equation (5-15) stablishes that the cost of the improvements to be installed in each stage must not exceed the budget available for that stage, which includes the maximum budget specifically allocated to the correspondent stage ($max\ {}^{stage\ j}_{budget}$) and the money left over from the budget of previous stages $\left(\sum_{stg=1}^{j-1}\left(max\ {}^{stage\ stg}_{budget} - C_0\left(\overline{ind_i}^{\,stage\ stg}\right)\right)\right)$.

5.4.2. IMPLEMENTATION OF THE MULTI-STAGE OPTIMIZATION ALGORITHMS

Before entering into the details of each algorithm, some indications must be made. The first of them only applies to the ESSs optimization, while the second one applies to the optimization of both types of improvements:

- As explained in Section 5.4.1, each individual is composed of a matrix with dimension $[number\ of\ features\ x\ N\ x\ M]$ that, in turn, can be decomposed into sub-matrices of $[1\ x\ N\ x\ M]$, each one corresponding to one of the features to be given a value for the RSs/ESSs and with an element-to-element correspondence. Although the optimization algorithms will treat each submatrix independently, in the case of the ESSs optimization there must be a coherency between the power and capacity values in each location and stage. Concretely, in case of selecting a non-zero value for the power in a certain location and stage, the value of the capacity must also be non-zero and vice versa. The same happens in case of selecting a zero value (no installation) for power or capacity in a certain location and stage. This restriction will be named 'constraint of coherency among features', is formulated in Equation (5-18) and must be applied in both GA and FA multistage optimization algorithms.

$$pow\left(\overline{ind_i}, stage\ j, k\right) = 0 \ \leftrightarrow \ \ cap\left(\overline{ind_i}, stage\ j, k\right) = 0 \quad \textbf{(5-18)}$$

- Attention must be also paid to the fact that, on the one hand, in each stage it is possible to add new installations only in those locations where no RSs/ESSs have been installed yet and, on the other hand, the RSs/ESSs already installed in previous stages cannot be neither modified nor uninstalled (although, from the

technical point of view, increasing the size of an RS/ESS already installed is possible, it is not efficient). This restriction can be named 'constraint of coherency among stages', is formulated in Equation (5-19) and is applied in both GA and FA multistage optimization algorithms.

$$\begin{aligned} pow(\overline{ind}_i, stage\ j, k) &= pow(\overline{ind}_i, stage\ j-1, k) \quad if\ pow(\overline{ind}_i, stage\ j-1, k) \neq 0 \\ cap(\overline{ind}_i, stage\ j, k) &= cap(\overline{ind}_i, stage\ j-1, k) \quad if\ cap(\overline{ind}_i, stage\ j-1, k) \neq 0 \end{aligned} \quad \textbf{(5-19)}$$

5.4.2.1. MULTI-STAGE GENETIC ALGORITHM (M-GA)

For the sake of clarity, the general nomenclature used in section 5.4.1 will be adapted to the usual nomenclature of the genetic algorithm:

- The individuals will be referred to as chromosomes.
- The sub-matrices with the power features will be referred to as power sub-chromosomes.
- The sub-matrices with the capacity features will be referred to as capacity sub-chromosomes.
- The power items will be referred to as power genes.
- The capacity items will be referred to as capacity genes.

The steps of the M-GA are the same as in the S-GA (see Figure 5-2):

M-GA 1. Random generation of a population of chromosomes: a population of CHR chromosomes is generated. The chromosomes are generated in increasing order of stages. At the beginning, all the genes of all the chromosomes in every stage are initialized with null values. For each stage and chromosome, one of the available genes (the same one for both power and capacity sub-chromosomes, in order to comply with the constraint of coherency among features) is randomly selected and given a value from the set of non-zero discrete values available. It must be noted that, in order to comply with the constraint of coherency among stages, the available genes in each stage correspond to those with null values in the previous stages (since those with non-zero values in the previous stages are replicated in the succeeding ones). This process is repeated until having an associated budget higher than a fraction of the budget available for the stage, discarding in every new selection the genes already selected.

M-GA 2. Fitness evaluation of the initial population of chromosomes. The configuration of RSs/ESSs associated with each chromosome is simulated successively: the first simulation only takes into account the RSs/ESSs to be installed in stage 1 and the following simulations add the new RSs/ESSs associated with succeeding stages. Therefore, the number of simulations to perform for each chromosome corresponds to the number of stages (M). The energy saving associated with the installation accumulated in each stage (composed of the new installation of the stage and the installation of the previous stages) is obtained from these simulations. Once obtained the energy saving of all the stages of each chromosome, the fitness function is evaluated for each chromosome with the formula of the NPV given in Equation (5-15).

M-GA 3. Selection: the ***tournament selection*** has been selected and the population resulting from this procedure is called *parent population.* A pair of chromosomes is randomly selected from the *children population* of the previous iteration or from the initial population in case of the first iteration. The fitness of both chromosomes is compared and the chromosome with the highest fitness is selected as a 'parent' chromosome for the next generation. This selection procedure is repeated until the number of selected parents equals the population size and the same chromosome can be selected more than once (every pair is randomly selected from the whole *children population* of the previous iteration/initial population). After having the parents for the new population, one of them is randomly selected and replaced by the chromosome with the best fitness of the *children population* of the previous iteration /initial population.

M-GA 4. Crossover: two types of crossover mechanisms have been selected: ***one-point crossover*** and ***uniform crossover*** (the same as in the single-stage approach). Each one has been applied in a different optimization case, as will be shown in Section 5.4.3.1. The crossover acts over the second dimension of each chromosome (location) and the application of the coherency constraints has two consequences:

- The same crossover is applied in all the stages of a chromosome to comply with the constraint of coherency among stages of Equation (5-19).
- In each stage, the same crossover is applied for both power and capacity sub-chromosomes to comply with the constraint of coherency among features of Equation (5-18).

The population resulting from this step is called *children population*.

M-GA 5. Mutation: it is a small modification consisting in adding or subtracting $step_{pow}$ or $step_{cap}$ (each possibility with a 50% probability) to, respectively, the power or capacity genes randomly selected for the mutations.
Every power/capacity sub-chromosome of the *children population* can be modified in one or two positions with, respectively, a probability mut_1 and mut_2 (to comply with the constraint of coherency among features, in the same position(s) in both sub-chromosomes, or what is the same, in the same power gene(s) and capacity gene(s)) or in none of them with a probability mut_0. The relationship among these probabilities is the same as in the single-stage approach, which has already been defined in Equation (5-3).
The modifications produced in the mutation are made in increasing order of stages and, in order to comply with the constraint of coherency among stages, the mutation in a certain stage can be only applied to those genes with zero-values in the previous stages (locations without installation in the previous stages) and the genes mutated in a stage are replicated in the succeeding stages.

If any mutated power or capacity gene crosses the maximum or minimum limits in power, the maximum or minimum power, respectively, is selected for that gene.
In case of having a null value in a power/capacity gene and a non-zero value in the associated power/capacity gene, the non-zero value is set to zero.

M-GA 6. Mutation-as-repair: there may be some chromosomes of the *children population* obtained after the crossover and the mutation that do not comply with the budget constraint in some of the stages. This mechanism is applied, in increasing order of stages, to each stage that do not comply with this constraint. The explanation of the mutation-as-repair mechanism is below:

M-GA 6.1: Random selection of a non-zero pair of power and capacity genes.

M-GA 6.2: Determination of the possible reductions in capacity and/or power to apply. There are three possible combinations for reducing the size: reducing only the power in $step_{pow}$, reducing only the capacity in $step_{cap}$ and reducing both power and capacity in, respectively, $step_{pow}$ and $step_{cap}$. These combinations are represented by the vector $\Delta size$, depicted in Equation (5-20).

$$\Delta size = \begin{bmatrix} -step_{pow} & 0 & -step_{pow} \\ 0 & -step_{cap} & -step_{cap} \end{bmatrix} \quad \textbf{(5-20)}$$

where the first row represents the possible reductions in the power gene selected, the second row the possible reductions in the associated capacity gene and each column corresponds to one of the three possible combinations.

M-GA 6.3: Selection of the reduction in capacity and/or size to apply: a minimization algorithm finds the combination that makes the chromosome to comply with the budget constraint in the stage studied with the smallest impact on the stage budget. If none of these combinations make the chromosome feasible (in terms of budget), the maximum reduction for that pair of genes is selected ($\begin{bmatrix} -step_{pow} \\ -step_{cap} \end{bmatrix}$) and the mutation-as repair mechanism is applied again.

Regarding the observation of the coherency constraints in the mutation-as-repair mechanism, it must be noted that:

- If in $stage\ j$ (that can be any stage of the M existing ones) the value of the power gene selected to be reduced is equal to $step_{pow}$ ($pow\left(\overline{ind}_i, stage\ j, k\right) = step_{pow}$) and the algorithm of step **M-GA 6.3** has determined that the reduction for that gene is $-step_{pow}$, the only possible reduction to apply to the power gene and the associated capacity gene is $\begin{bmatrix} -pow_k{}^{stage\ j} \\ -cap_k{}^{stage\ j} \end{bmatrix}$ in order to comply with the constraint of coherency among features. The same happens in the case of being the

value of the capacity gene $step_{cap}$ ($cap\left(\overline{ind}_i, stage\ j, k\right) = step_{cap}$) and then reduction to be applied - $step_{cap}$.

- The changes in a chromosome from applying the mutation as repair mechanism in a certain stage must be kept in the succeeding stages. Additionally, as happened with the mutation, the mutation-as-repair in a certain stage can be only applied to those genes with zero-values in the previous stages. Both conditions are designed to comply with the constraint of coherency among stages.

M-GA 7. Fitness evaluation of the new population of chromosomes: the children population is evaluated in the same way as in step 2 (**M-GA 2)**. Once obtained the new fitness values, the optimization algorithms goes to the next iteration, which starts in step 3 (**M-GA 3)**. This process is repeated for a number of iterations given by $num\ iter_{max}$.

5.4.2.2. MULTI-STAGE FIREWORKS ALGORITHM (M-FA)

For the sake of clarity, the general nomenclature used in the general formulation of Section 5.4.1 will be adapted to the usual nomenclature of the fireworks algorithm.

- The individuals will be referred to as sparks.
- The sub-matrices with the power features will be referred to as power sub-sparks.
- The sub-matrices with the capacity features will be referred to as capacity sub-sparks.
- The power items will be referred to as power dimensions.
- The capacity items will be referred to as capacity dimensions.

The steps of the M-FA discretized are the same as in the S-FA discretized (see Figure 5-4):

M-FA 1. Random generation of a population of fireworks: a population of F fireworks is generated. The fireworks are generated in increasing order of stages. At the beginning, all the dimensions of all the fireworks in every stage are initialized with null values. For each stage and firework, one of the available dimensions (the same one for both power and capacity sub-sparks, in order to comply with the constraint of coherency among features) is randomly selected and given a value from the set of non-zero discrete values available. It must be noted that, in order to comply with the constraint of coherency among stages, the available dimensions in each stage correspond to those with null values in the previous stages (since those with non-zero values in the previous stages are replicated in the succeeding ones). This process is repeated until having an associated budget higher than a fraction of the budget available for the stage, discarding in every new selection the dimensions already selected.

M-FA 2. Fitness evaluation of the initial population of fireworks. The configuration of RSs/ESSs associated with each firework is simulated successively: the first simulation only takes into account the RSs/ESSs to be installed in stage 1 and the following simulations add the new RSs/ESSs associated with the succeeding stages. Therefore, the number of simulations to

perform for each firework corresponds to the number of stages (M). The energy saving associated with the installation accumulated in each stage (composed of the new installation of the stage and the installation of the previous stages) is obtained from these simulations. Once obtained the energy saving of all the stages of each firework, the fitness function is evaluated for each firework with the formula of the NPV given by Equation (5-15).

M-FA 3. Regular sparks explosion: a variable number of regular sparks is set off from each firework. The set-off has the following steps:

M-FA 3.1. Selecting the number of regular sparks per firework: The number of regular sparks per firework is given by Equation (5-6).

As happened in the S-FA, it must be noted that the total number of regular sparks, SPK, generated from the F fireworks is variable in every iteration, due to rounding effects and to the restrictions in the minimum and maximum number of sparks that can be set off from a firework, although $SPK \cong SPK_{ctrl}$ (as a reminder, SPK_{ctrl} is a parameter that controls the number of regular sparks that can be set off from the F fireworks and that appears in Equation (5-6).

M-FA 3.2. Selecting the amplitude of explosion per firework: the continuous amplitude of explosion for firework i ($Ac_{\overline{fw_i}}$) is computed from Equation (5-7). Then, a discrete amplitude for the power and capacity will be assigned to each firework depending on its associated $Ac_{\overline{fw_i}}$:

- $step_{pow}$ and $step_{cap}$, for power and capacity respectively, when $Ac_{\overline{fw_i}}$ is within the xth percentile (which is equivalent to be within the x% of fireworks with the best fitness).
- $2 \cdot step_{pow}$ and $2 \cdot step_{cap}$, for power and capacity respectively, when $Ac_{\overline{fw_i}}$ is out of the xth percentile (which is equivalent to be within the (100-x)% of fireworks with the worst fitness).

After this transformation from continuous to discrete, each firework i will have an associated discrete amplitude of explosion, $Ad_{\overline{fw_i}}$, composed of a power explosion, $Adp_{\overline{fw_i}}$, and a capacity explosion $Adc_{\overline{fw_i}}$.

M-FA 3.3. Generating the regular sparks: regular sparks are generated in increasing order of stages. In order to comply with the constraint of coherency among stages:

- The spark dimensions that can be changed in a certain stage (with respect to the corresponding stage of the firework from which is set off) are those with null values in the previous stages of the spark.
- The power or capacity dimensions changed in a stage are replicated in the succeeding stages.

Therefore, each regular spark differs in each stage from the firework from which it is set off in z number of dimensions, z being a random number that varies for each spark and stage according to Equation (5-21).

$$z_{\overline{sp}_\alpha}{}^{stage\ j} = rdn(N - nzd_{\overline{sp}_\alpha}{}^{stage\ j-1}) \quad \textbf{(5-21)}$$

where:

- $z_{\overline{sp}_\alpha}{}^{stage\ j}$ is the number of dimensions to select randomly in the stage j of regular spark α.
- $nzd_{\overline{sp}_\alpha}{}^{stage\ j-1}$ is the number of non-zero dimensions in the previous stage (stage $j-1$) of regular spark α.
- $rdn(x)$ is a function that generates a integer random number comprised in the interval $[1-x]$.

Once having the number of dimensions z to be modified, the dimensions selected to be changed as well as the order in which they are going to be modified is determined randomly as well. In order to comply with the constraint of coherency among features, the same dimensions will be selected for each stage in the power and capacity sub-sparks.

Equation (5-22) shows how to apply the changes in a randomly selected dimension k in stage j of firework i ($\overline{fw}_i$) to obtain the power and capacity values of dimension k and stage j in the regular spark α ($\overline{sp}_\alpha$). As a reminder, $randsample$ is a logical operator that randomly selects one of the values of the given vector according to a uniform distribution.

$$\begin{bmatrix} pow(\overline{sp}_\alpha, stage\ j, k) \\ cap(\overline{sp}_\alpha, stage\ j, k) \end{bmatrix} = \quad \textbf{(5-22)}$$

$$\begin{bmatrix} pow(\overline{fw}_i, stage\ j, k) \\ cap(\overline{fw}_i, stage\ j, k) \end{bmatrix} + \begin{bmatrix} randsample\left(\left[-Adp_{\overline{fw}_i} : step_{pow} : 0\right) \cup \left(0 : step_{pow} + Adp_{\overline{fw}_i}\right]\right) \\ randsample\left(\left[-Adc_{\overline{fw}_i} : step_{cap} : 0\right) \cup \left(0 : step_{cap} + Adc_{\overline{fw}_i}\right]\right) \end{bmatrix}$$

After applying the changes:

- If any power or capacity dimension crosses the maximum or minimum limits in power, the maximum or minimum power, respectively, is selected for that dimension.
- In case of having a null value in a power/capacity dimension and a non-zero value in the associated power/capacity dimension, the non-zero value is set to zero.

Equation (5-22) will be applied to each of the $z_{\overline{sp}_\alpha}{}^{stage\ j}$ randomly selected dimensions in stage j of regular spark α. Before going to the next dimension, possible infeasibility problems with respect to the budget constraint are checked and corrected. There are two different possible situations where this constraint may not be complied:

- ***Budget infeasibility type A****: the spark is infeasible in terms of budget in a certain stage after changes have been applied in the dimension, but was feasible before those changes*. In these cases, the changes from applying Equation (5-22) have resulted in excessive increments in power or capacity that must be reduced. Particularly, the increment to be applied is determined by a function that selects the increment that, complying with the budget constraint, is closest to

the original increment that did not comply it.

- ***Budget infeasibility type B****: the spark is infeasible in terms of budget in a certain stage before the changes have been applied in the dimension*. The initial configuration of the spark in the stage of study is comprised by the non-zero power and capacity dimensions of the spark in the previous stage and the values of the firework in the stage of study for the rest of dimensions. This configuration can already overpass the budget limit for the stage. As an example, supposing that there are two stages and the firework from which the spark is set-off has a very small installation in the first stage and uses the remaining budget to increase the installation size in the second stage, if the changes in the first stage of the spark make the installation of that stage bigger (with respect to the one associated with the firework), it may happen that the initial configuration of the spark in the second stage (where the non-zero dimensions of the spark in the previous stage are replicated and the rest of dimensions are the same as those of the firework) becomes infeasible. In this case, Equation (5-22) is applied as normally. If the result from applying the random changes is a reduction in the power and/or capacity that makes the spark feasible again, nothing else is required; if not, the mutation-as-repair mechanism explained in **M-GA 6** is applied.

The values of the spark in the dimensions not selected are the same as the values of the firework from which the spark is set off.

M-FA 4. Gaussian sparks explosion: as in the S-FA, and according to (Tan & Zhu, 2010), with the aim of keeping a big diversity among sparks, the so-called 'Gaussian Explosion' is also performed in the M-FA. This type of explosion is applied to set off a very reduced number of Gaussian sparks, $GSPK$. Each Gaussian spark is set off from a different firework. The mechanism to set-off Gaussian sparks as well as the considerations that must be observed to ensure that the dimensions changed in the Gaussian sparks comply with all the constraints (power and capacity thresholds, budget and coherency among features and stages), are the same as those presented in the generation of regular sparks, with the exception of the algorithm used to determine the changes. Equation (5-23) presents the algorithm that applies the changes to each selected dimension k in stage j of firework i ($\overline{fw_i}$) to obtain the values of Gaussian spark δ ($\overline{spg_\delta}$) for that dimension and stage.

$$
\begin{aligned}
&while(\ coeff_{pow} < 0 \ \ or \ \ coeff_{cap} < 0) \\
&\quad coeff_{pow} = Gaussian\ (1{,}1) \\
&\quad coeff_{cap} = Gaussian\ (1{,}1) \\
&end
\end{aligned}
$$

$$
\begin{bmatrix} pow(\overline{spg}_{\delta}, stage\ j, k) \\ cap(\overline{spg}_{\delta}, stage\ j, k) \end{bmatrix} = \begin{bmatrix} round\left(\dfrac{pow(\overline{fw}_i, stage\ j, k)\cdot coeff_{pow}}{step_{pow}}\right)\cdot step_{pow} \\ round\left(\dfrac{cap(\overline{fw}_i, stage\ j, k)\cdot coeff_{cap}}{step_{cap}}\right)\cdot step_{cap} \end{bmatrix} \quad \textbf{(5-23)}
$$

where $coeff_{pow}$ and $coeff_{cap}$ are, respectively, the coefficients of Gaussian Explosion for the power and capacity sub-sparks. It must be noted that they must not be negative because the power of the RSs/ESSs and the capacity of the ESSs cannot be negative, just zero (which means no installation of an RS/ESS in the location associated with the selected dimension).

M-FA 5. Fitness evaluation of the new sparks: the new sparks are evaluated in the same way as described in step 2 (**M-FA 2)**.

M-FA 6. Selection of the locations of fireworks for the next generation: F new fireworks to set off the sparks of the next generation must be selected from the fireworks and sparks of the current generation. Among the F fireworks, SPK regular sparks and $GSPK$ Gaussian sparks of the current generation, the one with the best fitness is directly selected. The $F-1$ remaining fireworks are selected with a probability p, which depends on their distance to the rest of fireworks and sparks. This probability p is given by Equation (5-10).
Distance measure is computed according to the Manhattan distance (sum of the absolute value of the differences in every dimension of the sparks/fireworks). Equation (5-24) determines the way to apply the Manhattan distance for firework/spark x in the multi-stage formulation.

$$
R(x) = \sum_{\lambda \in I} \sum_{stage\ j=1}^{M} \sum_{k=1}^{N} (|pow(x, stage\ j, k) - pow(\lambda, stage\ j, k)| + |cap(x, stage\ j, k) - cap(\lambda, stage\ j, k)|) \quad \textbf{(5-24)}
$$

$$
where\ I = \{fw_1, \cdots, fw_F\ ,\ sp_1, \cdots, sp_{SPK}\ ,\ spg_1, \cdots, spg_{GSPK}\}
$$

Once the fireworks for the next generation have been obtained, the optimization algorithm goes to the next iteration, which starts in step 3 (**M-FA 3)**. This process is repeated for a number of iterations given by $num\ iter_{max}$.

5.4.3. COMPARISON OF THE PERFORMANCE OF THE MULTI-STAGE OPTIMIZATION ALGORITHMS

A test has been used to compare the performance of M-GA and M-FA. This test is particularized for 2 stages ($M = 2$) and the second stage takes place 2 years after the first stage. It also uses the final case study of this thesis and, as in Section 5.3.3 (and for the same reason), the results from the test will be normalized with respect to the best fitness obtained.

The infrastructure improvement selected for this test has also been the ESSs.

With respect to the variables of decision:

- Locations: Every SS location in the final case study is considered as a candidate to install the ESS (see Section 6.2.1), therefore $N = 11$.
- Power to be installed in each location: this variable of decision can take any value from the set $[0: step_{pow}: max_{pow}]$, where:
  - $step_{pow} = 500\ kW$
  - $max_{pow} = 3000\ kW$
- Capacity to be installed in each location: this variable of decision can take any value from the set $[0: step_{cap}: max_{cap}]$, where:
  - $step_{cap} = 5\ kWh$
  - $max_{cap} = 15\ kWh$

It must be noted that the search space for this multi-stage optimization has significantly increased with respect to the search space of the single-stage optimization of Section 5.3.3. The reason is that the capacity is already a variable of decision and that the optimum configuration must be determined not just for one stage but for two stages.

5.4.3.1. OPTIMIZATION CASES AND ALGORITHMS' PARAMETERS

The test comprises:

- Two optimization cases for each algorithm in order to check their robustness.
- Five instances to be run for each algorithm and case.

The reduction in the number of instances (with respect to those of the single-stage test of Section 5.3.3) is due to the increase in the simulation time required by each instance. This is because the computational burden increases with the size of the search space.

Parallel computing has also been used to speed up the simulation of this test: the configurations to be simulated in each iteration have been distributed among a number of workers equivalent to the number of logical processors of the server (the servers used are the same as in the test for the single-stage optimization). Considering that a single iteration takes around 40 minutes per stage (on average, having variations in time depending on the number of logical processors of the server used, which goes from 48 to 64), the time required to perform the whole test is around a month. This time is very

similar to the time required by the test performed in the single-stage optimization, since the increase in the number of simulations per iteration and the increase in the number of iterations required to achieve the optimum (the latter being a consequence of the bigger search space) is compensated with the reduction in the number of instances and the fact that only two algorithms are tested (one algorithm less than in the single-stage optimization).

The two cases of the M-GA differ in the crossover mechanism used: the one-point crossover has been used for Case 1 and the uniform crossover has been used for Case 2. The parameters of the M-GA have been selected experimentally and are depicted in Table 5-6.

Table 5-6: M-GA parameters

	Case 1 (M-GA1)	**Case 2 (M-GA2)**
Population size (number of chromosomes)	200	
Probability for a chromosome to mutate one gene, mut_1	20%	
Probability for a chromosome to mutate two genes, mut_2	10%	
Probability to swap each gene among parents in the uniform crossover mechanism, p_{swap}.	-	50%
Maximum number of iterations, $num\ iter_{max}$	100	

The two cases of the M-FA differ in the proportion between fireworks and regular sparks. Maintaining the average population of sparks in both cases, in Case 2 the number of fireworks doubles the number of fireworks of Case 1. Consequently, the number of regular sparks per firework, $n_{sp_{\overline{fw}_i}}$, in Case 2 is on average half than in Case 1. The parameters of the M-FA have been selected experimentally and are depicted in Table 5-7.

Table 5-7: M-FA parameters

	Case 1 (M-FA1)	**Case 2 (M-FA2)**
Average population of sparks ($SPK_{ctrl} + GSPK$)	200	
SPK_{ctrl} (percentage with respect to the average population of sparks)	93%	
$GSPK$ (percentage with respect to the average population of sparks)	7%	
Number of fireworks, F	20	40
***x*th** percentile to determine the radius of explosion	40	
Min. number of regular sparks that can be set off from a firework, $n_{sp_{min}}$	$\left(\frac{SPK_{ctrl}}{F}\right) \cdot 0.1$	
Max. number of regular sparks that can be set off from a firework, $n_{sp_{max}}$	$\left(\frac{SPK_{ctrl}}{F}\right) \cdot 1.5$	
Maximum number of iterations, $num\ iter_{max}$	100	

As can be seen, the population size in both algorithms has been increased with respect to the one used in the single-stage optimization algorithms (128 individuals). This is also due to the increase in the size of the search space: as the difficulty to find the optimum solution increases with the size of the search space, a bigger population is required to successfully tackle the search for the optimum solution.

5.4.3.2. RESULTS

Five instances have been run for each optimization algorithm and case. The same best fitness value has been achieved by both algorithms. The results presented in this section have been normalized with respect to it.

Figure 5-6 shows the evolution of the normalized fitness average and median for each algorithm and case with respect to the number of iterations. The average is more sensitive to outlier instances, while the median filters those outliers to a certain extent and represents what can be considered the normal behavior of the algorithm (the full explanation of the reasons why these two measures have been selected is in Section 5.3.3.2).

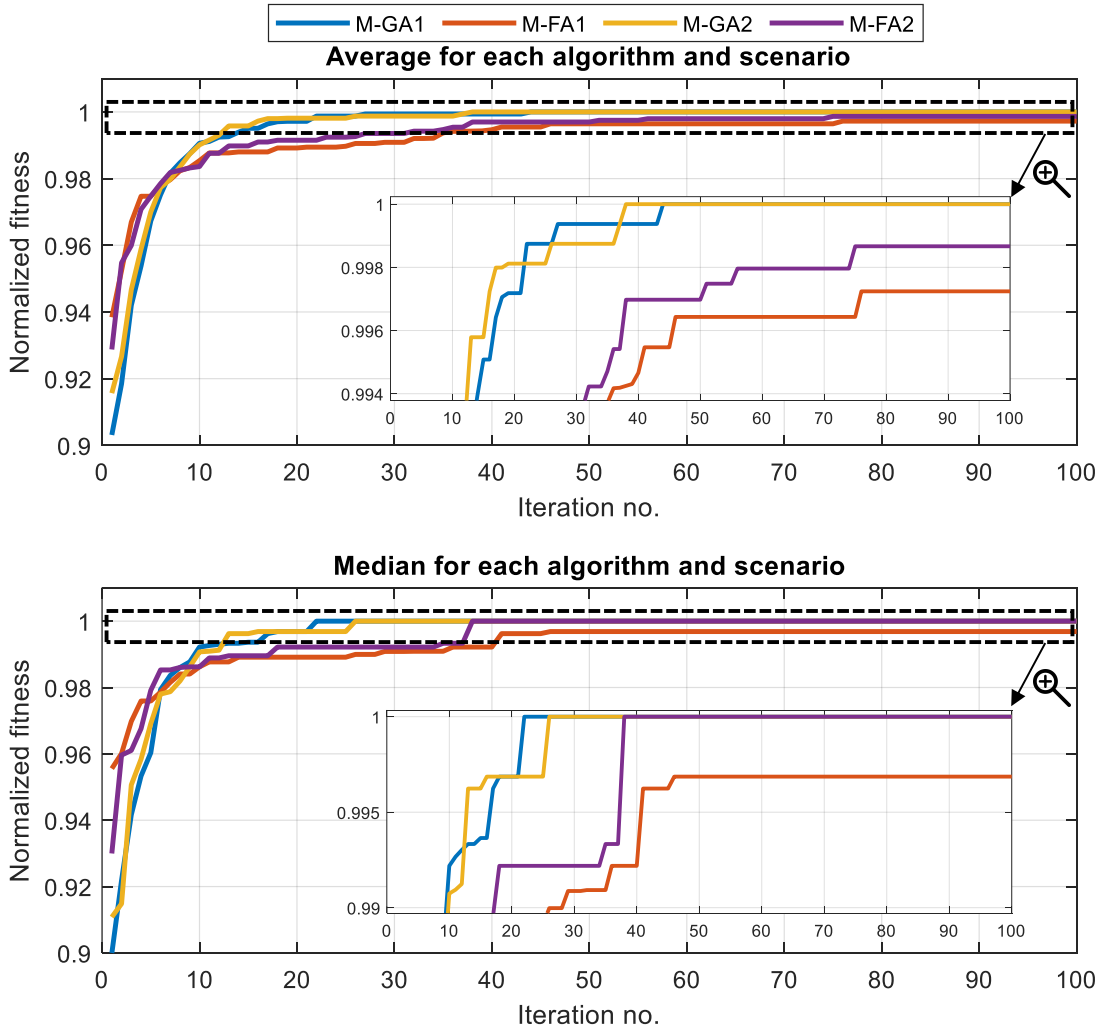

Figure 5-6: Evolution of the average and median of the normalized fitness for each algorithm and optimization case. Multi-stage optimization

Regarding the effectiveness of the algorithms, the M-GA clearly outperforms the M-FA:

- The M-GA always reaches the optimum solution, while the M-FA does not reach it in all its instances. This is clear when analyzing the evolution of the average: while this value is stabilized to 1 (as the results are normalized, this is the best fitness value obtained) in the two cases of the M-GA (M-GA1 and M-GA2), the average obtained in the two cases of the M-FA (M-FA1 and M-FA2) is bellow it.
- Even in a normal situation, the M-FA may not reach the optimum solution, as can be seen when analyzing the median, which only achieves the maximum fitness in one of its two cases (M-FA2).

As five instances may be considered a small number in order to compute the median, Figure 5-7 presents the same results but aggregating the instances of the two different optimization cases for each optimization algorithm.

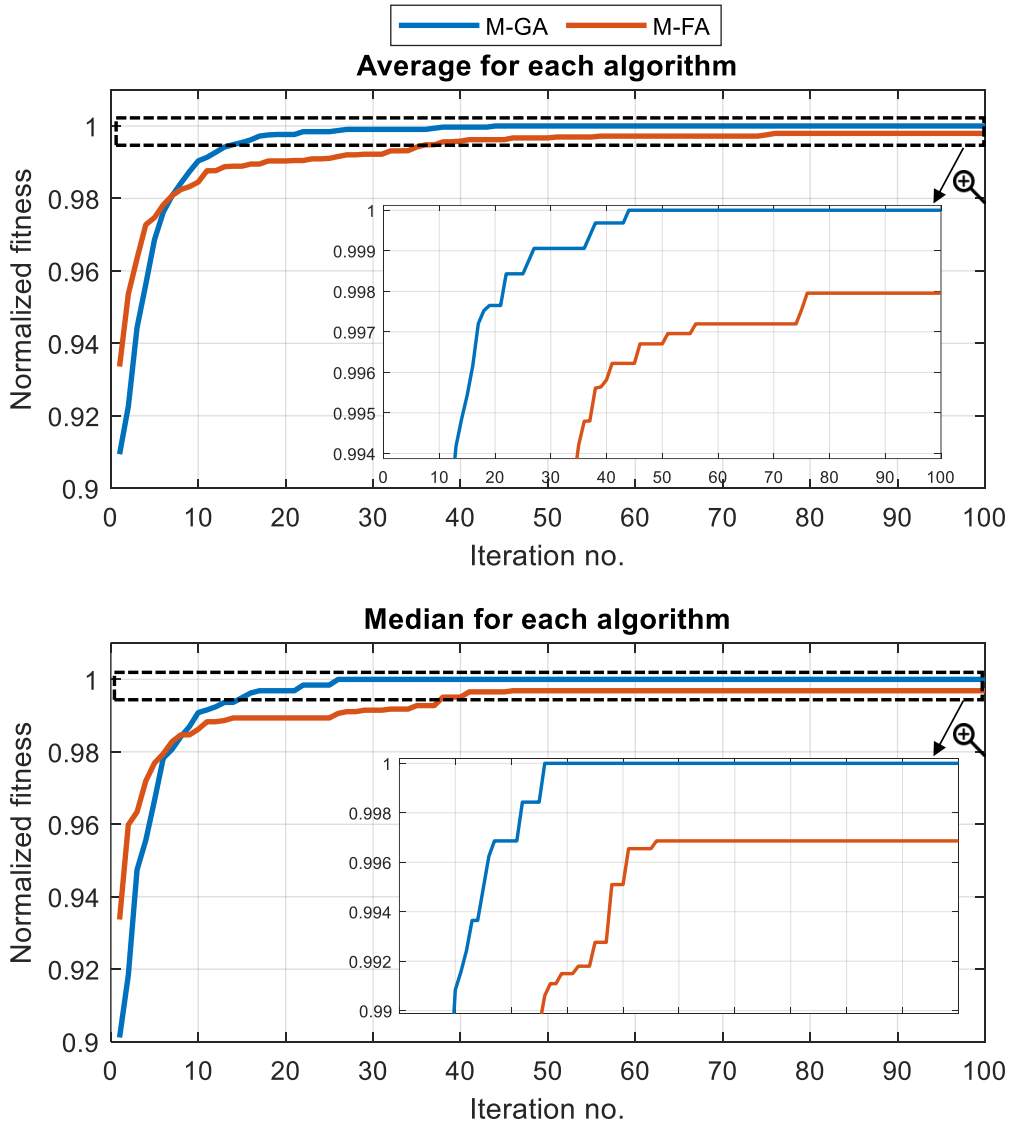

Figure 5-7: Evolution of the average and median of the normalized fitness for each algorithm. Multi-stage optimization

It must be noted that, despite putting the two optimization cases of the M-FA together (M-FA1 and M-FA2), the median of the M-FA still does not reach to the optimum fitness. This confirms the previous statement regarding the fact that, even in a normal situation, the M-FA may not reach the optimum solution.

Regarding the speed of convergence of the algorithms, the M-GA is faster than the M-FA. This is clearly seen in the vertical evolution of the averages and medians (especially in the medians, as they filter the outlier instances): the M-GA stabilizes before the M-FA (in addition to stabilizing with a higher fitness).

Additionally, the M-GA is very robust, since it presents a very similar performance in both optimization cases. On the contrary, the M-FA is less robust, as the fitness stabilizes in different values depending on the optimization case.

In conclusion, the M-GA presents the best performance in all the aspects studied: effectiveness, speed of convergence and robustness.

The detailed analysis of the solutions provided by the algorithms will be given in Chapter 6. Nevertheless, it must be noted that, although it is not possible to assure that the algorithms have reached the global optimum -this is only possible with mathematical optimization- it is very likely that they have reached it. This is because both algorithms (run each one five instances per optimization case and having two optimization cases per algorithm) have reached the same best solution (in all the instances run with the M-GA and in some of the instances run with the M-FA). Besides, the optimization algorithms selected present good exploration features that generally prevent them from getting “trapped” in local optima.

Additionally, those configurations provided by the instances of M-FA1 and M-FA2 that have not achieved the highest fitness are very close to the best solution in both fitness (the normalized fitness of the worst solution is 0.9962) and configuration (same number of ESSs installed in each stage, same power and capacity installed in each stage and only small differences in the locations).

5.4.4. MULTI-STAGE VS CASCADE SINGLE-STAGE OPTIMIZATION

The most common approach for solving the optimization problem where the installation is divided into stages is what can be called the cascade single-stage optimization. This approach optimizes separately each stage in increasing order of stages. Each stage would be optimized taking into account the improvements already installed in the previous stages and considering the money available for the stage, which would be the budget allocated to the stage in addition to the money from the budget allocated to previous stages not spent (in case there is).

The big difference between the cascade single-stage optimization and the multi-stage optimization relies on the way that the fitness function is evaluated and on its derived consequences:

- The multi-stage optimization evaluates the fitness function just once for each individual. This means that the investments in all the stages are evaluated as a whole, but taking into account their temporal sequence (see Equation (5-15)). Therefore, the optimization algorithm can see the whole investment at a time and take the best decision to maximize it (for example, in spite of having enough money to install a set of improvements at a time in a certain stage, some of them can be postponed to a later stage, if this decision makes the whole investment more profitable).
- The cascade single-stage optimization evaluates the fitness function once per stage and individual (the fitness is computed from the single-stage NPV of Equation (5-2)). Therefore, the optimization of each stage is performed separately and the only information available in each stage is the information from the previous stages and the money available for the stage. Unlike the multi-stage optimization, it cannot optimize the investment as whole, but it has to optimize each stage, without having information about the next ones.

As stated in Systems Theory, optimizing each part of a whole (in this case the improvements of each stage) does not necessarily result in the optimum for the whole (in this case the whole improvement divided into stages). Therefore, although being more complex from the modelling point of view, the multi-stage optimization is a better approach, since it presents the advantage of considering the infrastructure improvement as a whole.

In order to illustrate the differences between these two approaches, next paragraphs will compare the results from optimizing the ESSs installation with the best algorithm that can be applied for each approach (according to the results of Sections 5.3.3.2 and 5.4.3.2): the M-GA with the parameters of MGA-1 for the multi-stage optimization and the S-GA with the parameters of SGA-1 for the cascade single-stage optimization.

For this comparison it is important to know the differences among stages regarding budget and installation costs (the precise figures will be given in Chapter 6):

- The budget allocated to each stage is the same.
- The capital cost for power (the most relevant figure in the ESSs total installation cost) is reduced by 33% in the second stage (with respect to the cost in the first stage).

When analyzing the results provided by the two different approaches, it was found that the final installation is the same with both of them (regarding location, number of ESSs, total power installed and total capacity installed). Nevertheless, the decisions about the improvements to be installed in each stage vary depending on the optimization approach, as shown in Table 5-8. It must be noted that the term $Budget\ available$ that appears in the last row of the table corresponds to the maximum budget allocated to the stage together with the budget allocated to previous stages not spent.

Table 5-8: Distribution of the final installation among stages depending on the optimization approach

		Cascade single-stage optimization	Multi-stage optimization
FIRST STAGE	Number of ESSs installed	3	2
	Pow. of each ESS (kW)	500	500
	Cap. of each ESS (kWh)	5	5
	$\frac{Budget\ spent}{Max.\ budget\ allocated\ for\ the\ stage} \times 100$ (%)	99.3	66.2
SECOND STAGE	Number of ESSs installed	2	3
	Pow. of each ESS (kW)	500	500
	Cap. of each ESS (kWh)	5	5
	$\frac{Budget\ spent}{Max.\ budget\ allocated\ for\ the\ stage} \times 100$ (%)	44.8	67.2
	$\frac{Budget\ spent}{Budget\ available} \times 100$ (%)	44.5	50.2

The cascade single-stage optimization tries to install in the first stage as many ESSs as the budget allows. Concretely, in the first stage three ESSs are installed in the three positions that produce the biggest energy saving. In the second stage, two additional ESSs, which could not be installed in the first stage because of the lack of budget, are installed in the best positions that are still free after the installations of the first stage.

The multi-stage optimization changes the distribution of the installations between the two stages: the installation of one of the three ESSs installed in the first stage with the cascade single-stage optimization is postponed to the second stage. This implies a reduction of the installation cost (the capital cost for the ESS power considerably decreases in the second stage) that compensates the fact of not obtaining benefits from installing that ESS from the beginning. Only the multi-stage optimization can make this type of decisions because it is able to evaluate the investment as a whole and has the information of all the stages, while the cascade single-stage optimization cannot foresee the next stages and, therefore, optimizes the installation of each stage without taking into account the next ones. Owing to this reason, the multi-stage optimization outperforms the cascade single-stage optimization.

The increment in the NPV obtained with the multi-stage optimization with respect to the NPV obtained with cascade single-stage optimization is of 0.6%. Although this increment may seem small, the value is not so negligible taking into account the NPV figures (hundreds of thousands of euros, as will be seen in Chapter 6). Moreover, and more importantly, the differences between the two approaches, in both NPV and ESSs configuration in each stage, can be bigger if the differences among stages with respect to the budget and/or installation costs increase.

5.5. CONCLUSIONS AND CONTRIBUTIONS

This chapter has focused on the design of nature-inspired optimization algorithms that, working together with the railway simulator with the improvements in traffic modeling and topology developed in the previous chapters, determine the optimal installation of RSs/ESSs in a MTS line.

The variables of decision that must be optimized are:

- Number of RSs /ESSs to be installed.
- Location of the RSs /ESSs to be installed.
- Power (kW) of each RS / ESS to be installed.
- Capacity (kWh) of each ESS to be installed (this variable does not apply to the RSs optimization).

The optimization algorithms perform an intelligent search of the characteristics of the installation that yields the best fitness. The fitness has been defined as the Net Present Value (NPV), as it tries to find a balance between the energy saving and the installation costs associated with the infrastructure improvement.

The optimization problem has been addressed in two variants:

- Single-stage optimization: the whole budget for the installation of RSs/ESSs is available from the beginning.
- Multi-stage optimization: the whole budget is divided into stages, separated in time. Therefore, the improvement of the infrastructure must be undertaken gradually and the algorithm must try to find the optimum configuration for each stage without exceeding the budget limits of the stage and considering the installation as a whole.

The following sections will give the main conclusions of each one.

5.5.1. SINGLE-STAGE OPTIMIZATION CONCLUSIONS AND CONTRIBUTIONS

Three different optimization algorithms have been proposed in order to compare and validate their performance and results. The optimization algorithms proposed are the single-stage Genetic Algorithm (S-GA) as the main exponent of evolutionary algorithms, the single-stage Particle Swarm Optimization Algorithm (S-PSO) as the main exponent of swarm algorithms and the single-stage Fireworks Algorithm (S-FA) as another variant of swarm algorithms. A detailed explanation of each one and the implementation details required to adapt them to the optimization problem object of study have been given.

A test has been used to compare the performance of the single-stage optimization algorithms. This test comprises:

- Two optimization cases for each algorithm in order to check their robustness.
- Ten instances to be run for each algorithm and case.

The performance of the three proposed algorithms is excellent, although there are differences among them.

- Regarding the effectiveness, the S-GA and the S-FA achieve the optimal solution in all their instances and the S-PSO achieves it in most of them (although there are some outliers that do not reach the optimum, but solutions very close to it).
- Regarding the speed of convergence of the algorithms, the S-GA is faster than the S-FA, which, in turn, is faster than the S-PSO.
- Regarding the robustness, the S-GA and the S-FA are very robust, since they present a very similar performance in the two optimization cases designed to study the behavior of the algorithms (each case having a different parameterization). On the contrary, the S-PSO is less robust, as its performance is more affected by the optimization case.

In conclusion, the S-GA presents the best performance, followed by the S-FA and the S-PSO.

5.5.2. MULTI-STAGE OPTIMIZATION CONCLUSIONS AND CONTRIBUTIONS

The two algorithms with the best performance in the single-stage optimization have been selected to be applied to the multi-stage optimization problem: the multi-stage Genetic Algorithm (M-GA) and the multi-stage Fireworks Algorithm (M-FA). A detailed explanation of each one and the implementation details required to adapt them to the optimization problem object of study have been given.

A test has been used to compare the performance of M-GA and M-FA. This test is particularized for 2 stages ($M = 2$) and comprises:

- Two optimization cases for each algorithm in order to check their robustness.
- Five instances to be run for each algorithm and case.

The comparison of both algorithms has turn out that the M-GA clearly outperforms the M-FA:

- Regarding the effectiveness, the M-GA always reaches the optimal solution, while the M-FA does not reach it in all its instances. When studying what can be considered as the normal behavior of the M-FA (filtering the outliers), it has been found that this algorithm may not reach the optimum solution (although when not reaching it, the solutions provided are very close to the optimum).
- Regarding the speed of convergence of the algorithms, the M-GA is faster than the M-FA.
- Regarding the robustness, the M-GA is very robust, since it presents a very similar performance in the two optimization cases designed to study the behavior of the algorithms. On the contrary, the M-FA is less robust, as the fitness average and median stabilizes in different values depending on the case.

Additionally, and in order to illustrate the potential of the multi-stage formulation, it has been compared with what can be considered the most common approach to tackle with optimization problems where the installation is divided into stages: the cascade

single-stage optimization. This approach optimizes separately each stage in increasing order of stages. This way, each stage is optimized taking into account the improvements already installed in the previous stages and considering the money available for the stage, which would be the budget for the stage in addition to the money from the budget allocated to previous stages not spent (in case there is).

When comparing the results obtained with both approaches, it has been found that the multi-stage optimization outperforms the cascade single-stage optimization. This is because the multi-stage optimization is able to evaluate the investment as a whole and has the information of all the stages, while the cascade single-stage optimization cannot foresee the next stages and, therefore, optimizes the installation of each stage without taking into account the next ones.

CHAPTER 6

METHODOLOGY TO DETERMINE THE OPTIMUM INSTALLATION AND APPLICATION TO A FINAL CASE STUDY

This chapter formalizes the methodology proposed in this thesis to assess the installation of electrical infrastructure improvements and applies it to a final case study. It can be considered as the practical application of the knowledge obtained from the research of this PhD:

- The optimization of RSs and ESSs is addressed with the application of the single and multi-stage optimization algorithms of Chapter 5.
- These algorithms use the realistic railway simulator already incorporating the improvements with respect to the traffic model for small perturbations presented in Chapter 2 and for large perturbations presented in Chapter 3.
- The case study will incorporate the complex topologies developed in Chapter 4.

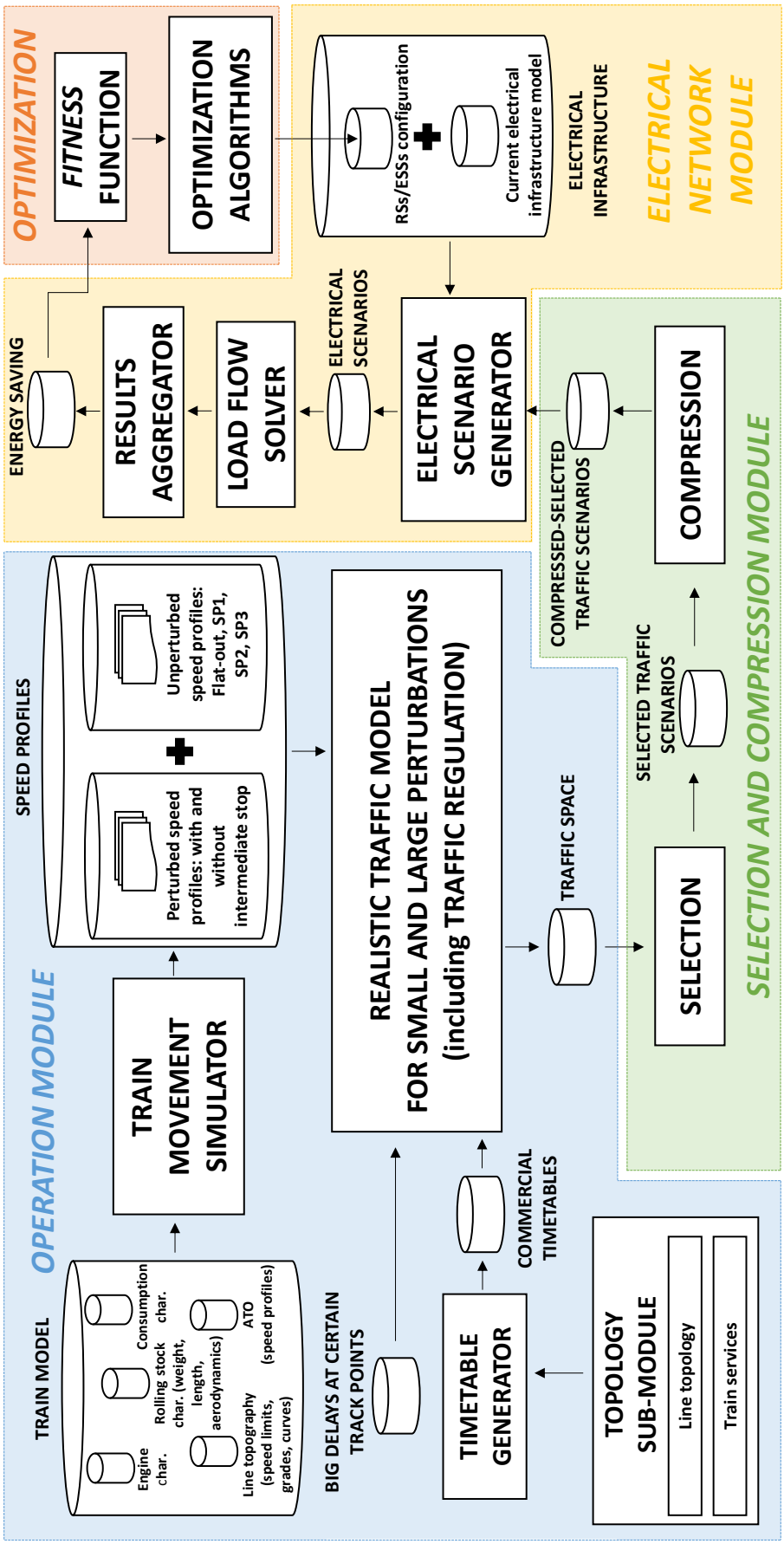

Figure 6-1: Methodology to determine the optimum installation of RSs/ESSs

6.1. METHODOLOGY

Figure 6-1 graphically depicts the methodology that must be followed to appropriately determine the optimum installation of RSs/ESSs in a MTS line. The next paragraphs will give the details of the four steps that compose this methodology: ***generation of the traffic space, selection and compression of the traffic space, electrical simulation and optimization***.

6.1.1. GENERATION OF THE TRAFFIC SPACE

The traffic space represents, in an accurate way, the real operation of the railway line. It is composed of a big number of representative traffic scenarios so as to take into account the traffic variability and its impact on the consumption.

The traffic variability of each scenario has two main sources:

- **Changes in the time shift**. As explained in Chapter 4, changing the time shift is equivalent to change the commercial return times, which in turn, is equivalent to generate different commercial timetables with the same headway in the ***timetable generator***. It must be noted that, as explained in Sections 3.4.2 and 4.1, the time shift is not relevant in traffic with large perturbations, so this source of randomness will be only considered for traffic with small perturbations.
- **Randomness associated with the dwell times.** It is generated by the dwell time models for traffic with small or large perturbations integrated within the ***realistic traffic model for small and large perturbations***. This randomness makes each scenario different from the rest, affecting the way the traffic regulation system (in the case of small perturbations) or the signalling system (in the case of large perturbations) manage the traffic operation, both also being integrated within the ***realistic traffic model for small and large perturbations***.

The representative traffic scenarios are generated by the **OPERATION MODULE**, which is the update of the **TRAIN MOVEMENT MODULE** of Chapter 1: while the **TRAIN MOVEMENT MODULE** only has the ***train movement simulator*** and a very ***simplified traffic model*** that, in some cases, can be directly substituted by the commercial timetables, the **OPERATION MODULE,** apart from the ***train movement simulator***, also includes the ***timetable generator***, the ***realistic traffic model for small and large perturbations*** developed in Chapters 2 and 3 and the ***topology sub-module*** developed in Chapter 4, whose information about the topology models is required to generate the commercial timetables. This sub-module is not explicitly mentioned in the literature, since all the previous studies have focused on very simple topologies whose associated models do not have enough entity to be considered in a separate sub-module. Nevertheless, the models developed in Chapter 4 to deal with complex topologies have increased its complexity considerably, reason why they have been included in this new sub-module.

In Sections 2.4.3 and 3.4.3, the criteria to determine the total number of traffic scenarios that composed the traffic space was to achieve the stabilization of the mean values of the variables of interest. This criteria is based on what is stated in (López-

López, Álvaro J. et al., 2017a). According to the authors, the traffic space is not known a priori and must be determined following a Monte-Carlo approach. This approach consists in increasing the number of scenarios in the traffic space until the mean and standard deviation of the main electrical variables defining each scenario are stabilized (e.g.: rheostat losses, consumption at SSs, etc).

6.1.2. SELECTION AND COMPRESSION OF THE TRAFFIC SPACE

This process is performed by the **SELECTION AND COMPRESSION MODULE** and can be divided into two sub-processes.

6.1.2.1. SELECTION

In Chapters 2 and 3, after generating the traffic space and the associated electrical scenarios, the assessment of the infrastructure improvements was made by performing the electrical simulations of all the traffic scenarios with and without the infrastructure improvements that were going to be assessed. This way, the energy saving associated with the improvement could be calculated from the comparison of the consumptions obtained with and without the improvement. This was affordable in terms of computational burden due to the low number of infrastructure improvements that were evaluated, since the main aim in those chapters was not to find the optimum configuration, but to evaluate the impact of the traffic model in the assessments.

Nevertheless, as seen in Chapter 5, when looking for the optimum installation, the electrical network module has to simulate each RSs/ESSs configuration provided by the individuals of the optimization algorithms in each iteration (which means to simulate that configuration in all the representative traffic scenarios). This makes the process absolutely unattainable from the computational burden point of view. Therefore, it is necessary to reduce the set of traffic scenarios that the electrical network module has to simulate.

The scenarios of this reduced set will be called **selected traffic scenarios** and must contain most of the information from the whole set of representative traffic scenarios that compose the traffic space. This selection has been based on (López-López, Álvaro J. et al., 2017a), where it is performed a characterization of the traffic scenarios based on the *Rheostat Loss Projection (RP)* function, that projects rheostat losses to a set of locations in the line. For this case, the set of locations is the set of N potential locations for installing the infrastructure improvements that, as stated in Sections 5.3.3.1 and 5.4.3.1, corresponds to the locations of the SSs.

The *RP* function tries, through complex procedures, to compute the potential reductions in rheostat losses that can be achieved by increasing the receptivity (which in practice will be achieved with infrastructure improvements). This function has been replaced by the so-called *Single infinite Reversible Substation Test (SIRS-Test).* The *SIRS-Test* can be considered as the application of the *RP* function, since the computation of the potential reductions in rheostat losses from the latter is substituted by the computation of the actual energy saving (directly correlated with the rheostat losses)

obtained from increasing the receptivity by means of installing an "infinite" RS (in theory, no limit in power; in practice, with a very big power). Therefore, this test stablishes the maximum amount of rheostat loss reductions that can be potentially achieved. The only disadvantage of the *SIRS-Test* with respect to the *RP* relies on the fact that it requires additional simulations (one simulation per traffic scenario and location to be evaluated). Nevertheless, this is not a problem, since these simulations are only performed once.

The condition to be met by the set of **selected traffic scenarios** is to obtain an error in the energy saving for all the locations tested in the *SIRS-Test* lower than 5% with respect to the whole set of representative traffic scenarios that compose the traffic space. All the possible random combinations of $n_{selected}$ scenarios among the whole set of scenarios must be tested and the one with the least $n_{selected}$ is chosen, as it achieves the highest reduction of scenarios (in case of having more than one combination with the least $n_{selected}$ complying with the requirement, the one with the lowest error is chosen).

6.1.2.2. COMPRESSION

Obtaining a set of selected traffic scenarios implies a great reduction in the number of scenarios to simulate when applying the optimization techniques. Nevertheless, each selected traffic scenario still has a very big amount of snapshots that must be solved. In order to reduce the number of snapshots that must be solved (each snapshot represents 1 second), the compression algorithm of (López-López, Álvaro J. et al., 2017b) has been applied. According to the authors, the compression algorithm consists of a clustering stage which groups similar snapshots in the uncompressed scenario and a second stage in charge of finding a set of optimized trains' load and regeneration profiles which may be directly fed into the MTS infrastructure of the case study. In the case of compressing the scenarios for the ESSs optimization, the energy accumulated in the ESSs is a state variable that forces to group only consecutive snapshots in the clustering stage of the compression algorithm.

This algorithm reduces the number of snapshots to be included in a given traffic scenario while keeping enough accuracy. As can be supposed, the higher the compression, the lower the accuracy. Therefore, the requirement to classify a **compressed scenario** as an accurate one is to achieve a relative energy-saving error (with respect to the energy saving in the associated uncompressed scenario) lower than 5%.

6.1.3. ELECTRICAL SIMULATION

The electrical simulation takes place in the **ELECTRICAL NETWORK MODULE**. The electrical scenarios associated with the compressed-selected traffic scenarios are generated in the ***electrical scenario generator***, which requires the information of the electrical infrastructure. After that, they are solved in the ***load flow solver***. As a reminder, ***load flow solver*** applies the **unified mixed AC-DC Newton-Raphson** method. Finally, and after the information processing of the ***results aggregator***, the electrical variables of interests are selected and given as the output of the electrical simulation. In order to determine the optimum installation of RSs/ESSs, the main variable of interest

is the energy saving associated with the installation, which is computed by comparing the consumption with and without it.

6.1.4. OPTIMIZATION

The nature-inspired optimization algorithms developed in Chapter 5 use the **ELECTRICAL NETWORK MODULE** to make the search for the optimum configuration. They try in every iteration different RSs/ESSs configurations (as many as individuals of the population) and give the order to the **ELECTRICAL NETWORK MODULE** to simulate them, for which the data of the electrical infrastructure must be updated with the information of the RSs/ESSs installations that are going to be tested.

It must be noted that, while the generation of the traffic space and the selection and compression of the traffic scenarios are performed only once, the electrical simulation and the optimization are repeated, in a kind of feedback loop, until achieving the optimum solution. The details of the communication between the algorithms and the electrical network module are given in Section 5.2.

6.2. FINAL CASE STUDY

6.2.1. TOPOLOGY, INFRASTRUCTURE AND ROLLING STOCK CHARACTERISTICS

The line topology selected for the final case study is a line with branches, short-turn and terminal stations, particularly a Y-shaped line with short-turn and terminal stations in the branches and a terminal station in the common section. This choice is due to the fact that this is the most complex topology among those studied in Chapter 4 and, somehow, covers the different aspects of complex topologies that have been studied. Additionally, from the point of view of the decisions that the optimization algorithms must take to find the optimum RSs/ESSs installation, this type of topology makes the optimization problem more difficult to be solved.

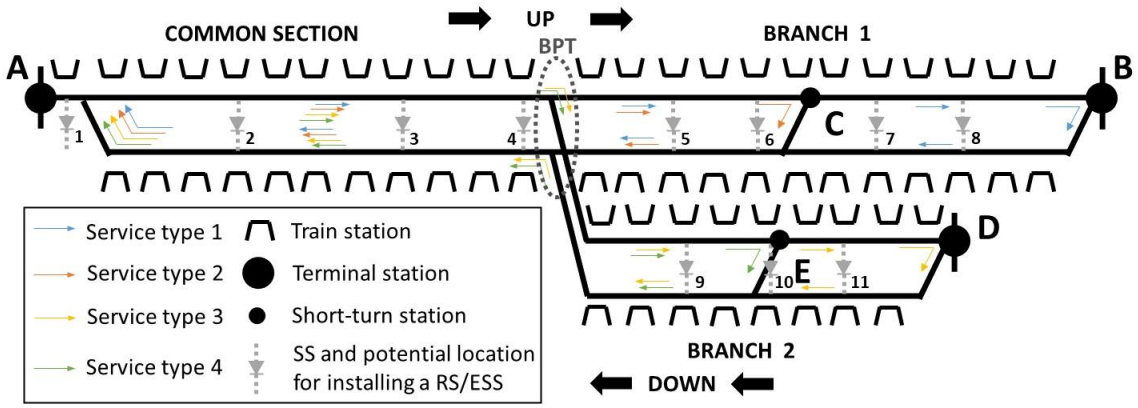

Figure 6-2: Final case-study line topology

As can be seen, there is a common section, two branches, a bifurcation point (BPT) and three terminal stations (n_T=3): A in the common section, B in branch 1 and D in branch 2. Additionally, there are two short-turn stations ($n_{SH-T} = 2$), one in each of the two

branches: C in branch 1 and E in branch 2. The different possibilities of itinerary selection makes it possible to have four different types of service ($n_{services} = 4$).

- Type 1: the itinerary of the trains providing this type of service is A-BPT-C-B-C-BPT-A.
- Type 2: the itinerary of the trains providing this type of service is A-BPT-C-BPT-A.
- Type 3: the itinerary of the trains providing this type of service is A-BPT-E-D-E-BPT-A.
- Type 4: the itinerary of the trains providing this type of service is A-BPT-E-BPT-A.

The different types of service in this case study are repeated periodically according to this pattern: [Type 1-Type 4- Type 2- Type 3].

The line is inspired by the real Spanish metro line used in the case study of Chapters 2 and 3 but with changes to adapt it to this type of topology. Indeed, the stretch included within the common section and branch 1 corresponds to the line with two terminal stations of the mentioned chapters, to which an additional short-turn station has been added (C). Branch 2 is symmetric to branch 1, but its extension has been reduced in three stations and, therefore, the locations of its short-turn and terminal stations are different.

Table 6-1 shows the main electrical and topological characteristics of this line, as well as the information regarding the rolling stock.

Regarding the RS management, the regenerated energy not used by other trains is sent back to the grid when the inversion mode is activated. The activation of this mode takes place when the catenary voltage exceeds the threshold of $1.0001 \times$ no-load voltage. The behavior of the RS in the inversion mode is determined by the constant voltage control (for more details, see Appendix 1).

Table 6-1: Case study topological, electrical and rolling stock characteristics

Topological and electrical and characteristics	Rolling stock characteristics

• **Line length.**
  ○ **Common section:** 9.8 km
  ○ **Branch 1:** 10 km
  ○ **Branch 2:** 8.3 km
• **Maximum speed:** 70 km/h.
• **Passenger stations.**
  ○ **Common section:** 12
  ○ **Branch 1:** 12
  ○ **Branch 2:** 9
• **Traction SSs:** 11
  ○ **Common section:** 4
  ○ **Branch 1:** 4
  ○ **Branch 2:** 3
• **Rectifier type (all SSs):** 6-pulse diode rectifiers (one-quadrant)
• **Rectifier nominal power.**
  ○ **SSs 1-4 (common section):** 6.6 MVA.
  ○ **SSs 5-11 (branches):** 4.8 MVA.
• **Nominal voltage of the line / No-load voltage:** 1600 / 1650 V
• **Feeder lines:** Conventional overhead conductor with a support feeder connected to the contact lines every 700 m (at these points, both track overhead conductor lines are paralleled).
• **Return circuit:** Both rails are used to carry the return current.
• **Total impedance of the active + return line:** 26 mΩ/km.
	• **Empty train mass:** 192.96 tons (only one type of train composition used).
	• **Train maximum load:** 76.58 tons.
	• **Train load in the study:** varies depending on the headway from 25% of maximum load to 90% of maximum load (for more details see Section 6.2.2)
	• **Type of braking:** Blend of pneumatic and electrical braking. The pneumatic braking is only used when the electrical braking is not able to provide the braking force commanded.
	• **Electrical braking:** Regenerative. Trains feed braking power into the railway line if possible. If the maximum voltage is reached, the power surplus is sent to rheostats.
	• **Maximum motoring power:** 5MW
	• **Maximum regenerating power:** 4MW
	• **Type of driving:** Automatic Train Operation (ATO) guided trains.
	• **Auxiliary consumption power:** 200 kW.
	• **Voltage threshold for the activation of the rheostatic braking:** 1800 V

Regarding the ESSs, the storage technology chosen consists in electrochemical double layer capacitors (EDLC), due to their good balance between its power and energy densities. The ESS management control will be according to the ESS control curve described in (Roch-Dupré et al., 2017) and represented in Figure 6-3. It must be noted that the reference voltage value for defining the unitary units (p.u.) is the no-load voltage: 1650 V.

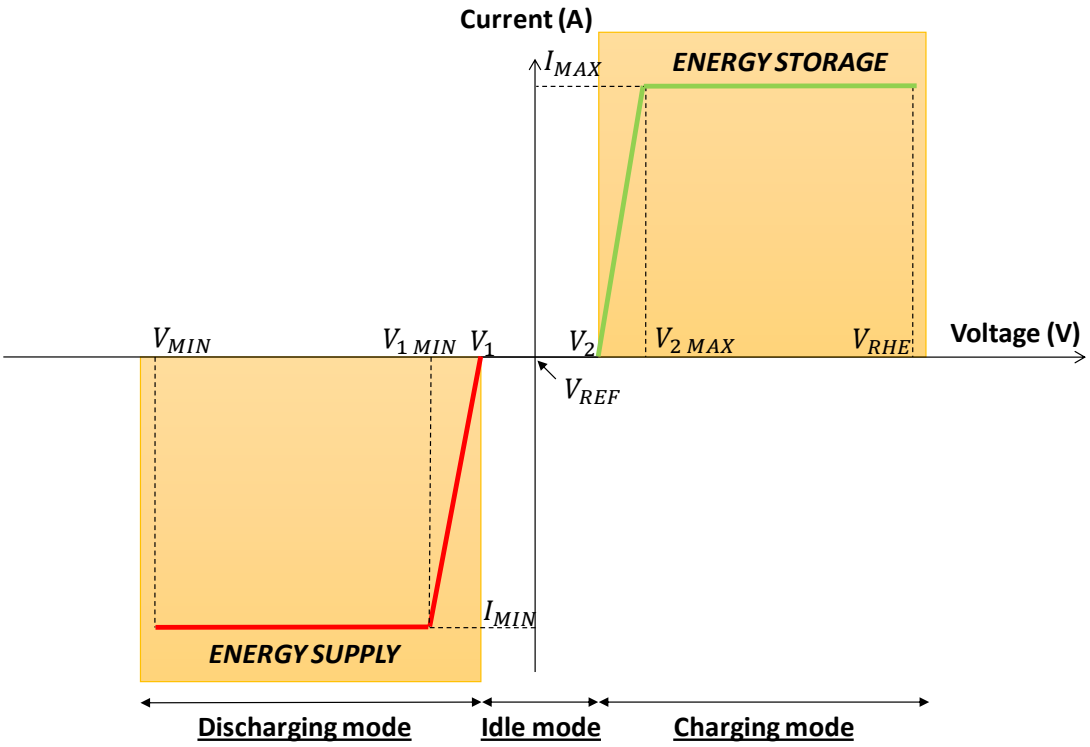

Figure 6-3: ESS control curve

where:

- V_{RHE}: voltage threshold for the activation of the rheostatic braking: 1800 V.
- V_{REF}: reference voltage level, which coincides with the no-load voltage level: 1 p.u.
- V_1**:** voltage level at which the ESS starts the discharging phase: 0.99 p.u.
- $V_{1\,MIN}$ **:** voltage level at which the ESS reach its maximum discharging current (I_{MIN}): 0.95 p.u.
- V_2 : voltage level at which the ESS starts the charging phase: 1.01 p.u.
- $V_{2\,MAX}$: voltage level at which the ESS reach the maximum charging current (I_{MAX}): 1.05 p.u.
- V_{MIN} is the lowest admissible operating voltage: 0.66 p.u.

As can be seen, according to the values of the control curve parameters, both charging and discharging phases are activated as soon as possible, since their activation values, respectively determined by V_1 and V_2, are very close to the reference voltage. Therefore, and compared to other control curves that prioritize voltage stabilization or peak power shaving (where the value of V_1 is higher in order to preserve the stored energy for situations of voltage drops or power peaks), this control curve is designed to save the highest possible amount of energy.

The Jacobian matrix used to solve the load flow has a set of terms where the derivative of the power with respect to the voltage is calculated for all the DC power nodes (in particular, the expression of these terms is $\frac{\partial P_{DC}}{\partial V_{DC}} \cdot V_{DC}$). ESSs are considered as power

nodes, where the power is obtained by multiplying the voltage by the current, the latter being defined by a piecewise linear function (see Figure 6-3). Consequently, in the case of the ESSs, $\frac{\partial P_{DC}}{\partial V_{DC}} \cdot V_{DC}$ has different expressions depending on the voltage value, which can generate convergence problems in the load flow. In order to have a unique expression and to avoid these convergence problems, the ESS control curve must become continuous derivable throughout the whole voltage domain ($[V_{MIN} - V_{RHE}]$), for which it has been approximated as a sum of sigmoid functions. Appendix 2 give the details of the procedure followed to make this approximation and analyzes its impact on the convergence of the load flow.

6.2.2. OPERATION CHARACTERISTICS

In order to represent the different types of operation during the day (peak hours, off-peak hours, etc.), four different headways have been chosen for the common section: 3.5, 5, 7 and 15 minute headways.

Simulations with large perturbations only take place at 3.5 minute headway, while simulations with small perturbations take place at all the headways. The train load varies depending on the headway:

- At peak hours, represented by 3.5 minute headway, and semi-peak hours, represented by 5 minute headway, the number of passengers is very high and train load is 90% of the maximum load.
- At off-peak hours, represented by 7 minute headway, the number of passengers is lower and train load is 50% of the maximum load.
- At sparse traffic conditions, represented by 15 minute headway, the train is almost empty, thus its load is 25% of the maximum load.

Regarding the speed profiles:

- The set of four predesigned and unperturbed speed profiles (flat-out, SP1, SP2, SP3) is the same as the one presented in Section 2.4.2.
- In the case of perturbed speed profiles, the delays that create the accumulation of trains are introduced at the end of the common section in the down direction. As a consequence, the interstations with perturbed speed profiles are the last three interstations before arriving to terminal station A (see Figure 6-2). Since the topology of the case-study line in the common section is the same as the topology of the case-study line of Chapter 3, the interstations with perturbed speed profiles are those of Chapter 3 and, consequently, the perturbed speed profiles -with and without intermediate stops- are the same as those presented in Section 3.4.2.

6.2.3. SIMULATION CHARACTERISTICS

As previously explained, the traffic space must comprise a big enough number of different traffic scenarios so as to achieve the stabilization of the mean values of the variables of interest, which have been the energy consumption at SSs, the regenerated energy, the rheostat losses and the receptivity. The values of these variables first

stabilize when generating 200 different traffic scenarios in each of the five different moments of operation (defining each moment of operation the headway and the type of perturbation). The two sources of randomness in the generation of the traffic space explained in Section 6.1.1 have been taken into account in the following way:

- In traffic with small perturbations, each traffic scenario has been generated with the randomness associated with the dwell time model for small perturbations (see Section 2.3.2.1) and with different time shifts. The selection of the values for the time shift has been performed very carefully, so as to properly include all the variability that may be due to it. Specifically, as there are four different types of service (see Section 6.2.1), the duration of a whole interval of operation is four times the headway in the common section and, therefore, the values chosen for the time shift are equally separated and within the interval $[-headway \cdot 2, headway \cdot 2]$ (in addition to the null-time shift, which is the most common in the literature).
- In traffic with large perturbations, each traffic scenario has been generated with the randomness associated with the dwell time model for large perturbations (see Section 3.3.2.1) and with null time shift.

After the generation of the traffic space, the selected traffic scenarios have been obtained by applying the procedure explained in Section 6.1.2.1, achieving a reduction of 99% with respect to the initial number of scenarios composing the traffic space.

With the aim of representing a typical operation cycle, the simulation length for each traffic scenario must be approximately the time required by a train to go from one terminal station to the other. As there are four different travel times (one for each type of service), the simulation length has been defined as the longest travel time. This value varies from 3700 secs to 6400 secs depending on the headway, which means to solve from 3700 to 6400 snapshots in the electrical simulation of each traffic scenario. In order to reduce the computational burden, the compression procedure explained in Section 6.1.2.2 has been applied, reducing the number of snapshots in 85%.

The error between the compressed-selected scenarios and the whole set of non-compressed scenarios that compose the traffic space is less than 5% when applying the *SIRS-Test*.

6.2.4. OPTIMIZATION DETAILS

The single and multi-stage optimization (the latter particularized for two stages, where the second stage takes place 2 years after the first stage) of both RSs and ESSs has been performed. The algorithms selected for the optimization have been those that presented the best results in the tests of Chapter 5: the S-GA for the single-stage optimization with the S-GA1 parameterization and the M-GA for the multi-stage optimization with the M-GA1 parameterization. The parameterization of both algorithms is given in Table 6-2 (note that the population size in S-GA1 has been also increased to 200 chromosomes).

Table 6-2: S-GA1 and M-GA1 parameters

	S-GA1	M-GA1
Population size (number of chromosomes)	200	
Probability for a chromosome to mutate one gene, mut_1	20%	
Probability for a chromosome to mutate two genes, mut_2	10%	
Maximum number of iterations, $num\ iter_{max}$	100	

With respect to the variables of decision:

- Locations: Every SS location in the final case study is considered as a candidate to install the RS/ESS, therefore $N = 11$.
- Power to be installed in each location: this variable of decision can take any value from the set $[0: step_{pow}: max_{pow}]$. This set changes depending on the infrastructure improvement:
  - With RSs:
    - $step_{pow} = 1000\ kW$
    - $max_{pow} = 3000\ kW$
  - With ESSs:
    - $step_{pow} = 500\ kW$
    - $max_{pow} = 3000\ kW$
- Capacity to be installed in each location: this variable of decision (only applicable for the ESSs installation) can take any value from the set $[0: step_{cap}: max_{cap}]$.
  - $step_{cap} = 5\ kWh$
  - $max_{cap} = 15\ kWh$

Regarding the simulation time, achieving convergence took around a day in the single-stage optimization and two days in the multi-stage optimization. The server used for the optimization has the following characteristics:

- CPU: Intel(R) Xeon(R) Silver 4116, 24 Cores-2100 MHz (48 logical processors).
- RAM: 128 GB.
- Disk: DELL PERC H330 1.65 TB.

In order to check the validity of the solutions, several instances have been run for all the optimizations and all of them reached the same solution.

The values for the parameters of the fitness function, as well as the reason why they have been chosen are given bellow:

- e_{cost}: 0.0642 €/kWh. This is a realistic value obtained from the addition of the average energy price in Spanish market in the year 2018 and the energy tolls established by the Spanish Government for that year. For more details about the procedure to compute the energy cost, see (Roch-Dupré et al., 2017).
- $C_0\left(\overline{ind_i}^{\,stage\ j}\right)$ this value is computed differently depending on the type of infrastructure improvement:
  - In the case of the RSs, the cost of the installation associated with each stage is the combination of a fixed term (which represents the costs

related with personnel, the works to install the RS, etc...) and a variable term that depends on the RS size. The fixed term is computed by multiplying the total number of RSs installed in the stage by the fixed cost, while the variable term is obtained from adding the total power installed in the stage and multiplying it by the unitary power cost (see Equation (6-1)).

$$\left[C_0\left(\overline{ind}_i^{\,stage\ j}\right)\right]_{RSs} = \#RSs\left(\overline{ind}_i, stage\right)\cdot f_{cost}(stage\ j) + \sum_{k=1}^{N} pow\left(\overline{ind}_i, stage\ j, k\right)\cdot pow_{cost}(stage) \quad \textbf{(6-1)}$$

where:

- ✓ $\left[C_0\left(\overline{ind}_i^{\,stage\ j}\right)\right]_{RSs}$ is the cost of the RSs installation associated with individual i in stage j.
- ✓ $\#RSs\left(\overline{ind}_i, stage\ j\right)$ is the number of RSs installed in stage j by individual i.
- ✓ $f_{cost}(stage\ j)$ is the installation fixed cost in stage j.
- ✓ $pow_{cost}(stage\ j)$ is the unitary cost for power in stage j.

Table 6-3 shows the values of these costs in each of the stages (in the case of the single-stage optimization, the costs correspond to those of stage 1). It must be noted that there is almost no literature providing economic figures about the RSs costs, so reasonable values have been selected (the unitary costs for power are inspired by the information provided in (Gelman, 2013)).

Table 6-3: RSs installation costs

Fixed cost [€]		**Unitary power cost [€/kW]**	
Stage 1	**Stage 2**	**Stage 1**	**Stage 2**
25000	20000	65	50

- In the case of the ESSs, only the variable term has been observed, since their installation is much simpler than the installation of the RSs. The value of this term for each stage is obtained from adding the total power and capacity installed in the stage and multiplying them by their unitary costs (see Equation (6-2)). The unitary costs for the EDLCs in each stage are depicted in Table 6-4 (in the case of the single-stage optimization, the costs correspond to those of stage 1). It must be noted that a sensitivity analysis has been included in the optimization of the ESSs, stablishing two different cases differentiated by the values given to the unitary costs for power: in **sensitivity case 1** the values are included within the range of values proposed by (González-Gil, Arturo et al., 2013), while in **sensitivity case 2** the values are considerably cheaper. In both cases, the costs are reduced by 33% in the second stage. The unitary cost for capacity, also obtained from the range of values proposed by

(González-Gil, Arturo et al., 2013), is common for both stages and for both cases.

$$\left[C_0\left(\overline{ind_i}^{\,stage\ j}\right)\right]_{ESSs} = \sum_{k=1}^{N} pow\left(\overline{ind_i}, stage\ j, k\right) \cdot pow_{cost}(stage\ j) + \sum_{k=1}^{N} cap\left(\overline{ind_i}, stage\ j, k\right) \cdot cap_{cost}(stage\ j) \quad \textbf{(6-2)}$$

where:

- ✓ $\left[C_0\left(\overline{ind_i}^{\,stage\ j}\right)\right]_{ESSs}$ is the cost of the ESSs installation associated with individual i in stage j.
- ✓ $cap_{cost}(stage\ j)$ is the unitary cost for capacity in stage j.

Table 6-4: ESSs installation costs

Sensitivity case	Unitary power cost [€/kW]		Unitary capacity cost [€/kWh]	
	Stage 1	Stage 2	Stage 1	Stage 2
1	160	106.7	270	
2	70	46.7	270	

- $wacc$: 2.5%. This is a reasonable interest rate.
- T: 15 years. This is a very reasonable estimation for the ESSs life cycle (ESSs are more restrictive with respect to this aspect than RSs) according to (Ralon, Taylor, Ilas, Diaz-Bone, & Kairies, 2017).
- $budget$: Table 6-5 shows the budget figures selected for the RSs and ESSs installation. In the case of having two stages, half of the total budget is allocated to each stage. These figures are flexible enough to allow a high number of different configurations to be installed, and restrictive enough so as not to allow very expensive configurations. For real implementation, railway operators must set the budget.

Table 6-5: Budget figures

Budget for RSs (k€)	Budget for ESSs (k€)
340	280

6.2.5. ENERGY CALCULATION PROCEDURE

The energy saving required to compute the fitness function must be given in annual terms. The procedure to calculate the annualized energy saving is the same as the one presented in Section 3.4.5.

The distribution of the annual hours of operation with each headway and perturbation type is depicted in Table 6-6 (operation is from 6:00 AM to 2:00^{+1} AM, while maintenance is from 2:00 AM to 6:00 AM).

Table 6-6: Main characteristics of the annual operation in the case-study line

	3.5 min with large pert.	3.5 min with small pert.	5 min with small pert.	7 min with small pert.	15 min with small pert.
Hours of operation in a year	942.5	942.5	1885	2782	728
Percentage of total operation	12.95%	12.95%	25.9%	38.2%	10%

6.3. OPTIMIZATION RESULTS

6.3.1. ANALYSIS OF THE OPTIMIZED CONFIGURATIONS

Figure 6-4 provides the properties (locations and sizes) of the solutions achieved by the RSs optimization, as well as the fitness of the solutions. Figure 6-5 and Figure 6-6 do the same for the ESSs optimization in both sensitivity cases.

In pre-optimization tests performed to gain a first understanding of the search space corresponding to the case-study line, it was found that the receptivity of the line was reasonably high. Indeed, it was also found that the receptivity is almost absolute (which means that practically the whole amount of regenerated energy is recovered) with installations with a total power greater or equal to 3 MW. The solutions provided by the optimization algorithms are completely in line with the results of these pre-optimization tests.

The following sections will get into the details of each of the solutions.

6.3.1.1. ANALYSIS OF THE OPTIMIZED RSs CONFIGURATIONS

In the RSs single-stage optimization the total power installed is 2 MW. This means that although there is room to increase the energy saving with a bigger installation (at least until a total power of 3 MW), the marginal benefit from increasing it does not economically compensate the extra-investment required for it. When moving to the RSs multi-stage optimization, the total power installed is 3 MW, divided into 2 MW in the first stage and 1 MW in the second stage. This means that the prices in the second stage have been reduced enough to install 1 additional MW.

Once having analyzed the total amount of power installed, it is also very important to study the distribution of this power among the potential locations where the RSs can be installed. As can be seen, the total power installed is very reasonably distributed:

- In the **RSs single-stage optimization**, two 1MW RSs are installed in positions no.2 and 6. These locations are centered in, respectively, the common section (along which the largest number of trains run) and branch 1 (the longest of the two branches).

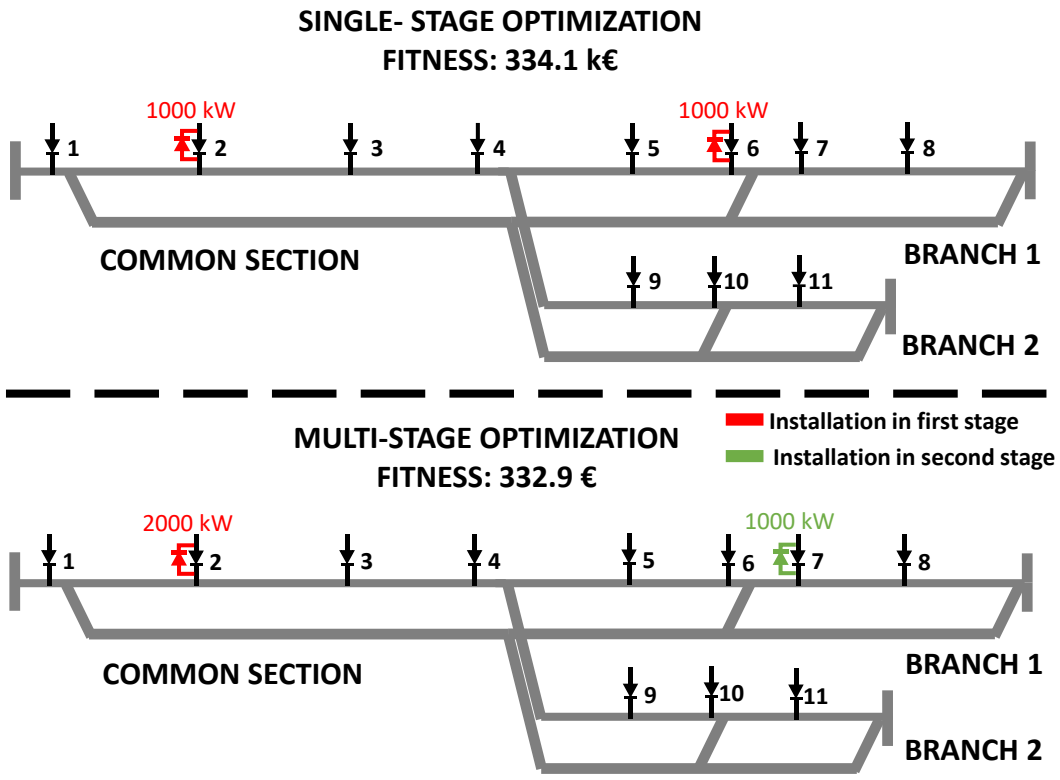

Figure 6-4: RSs optimization

- In the first stage of **RSs multi-stage optimization** one RS is installed in position no.2 with twice the power of the RS installed in that position in the single-stage optimization. The reason of installing just a 2 MW RS instead of two 1 MW RSs is the budget limit in the first stage and the fixed cost, which makes more expensive to install two small RSs than one big RS. In the second stage, since installation costs are lower, another 1 MW RS is installed in position no.7, which is very close to position no. 6 (the other position selected in the single-stage optimization). The reason for this small change in position (7 vs 6) may be due to the fact that, since the size of the RS in position 2 is bigger, its area of influence is bigger too (the area of influence being the area from which it can receive regenerated energy), so it can be better for the RS installed in branch 1 to separate from this area of influence (so that it can focus more on the regeneration taking place in the branch).

6.3.1.2. ANALYSIS OF THE OPTIMIZED ESSS CONFIGURATIONS

6.3.1.2.1. Sensitivity case 1

In the ESSs single-stage optimization with the prices of sensitivity case 1 the total power installed is 1.5 MW. This means that although there is room to increase the energy saving (at least until a total power of 3 MW), the marginal benefit from increasing it does not economically compensate the extra-investment required for it. In the case of the multi-stage optimization, the total power installed is the same and, indeed, all the installation has been moved to the second stage. This means that the reduction in the installation cost derived from undertaking all the installation in the second stage (the capitals cost for the ESS power considerably decreases in this stage) compensates the

fact of not obtaining benefits from installing the ESSs from the beginning. This is a very extreme case but it can be very illustrative to show the potential of the multi-stage optimization with respect to the cascade single-stage optimization explained in Section 5.4.4 (which, unlike the multi-stage optimization, would have opted to undertake the whole installation in the first stage).

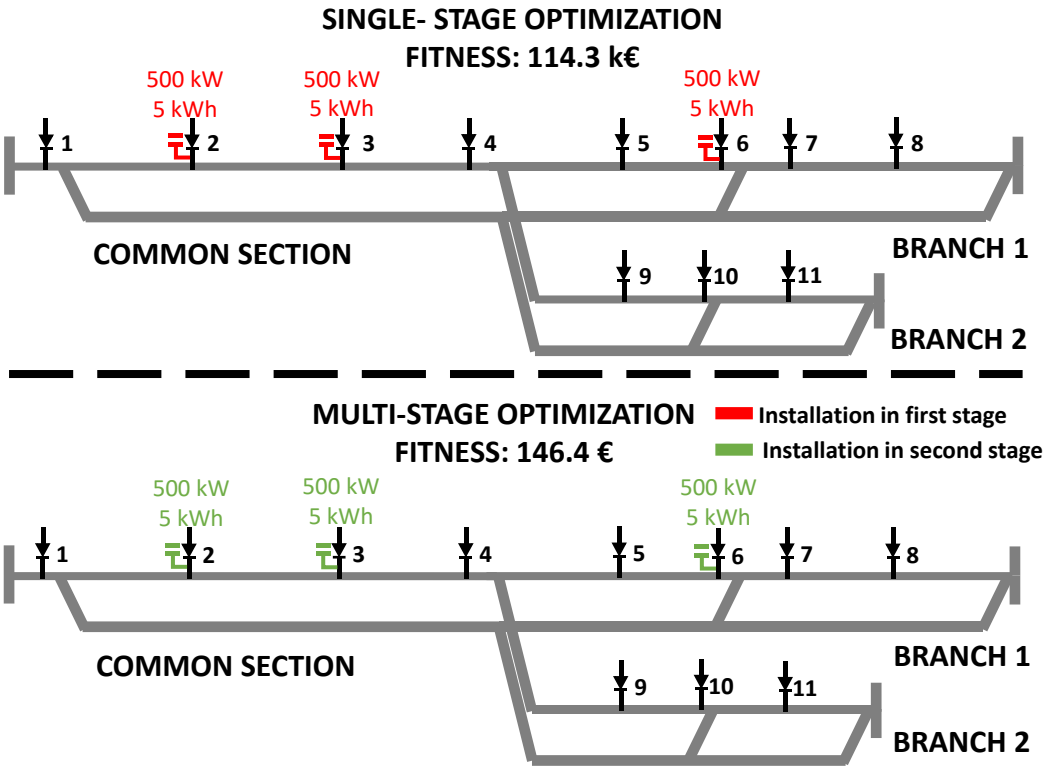

Figure 6-5: ESSs optimization sensitivity case 1

Regarding the distribution of the power installed, it is very similar to the proposed in the RSs single-stage optimization. In this case, as there is no fixed cost and the minimum power that can be installed is smaller than in the case of the RSs (500 kW vs 1000 kW), the 1 MW RS installed in position no.2 is replaced by two 500 kW ESSs in positions no.2 and 3 (so that the power installed is more distributed). Additionally, there is also an ESS installed in the same position where the other RS was installed; in this case the power of the ESS is 500 kW and not 1000 kW (as happened with the RS), which means that the increase in the energy saving from installing a bigger size (or an additional 500 kW ESS in the next position) does not compensate the increase of the installation cost.

Regarding the capacity, all the ESSs have 5 kWh, since this value is enough to avoid losing significant amounts of regenerated energy due to lack of storage capacity. It must be noted that, according to the ESS control curve explained in Section 6.2.1, ESSs try to discharge as soon as possible and, consequently, neither the energy is accumulated for a long time, nor big capacities are required (the small extra energy saving that could be obtained with higher capacities does not compensate the increase of the installation cost).

6.3.1.2.2. Sensitivity case 2

In sensitivity case 2 the prices are quite lower, which makes the total power installed to increase until 2.5 MW in the single-stage optimization and even to 3 MW in the multi-stage optimization (thanks to the additional reduction in the prices of the second stage).

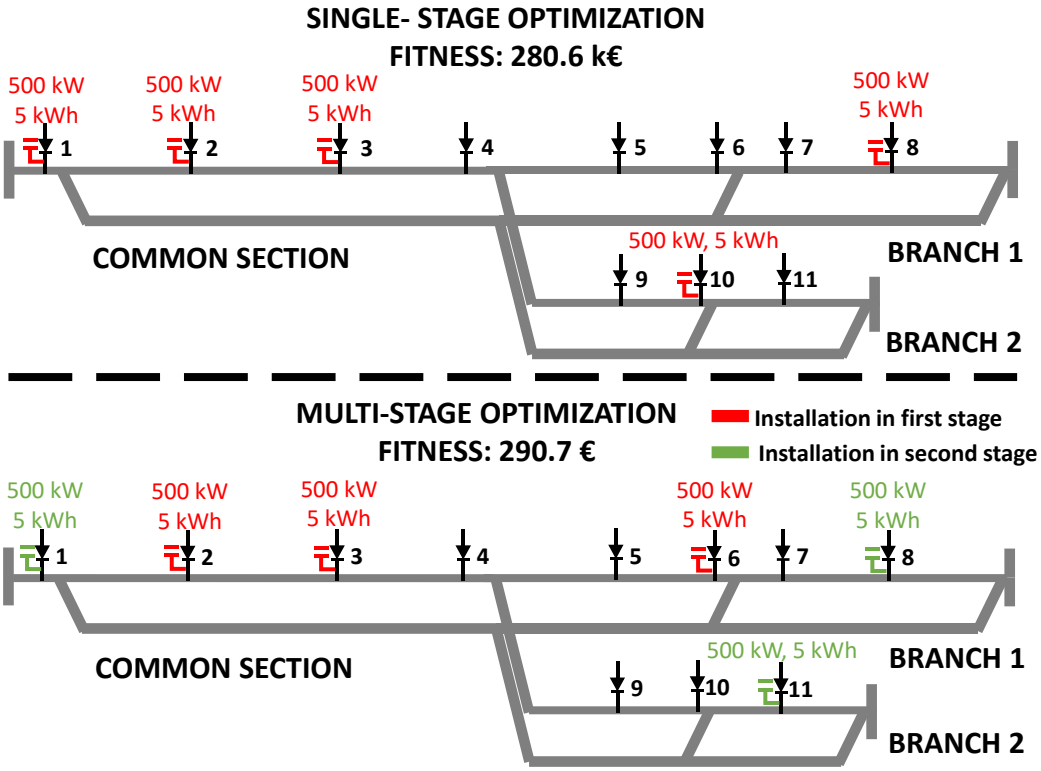

Figure 6-6: ESSs optimization sensitivity case 2

Regarding the distribution of the power installed, the results are very interesting:

- In the **ESSs single-stage optimization**, three 500 kW ESSs are installed in positions no.1, 2 and 3 of the common section (along which the largest number of trains run) and one 500 kW ESS is installed in each of the two branches. Since installation costs are lower, each branch can have, at least, one installation. Besides, the ESS installed in branch 1 is in position no.8, which means that it has moved to the right with respect to the position selected for the ESS installed in that branch in sensitivity case 1. This is because, in comparison to sensitivity case 1, there are more ESSs installed in the common section, some of them being close to the bifurcation point, which enables them to easily deal with the regeneration taking place in the beginning of branch 1, so it may be preferable for the ESS installed in that branch to focus on the regeneration taking place in the last part of the branch, which is more distanced from the bifurcation point, since branch 1 is the longest of the two branches.
- The ESSs installed in the first stage of the **ESSs multi-stage optimization** with the prices of sensitivity case 2 are exactly the same as those installed in the optimization with the prices of sensitivity case 1: three 500 kW ESSs installed in positions no. 2, 3 and 6, what reaffirms that this configuration is the basic

optimum ESSs installation, which can be enhanced if the installation costs are not too big. In the second stage of the optimization, three additional 500 kW ESSs have been installed:

- One additional 500 kW ESS in the common section (position no.1) to match the installation proposed in the single-stage optimization for this branch. In this case the reduction in the prices of the second stage makes it worthy to wait to install that ESS until the second stage.
- The reduction of the prices in the second stage also enables to reinforce the installation in branch 1 with an additional 500 kW ESS in the same position than the ESS installed in that branch in the single-stage optimization (position no.8). The final configuration for branch 1 (one ESS in position no.6 installed in the first stage and another in position no.8 installed in the second stage) allows each ESS to focus on the regeneration that takes place in the different sections of the branch: while the ESS in position no. 6 will focus on the first part of the branch, the ESS in position no.8 will focus on the last part.
- A 500 kW ESS in the end of branch 2 (position no.11). In this case, the ESSs installed near to the bifurcation point (specially those in positions no. 3 and 6) can tackle with the regeneration taking place in the beginning of branch 2, while the ESS in position no.11 can focus on the regeneration taking place in the last section of the branch (besides, this branch is shorter, which makes it easier for the ESS in position no.11 to store also energy from regeneration taking place in the beginning of the branch, if necessary).

Attention must be paid to the fact that, after the two stages, three ESSs have been installed in the common section (along which the largest number of trains run), two ESSs in branch 1 (the longest branch) and one ESS in branch 2 (the shortest branch).

Regarding the capacity, all the ESSs have 5 kWh. The reason for this choice has been already given in Section 6.3.1.2.1.

6.3.2. ANALYSIS OF THE FITNESS RESULTS

As previously explained, although the main aim of installing infrastructure improvements is to increase the energy efficiency, railway operators must check that these installation are also feasible from the economic point of view. This has been taken into account when selecting the NPV of the installation as the fitness function, instead of other possible measures only focused on the energy saving. The NPV tries to find a balance between energy saving and installation costs and, consequently, the higher the NPV, the better this balance (as a minimum requirement, the NPV must be positive, which means that the investment will be economically profitable).

Table 6-7 shows the economic figures of the optimized installations: costs and NPVs. In all cases it is clearly seen that the profitability of the installation is assured, although it is true that, of course, the NPV value considerably changes depending on the installation costs.

It must be noted that the only case where the multi-stage optimization provides a lower NPV than the single-stage optimization is in the RS optimization. This is due to the fact that in this case, the budget restriction in the RS multi-stage optimization clearly affects the installation decisions in the first stage, where more power would have been installed (with bigger sizes or additional RSs in other locations) if the budget allocated to that stage had been bigger.

Table 6-7: Economic figures of the optimized RSs/ESSs installations

Infrastructure improvement	Single-stage optimization		Multi-stage optimization		
	Installation cost (k€)	NPV (k€)	Installation cost (k€)		NPV (k€)
			First stage	Second stage	
RSS	180	334.1	155	70	332.9
ESSs *sensitivity case 1*	244.05	114.3	0	164.1	146.4
ESSs *sensitivity case 2*	181.75	280.6	109.05	74.1	290.7

6.4. CONCLUSIONS AND CONTRIBUTIONS

This chapter formalizes the methodology proposed in this thesis to assess the installation of electrical infrastructure improvements. This methodology combines the use of a realistic railway simulator and the application of nature-inspired optimization algorithms.

The railway simulator is used to obtain accurate enough energy figures to characterize the energy saving potential of the railway line. Since it is fundamental for the reliability of the methodology to improve the accuracy of the results provided by the railway simulator, a new structure for the railway simulator to be used in the assessments is proposed. This structure is divided into two main modules:

- The **operation module**, which represents the real operation of the railway line and models in detail situations of traffic with small and large perturbations. This module is the update of the **train movement module** (most common in the literature and explained in Chapter 1): while the **train movement module** only has the ***train movement simulator*** and a very ***simplified traffic model*** that, in some cases, can be directly substituted by the commercial timetables, the **operation module,** apart from the ***train movement simulator***, also includes the ***timetable generator***, the ***realistic traffic model for small and large perturbations*** developed in Chapters 2 and 3 and the ***topology sub-module*** developed in Chapter 4.
- The **electrical network module**, which performs the electrical simulations of the traffic scenarios generated by the operation module.

The nature-inspired optimization algorithms, designed in Chapter 5, perform an intelligent search to find the characteristics of the RSs/ESSs installation, (in terms of

number, location and size) that yields the best balance between energy saving and installation costs.

The steps of the methodology are:

- **Generation of the traffic space**: the traffic space represents in an accurate way the real operation of the railway line. It is composed of a big number of representative traffic scenarios so as to take into account the traffic variability and its impact on consumption. The traffic space is generated by the **operation module**.
- **Selection and compression of the traffic space:** with the aim of not making the optimization problem intractable in terms of computational burden, two procedures have been carried out:
    - A **selection procedure** has been applied to the whole set of representative traffic scenarios that compose the traffic space in order to obtain a reduced set of ***selected traffic scenarios*** that contain most of the information of the initial set.
    - A **compression procedure** has been applied to the set of ***selected traffic scenarios*** in order to reduce the number of snapshots to be solved by the **electrical network module** without compromising the accuracy of the results.
- **Electrical simulation**: it is performed by the **electrical network module**.
- **Optimization**: it is performed by the nature-inspired optimization algorithms.

The methodology has been applied to optimize the installation of RSs and ESSs in a final case study. The case study used takes into account the improvements made in Chapters 2, 3 and 4: simulation of representative traffic scenarios with large and small perturbations and use of a complex topology, in particular a line with branches, short-turn and terminal stations.

The results obtained are very satisfactory: the increase of the energy saving associated with the installation of the improvements is always accompanied with the economic profitability of the investment. Additionally, a sensitivity analysis for the ESSs optimization has been performed. In this sensitivity analysis different values of the ESSs unitary power costs have been given in order to study the influence of the installation costs on the decision-making. The results clearly show how the installation of the infrastructure improvements varies depending on the economic factor, which means that the optimization algorithms are able to successfully combine this important factor with the main target of this thesis: increasing the energy efficiency.

The a posteriori analysis of the solutions shows that the decisions taken by the optimization algorithms are very reasonable with respect to the configuration details (number, location and size of the improvements). Nevertheless, they are not so intuitive in an *a priori* analysis*,* which reinforces the idea defended in this thesis about the necessity of applying a comprehensive methodology, such as the one proposed in this chapter, in order to provide an accurate assessment for the installation of infrastructure improvements.

CHAPTER 7

CONCLUSIONS, CONTRIBUTIONS, PUBLICATIONS AND FUTURE WORK

The thesis is finished with this chapter, which tries to summarize the main results from the research, as well as to propose some future work.

Section 7.1 presents the main conclusions that can be drawn from the thesis. Section 7.2 lists the main contributions derived from the development of the thesis. Section 7.3 shows the publications obtained within the framework of the thesis. Finally, Section 7.4 proposes some research lines for future work.

7.1. CONCLUSIONS

Section 7.1.1 presents the main conclusions regarding the improvements developed in the railway simulator to include some important features missing in the literature.

Section 7.1.2 presents the main conclusions regarding the design of the nature-inspired optimization algorithms that are used to find the optimum installation of RSs/ESSs.

Finally, section 7.1.3 summarizes the methodology proposed in this thesis to assess the installation of the infrastructure improvements, which combines the use of the improved railway simulator and the optimization algorithms.

7.1.1. RAILWAY SIMULATOR IMPROVEMENTS (CHAPTERS 2, 3 AND 4)

Improving the railway electrical infrastructure of DC railway systems with the installation of RSs or ESSs implies considerable investments that must be carefully studied. Railway simulators are usually the tool in charge to assess the impact of these improvements. Therefore, the more precise and realistic the simulator, the better assessments will be obtained and the more confidence on the investment will have the railway operators.

With this aim, chapters 2, 3 and 4 have focused on the development of different features of the railway simulator that will improve its accuracy and realism.

7.1.1.1. IMPROVEMENTS IN THE TRAFFIC MODEL (CHAPTERS 2 AND 3)

One of the most important parts of the railway simulator is the traffic model, which represents the real operation conditions. Despite its importance, the vast majority of studies in the literature propose oversimplified traffic models that provide inaccurate results, which directly affects the reliability of the assessments made with the railway simulators.

Two main types of traffic scenarios can be differentiated according to the degree of perturbations that take place in operation (perturbation being the deviation of train departures with respect to the commercial timetable)*: **a) traffic with small perturbations*** and ***b) traffic with large perturbations***.

This thesis has proposed the models to accurately represent both traffic scenarios. Particularly, Chapter 2 has presented an accurate model for traffic with small perturbations and has analysed its impact on the simulation results, while Chapter 3 has done the same for the case of large perturbations. The combination of both models allows obtaining a detailed traffic model able to generate representative traffic scenarios that properly replicate the real behaviour of railway operation.

TRAFFIC MODEL FOR SMALL PERTURBATIONS (CHAPTER 2)

This chapter has demonstrated that the results obtained in electric railway simulations can be significantly different depending on the accuracy of the traffic model used.

The most common traffic model for small perturbations used in the literature is too simplified and produces not very accurate results. The main simplifications of this model are: the consideration that the departures of trains from each terminal station are synchronized (null time shift), the lack of stochastic models for dwell times and the use of only one speed profile, generally the flat-out one (minimum running time).

Opposite to this model, Chapter 2 has proposed a novel traffic model for small perturbations with the following features:

- Use of different values of time shift to cover the variability associated with this variable.

- Use of realistic dwell times, taking into account the stochastic behavior of this variable and the behavior of the driver, who tries to shorten the dwell time when the train is delayed.
- Use of four different speed profiles (flat-out and three additional speed profiles with higher travel times and less energy consumption).
- Integration of a traffic regulator module to decide about the speed profile to be used in each interstation.

To demonstrate the necessity of improving the accuracy of the traffic model, the results obtained with both traffic models (the most common in the literature and the one proposed in Chapter 2) have been compared in an illustrative case study, where the installation of an RS has been simulated and the energy saving associated with this installation has been analyzed. The comparison showed that the simplified traffic model used in the literature can yield non-accurate results (energy saving overestimations higher than the 30% have been obtained in this particular case).

TRAFFIC MODEL FOR LARGE PERTURBATIONS (CHAPTER 3)

Traffic with large perturbations has a direct impact in the energy saving that can be obtained when installing RSs or ESSs. Nevertheless, and despite the fact that this type of perturbations can appear not just punctually, but repetitively (especially during peak hours), there are no studies in the literature on this topic. With the aim of filling this gap, this chapter has proposed a realistic traffic model for traffic with large perturbations with the following features:

- Introduction of big delays, characteristic of the operation with large perturbations, which generate great decompensations in the distribution of trains along the line (with some parts where trains are accumulated and other parts where they are very disperse).
- Realistic dwell times models that take into account the traffic conditions (if trains are accumulated or not), the stochasticity inherent to dwell times and the driver's behavior.
- Realistic speed profiles which take into account the traffic conditions (if trains are accumulated or not). In case of not having trains accumulated (traffic with small perturbations) the speed profiles are designed with eco-driving techniques.
- Simulation of the most appropriate speed profile, for each train in each moment, based on the traffic conditions:
    - When trains are not accumulated and the signalling system is not activated, the traffic regulator selects the most appropriate unperturbed speed profile.
    - When there is an accumulation of trains, the speed profiles are perturbed by the signalling system. The application of different types of perturbed speed profiles is considered in the model: speed reduction or train stop at the interstation.

The use of the realistic traffic model for small perturbations of Chapter 2 together with the realistic traffic model for large perturbations of Chapter 3 allows to take into

account all type of traffic situations. This improves the realism and the accuracy of the energy saving results provided by the simulator, which in turn, will facilitate decision-making process about the most appropriate investments required for the electrical infrastructure.

The results presented in Chapter 3 have demonstrated that using *a) the oversimplified traffic model of the literature, b) only the realistic traffic model for small perturbations or c) a combination of both realistic traffic models (with small and large perturbations)*, can lead to different decisions about the most appropriate infrastructure improvement to be installed. The results provided by the realistic traffic models are the most reliable and accurate ones. More concretely, for the case study of Chapter 3, where the energy saving obtained from installing an RS has been evaluated, differences in the energy saving estimations higher than the 30% have been obtained when comparing the results provided by the simplified traffic model and the realistic ones. Additionally, there were also significant differences (higher than the 18% for the case study) between the results obtained only with the realistic traffic model for small perturbations or with the combination of both realistic traffic models (for small and for large perturbations). Finally, it has also been proven that even the decision about the location of the RS may differ depending on the traffic model used for the simulations.

7.1.1.2. IMPROVEMENTS IN THE TOPOLOGY MODELS (CHAPTER 4)

Although real MTS lines have different types of line topologies, only the simplest one (line with two terminal stations) has been used in all the studies of the literature about simulation-based assessments of infrastructure improvements. This chapter has covered this gap in the literature, since it has incorporated the information required by the simulator (the tool in charge of the assessments) in order to work with different types of topologies, including the complex ones.

For a better understanding and modularization of the railway simulator, all the developments made in this chapter with respect to the topologies can be grouped in a ***topology sub-module***, which is the one that provides the information to the ***timetable generator*** in order to obtain the commercial timetables associated with the different types of topology. Once having the commercial timetables of the complex topologies, the realistic traffic models for small and large perturbations can be applied to them in order to obtain the associated representative traffic scenarios.

The topologies studied in this chapter have been the following ones:

- Line with two terminal stations.
- Line with short-turn and terminal stations.
- Line with branches.
- Line with branches, short-turn and terminal stations.

7.1.1.3. PROPOSAL OF A NEW STRUCTURE FOR THE RAILWAY SIMULATOR

As a result of the improvements developed in Chapters 2, 3 and 4, a new structure for the railway simulator is proposed. This structure implies an evolution with respect to the railway simulator structure more spread in the literature and is divided into two main modules:

- The **operation module**, which represents the real operation of the railway line and models in detail situations of traffic with small and large perturbations. This module is the update of the **train movement module** (most common in the literature): while the **train movement module** only has the ***train movement simulator*** and a very ***simplified traffic model*** that, in some cases, can be directly substituted by the commercial timetables, the **operation module**, apart from the ***train movement simulator***, also includes the ***timetable generator***, the ***realistic traffic model for small and large perturbations*** developed in Chapters 2 and 3 and the ***topology sub-module*** developed in Chapter 4.
- The **electrical network module**, which performs the electrical simulations of the traffic scenarios generated by the operation module. This module includes the ***electrical scenarios generator***, the ***load flow solver*** and the ***results aggregator.***

7.1.2. DESIGN OF NATURE-INSPIRED OPTIMIZATION ALGORITHMS (CHAPTER 5)

Optimization algorithms use the information provided by the railway simulator (which includes the improvements already explained) to find the optimal installation of RSs or ESSs.

There are two types of optimization algorithms that can be used to tackle the optimal design of the infrastructure improvements: formal mathematical models or nature-inspired optimization algorithms. This thesis has focused on the second ones, since they present high flexibility and a great capacity to successfully deal with the computationally-intensive and highly non-linear and non-convex problem posed by the railway simulator.

The fitness function that guides the intelligent search of the algorithms has been defined as the Net Present Value (NPV), since it tries to find a balance between the energy saving and the installation costs associated with the infrastructure improvement required to achieve it. The variables of decision that have been optimized are:

- Number of RSs /ESSs to be installed.
- Location of the RSs /ESSs to be installed.
- Power (kW) of each RS / ESS to be installed.
- Capacity (kWh) of each ESS to be installed (this variable does not apply to the RSs optimization).

The optimization problem has been addressed in two variants:

- Single-stage optimization: the whole budget for the installation of RSs/ESSs is available from the beginning.
- Multi-stage optimization: the whole budget is divided into stages, separated in time. Therefore, the improvement of the infrastructure must be undertaken gradually and the algorithm must try to find the optimum configuration for each stage without exceeding the budget limits of the stage and considering the installation as a whole.

While the single-stage optimization has already been addressed in the literature, (but in few examples and with very simplified simulations), the multi-stage optimization is a true novelty that can be of great interest and application.

In order to fit with the optimization problem, the nature-inspired optimization algorithms selected from the literature have been reformulated according to the knapsack problem formulation. The knapsack problem consists in picking and choosing a set of items from a given larger set to put in the knapsack so as to maximize the total value, under certain constraints. The knapsack optimization problem is generally coded as a bit string containing zeros and ones – a "one" representing the fact that a certain item is selected and a "zero" representing the fact that a certain item is not selected. For the particular case of this optimization problem, each item represents one of the potential locations where an RS/ESS can be installed and, instead of having a bit string containing zeros and ones, each item has a value from a set of discrete values that represent the possible amounts of power or capacity that can be installed. The constraints are related to the maximum sizes and maximum admissible budget that cannot be exceeded.

SINGLE-STAGE OPTIMIZATION

Three different optimization algorithms have been proposed in order to compare and validate their performance and results. The optimization algorithms proposed are the single-stage Genetic Algorithm (S-GA) as the main exponent of evolutionary algorithms, the single-stage Particle Swarm Optimization Algorithm (S-PSO) as the main exponent of swarm algorithms and the single-stage Fireworks Algorithm (S-FA) as another variant of swarm algorithms. A detailed explanation of each one and the implementation details required to adapt them to the optimization problem object of study have been given.

A test has been designed to compare the performance of the single-stage optimization algorithms. This test used the final case study of this thesis (which takes into account the improvements made in Chapters 2, 3 and 4) and comprised:

- Two optimization cases for each algorithm in order to check their robustness.
- Ten instances to be run for each algorithm and case.

The performance of the three proposed algorithms was excellent, although there were differences among them.

- Regarding the effectiveness, the S-GA and the S-FA achieved the optimal solution in all their instances and the S-PSO achieved it in most of them (although there were some outliers that did not reach the optimum, but solutions very close to it).
- Regarding the speed of convergence of the algorithms, the S-GA was faster than the S-FA, which, in turn, was faster than the S-PSO.
- Regarding the robustness, the S-GA and the S-FA were very robust, since they presented a very similar performance in the two optimization cases designed to study the behavior of the algorithms. On the contrary, the S-PSO was less robust, as its performance was more affected by the optimization case.

In conclusion, the S-GA presented the best performance, followed by the S-FA and the S-PSO.

MULTI-STAGE OPTIMIZATION

The two algorithms with the best performance in the single-stage optimization have been selected for the multi-stage optimization problem. Consequently, the optimization algorithms proposed were the multi-stage Genetic Algorithm (M-GA) and the multi-stage Fireworks Algorithm (M-FA). A detailed explanation of each one and the implementation details required to adapt them to the optimization problem object of study have been given.

A test has been designed to compare the performance of M-GA and M-FA. This test was particularized for 2 stages ($M = 2$), also used the final case study of this thesis and comprised:

- Two optimization cases for each algorithm in order to check their robustness.
- Five instances to be run for each algorithm and case.

The comparison of both algorithms has turn out that the M-GA clearly outperformed the M-FA:

- Regarding the effectiveness, the M-GA always reached the optimal solution, while the M-FA did not reach it in all its instances. When studying what can be considered as the normal behavior of the M-FA (filtering the outliers), it has been found that this algorithm may not reach the optimum solution (although when not reaching it, the solutions provided were very close to the optimum).
- Regarding the speed of convergence of the algorithms, the M-GA was faster than the M-FA.
- Regarding the robustness, the M-GA was very robust, since it presented a very similar performance in the two optimization cases designed to study the behavior of the algorithms. On the contrary, the M-FA was less robust, as the average and median value of the fitness stabilized in different values depending on the case.

Additionally, and in order to illustrate the potential of the multi-stage formulation, this approach has been compared with what can be considered the most common approach to tackle with the optimization problem where the installation is divided into stages: the cascade single-stage optimization. The latter approach (cascade single-stage optimization) optimizes separately each stage in increasing order of stages. This way, each stage is optimized taking into account the improvements already installed in the previous stages and considering the money available for the stage, which would be the budget for the stage in addition to the money from the budget allocated to previous stages not spent (in case there is).

When comparing the results obtained with both approaches, it has been found that the multi-stage optimization clearly outperformed the cascade single-stage optimization. This is because the multi-stage optimization is able to evaluate the investment as a whole and has the information of all the stages, while the cascade single-stage

optimization cannot foresee the next stages and, therefore, optimizes the installation of each stage without taking into account the next ones.

7.1.3. METHODOLOGY PROPOSAL (CHAPTER 6)

This chapter has formalized the methodology proposed in this thesis to assess the installation of electrical infrastructure improvements. As explained, this methodology combines the use of a realistic railway simulator and the application of nature-inspired optimization algorithms. In particular, the railway simulator used incorporates the improvements of Chapters 2, 3 and 4 and the optimization algorithms are the ones designed in Chapter 5.

The steps of the methodology are:

- **Generation of the traffic space**: the traffic space represents in an accurate way the real operation of the railway line. It is composed of a big number of representative traffic scenarios so as to take into account the traffic variability and its impact on consumption. The traffic space is generated by the **operation module**.
- **Selection and compression of the traffic space:** with the aim of not making the optimization problem intractable in terms of computational burden, two procedures have been carried out:
    - A **selection procedure** has been applied to the whole set of representative traffic scenarios that compose the traffic space in order to obtain a reduced set of ***selected traffic scenarios*** that contain most of the information of the initial set.
    - A **compression procedure** has been applied to the set of ***selected traffic scenarios*** in order to reduce the number of snapshots to be solved by the **electrical network module** without compromising the accuracy of the results.
- **Electrical simulation**: it is performed by the **electrical network module**.
- **Optimization**: it is performed by the nature-inspired optimization algorithms.

The methodology has been applied to optimize the installation of RSs and ESSs in a final case study. This final case study includes the simulation of representative traffic scenarios with large and small perturbations in a complex topology, particularly a line with branches, short-turn and terminal stations.

The results obtained were very satisfactory: the increase of the energy saving associated with the installation of the improvements was always compatible with the economic profitability of the investment. Additionally, a sensitivity analysis for the ESSs optimization has been performed. In this sensitivity analysis different values for the ESSs unitary power costs have been given in order to study the influence of the installation costs on the decision-making. The results clearly showed how the installation of the infrastructure improvements varied depending on the economic factor, which means that the optimization algorithms are able to successfully combine this important factor with the main target of this thesis: increasing the energy efficiency.

The a posteriori analysis of the solutions showed that the decisions taken by the

optimization algorithms were very reasonable with respect to the configuration details (number, location and size of the improvements). Nevertheless, they were not so intuitive in an *a priori* analysis*,* which reinforces the idea defended in this thesis about the necessity of applying a comprehensive methodology, such as the one proposed, in order to provide an accurate assessment for the installation of infrastructure improvements.

7.2. CONTRIBUTIONS

The following lines will try to list the main contributions derived from this thesis, which can be grouped into two main fields: railway simulation modelling and decision support mechanisms for improving railway infrastructures.

CONTRIBUTIONS TO RAILWAY SIMULATION MODELLING

1. ***Development of a realistic model for traffic with small perturbations.***
   The proposed model uses different headways, different time shifts, realistic and stochastically modelled dwell times, different train speed profiles (including speed profiles designed according to eco-driving techniques) and a specific module of the traffic regulation system in real time that decides the speed profile to be sent to each train in each interstation. This model has been compared with the models proposed in the literature and has demonstrated that it clearly outperforms them in accuracy as well as in realism.
2. ***Development of a realistic model for traffic with large perturbations.***
   The proposed model introduces big delays in certain points of the line that produce accumulation of trains, as well as decompensations in their distribution along the line, both being characteristic of this type of operation. It also uses realistic and stochastically modelled dwell times, perturbed speed profiles and a module to decide which speed profile is to be selected for each train in each interstation depending on the degree of perturbation of the train. This is a true novelty in the literature, as traffic operation with large perturbations, although having a great impact in consumption, has not been observed before when using railway simulators to assess electrical infrastructure improvements.
3. ***Development of a topology sub-module to generate commercial timetables associated with complex topologies.***
   This topology sub-module is able to work with the following complex topologies: line with short-turn and terminal stations, line with branches and line with branches, short-turn and terminal stations (the combination of the two previous ones). This is also a true novelty in the literature, since all the previous studies only worked with simple topologies. Therefore, this sub-module allows to extend the assessment of the installation of infrastructure improvements to any type of topology.
4. ***Proposal of a new structure for detailed railway simulation models.***
   This structure includes the aforementioned developments in traffic and topology modelling and is able to generate representative traffic scenarios that, after their electrical simulation, provide accurate and realistic information about the electrical variables required for the assessment of the infrastructure improvements.

CONTRIBUTIONS TO DECISION SUPPORT MECHANISMS FOR IMPROVING RAILWAY INFRASTRUCTURES

1. ***Design, comparison and application of nature-inspired optimization algorithms to determine the optimal installation of RSs/ESSs in two approaches***
    a. Single-stage optimization: in this approach the whole installation is undertaken at a time, since the budget is available from the beginning. Three different algorithms have been designed and compared -the Genetic Algorithm, the Particle Swarm Optimization Algorithm and the Fireworks Algorithm-, selecting the best of them -the Genetic Algorithm- for the application in a final case study, where the installation of RSs and ESSs has been addressed.
    b. Multi-stage optimization: in this approach the budget is divided into stages separated in time and the installation is undertaken gradually -in stages- and complying with the budget limits of each stage. The key idea of this approach (with respect to optimizing separately each stage) is that the algorithms must take the decisions for each stage considering the installation as a whole (not separately per stages). Two different algorithms have been designed and compared -the Genetic Algorithm and the Fireworks Algorithm-, selecting the best of them -the Genetic Algorithm- for the application in a final case study, where the installation of RSs and ESSs has been addressed.
2. ***Proposal of a comprehensive methodology for designing the installation of RSs/ESSs that combines the use of detailed railway simulation models and efficient optimization algorithms.***
    This methodology has been applied for optimizing the installation of RSs and ESSs in a realistic and complex final case study, providing excellent results.

7.3. PUBLICATIONS

JCR Journals

Roch-Dupré, D., Cucala, A.P., Pecharromán, R.R., López-López, ÁJ., Fernández-Cardador, A., 2020. Simulation-based assessment of the installation of a Reversible Substation in a railway line, including a realistic model of large traffic perturbations. International Journal of Electrical Power & Energy Systems 115, 105476. DOI: https://doi.org/10.1016/j.ijepes.2019.105476. JCR: 4.418 - Q1 (2018).

Roch-Dupré, D., Cucala, A.P., R. Pecharromán, R., López-López, ÁJ., Fernández-Cardador, A., 2018. Evaluation of the impact that the traffic model used in railway electrical simulation has on the assessment of the installation of a Reversible Substation. International Journal of Electrical Power & Energy Systems 102, 201-210. DOI: https://doi.org/10.1016/j.ijepes.2018.04.030. JCR: 4.418 - Q1 (2018).

Roch-Dupré, D., López-López, ÁJ., Pecharromán, R.R., Cucala, A.P., Fernández-Cardador, A., 2017. Analysis of the demand charge in DC railway systems and reduction of its economic impact with Energy Storage Systems. International Journal of Electrical Power & Energy Systems 93, 459-467. DOI: https://doi.org/10.1016/j.ijepes.2017.06.022. JCR: 3.610 - Q1 (2017); 4.418 - Q1 (2018)

Roch-Dupré, D., Gonsalves, T., Cucala, A.P., Pecharromán, R.R., López-López, ÁJ., Fernández-Cardador, A., [*Under Review*]. Determining the optimum installation of Energy Storage Systems in railway electrical infrastructures by means of swarm and evolutionary optimization algorithms. International Journal of Electrical Power & Energy Systems.

Roch-Dupré, D., Gonsalves, T., Cucala, A.P., Pecharromán, R.R., López-López, ÁJ., Fernández-Cardador, A., [*In Process*]. Multi-stage optimization of the installation of Energy Storage Systems in railway electrical infrastructures with nature-inspired optimization algorithms.

Congress presentations

Roch-Dupré, D., López-López, ÁJ., Pecharromán, R.R., Cucala, A.P., Fernández-Cardador, A., 2017. Dimensioning DC Traction Substations with Realistic Traffic Scenarios. 2017 IEEE Vehicle Power and Propulsion Conference (VPPC 2017). Belfort, France.

Books and book chapters

Roch-Dupré, D., Gonsalves, T., 2020. Increasing energy efficiency by optimizing the electrical infrastructure of a railway line using fireworks algorithm, in Handbook of Research on Fireworks Algorithms and Swarm Intelligence, IGI Global, Hershey, PA, USA, pp. 263-282. DOI: 10.4018/978-1-7998-1659-1.ch012.

7.4. FUTURE WORK

Some research lines are proposed to continue the work presented in this thesis.

7.4.1. SINGLE AND MULTI-STAGE MULTI-OBJECTIVE OPTIMIZATION

Multi-objective optimization refers to problems where the aim is to optimize simultaneously two or more conflicting objectives. In the case of this thesis, the single and multi-stage optimization algorithms search for the optimal RSs or ESSs installations, resulting in what can be considered as a conflict between the energy saving -the higher, the better- and the installation costs -the lower, the better- (the conflict relies on the fact that higher energy saving is achieved with higher installation costs and vice-versa).

Since the optimization algorithms designed in this thesis are single-objective, the balance between the two objectives has been stablished with the fitness function, which is the Net Present Value (NPV) computed from evaluating the cash flows in the period studied (the positive cash flows being associated with the energy saving and the negative cash flows with the installation costs).

The development of multi-objective optimization algorithms would make it possible to obtain as result a Pareto front with the set of non-dominated solutions (non-dominated solutions being those that cannot be improved at the same time in energy saving and installation costs) instead of a single solution that balances both objectives. The information provided by the Pareto front would be very useful for the decision-making of railway operators because it would clearly reflect the trade-off between energy saving and installation costs.

7.4.2. MULTI-STAGE OPTIMIZATION INCLUDING UNCERTAINTY

In the multi-stage optimization developed in this thesis the energy prices and installation costs are given for all the stages, as well as the hours of operation at each headway. Nevertheless, in real world there is uncertainty with respect to these variables. On the one hand, energy prices and installation costs can increase or decrease depending, among others, on environmental conditions, development in the storage and power electronics technologies, etc. On the other hand, the distribution of the hours of operation with each headway can vary depending on mobility policies, population behaviour…, etc.

Therefore, it is very interesting to apply a multi-stage optimization with a stochasticity component associated with possible variations in any of the following variables:

- Energy price.
- RSs/ESSs installation costs.
- Distribution of hours of operation with each headway and also with the different types of traffic perturbations (if the number of peak hours increase, it is very likely that the number of hours of operation with large perturbations also increase).

In order to tackle with this problem it would be necessary to develop a scenario tree, where each scenario from any stage different from the initial one has different values for the variables previously presented and an associated probability.

Once having defined the scenario tree, it is only necessary to change the fitness function. Maintaining the NPV to evaluate the fitness, different fitness functions can be designed, each one with a different criterion to face the uncertainty. If the reliability on the probability figures of the scenario tree is high, the most popular criteria is the "Expected Value Criteria", which selects the alternative with the highest mean benefit (NPV in this case). If the reliability on the probability figures of the scenario tree is low, it is also possible to use criteria that ignore the probabilities, such as the "Savage Criteria", which takes into account the opportunity cost/penalty for not correctly anticipating the state of nature and selects the alternative with the lowest penalty.

As an example, Equation (7-1) provides the formulation of the fitness function provided that the Expected Value Criteria is used.

$$\overline{NPV(\overline{ind_i})} = \sum_{x=1}^{N_{scen}} prob(x) \cdot NPV(p_{\mathrm{i}})^x \quad \textbf{(7-1)}$$

where:

- $\overline{NPV(\overline{ind_i})}$ is the mean NPV associated with individual $\overline{ind_i}$. This is the value that must be maximized.
- $prob(x)$ is the probability of scenario x to happen.
- N_{scen} is the total number of scenarios.
- $NPV(p_{\mathrm{i}})^x$ is the NPV associated with scenario x. The NPV in each scenario is different because:
    - The energy saving can be different due to the changes in the distribution of hours of operation with each headway.
    - The energy price can be different.
    - The installation cost can be different.

7.4.3. APPLICATION OF ARTIFICIAL INTELLIGENCE TECHNIQUES TO SPEED UP THE OPTIMIZATION PROCESS

Despite the selection and compression procedures explained in Section 6.1.2, the high computational burden of the electrical simulations make each algorithm iteration last, on average, 40 minutes × the number of stages of the optimization. Although the simulation time scale is affordable (it must be taken into account that these studies are off-line), it would be very interesting to explore the use of neural networks for different purposes related with the reduction of the simulation-time.

In a first approach, neural networks can solve a classification problem, which would help to reduce the search space of the subsequent optimization. Different groups can be

created according to their fitness value (e.g.: four groups, each one corresponding to one fitness quartile) and, after a first training stage with a big enough set of configurations with known fitness, the neural network can start classifying new configurations (not previously simulated) in order to find those corresponding to the group with the best fitness. Once having defined the main characteristics shared by the configurations corresponding to this group (e.g ranges of total power installed, total number of installations, etc.), the optimization could be performed observing only the search space associated with these characteristics.

In the next step, the regression problem can be tackled. After a first training stage (where the input is the fitness of a set of configurations previously simulated), the neural networks can try to predict (instead of classifying into groups) the NPV of the solutions.

7.4.4. FURTHER STUDIES OF THE TRAFFIC SPACE

As explained in Section 6.1.1, the traffic variability of each scenario has two main sources: **changes in the time shift** and **randomness associated with dwell times.** The operation module proposed for the traffic simulation takes into account both sources and the final case study presented in this thesis simulated a very big amount of traffic scenarios, each one with a different time shift and with noise in the dwell time.

In order to improve the characterization of the traffic space (and maybe to reduce its size), it is very interesting to determine a methodology to:

- Analyze in detail the influence of these two sources of traffic variability and the relationship between them (which, in turn, can vary depending on the topology or the operation characteristics).
- Determine the number of time shifts to be selected, as well as the number of traffic scenarios with different dwell times to be simulated with each time shift.

This may allow to obtain the smallest possible traffic space.

APPENDIX 1

RS CONSTANT VOLTAGE CONTROL IMPLEMENTATION

This appendix gives the details about the equations that must be included in the Jacobian matrix of the N-R used by the load flow solver in order to implement the constant voltage control method that defines the behavior of the RS when it is in the inversion mode. These equations have been obtained from (Tzeng et al., 1998).

The aforementioned paper states than when a constant voltage controlled RS, connected between AC bus p and DC bus t (see Figure APP 1-1), activates its inversion mode:

1) The bus power mismatch (BPM) equation associated must be modified according to Equation APP 1-1.
2) A set of independent residual equations (Equations (APP 1-2), (APP 1-3) and (APP 1-4), which constraint the converter terminal behaviors, must be added into the Jacobian matrix of the N-R to solve the converter variables γ, β and I_{dI}.

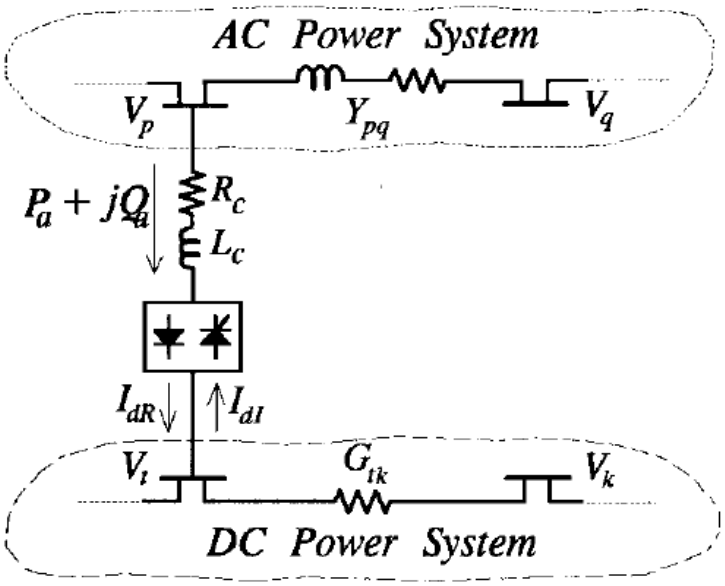

Figure APP 1-1: RS connection (Tzeng et al., 1998)

$$\Delta P_p + j\Delta Q_p = P_p^{spec} + jQ_p^{spec} - V_p\left(\sum_{q=1}^{Nac} Y_{p,q}\cdot V_q\right)^* - P_{aI} + jQ_{aI} \qquad \textbf{(APP 1-1)}$$

$$R_{I1} = V_t - \frac{n_{IR}\cdot|V_p|}{2}\cdot[\cos\gamma + \cos\beta] - \frac{\pi^2}{18}\cdot\left[2 - \frac{3(\beta-\gamma)}{2\pi}\right]\cdot R_c\cdot I_{dI} \qquad \textbf{(APP 1-2)}$$

$$R_{I2} = I_{dI} - \frac{6\,n_{IR}V_p\cos\xi}{\pi\cdot X_c\cdot[1+e^{-\lambda(\beta-\gamma)}]}\cdot\left[\cos(\xi-\gamma) - e^{-\lambda(\beta-\gamma)}\cos(\xi-\beta)\right] \qquad \textbf{(APP 1-3)}$$

$$R_{I3} = \left(\sum_{k=1}^{Ndc} G_{t,k}\cdot V_k\right) + I_{dI} \qquad \textbf{(APP 1-4)}$$

where:

- $G_{t,k}$ is the mutual conductance between DC buses t and k.
- I_{dI} is the inverter DC current.
- $\Delta P_p, \Delta Q_p$ are the increments in active and reactive power in AC bus p.
- P_p^{spec}, Q_p^{spec} are the specified active and reactive power of AC bus p (this bus must be a **load** bus).
- P_{aI}, Q_{aI} are the inverter-consumed rms fundamental active and reactive power.
- $R_{In^{\underline{o}}}$ is the residual equation $n^{\underline{o}}$.
- R_c is the commutation resistance.
- V_x is the voltage in AC or DC node x.

- X_c is the commutation reactance.
- $Y_{p,q}$ is the mutual admittance between AC buses p and q.
- γ is the inverter extinction angle.
- β is the inverter advance angle.
- $\lambda = {R_c}/{X_c}$
- $\xi = \tan^{-1}\gamma$
- n_{IR} is the turns ratio of the inverter transformer secondary winding to the rectifier transformer secondary winding. The value can be obtained from Equation (APP1-5).

$$n_{IR} = \frac{1}{|V_a| \cdot \cos\gamma} \cdot \left(V_{dI} + \frac{\pi}{6} \cdot X_c \cdot I_{dI}\right) \quad \textbf{(APP 1-5)}$$

where:

  - $|V_a|$ is the rectifier transformer secondary rms line voltage.
  - V_{dI} is the inverter DC average output voltage.

Once the BPM and residual equations are specified and added to the Jacobian matrix, the power flow of the transit system at each snapshot can be solved iteratively using a unified N–R, such as the proposed in (Tzeng & Wu, 1995).

APPENDIX 2

APPROXIMATION OF THE ESS CONTROL CURVE WITH SIGMOID FUNCTIONS

This appendix give the details of the procedure followed to approximate the ESS control curve as a sum of sigmoid function and analyzes its impact on the convergence of the load flow.

As stated in Section 6.2.1, having a piecewise linear function defining the ESS current forces to have different expressions for $\frac{\partial P_{DC}}{\partial V_{DC}} \cdot V_{DC}$ in the DC power nodes of the Jacobian matrix associated with the ESSs. Concretely there are five different expressions depending on the voltage values, as showed in Equation (APP 2-1).

$$\left[\frac{\partial P_{DC}}{\partial V_{DC}} \cdot V_{DC}\right]_{ESS\ power\ node} = \frac{\partial P_{ESS}}{\partial V_{ESS}} \cdot V_{ESS} =$$

$$\begin{cases} \frac{\partial (V_{ESS} \cdot I_{MIN})}{\partial V_{ESS}} \cdot V_{ESS} = V_{ESS} \cdot I_{MIN}\ , & if\ V_{alm} < V_{1\,MIN} \\ \frac{\partial \left(V_{ESS} \cdot \frac{I_{MIN}}{V_{1\,MIN} - V_1} \cdot (V_{ESS} - V_1) \right)}{\partial V_{ESS}} \cdot V_{ESS} = \frac{I_{MIN}}{V_{1\,MIN} - V_1} \cdot (2 \cdot {V_{ESS}}^2 - V_{ESS} \cdot V_1), & if\ V_{alm} \in (V_{1\,MIN}, V_1) \\ 0, & if\ V_{alm} \in (V_1, V_2) \\ \frac{\partial \left(V_{ESS} \cdot \frac{I_{MAX}}{V_{2\,MAX} - V_2} \cdot (V_{ESS} - V_2) \right)}{\partial V_{ESS}} \cdot V_{ESS} = \frac{I_{MAX}}{V_{2\,MAX} - V_2} \cdot (2 \cdot {V_{ESS}}^2 - V_{ESS} \cdot V_2), & if\ V_{alm} \in (V_2, V_{2\,MAX}) \\ \frac{\partial (V_{ESS} \cdot I_{MAX})}{\partial V_{ESS}} \cdot V_{ESS} = V_{ESS} \cdot I_{MAX}\ , & if\ V_{alm} > V_{2\,MAX} \end{cases} \quad \textbf{(APP 2-1)}$$

where P_{ESS} is the ESS power demand and V_{ESS} is the ESS voltage (the rest of the terms are defined in Section 6.2.1, where the ESS control curve is explained).

The abrupt changes in slope between the different sections may shoot up the number of iterations required to achieve the convergence of the load flow when the ESS voltage is close to any of the corners, as the voltage can start switching from one section to the other without stabilizing its value.

In order to avoid problems in the convergence of the load flow, the ESS control curve must become continuous derivable throughout the whole voltage domain ($[V_{MIN} - V_{RHE}]$), for which it is going to be approximated as a sum of sigmoid functions. Concretely, the approximation has been made by superimposing three different sigmoid. The new expression for $\frac{\partial P_{ESS}}{\partial V_{ESS}} \cdot V_{ESS}$ is given in Equation (APP 2-2).

$$\frac{\partial P_{ESS}}{\partial V_{ESS}} \cdot V_{ESS} = \frac{\partial \left(V_{ESS} \cdot I(V_{ESS}) \right)}{\partial V_{ESS}} \cdot V_{ESS} = V_{ESS} \cdot I(V_{ESS}) + {V_{ESS}}^2 \cdot \frac{\partial I(V_{ESS})}{\partial V_{ESS}} \quad \textbf{(APP 2-2)}$$

where:

- $I(V_{ESS})$ is the ESS control curve approximated with the sigmoid functions, represented by Equation (APP 2-3).

$$I(V_{ESS}) = \sum_{i=1}^{i=3} a_i + \frac{b_i - a_i}{1 + 10^{(c_i - V_{ESS}) \cdot d_i}} \quad \textbf{(APP 2-3)}$$

  where a_i, b_i, c_i, d_i are the four parameters of sigmoid function i (it must be noted that the parameters of the three sigmoid functions have been adjusted with the function sigm_fit (MATLAB Central File Exchange, 2016)).

- $\frac{\partial I(V_{ESS})}{\partial V_{ESS}}$ is the first derivative of the ESS control curve approximated with the sigmoid functions. As shown in Equation (APP 2-4), it is continuous derivable throughout the whole voltage domain.

$$\frac{\partial\, I(V_{ESS})}{\partial\, V_{ESS}} = \sum_{i=1}^{i=3} \frac{(b_i - a_i)\cdot d_i \cdot \ln(10) \cdot 10^{(c_i - V_{ESS})\cdot d_i}}{(1+10^{(c_i - V_{ESS})\cdot d_i})^2} \qquad \textbf{(APP 2-4)}$$

The first subplot of Figure APP 2-1 depicts the original piecewise linear ESS control curve together with the ESS control curve approximated with the sigmoid functions, while the second subplot depicts the first derivative of the ESS control curve approximated with the sigmoid functions.

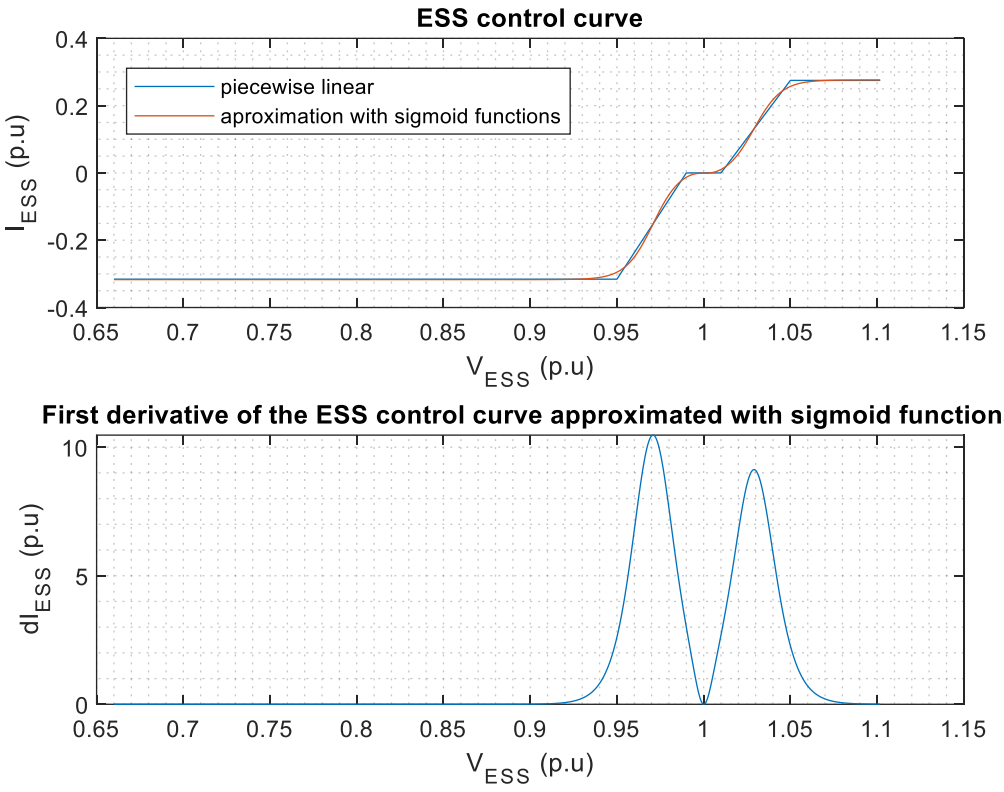

Figure APP 2-1: Results from the approximation of the ESS control curve with sigmoid functions

Achieving a continuous derivable ESS control curve in the whole voltage domain and, consequently, having a unique expression for the terms of the Jacobian matrix corresponding to $\frac{\partial\, P_{ESS}}{\partial\, V_{ESS}} \cdot V_{ESS}$ has had a positive impact on the resolution of the load flow problem, yielding a considerable reduction in the number of iterations required to achieve convergence, especially in those snapshots that had problems with the piecewise linear curve.

With the aim of quantifying the impact of this improvement, a set of 288 different ESS configurations have been simulated with the two ESS control curves: the piecewise linear one and the one approximated with sigmoid functions. Results have shown that the total simulation time has been reduced in more than 74% with the latter. Additionally, Figure APP 2-2 shows the boxplots with the distribution of the simulation times obtained with both control curves. For the sake of clarity, results have been

normalized with respect to the median of the simulation times obtained with the piecewise linear ESS control curve.

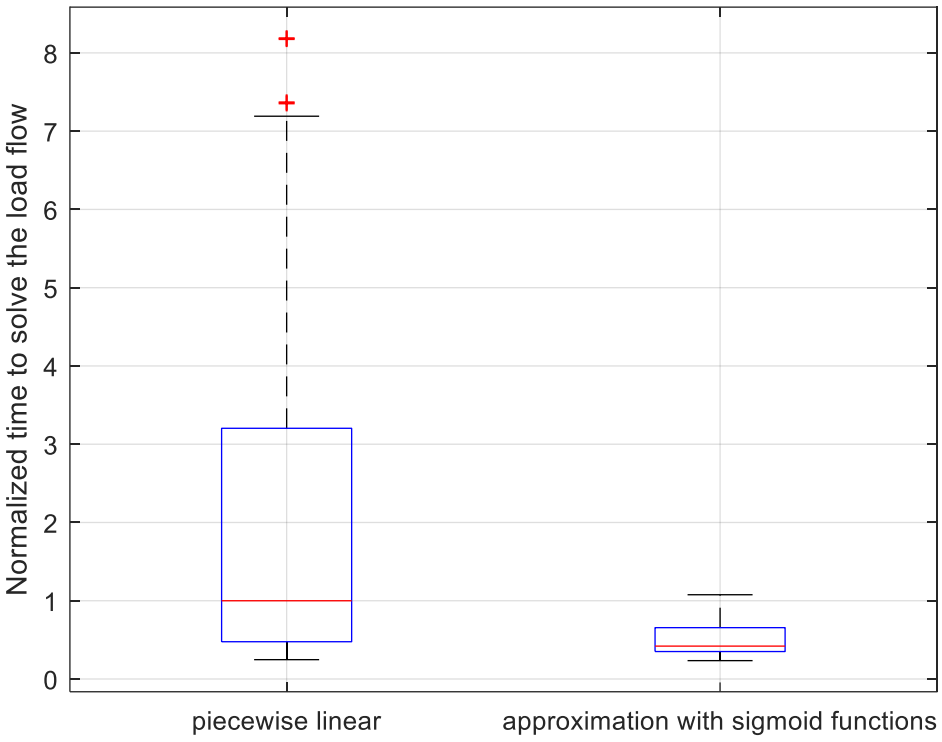

Figure APP 2-2: Distribution of the simulation times with both ESS control curves

References

Abrahamsson, L., Kjellqvist, T., Östlund, S., 2012. High-voltage DC-feeder solution for electric railways. IET Power Electronics 5(9), 1776-1784.

Albrecht, T., 2004. Reducing power peaks and energy consumption in rail transit systems by simultaneous train running time control. Computers in railways IX, 885-894.

Alnuman, H., Gladwin, D., Foster, M., 2018. Electrical Modelling of a DC Railway System with Multiple Trains. Energies 11(11), 3211.

Arboleya, P., Bidaguren, P., Armendariz, U., 2016. Energy Is On Board: Energy Storage and Other Alternatives in Modern Light Railways. IEEE Electrification Magazine 4(3), 30-41.

Arboleya, P., Coto, M., González-Morán, C., Arregui, R., 2014. On board accumulator model for power flow studies in DC traction networks. Electric Power Systems Research 116, 266-275.

Arboleya, P., Diaz, G., Coto, M., 2012. Unified AC/DC Power Flow for Traction Systems: A New Concept. IEEE Transactions on Vehicular Technology 61(6), 2421-2430.

Arboleya, P., Mohamed, B., El-Sayed, I., 2020. Off-board and on-board energy storage versus reversible substations in DC railway traction systems. IET Electrical Systems in Transportation 10(2), 185-195.

Arboleya, P., Mohamed, B., El-Sayed, I., 2018. DC Railway Simulation Including Controllable Power Electronic and Energy Storage Devices. IEEE Transactions on Power Systems 33(5), 5319-5329.

Bae, C.H., 2009. A simulation study of installation locations and capacity of regenerative absorption inverters in DC 1500 V electric railways system. Simulation Modelling Practice and Theory 17(5), 829-838.

Barrero, R., Mierlo, J., Tackoen, X., 2008. Energy savings in public transport. IEEE Vehicular Technology Magazine 3(3), 26-36.

Barrero, R., Tackoen, X., Van Mierlo, J., 2008. Improving energy efficiency in public transport: stationary supercapacitor based energy storage systems for a metro network. 2008 IEEE Vehicle Power and Propulsion Conference (VPPC), Harbin, China, 3/5 September, pp. 1-8.

Battistelli, L., Ciccarelli, F., Lauria, D., Proto, D., 2009. Optimal design of DC electrified railway stationary storage system. International Conference on Clean Electrical Power (ICCEP), Capri, Italy, 9-11 June, pp. 739-745.

Beusen, B., Degraeuwe, B., Debeuf, P., 2013. Energy savings in light rail through the optimization of heating and ventilation. Transportation Research Part D: Transport and Environment 23, 50-54. DOI: https://doi.org/10.1016/j.trd.2013.03.005.

Binitha, S., Sathya, S.S., 2012. A survey of bio inspired optimization algorithms. International journal of soft computing and engineering 2(2), 137-151.

Bocharnikov, Y.V., Tobias, A.M., Roberts, C., Hillmansen, S., Goodman, C.J., 2007. Optimal driving strategy for traction energy saving on DC suburban railways. IET Electric Power Applications 1(5), 675-682.

Boizumeau, J., Leguay, P., Navarro, E., 2011. Braking energy recovery at the Rennes metro. Workshop on Braking Energy Recovery Systems–Ticket to Kyoto Project.

Buckingham, E., 1988. Analytical Mechanics of Gears. Courier Corporation.

Cai, Y., Irving, M.R., Case, S.H., 1995. Iterative techniques for the solution of complex DC-rail-traction systems including regenerative braking. IEE Proceedings-Generation, Transmission and Distribution 142(5), 445-452.

Calderaro, V., Galdi, V., Graber, G., Piccolo, A., 2015. Optimal siting and sizing of stationary supercapacitors in a metro network using PSO. Industrial Technology (ICIT), 2015 IEEE International Conference On, pp. 2680-2685.

Chen, J.F., Lin, R.L., Liu, Y.C., 2005. Optimization of an MRT train schedule: reducing maximum traction power by using genetic algorithms. IEEE Transactions on Power Systems 20(3), 1366-1372.

Chuang, H.J., 2005. Optimisation of inverter placement for mass rapid transit systems by immune algorithm. IEE Proceedings - Electric Power Applications 152(1), 61-71.

Chymera, M., Renfrew, A.C., Barnes, M., 2006. Analysis of Power Quality in a DC Tram System. The 3rd IET International Conference on Power Electronics, Machines and Drives, 2006., pp. 96-100.

Chymera, M.Z., Renfrew, A.C., Barnes, M., Holden, J., 2010. Modeling Electrified Transit Systems. IEEE Transactions on Vehicular Technology 59(6), 2748-2756.

Ciccarelli, F., Iannuzzi, D., Tricoli, P., 2012. Control of metro-trains equipped with onboard supercapacitors for energy saving and reduction of power peak demand. Transportation Research, Part C: Emerging Technologies 24, 36-49.

Cornic, D., 2010. Efficient recovery of braking energy through a reversible dc substation. Electrical Systems for Aircraft, Railway and Ship Propulsion (ESARS), pp. 1-9.

de la Torre, S., Sánchez-Racero, A.J., Aguado, J.A., Reyes, M., Martínez, O., 2015. Optimal Sizing of Energy Storage for Regenerative Braking in Electric Railway Systems. IEEE Transactions on Power Systems 30(3), 1492-1500.

Domínguez, M., Cucala, A., Fernández, A., Pecharromán, R., Blanquer, J., 2011. Energy efficiency on train control: design of metro ATO driving and impact of energy accumulation devices. 9 Th World Congress on Railway Research (22.05–26.05. 2011). Madrid, pp. 1-12.

Domínguez, M., Fernández-Cardador, A., Cucala, A.P., Lukaszewicz, P., 2011. Optimal design of metro automatic train operation speed profiles for reducing energy consumption. Proceedings of the Institution of Mechanical Engineers, Part F (Journal of Rail and Rapid Transit) 225, 463-473.

Domínguez, M., Fernández-Cardador, A., Cucala, A.P., Gonsalves, T., Fernández-Rodríguez, A., 2014. Multi objective particle swarm optimization algorithm for the design of efficient ATO speed profiles in metro lines. Engineering Applications of Artificial Intelligence 29, 43-53.

Domínguez, M., Fernandez-Cardador, A., Cucala, A.P., Pecharroman, R.R., 2012. Energy Savings in Metropolitan Railway Substations Through Regenerative Energy

Recovery and Optimal Design of ATO Speed Profiles. IEEE Transactions on Automation Science and Engineering 9(3), 496-504.

Douglas, H., Roberts, C., Hillmansen, S., 2016. Optimising energy saving in metro systems through characteristic evaluation. The International Conference on Railway Engineering (ICRE) 2016, 1-9.

Douglas, H., Roberts, C., Hillmansen, S., Schmid, F., 2015. An assessment of available measures to reduce traction energy use in railway networks. Energy Conversion and Management 106, 1149-1165. DOI: https://doi.org/10.1016/j.enconman.2015.10.053.

Episcopal Church, Evangelical Lutheran Church in America, Church of Sweden, 2019. A Call to Join in the Care of Creation.

Ertenlice, O., Kalayci, C.B., 2018. A survey of swarm intelligence for portfolio optimization: Algorithms and applications. Swarm and Evolutionary Computation 39, 36-52. DOI: https://doi.org/10.1016/j.swevo.2018.01.009.

Falvo, M.C., Lamedica, R., Bartoni, R., Maranzano, G., 2011. Energy management in metro-transit systems: An innovative proposal toward an integrated and sustainable urban mobility system including plug-in electric vehicles. Electric Power Systems Research 81(12), 2127-2138.

Falvo, M.C., Sbordone, D., Fernández-Cardador, A., Cucala, A.P., Pecharromán, R.R., López-López, A., 2014. Energy savings in metro-transit systems: A comparison between operational Italian and Spanish lines. Proceedings of the Institution of Mechanical Engineers, Part F: Journal of Rail and Rapid Transit 230(2), 345-359.

Fazel, S.S., Firouzian, S., Shandiz, B.B., 2014. Energy-Efficient Emplacement of Reversible DC Traction Power Substations in Urban Rail Transport through Regenerative Energy Recovery. International Journal of Railway Research 1(2), 11-22.

Fernández-Cardador, A., Cucala, A.P., Vitoriano, B., de Cuadra, F., 2006. Predictive traffic regulation for metro loop lines based on quadratic programming. Proceedings of the Institution of Mechanical Engineers, Part F: Journal of Rail and Rapid Transit 220(2), 79-89.

Fernández-Rodríguez, A., 2018. Train eco-driving optimisation based on simulation models. PhD thesis. Comillas Pontifical University. Madrid, Spain.

Fernández-Rodríguez, A., Fernández-Cardador, A., Cucala, A.P., Domínguez, M., Gonsalves, T., 2015. Design of Robust and Energy-Efficient ATO Speed Profiles of Metropolitan Lines Considering Train Load Variations and Delays. Intelligent Transportation Systems, IEEE Transactions on PP(99), 1-11.

Fernández-Rodríguez, A., Fernández-Cardador, A., Cucala, A.P., 2018. Balancing energy consumption and risk of delay in high speed trains: A three-objective real-time eco-

driving algorithm with fuzzy parameters. Transportation Research Part C: Emerging Technologies 95, 652-678. DOI: https://doi.org/10.1016/j.trc.2018.08.009.

Gao, Z., Fang, J., Zhang, Y., Jiang, L., Sun, D., Guo, W., 2015. Control of urban rail transit equipped with ground-based supercapacitor for energy saving and reduction of power peak demand. International Journal of Electrical Power & Energy Systems 67, 439-447.

Gelman, V., 2013. Energy Storage That May Be Too Good to Be True: Comparison Between Wayside Storage and Reversible Thyristor Controlled Rectifiers for Heavy Rail. Vehicular Technology Magazine, IEEE 8(4), 70-80.

Glover, F.W., Kochenberger, G.A., 2006. Handbook of Metaheuristics. Springer Science & Business Media.

Goldberg, D.E., Holland, J.H., 1988. Genetic algorithms and machine learning. Machine Learning 3(2), 95-99.

Gong, C., Zhang, S., Zhang, F., Jiang, J., Wang, X., 2014. An integrated energy-efficient operation methodology for Metro systems based on a real case of Shanghai Metro line one. Energies 7(11), 7305-7329.

Gonsalves, T., 2017. Artificial Intelligence: A Non-Technical Introduction . Sophia University Press.

González-Gil, A., Palacin, R., Batty, P., Powell, J.P., 2014. A systems approach to reduce urban rail energy consumption. Energy Conversion and Management 80, 509-524.

González-Gil, A., Palacin, R., Batty, P., 2013. Sustainable urban rail systems: Strategies and technologies for optimal management of regenerative braking energy. Energy Conversion and Management 75, 374-388.

Goodman, C.J., Chymera, M., 2013. Modelling and simulation. Railway Electrification Infrastructure and Systems (REIS 2013), 6th IET Professional Development Course On, pp. 16-25.

Goodman, C.J., Siu, L.K., Ho, T.K., 1998. A review of simulation models for railway systems. International Conference on Developments in Mass Transit Systems, London, UK, 20-23 April, pp. 80-85.

Gunselmann, W., 2005. Technologies for increased energy efficiency in railway systems. 2005 IEEE 11th European Conference on Power Electronics and Applications, Dresden, Germany, 11-14 September, pp. 1-10.

He, L., Li, W., Zhang, Y., Cao, Y., 2019. A discrete multi-objective fireworks algorithm for flowshop scheduling with sequence-dependent setup times. Swarm and Evolutionary Computation, 100575. DOI: https://doi.org/10.1016/j.swevo.2019.100575.

Holguín-Veras, J., Amaya Leal, J., Sánchez-Diaz, I., Browne, M., Wojtowicz, J., 2018a. State of the art and practice of urban freight management Part II: Financial approaches, logistics, and demand management. Transportation Research Part A: Policy and Practice. DOI: https://doi.org/10.1016/j.tra.2018.10.036.

Holguín-Veras, J., Amaya Leal, J., Sánchez-Diaz, I., Browne, M., Wojtowicz, J., 2018b. State of the art and practice of urban freight management: Part I: Infrastructure, vehicle-related, and traffic operations. Transportation Research Part A: Policy and Practice. DOI: https://doi.org/10.1016/j.tra.2018.10.037.

Holman, C., Harrison, R., Querol, X., 2015. Review of the efficacy of low emission zones to improve urban air quality in European cities. Atmospheric Environment 111, 161-169. DOI: https://doi.org/10.1016/j.atmosenv.2015.04.009.

Huang, H., Fu, D., Qi, W., 2017. Effect of driving restrictions on air quality in Lanzhou, China: Analysis integrated with internet data source. Journal of Cleaner Production 142, 1013-1020. DOI: https://doi.org/10.1016/j.jclepro.2016.09.082.

Hui-Jen, C., Chao-Shun, C., Chia-Hun, L., Shi-Hong, C., 2005. Optimization of inverter placement for mass rapid transit systems using genetic algorithm. , Dalian, 01/01, pp. 1-6.

Ianuzzi, D., Ciccarelli, F., Lauria, D., 2012. Stationary ultracapacitors storage device for improving energy saving and voltage profile of light transportation networks. Transportation Research, Part C: Emerging Technologies 21, 321-337.

Ibaiondo, H., Romo, A., 2010. Kinetic energy recovery on railway systems with feedback to the grid. Power Electronics and Motion Control Conference (EPE/PEMC), 2010 14th International, pp. T9-94-T9-97.

Ichikawa, S., Miyatake, M., 2019. Energy Efficient Train Trajectory in the Railway System with Moving Block Signaling Scheme. IEEJ Journal of Industry Applications 8(4), 586-591.

IPCC, 2018. Global warming of 1.5°C. An IPCC Special Report on the impacts of global warming of 1.5°C above pre-industrial levels and related global greenhouse gas emission pathways, in the context of strengthening the global response to the threat of climate change, sustainable development, and efforts to eradicate poverty.

IPCC, 2015. Climate Change 2014: Mitigation of Climate Change: Working Group III Contribution to the IPCC Fifth Assessment Report. Cambridge University Press, Cambridge.

IPCC, 2014. *Climate Change 2014: Synthesis Report. Contribution of Working Groups I, II and III to the Fifth Assessment Report of the Intergovernmental Panel on Climate Change* [Core Writing Team, R.K. Pachauri and L.A. Meyer (eds.)].

Ise, T., Kita, M., Taguchi, A., 2005. A hybrid energy storage with a SMES and secondary battery. Applied Superconductivity, IEEE Transactions on 15(2), 1915-1918.

J. Xin, G. Chen, Y. Hai, 2009. A Particle Swarm Optimizer with Multi-stage Linearly-Decreasing Inertia Weight. 2009 International Joint Conference on Computational Sciences and Optimization 1, 505-508.

Jefimowski, W., Szeląg, A., 2018. The multi-criteria optimization method for implementation of a regenerative inverter in a 3kV DC traction system. Electric Power Systems Research 161, 61-73. DOI: https://doi.org/10.1016/j.epsr.2018.03.023.

Kennedy, J., Eberhart, R.C., 1995. Particle swarm optimization. Neural Networks, 1995. Proceedings., IEEE International Conference On, pp. 1942-1948 vol.4.

Kondo, K., 2010. Recent Energy Saving Technologies on Railway Traction Systems. IEEJ Transactions on Electrical and Electronic Engineering 5(3), 298-303.

Kondo, M., Miyabe, M., Manabe, S., 2014. Development of a High Efficiency Induction Motor and the Estimation of Energy Conservation Effect. Quarterly Report of RTRI 55(3), 138-143.

Konishi, T., Morimoto, H., Aihara, T., Tsutakawa, M., 2010. Fixed Energy Storage Technology Applied for DC Electrified Railway. IEEJ Transactions on Electrical and Electronic Engineering 5(3), 270-277.

Lee, H.M., Oh, S.C., Lee, C.M., Kim, G.D., 2008. Factory test for development of energy storage system. International Conference on Control, Automation and Systems (ICCAS), Seoul, South Korea, 14-17 October, pp. 1495-1498.

Lee, H., Jung, S., Cho, Y., Yoon, D., Jang, G., 2013. Peak power reduction and energy efficiency improvement with the superconducting flywheel energy storage in electric railway system. Physica C: Superconductivity 494(0), 246-249.

Long, Q., Wu, C., Huang, T., Wang, X., 2015. A genetic algorithm for unconstrained multi-objective optimization. Swarm and Evolutionary Computation 22, 1-14. DOI: https://doi.org/10.1016/j.swevo.2015.01.002.

López-López, ÁJ., Abrahamsson, L., Pecharromán, R.R., Fernández-Cardador, A., Cucala, A.P., Östlund, S., et al, 2014. A variable no-load voltage scheme for improving energy efficiency in DC- electrified mass transit systems. ASME-IEEE Joint Rail Conference (JRC), Colorado Springs, Colorado, USA, April 2–4, pp. 1-7.

López-López, ÁJ., Pecharromán, R.R., Pilo de la Fuente, E., Cucala, A.P., Fernández-Cardador, A., 2011. Analysis of energy-saving strategies in railway power supply systems. 9th World Congress on Railway Research - WCRR 2011, Lille, France, May 22-26, pp. 1-10.

López-López, ÁJ., 2016. Optimising the electrical infrastructure of mass transit systems to improve the use of regenerative braking. PhD thesis. Comillas Pontifical University. Madrid, Spain.

López-López, ÁJ., Pecharromán, R.R., Fernández-Cardador, A., Cucala, A.P., 2017a. Improving the Traffic Model to Be Used in the Optimisation of Mass Transit System Electrical Infrastructure. Energies 10(8), 1134.

López-López, ÁJ., Pecharromán, R.R., Fernández-Cardador, A., Cucala, A.P., 2017b. Smart traffic-scenario compressor for the efficient electrical simulation of mass transit systems. International Journal of Electrical Power & Energy Systems 88, 150-163.

López-López, ÁJ., Pecharromán, R.R., Fernández-Cardador, A., Cucala, A.P., 2014. Assessment of energy-saving techniques in direct-current-electrified mass transit systems. Transportation Research Part C: Emerging Technologies 38, 85-100.

Lukaszewicz, P., 2001. Energy Consumption and Running Time for Trains. PhD thesis. Royal Institute of Technology. Stockholm, Sweden.

Lynn, N., Suganthan, P.N., 2015. Heterogeneous comprehensive learning particle swarm optimization with enhanced exploration and exploitation. Swarm and Evolutionary Computation 24, 11-24. DOI: https://doi.org/10.1016/j.swevo.2015.05.002.

M. Khodaparastan, O. Dutta, M. Saleh, A. A. Mohamed, 2019. Modeling and Simulation of DC Electric Rail Transit Systems With Wayside Energy Storage. IEEE Transactions on Vehicular Technology 68(3), 2218-2228.

Martin, P., 2010. Train performance & simulation. Electric Traction Systems, 2010 IET Professional Development Course On, pp. 191-206.

Martin, P., 1997. The development of an object-oriented, discrete-event simulation language using Java. Software Engineering Conference, 1997. Asia Pacific ... and International Computer Science Conference 1997. APSEC '97 and ICSC '97. Proceedings, pp. 123-130.

Martínez, I., Vitoriano, B., Fernandez-Cardador, A., Cucala, A.P., 2007. Statistical dwell time model for metro lines. WIT Transactions on The Built Environment 96, 1-10.

MATLAB Central File Exchange, 2016. sigm_fit. 2020(01/28).

Matsuoka, K., Kondo, M., 2010. Energy Saving Technologies for Railway Traction Motors. IEEJ Transactions on Electrical and Electronic Engineering 5(3), 278-284.

Mavrovouniotis, M., Li, C., Yang, S., 2017. A survey of swarm intelligence for dynamic optimization: Algorithms and applications. Swarm and Evolutionary Computation 33, 1-17. DOI: https://doi.org/10.1016/j.swevo.2016.12.005.

Mellitt, B., Mouneimne, Z., Goodman, C., 1984. Simulation study of DC transit systems with inverting substations. IEE Proceedings B - Electric Power Applications 131(2), 38-50.

Mellitt, B., Goodman, C.J., Arthurton, R.I.M., 1978. Simulator for studying operational and power-supply conditions in rapid-transit railways. Proceedings of the Institution of Electrical Engineers 125(4), 298-303.

Miyatake, M., 2011. A Simple Mathematical Model for Energy-saving Train Scheduling. IEEJ Transactions on Industry Applications 131(6), 860-861.

Miyatake, M., Haga, H., Suzuki, S., 2009. Optimal speed control of a train with On-board energy storage for minimum energy consumption in catenary free operation. 13th European Conference on Power Electronics and Applications (EPE '09), Barcelona, 8-10 September, pp. 1-9.

Miyatake, M., Ko, H., 2010. Optimization of Train Speed Profile for Minimum Energy Consumption. IEEJ Transactions on Electrical and Electronic Engineering 5(3), 263-269.

Nasri, A., Moghadam, M.F., Mokhtari, H., 2010. Timetable optimization for maximum usage of regenerative energy of braking in electrical railway systems. International Symposium on Power Electronics Electrical Drives Automation and Motion (SPEEDAM), 14-16 June, pp. 1218-1221.

National Religious Coalition on Creation Care, 2019. Religious Declaration of Unprecedented Human Emergency.

Nomura, K., Miyatake, M., 2016. Scheduling method for minimum energy consumption considering constraints of time intervals between local and express trains. 2016 IEEE International Conference on Intelligent Rail Transportation (ICIRT), 469-475.

Oettich, S., Albrecht, T., Scholz, S., 2004. Improvements of energy efficiency of urban rapid rail systems. Publication of: WIT Press.

Pena-Alcaraz, M., Fernández-Cardador, A., Cucala, A.P., Ramos, A., Pecharromán, R.R., 2012. Optimal underground timetable design based on power flow for maximizing the use of regenerative-braking energy. Proceedings of the Institution of Mechanical Engineers, Part F: Journal of Rail and Rapid Transit 226(4), 397-408.

Pereira, F.H., Pires, C.L., Nabeta, S.I., 2014. Optimal placement of rectifier substations on DC traction systems. IET Electrical Systems in Transportation 4(3), 62-69.

Pilo, E., Rouco, L., Fernandez, A., Burleson, D.P., Cackovic, D., 2003. A reduced representation of 2x25 kV electrical systems for high-speed railways. Proceedings of the 2003 IEEE/ASME Joint Rail Conference (Cat. no.03CH37424), 01/01, pp. 199-205.

Pilo, E., Rouco, L., Fernandez, A., Hernandez-Velilla, A., 2000. A simulation tool for the design of the electrical supply system of high-speed railway lines. 2000 Power Engineering Society Summer Meeting (Cat. no.00CH37134), 16-20 July, pp. 1053-1058 vol. 2.

Pires, C.L., Nabeta, S.I., Cardoso, J.R., 2007. ICCG method applied to solve DC traction load flow including earthing models. IET Electric Power Applications 1(2), 193-198.

Pope Francis, 2015. Encyclical Letter Laudato Si' of the Holy Father Francis On Care For Our Common Home.

Rahimi, A., Zarghami, M., Vaziri, M., Vadhva, S., 2013. A simple and effective approach for peak load shaving using Battery Storage Systems. North American Power Symposium (NAPS), 2013, pp. 1-5.

Ralon, P., Taylor, M., Ilas, A., Diaz-Bone, H., Kairies, K., 2017. Electricity storage and renewables: costs and markets to 2030. International Renewable Energy Agency: Abu Dhabi, UAE.

Ratniyomchai, T., Hillmansen, S., Tricoli, P., 2015. Energy loss minimisation by optimal design of stationary supercapacitors for light railways. 2015 International Conference on Clean Electrical Power (ICCEP), pp. 511-517.

Ratniyomchai, T., Hillmansen, S., Tricoli, P., 2014. Optimal capacity and positioning of stationary supercapacitors for light rail vehicle systems. 2014 International Symposium on Power Electronics, Electrical Drives, Automation and Motion, pp. 807-812.

Ripple, W.J., Wolf, C., Newsome, T.M., Barnard, P., Moomaw, W.R., 2019. World Scientists' Warning of a Climate Emergency. Bioscience 70(1), 8-12.

Roch-Dupré, D., Cucala, A.P., Pecharromán, R.R., López-López, ÁJ., Fernández-Cardador, A., 2020. Simulation-based assessment of the installation of a Reversible Substation in a railway line, including a realistic model of large traffic perturbations. International Journal of Electrical Power & Energy Systems 115, 105476. DOI: https://doi.org/10.1016/j.ijepes.2019.105476.

Roch-Dupré, D., Cucala, A.P., R. Pecharromán, R., López-López, ÁJ., Fernández-Cardador, A., 2018. Evaluation of the impact that the traffic model used in railway electrical simulation has on the assessment of the installation of a Reversible Substation. International Journal of Electrical Power & Energy Systems 102, 201-210. DOI: https://doi.org/10.1016/j.ijepes.2018.04.030.

Roch-Dupré, D., López-López, ÁJ., Pecharromán, R.R., Cucala, A.P., Fernández-Cardador, A., 2017. Analysis of the demand charge in DC railway systems and reduction of its economic impact with Energy Storage Systems. International Journal of Electrical Power & Energy Systems 93, 459-467. DOI: https://doi.org/10.1016/j.ijepes.2017.06.022.

Rufer, A., Hotellier, D., Barrade, P., 2004. A supercapacitor-based energy storage substation for voltage compensation in weak transportation networks. IEEE Transactions on Power Delivery 19(2), 629-636.

S. Su, X. Li, T. Tang, Z. Gao, 2013. A Subway Train Timetable Optimization Approach Based on Energy-Efficient Operation Strategy. IEEE Transactions on Intelligent Transportation Systems 14(2), 883-893.

Saka, M.P., Hasançebi, O., Geem, Z.W., 2016. Metaheuristics in structural optimization and discussions on harmony search algorithm. Swarm and Evolutionary Computation 28, 88-97. DOI: https://doi.org/10.1016/j.swevo.2016.01.005.

Sanjula Weerasinghe, 2018. In Harm's Way: International Protection in the Context of Nexus Dynamics Between Conflict or Violence and Disaster or Climate Change. UN High Commissioner for Refugees (UNHCR).

Sheu, J., Lin, W., 2012. Energy-Saving Automatic Train Regulation Using Dual Heuristic Programming. IEEE Transactions on Vehicular Technology 61(4), 1503-1514.

Shigen Gao, Hairong Dong, Yao Chen, Bin Ning, Guanrong Chen, Xiaoxia Yang, 2013. Approximation-Based Robust Adaptive Automatic Train Control: An Approach for Actuator Saturation. Intelligent Transportation Systems, IEEE Transactions on 14(4), 1733-1742.

Stephan, A., 2010. Openpowernet - the new co-simulation tool for traction power supply. IET Conference on Railway Traction Systems (RTS 2010), pp. 1-6.

Sumpavakup, C., Suwannakijborihan, S., Ratniyomchai, T., Kulworawanichpong, T., 2018. Peak Demand Cutting Strategy with an On-Board Energy Storage System in Mass Rapid Transit. Iranian Journal of Science and Technology, Transactions of Electrical Engineering 42(1), 49-62.

Suzuki, S., Baba, J., Shutoh, K., Masada, E., 2004. Effective application of superconducting magnetic energy storage (SMES) to load leveling for high speed transportation system. Applied Superconductivity, IEEE Transactions on 14(2), 713-716.

Takagi, R., 2012. Preliminary evaluation of the energy-saving effects of the introduction of superconducting cables in the power feeding network for DC electric railways using the multi-train power network simulator. IET Electrical Systems in Transportation 2(3), 103-109.

Takagi, R., 2010. Energy Saving Techniques for the Power Feeding Network of Electric Railways. IEEJ Transactions on Electrical and Electronic Engineering 5(3), 312-316.

Tan, Y., Zhu, Y., 2010. Fireworks algorithm for optimization. International Conference in Swarm Intelligence, pp. 355-364.

Tian, Z., Kamel, T., Tricoli, P., 2019. A study to design the locations of reversible traction substations for minimizing power losses of DC railways. 2019 21st European Conference on Power Electronics and Applications (EPE'19 ECCE Europe), pp. P. 1-P. 9.

Tzeng, Y.S., Wu, R.N., Chen, N., 1998. Electric network solutions of DC transit systems with inverting substations. IEEE Transactions on Vehicular Technology 47(4), 1405-1412.

Tzeng, Y.S., Wu, R.N., 1995. A detailed R-L fed bridge converter model for power flow studies in industrial AC/DC power systems. IEEE Transactions on Industrial Electronics 42(5), 531-538.

Tzeng, Y.S., Wu, R.N., Chen, N., 1995. Unified AC/DC power flow for system simulation in DC electrified transit railways. IEE Proceedings - Electric Power Applications 142(6), 345-354(9).

van Oort, N., van Nes, R., 2010. Impact of Rail Terminal Design on Transit Service Reliability. Transportation Research Record 2146(1), 109-118.

Wang, B., Yang, Z., Lin, F., Zhao, W., 2014. An Improved Genetic Algorithm for Optimal Stationary Energy Storage System Locating and Sizing. Energies 7(10), 6434.

World Health Organization, 2019. Health, environment and climate change. Draft WHO global strategy on health, environment and climate change: the transformation needed to improve lives and well-being sustainably through healthy environments. Report by the Director-General.

Xia, H., Chen, H., Yang, Z., Lin, F., Wang, B., 2015. Optimal energy management, location and size for stationary energy storage system in a metro line based on genetic algorithm. Energies 8(10), 11618-11640.

Yii-Shen Tzeng, Nanming Chen, Ruay-Nan Wu, 1995. A detailed R-L fed bridge converter model for power flow studies in industrial AC/DC power systems. IEEE Transactions on Industrial Electronics 42(5), 531-538.

Zhang, G., Tian, Z., Tricoli, P., Hillmansen, S., Liu, Z., 2019. A new hybrid simulation integrating transient-state and steady-state models for the analysis of reversible DC traction power systems. International Journal of Electrical Power & Energy Systems 109, 9-19. DOI: https://doi.org/10.1016/j.ijepes.2019.01.033.

Zhu, X., Zhang, R., Dai, W., Zhang, Z., Li, J., 2013. Performance and Safety Assessment of ATO Systems in Urban Rail Transit Systems in China. Journal of Transportation Engineering 139(7), 728-737.

We would like to the express our gratitude to the Ministerio de Educación, Cultura y Deporte of Spain through the “Training Programme for Academic Staff (FPU)” (Grant No. FPU15/03765) for supporting this research.

This research has also been partially supported by Comunidad de Madrid, PROMINT-CM project (grant ref: P2018/EMT-4366) and Ministerio de Economía, Industria y Competitividad of Spain (grant ref. TIN2017-85887-C2-2-P, TIN2017-85887-C2-1-P).